A Click-Chemistry based approach for the synthesis of new BODIPY-labelled fluorescent ligands

Daniel Speed BSc. MSc

Thesis submitted to the University of Nottingham for the degree of Doctor of Philosophy

July 2013

Abstract

Fluorescent ligands have found numerous applications for studying interactions of drug molecules with their target and as a probe of biological systems. A common approach when designing and synthesising a fluorescent ligand is to separate the fluorophore and pharmacophore via a linker. One novel approach is to utilise click chemistry to allow the coupling of fluorophore to a pharmacophore. This thesis reports the results of an investigation into utilising click chemistry, specifically the alkyne-azide copper (I) cycloaddition to synthesis novel fluorescent GPCR ligands. Targets included the β_1, β_2 adrenoceptor and the muscarinic M_3 receptor.

Investigations into the introduction of a 1,2,3-triazole within the linker to the fluorophore resulted in 14 novel fluorescent antagonists active at the β_1 and β_2 adrenoceptor. The most promising ligand had log K_i values of -6.77 ± 0.20 (β_1) and -7.32 ± 0.05 (β_2). These ligands were used in a confocal microscopy studies to visualise the β_1 and β_2 adrenoceptors on the surface of CHO cells. However the ligands internalistion, and receptor visualisation was not possible. A range of structural modifications were made to reduce this with the introduction of a polar linker but this did not reduce the intracellular accumulation. The change to a longer wavelength fluorophore stopped intracellular accumulation but reduced the binding log K_i to -5.16 ± 0.06 (β_1) -5.96 ± 0.20 (β_2).

Twenty two novel fluorescent M_3 ligands were synthesised and their inhibitory properties were investigated. An initial screen showed four promising ligands and further study into the binding affinities showed the ligands to have high potency (log K_b -7.97 ± 0.07 to -8.89 ± 0.11). These ligands were studied with confocal microscopy and intracellular accumulation did not occur. Structural changes to include a polar side chain or a sulfonic acid onto the fluorophore were investigated and led to three novel fluorescent ligands that had reduced lipophilicity. With this reduced lipophilicity, binding affinities were also reduced by ten fold compared to the original fluorescent ligand. The seven ligands were fully profiled physiochemically and kinetically. The physioschemical properties of these seven ligands gave a wide variety of lipophilic values. The kinetic profiles of the ligands exhibited very similar dissociation properties to those of the parent ligand with varying association rates.

The Muscarinic M_3 ligands synthesised show great binding affinities for fluorescent ligands and kinetic profiles that are extremely similar to the parent ligand. These fluorescent ligands hold characteristics that can be used to further examine the pharmacology of muscarinic receptors and be used to replace radioligands for binding studies.

Acknowledgements

Many thanks to my supervisors Barrie Kellam, Stephen Hill, Stephen Charlton and Robin Fairhurst for their excellent guidance and knowledge throughout my PhD. I would also like to thank Tim Self, David Sykes and John Reilly for their direction and support in confocal microscopy, kinetic experiments and physchem HPLC analysis.

I would like to acknowledge the help and time given by all the people in chemistry, and at Novartis. In particular I would like to thank Austin, Jim, Leigh, and Shailesh for their continuous advice and patience. Jack and Jo I thank you for the distraction of a coffee every now and again.

Finally I would like to thank Mum, Dad, Paul and Kayleigh for endless support and for listening to me as I ramble on about chemistry and pharmacology when they have absolutely no idea what I was talking about.

I am extremely grateful to the BBSRC and Novartis for funding my work.

Abbreviations

5-TAMRA	5-carboxytetramethylrhodamine
6-TAMRA	6-carboxytetramethylrhodamine
ATP	adenosine triphosphate
βAR	β-adrenoceptor
β_1AR	β_1-adrenoceptor
β_2AR	β_2-adrenoceptor
β_3AR	β_3-adrenoceptor
BBSRC	Biotechnology & biological science research council
Boc	*tert*-Butoxycarbonyl
BODIPY	boron-dipyrromethene
br	broad
Calc.	calculated
cAMP	cyclic adenosine monophosphate
CHI	chromatographic hydrophobicity Index
$CHI_{IAM\ 7.4}$	chromatographic hydrophobicity Index at pH 7.4
CHO	chinese hamster ovary
CGP 12177	4-[3-[(1,1-dimethylethyl)amino]2-hydroxypropoxy]-1,3-dihydro-2*H*-benzimidazol-2-one hydrochloride
CNS	central nervous system
COPD	chronic obstructive pulmonary disease
d	doublet
Dansyl chloride	5-(dimethylamino)naphthalene-1-sulfonyl chloride
dd	doublet of doublets
DCE	1,2 – dichloroethane
DCM	dichloromethane
DDQ	2,3-dichoro-5,6-dicyano-1,4-benzoquinone
DIAD	diisopropyl azodicarboxylate
DIPEA	*N,N,*-diisopropylethylamine
DMF	*N,N,*- dimethylformamide
DMSO	dimethyl sulfoxide
DMSO-*d*6	dueterated dimethyl sulfoxide
DR	dose ratio

ES	electrospray
FCS	fluorescence correlation spectroscopy
FP	fluorescence polarisation
FRET	fluorescence resonance energy transfer
FT-IR	fourier transform -infrared
Fura-2	acetoxymethyl 2-[5-[bis[(acetoxymethoxy-oxo- methyl)methyl]amino]-4-[2-[2-[bis[(acetoxymethoxy-oxo- methyl)methyl]amino]-5-methyl-phenoxy]ethoxy]benzofuran-2-yl]oxazole-5-carboxylate
GABA	γ-amino butyric acid
GDP	guanosine diphosphate
GPCR	G-protein coupled receptor
GTP	guanosine triphosphate
HBSS	Hank's buffered saline solution
HBTU	*O*-(benzotriazol-1-yl)-*N,N,N′,N′*-tetramethyluronium hexafluorophosphate
HPLC	high performance liquid chromatography
h	hours
HSQC	heteronuclear single-quantum correlation spectroscopy
IC_{50}	molar concentration which inhibits 50% of the maximal stimulatory response.
IAM	immobilised artificial membrane
ICI 118,551	3-(isopropylamino)-1-[(7-methyl-4-indanyl)oxy]butan-2-ol
IP_3	inositol 1,4,5-triphosphate
IR	infrared
J	coupling constant
k3	calculated associated rate
k4	calculated dissociation rate
k_D	dissociation constant
k_i	equilibrium association constant
k_{ob}	observed rate constant
k_{on}	dissociation rate
k_{off}	association rate
Log D	partition coefficient
Log $D_{7.4}$	partition coefficient at pH 7.4
M	molar

m	multiplet
MeCN	acetonitrile
MeOH	methanol
Min	minutes
MS	mass spectroscopy
MW	microwave
NBD	nitrobenzofuran
NMR	nuclear magnetic resonance spectroscopy
q	quartet
QNB	3-quinuclidinyl-benzilate
RLB	radio ligand binding
Rt	retention time
s	singlet
SAR	structure activity relationships
SBD	benzo-2-oxa-1,3-diazole-4-sulfonate
t	triplet
TAMRA	carboxytetramethylrhodamine
TFA	trifluoroacetic acid
THF	tetrahydrofuran
TLC	thin layer chromatography
TM	transmembrane
TOF	time of flight
s.e.m	standard error of the mean
W	Watt
XAC	xanthine amine congener

Table of Contents

1. Introduction

1.1. G-protein coupled receptors

Guanine nucleotide binding protein coupled receptors (GPCRs) are the largest class of cell surface receptors. The amino acids of a GPCR protein molecule are wound into seven helices, which span the cell membrane and are often referred to as transmembrane domains.[1] GPCRs consist of a single polypeptide chain of up to 1100 residues and compose the greatest single gene family, with approximately 800 genes in the human genome.[2] The seven membrane-spanning domains are connected by three intracellular and three extracellular loops. The N-terminus resides outside the cell while the C-terminal domain is located inside the cell (Figure 1.1).[1] GPCRs play a critical role in the human body by controlling numerous biological and physiological functions, and can be activated by many different endogenous stimuli, including neurotransmitters, peptides and hormones, e.g. dopamine, adenosine, acetylcholine and glucagon.[3] GPCRs are a major target area in pharmaceutical research and more than 60 new GPCR drugs have been launched in the past decade, representing approximately 24% of all drugs reaching the market.[4]

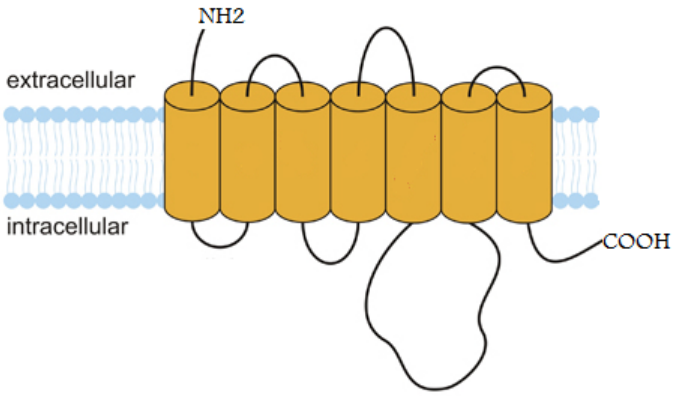

Figure 1.1. Representation of a GPCR. The structure of the protein shows the seven transmembrane domains, the extracellular and intracellular loops, the NH_2 and COOH termini.

GPCRs can be categorised into six families based on their activating ligands and sequence similarity. Three of these exist in mammals and are named 'A', 'B' and 'C'.[5] Group A is the largest subgroup, often known as the rhodopsin-like family, and contains receptors for odorants,

small molecules such as biogenic amines, some small peptides, glycoprotein hormones and photons.[6] This group is characterised by several conserved amino acids and a disulfide bridge that connects the first and second extracellular loop.[5,7,8] The second largest subgroup is group B, also known as the secretin family, and its members are activated by hormones such as glucagon, gonadtropin-releasing hormones and parathyroid hormones.[9] These peptides activate their receptors by a two-domain model in which the peptides bind at two sites before receptor activation.[10] The final GPCR group found in mammals is Group C, also known as the metabotropic glutamate family, which contains receptors such as the metabotropic glutamate, Ca^{2+}-sensing and γ-aminobutyric $(GABA)_B$. These receptors are characterised by a long amino terminus region and carboxy tail. The ligand-binding domain is located in the amino terminus, which has a large lobed structure.[11]

1.1.1 G-proteins

GPCRs are molecules that recognise external stimuli such as hormones, odorants and neurotransmitters. For this recognition to be transmitted to the cell, GPCRs are coupled to transducer molecules. These transducer molecules are heterotrimeric G-proteins that are capable of transferring the recognised external stimuli into an intracellular signal.[12] Each G-protein contains three subunits: α, β and γ. Following receptor activation, GPCRs catalyse the exchange of guanosine diphosphate (GDP) for guanosine triphosphate (GTP) on the Gα subunit, which leads to a decreased affinity for βγ and this results in dissociation.[13] This allows subunits to activate a range of downstream signalling pathways, dependent on the G-protein. G-proteins belong to five different families ($G_{\alpha s}$, $G_{\alpha i}$, $G_{\alpha q/11}$ $G_{\alpha o}$ and $G_{\alpha 12/13}$) based on the α subunit sequence identity and signaling activity.[12,13]

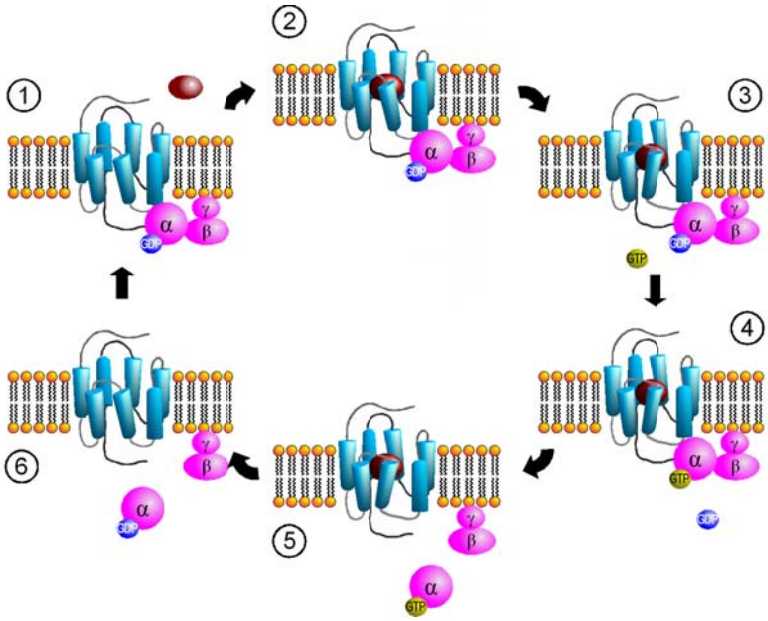

Figure 1.2. G-protein activation by GPCRs. **Source:** Hamm, Biol. Chem. 1998, 273, 669–672.[12]

1.The GPCR in the inactive state is bound to the G-protein. The G-protein α subunit is in the inactive complex and is bound to GDP. 2 and 3. The agonist binds to the receptor, which undergoes a conformation shift. 4. The active receptor causes the exchange of GDP for GTP on the G-protein subunit. 5. GTP binding causes dissociation of the G-protein into the α subunit and βγ subunit, which can modulate downstream signaling. 6. The G-protein α subunit possesses intrinsic GTPase activity, causing hydrolysis of GTP to GDP, and the GDP-bound α subunit can associate with the βγ subunit and associate with the GPCR in the inactive state.

1.2 Studying GPCRs as drug targets

Fifty percent of established drug targets are located on the cell surface and half of these are GPCRs, thus making GPCRs a large area for drug discovery.[14] There have been extensive developments in the methods used to investigate the ligand–receptor interface at GPCRs as well as structure elucidation. These proteins are active in almost every organ system and present a wide range of opportunities for therapeutic targets. Techniques for drug discovery have developed from the understanding of structure–activity relationships (SAR) and rational lead optimisation to modern techniques, such as molecular modelling, compound library screening, natural product basis, allosteric modulation and ligand–receptor kinetics. The SAR and rational lead optimisation approach has been successful for many drug candidates, but it is not the most cost and time effective method in drug discovery. Drugs that have been discovered from SAR studies include (Imatinib).[15] Drugs discovered through natural products include (Taxol)[16] and a druge that had been discovered through chance discovery include (penicillin).[17]

1.2.1 Molecular modelling

Molecular modelling is a collective term that refers to the theoretical methods and computational techniques used to model or mimic the behavior of molecules that can be applied for drug design and discovery. These techniques, such as *de novo* ligand design methods, use computational methods for designing molecules that complement a receptor or binding site structurally and energetically from X-ray crystal structures or receptors of similar nature.[18] The aim of this approach is to design ligands that have high binding affinities for their respective target. *De novo* ligand design has been argued to be most successful when it benefits from established biological and experimental knowledge of the target and receptor.[19] Designing ligands from fundamentals can be applied from two approaches: molecular fragment[20] and sequential growth.[21]

Sequential growth is a technique that 'grows' molecules into an active site, starting from a seed (small molecule or fragment) bound into the active site. The ligand can be grown via the addition of either a single atom or molecular fragment calculated as being complementary to the active site geometrically and/or energetically.[22,23] The second molecular fragment approach docks molecular fragments on the active site to determine favourable positions based on energetically superior configurations. These fragments are then linked together. The initial step in this process is to discover the key locations of the active site and then bind small fragments to these positions. Once this is achieved, linking the fragments with a scaffold is carried out.[19,20] Firth-Clark *et al*.[24] used this process to develop lead compounds for the ATP-binding site of DNA gyrase.

An in-depth review of GPCR *de novo* ligand screening was published by de Graaf and Rognan,[25] and readers are directed to this publication.

1.2.2 X-ray crystallography

In recent years, the study of GPCRs at the molecular level has developed significantly within X-ray crystallography that affords new dimensions to the use of computational chemistry.

X-ray crystallography produces a three-dimensional molecular structure by X-ray diffraction. Unfortunately, members of the GPCR family possess attributes that are undesirable in relation to the classical techniques employed in crystallising proteins. GPCRs require the cell

membrane for structural integrity and are generally unstable in detergent solutions.[26] Since the first X-ray crystal structure of a human GPCR was solved in 2000 by Palczewski *et al*.[27] there has been large scope for development with more than 40 crystal structures of GPCRs entered in the protein data bank.[4] Many of these crystal structures have been solved with a medium to high resolution, in most cases with a small molecule ligand incorporated into the structure. Examples of these include rhodopsin, adenosine A_{2A},[28] chemokine CXCR4,[29] dopamine D_3,[30] the β_1 and β_2 adrenoceptors,[26,31,32] and the histamine H_1 receptor.[33] Some receptors have been engineered for stability using either point mutations of amino acids or the replacement of intracellular loops with lysozymes,[34] and these modifications are shown not to affect ligand binding.[26,35]

1.2.3.GPCR Pharmacology

It is important to evaluate whether a new ligand is an agonist or antagonist and what the potency of the ligand is. It is critical to differentiate between an agonist and antagonist as these will give different effects on the receptor and the possible downstream effects. An agonist is defined as a ligand that binds to a receptor and alters the receptor state resulting in a pharmacological response. Agonists can be sub categorised into full agonists, partial agonists and inverse agonists. Full agonists activate the receptor and display full efficacy for the receptor, while a partial agonist will only have partial efficacy for the receptor relative to a full agonist. An inverse agonist is a ligand that binds to the orthosteric binding site but induces a pharmacological effect opposite to that of the agonist. This is usually shown with a decrease in basal level of activity of the receptor when no ligand is bound. An antagonist is ligand that does not induce a biological response when bound to the orthosteric binding site, but can block or dampen agonist-mediated responses. Figure 1.3 shows typical dose response curves for full, partial and inverse agonist as well as antagonists.

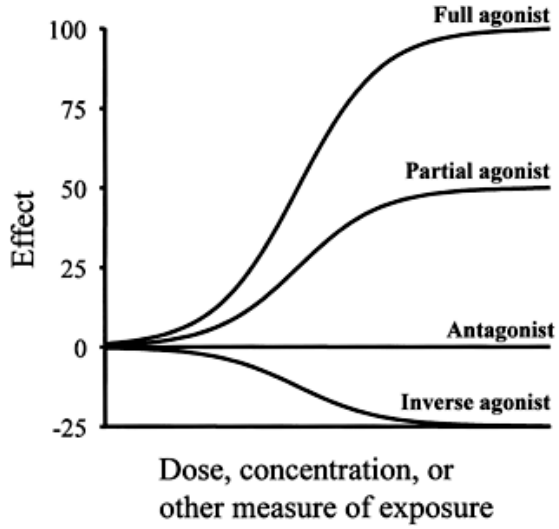

Figure 1.3. Effect of various types of ligands on receptor response. (Effect is quote in %)

Some assays do not give functional results and just identify what that binding affinity of the ligand is while other assays give more accurate and comprehensive data of the compound targeting the GPCR.

1.2.3.1.Radioligand binding experiments

Radioligand based assays examine the binding of radioactive ligands to their counter-receptors. These assays are excellent for the determination of ligand affinity, but do not provide any information on the function of the ligand. There are three main types of radioligand binding assay: saturation assays, competition assays[36] and kinetic assays.[37] Saturation experiments can determine the affinity (K_d) of a radioligand and the maximal specific binding of a ligand (B_{max}), while competition experiments are used to determine the affinity of unlabelled ligands (K_i).[36] Receptor kinetic experiments allow the calculation of association and dissociation rates of radiolabelled ligands and non-labelled ligands. The drawbacks to using radioligands are the requirement of a large cell population ($>10^4$) if using whole cells. Radioligands are hazardous substances that need to be accounted for and must be disposed of in the correct manner, which can be expensive. When there is no commercially available radioligand for the receptor, synthesis of a radioligand is required, which is associated with drawbacks such as half-life of the radioligand and synthesis time.

1.2.3.2. GTPγS binding assays

GTPγS binding assays directly measure the guanine nucleotide exchange of G-proteins. Typically the acculimation of non hydrolysable GTP analogue, Upon receptor activation of the GPCR by an agonist, the receptor changes conformation exposing a binding site for a G-protein complex. Once this G-protein complex is bound, the Gα protein can release GDP and bind GTP. As the GTP is radiolabelled, usually [^{35}S] GTPγS, it is possible to measure the activation of the GPCR bing studied by measuring the amount of radiolabled GTP bound to the cell membrane,As this assay depends on receptor activation it is possible to determine whether a ligand is an agonist, antagonist or inverse agonist.[38]

The disadvantages to this assay are that radioactive compounds are being used which have already been stated, and also a filtration step is required to separate the membrane bound [^{35}S] GTPγS to the unbound which can cause problems when using this as a high throughput assay.

1.2.3.3. cAMP assays

$G\alpha_s$ and $G\alpha_{i/o}$ G proteins when activated, affect andenylyl cylase and the production of cyclic adenosine monophosphate (cAMP). In cAMP assays, cAMP levels are typically measured using competition assays in which a cellular cAMP competes with an introduced labeled form of cAMP for binding to an anti-cAMP antibody.[39] When $G\alpha_s$ is activated, a stimulatory effect of adenylyl cyclase is caused resulting in an increase in cellular cAMP which can be calculated. When $G\alpha_{i/o}$ is stimulated an inhibitory effect of adenylate cyclase occurs and a decrease in cAMP levels occur. [40]

This style of assay is only applicable to GPCRs that stimulate a cAMP response. $G\alpha_{i/o}$ dependent receptors can be difficult to screen as well as antagonists for both G-proteins.

1.2.3.4. Reporter assays

A reporter gene is a sequence of DNA that encodes for an easily measured protein product that is synthesised in response to the activation of a particular signalling cascade. The DNA sequence consists of three essential parts, a promoter, where transcription factors bind to control transcription, the reporter gene itself and a transcription stop signal.[41] When a GPCR is activated, downstream signalling occurs and one response from a secondary messenger is gene transcription alteration. These secondary messengers are all located within the gene promoter

regions and can therefore be used for cell based assays for GPCR drug discovery.[42] The reporter gene assays have the potential to determine the affinities, efficacies and potencies of respective antagonists and agonists.

There are a range of disadvantages of the report gene assay. Firstly a long assay time is required, usually in the range of four to six hours, this is for the expression of the report gene product. Another disadvantage of the assay is the requirement of the cells to be transfected with the receptor gene and possible drugs used in the assay may effect other mechanisms further along the signal pathway. This could lead to the reporter readout becoming a mixture of activity at the receptor and a point elsewhere in the signalling cascade which generates false potencies for ligand-binding interactions.[41]

1.2.3.5. Ca^{2+} assay

Upon GPCR activation of a $G\alpha_q$ or $G\alpha_i$ coupled receptor, activation of phospholipase C to hydrolyse phosphatidylinositol biphosphate to form two secondary messengers, inositol 1,4,5-triphosphate (IP3) and diacylglycerol. IP3 activates the IP3 receptors located on the endoplasmic reticulum resulting in an efflux of Ca^{2+} into the cytoplasm and an elevation of intracellular Ca^{2+}.[43] The Ca^{2+} assay utilises cell permeable Ca^{2+} sensitive fluorescent dyes that when bound to Ca^{2+} change their fluorescent properties that can determine whether a ligand is an agonist or an antagonist.

This style of assay does have some disadvantages such as it cannot be used to screen for inverse agonists due to increase of basal Ca^{2+} is not observed. The assay is not suitable for ligands that have slow associate rates as calcium flux occurs rapidly and transiently.[44]

1.2.4 Fluorescence

Fluorescent probes have been used to study various receptors[45-53] and these fluorescent probes offer many advantages over the conventional techniques currently used, and fluorescent probes are now being used in the assays previously mentioned. There are binding assays based on time resolved fluorescent resonance energy transfer, and homogenous time-resolved fluorescence technology.[54] These assays remove the health and safety issues, synthetic problems and inconvenient short half lives of the radio isoptopes. Modifications to the cAMP assays has resulted in a fluorescent polarisation assay. This assay works in similar fashion but the

competition is a between fluorescently labeled cAMP and non-labeled cAMP for a fixed number of antibody binding sites, again removing the hazardous radio isotope from the assay.[55]

Another benefit to using fluorescence for studying GPCRs is the conjugation of a fluorescent molecule to an established orthosteric ligand can be used to study ligand-binding interactions at the cellular level. They have the advantage of an easier less restrictive synthetic procedure as well as allowing direct visualisation using confocal microscopy, amongst other techniques, to determine the actual location of receptors within a single cell. This allows small numbers of cells to be used for each experiment and results can be obtained in real time.[56] Fluorescent molecules can also be displaced by non-fluorescent ligands to examine specific and non-specific binding. There are, however, some perceived disadvantages of using fluorescence-based techniques. The addition of a fluorescent probe to a pharmacologically active ligand or indeed the receptor itself can alter their properties, and this needs to be considered. In addition, cells and tissues exhibit background fluorescence, which can cause problems when studying fluorescent receptors and ligands. When studying fluorescent proteins or ligands within a biological sample the signal of interest must be from the molecule or protein. Background fluorescence can add intensity to the signal of interest and it can be sourced from a range of cellular components, depending on the specimen being used. Examples consist of NADH, riboflavins and flavin coenzymes.[57] Collagen, elastin and monomers of tubulin can also cause background fluorescence. If using cells, cell culture media that contain phenol red, vitamins and other components that fluoresce can cause issues if the samples are not washed thoroughly.[58] Background fluorescence is known to be stronger at all wavelengths in the green and blue spectral region below 500 nm.[59]

1.2.4.1 Principles of fluorescence

Fluorescence is based on the properties of some molecules (generally polyaromatic hydrocarbons or heterocycles) that when excited by a photon can absorb the energy of that photon causing an excited electronic state (S_1, S_2). Upon relaxation from the excited state the same molecule releases a photon, this process is known as fluorescence emission. The photon that is released from the molecule is of lower energy than the exciting photon. This is referred to as the Stokes shift, reducing the excited electronic state back to the ground state (S_0). If a molecule that absorbs a photon does not emit a photon, it is regarded that the energy is lost

through vibration and rotation of bonds. These processes are called radiation less transfer of energy.[60]

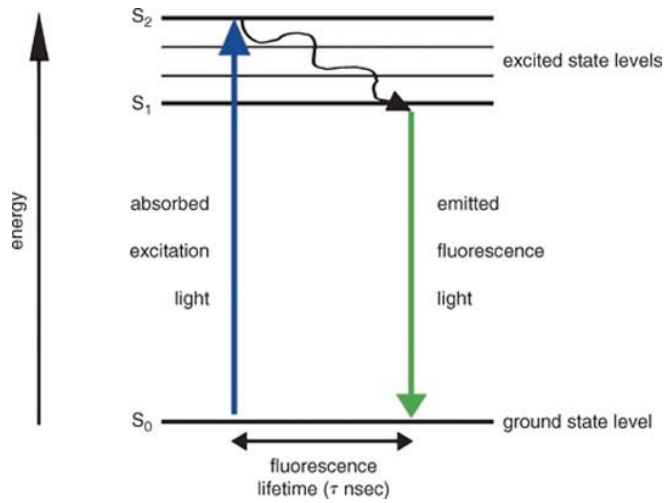

Figure 1.4. Energy diagram for a fluorescent molecule (S_0, electronic ground state; S_1 and S_2, electronic excited state.)

1.2.4.2 Fluorescence techniques

1.2.4.2.1 Confocal microscopy

Confocal microscopy is a powerful tool for generating high-resolution images and 3-D reconstructions of a specimen. In confocal microscopy a laser light beam is focused onto a fluorescent specimen through the objective lens. The mixture of reflected and emitted light is captured by the same objective and is sent to the dichroic mirror. The reflected light is deviated by the mirror while the emitted fluorescent light passes through a confocal aperture (pinhole) to reduce the 'out of focus' light. The focused light then passes through the emission filter and proceeds to the photomultiplier.[61]

Confocal microscopy can allow the study of ligand–receptor binding interactions at the single cell level and can capture biological processes such as localisation. Confocal microscopy has been used to visualise fluorescent probes on a range of receptors, including cannabinoid CB_2,[62] adenosine,[63] adrenergic[64] and mu opioid receptors.[65]

1.2.4.2.2 Fluorescence polarisation

Fluorescent polarisation (FP) is becoming an alternative to radioligand binding experiments and has many benefits over radioligand binding, such as low health and safety implications, homogenous format, high sensitivity and flexibility.[66] FP uses polarised light to detect how

much fluorescent ligand is bound and not bound to a receptor. When polarised light is reflected from a bound ligand the light returns polarised as the bound ligand has little free rotation, unlike the free ligand, which can rotate freely in the extracellular media. This results in the return of non-polarised light.[67] This can determine how much fluorescent ligand is bound when used in a competition assay, for example.

1.2.4.2.3 Fluorescence correlation spectroscopy

Fluorescence correlation spectroscopy (FCS) depends on small fluctuations in the fluorescence intensity as fluorescent particles move through a small defined volume.[68] Statistical analyses of these fluctuations provide information regarding the diffusion coefficient of the labelled molecules being studied and their concentration. FCS is able to distinguish between bound and unbound species when studying receptor–ligand interactions.[68] An unbound fluorescently tagged ligand in solution will show a fast diffusion coefficient, at a rate corresponding to its molecular mass. If that ligand subsequently binds to a slow-moving membrane-localised receptor, its diffusion coefficient will be significantly reduced, thus showing as a bound ligand.[69] This reduction in the diffusion coefficient allows differentiation between free and bound ligand.

1.2.4.2.4 Fluorescence resonance energy transfer

Fluorescence resonance energy transfer (FRET) is a technique that utilises two separate fluorophores and the process of energy transfer. FRET uses the excited energy from one fluorophore (donor) to excite a separate fluorophore (acceptor) through a non-radiative process. This process is distance dependent and can be used to probe biological structures.[70] FRET can allow the quantification of molecular interactions, such as between labelled receptors and ligands,[71] protein conformational changes, and protein interactions.[72]

For a more detailed review on fluorescence techniques, readers are directed to excellent reviews by Joo *et al*.[73] and Hovius *et al*.[71]

1.3 Current GPCR fluorescent ligands

GPCRs have had a range of fluorescent ligands designed, synthesised and tested to investigate their pharmacology at the molecular level, and several thorough reviews have been published

covering fluorescent ligands and fluorescent imaging of GPCRs.[66,68,74-77] McGrath *et al*.[56] published a comprehensive review of research on fluorescent ligands before 1996 and Middleton *et al*.[74] provided a further review in 2005. There are also many examples of fluorescently labelled peptide ligands in the current literature; however, these will not be reviewed herein as our focus has been on small molecules.

Xie *et al*.[53] successfully developed an alternative for radioligand binding assay for histamine H_2 receptors by synthesising antagonists based upon the structure of aminopotentidine. These compounds were coupled with the commercially available fluorescent dyes S0536 or BODIPY 650/665. The binding assays were performed on both human H_2 receptors and guinea pig H_2 receptors. It was found that compound (**1**) bound with relatively high affinity (log K_b = −7.33) to the human H_2 receptor as well as to the guinea pig H_2 receptor (log K_b = −7.23). The coupling of the fluorophore to the pharmacophore was through amide bond formation.

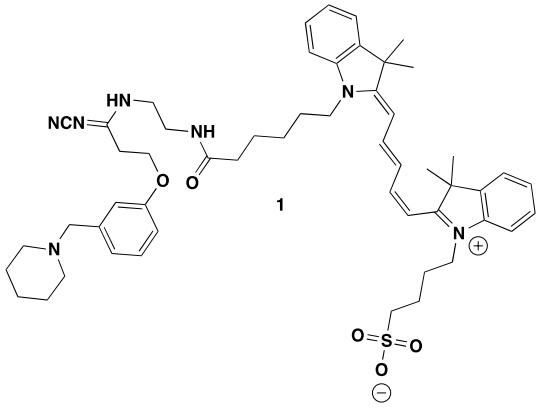

Figure 1.5. Structure of fluorescently labelled histamine H_2 ligand.

Cowart *et al*.[78] synthesised and investigated eight benzofuran histamine H_3 receptor antagonists. These compounds were based on ABT-239 and had a range of commercial fluorophores attached, including: nitrobenzofuran (NBD), benzo-2-oxa-1,3-diazole-4-sulfonate (SBD), 5-(dimethylamino)naphthalene-1-sulfonyl chloride (dansyl chloride), *5-carboxytetramethylrhodamine* (5-TAMRA) and *6-carboxytetramethylrhodamine* (6-TAMRA). The concept behind the fluorophores was to produce ligands with drug-like properties, such as good lipophilicity and no highly polar groups. The K_i values for the series of antagonists were in the range of log K_i = −10 to −8.22 at the human H_3 receptor while the values were −9.92 to

−7.77 at the rat histamine H_3 receptor, with the most potent antagonist (**2**) containing the NBD fluorophore.

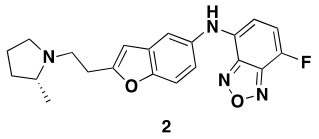

2

Figure 1.6. Structure of fluorescent histamine H_1 ligand.

Bonnet and co-workers synthesised fluorescent compounds through 'click' chemistry using Cu(I) catalysed 1,3-dipolar cycloaddition in an attempt to side-step some of the limitations of fluorescent probe synthesis; *e.g.* the requirement of excess reagents, and the generation of deleterious by-products that compromise both overall yield and purity. This approach focused on the insertion of a fluorophore onto a muscarinic antagonist scaffold that was derived from pirenzepine. The fluorophore incorporated into the scaffold was lissamine rhodamine B. The synthesis was performed in acetonitrile/water in the presence of $CuSO_4$ and copper wire. This procedure afforded novel pirenzepine derivatives with nanomolar affinity for the muscarinic M_1 receptor. The fluorescent ligand (**3**) was also examined in FRET based assays.[79]

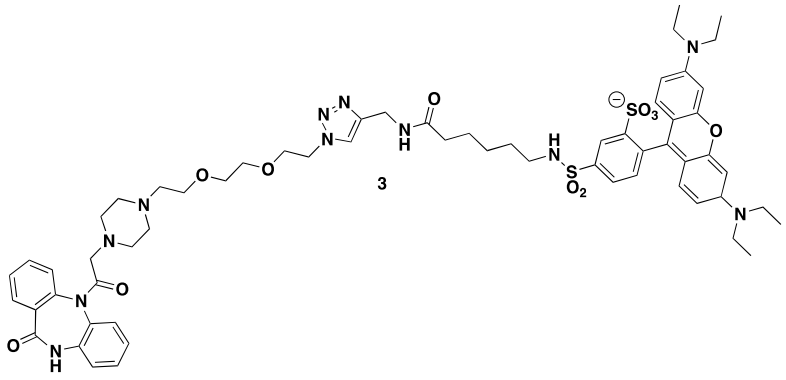

3

Figure 1.7. Fluorescently labelled muscarinic M_1 ligand.

Lacivita *et al.*[52] synthesised and developed a range of weakly fluorescent 5-HT_{1A} ligands with nanomolar affinity for the receptor. Ligands were synthesised by a condensation reaction of the pharmacophore with the weakly fluorescent amine, 2-quinolinamine. The ligand with optimum binding (**4**) had a $\log K_D$ = -9.39 and remained an antagonist. Within the same research group, red shifted 5HT-$_{1A}$ ligands were synthesised with the most potent ligand, **5**, having a $\log K_D$ -7.20. Confocal microscopy was utilised and observed intracellular ligand accumulation. When

lower temperatures (4 °C) were used, less intracellular accumulation occurred and displacement of fluorescent ligand was achieved with serotonin.[80]

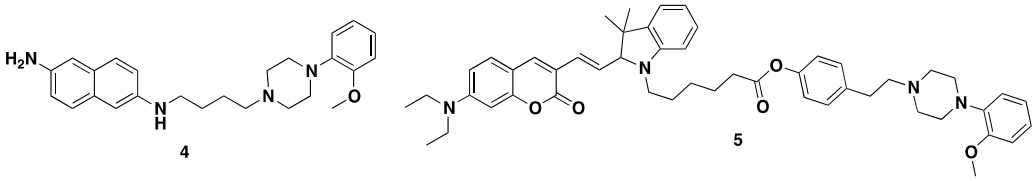

Figure 1.8. Structure of weakly fluorescent and red shifted 5HT-$_{1A}$ ligands.

Dopamine D_3 fluorescent ligands were also synthesised within the same group. Two ligands (**6** & **7**) were highly potent ($logK_D$ = -8.79 and -9.14). Epifluorescent microscopy was attempted but unfortunately visualisation was not possible.[81]

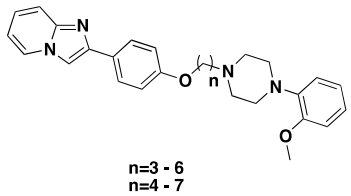

Figure 1.9. Structure of fluorescent dopamine D_3 ligands

Briddon *et al.*[47] describe FCS analysis of antagonist (**8**) with the adenosine A_1 receptor. Confocal imaging allowed visualisation of the ligand at the receptor showing specific binding. The xanthine amine congener (XAC) derived fluorescent ligand had a binding affinity constant of -6.7 ($logK_b$) calculated by cAMP accumulation and -6.5 ($logK_B$) calculated by inositol phosphate accumulation. The ligand was readily synthesised by acylation of XAC by the commercially available BODIPY 630/650-X-succinimidyl ester.

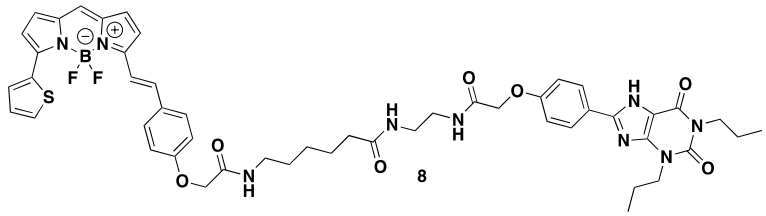

Figure 1.10. Structure of XAC-BODIPY

Within the same research group Middleton *et al.*[82] described the design and synthesis of a range of adenosine-A_1 fluorescent agonists and the subsequent use of these in FCS-based studies of receptor- ligand interactions in live cells. The commercially available fluorophore

BODIPY 630/650 was again employed as the fluorophore of choice. FCS analysis allowed detection and quantification of receptor-ligand binding alongside confocal imaging demonstrating the specific nature of the receptor binding. The ligands displayed a range of pEC_{50} values ranging between 7.92 – 9.16.

Further work in the group published by Cordeaux *et al.*[83] described the use of FCS to investigate the diffusional characteristics of an agonist occupied A_3 receptor using a fluorescent adenosine-A_3 ligand. Studies included confocal microscopy utilising fluorescent ligands and fluorescent intracellular calcium detectors to visualise receptor binding and receptor activation. This allowed visualisation of both ligand and intracellular calcium production. The fluorescent ligand (**9**) utilised the commercially available BODIPY 630/650 fluorophore.

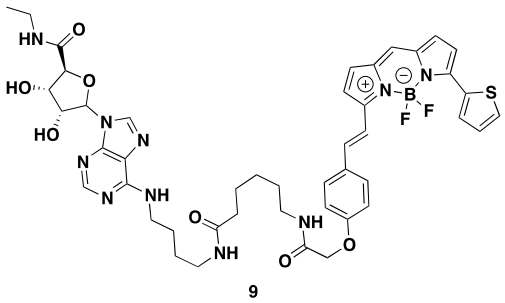

9

Figure 1.11. Structure of ABEA-X-BY630

Baker *et al.*[84] described a fuller investigation surrounding adenosine-A_1 fluorescent ligands and how the linker and choice of fluorophore influences the pharmacology of the conjugated ligand. It was suggested from the results of two separate pharmacophores with different linkers and fluorophores that the physiochemical properties of the fluorophore and linker determine the ultimate utility of the fluorescent ligand. A range of fluorophores were investigated including Dansyl, Cy5, BODIPY 630/650, BODIPY FL and Texas Red with a range of linkers of differing length and chemical composition.

Jones *et al.*[85] developed a fluorescent muscarinic M_3 antagonist based upon tolterodine. This scaffold had a commercially available BODIPY tag again attached through an amide bond and this resulted in a fluorescent M_3 antagonist (**10**) with a log K_i = -8.33 calculated from radioligand binding experiments. It was later found that this ligand displayed poor stability and

degradation in solution with a $t_{1/2}$ of one week. No other biological investigation was carried out on the ligand.

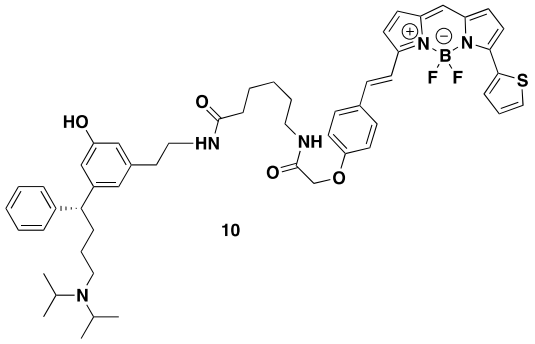

Figure 1.12. Structure of fluorescent M_3 ligand

Baker *et al.*[86] also described the use of a commercially available fluorescent ligand BODPIY-TMR-CGP 12177 (**11**). Investigations into agonist activity through radioligand binding studies and confocal microscopy resulted in receptor visualisation and affinities to be calculated. Receptor binding could be reduced by pre-incubation with 3-(isopropylamino)-1-[(7-methyl-4-indanyl)oxy]butan-2-ol (ICI 118551) or 4-[3-[(1,1-Dimethylethyl)amino]2-hydroxypropoxy]-1,3-dihydro-2*H*-benzimidazol-2-one hydrochloride (CGP 12177). The fluorescent ligand had a low nanomolar affinity with values dependent upon on which assay was used.

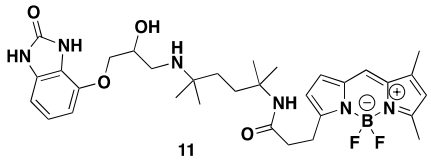

Figure 1.13. Structure of BODIPY-TMR-CGP

A fluorescently labelled arterenol derived fluorescent ligand has been investigated by Hegener *et al*.[87] The labelling of an arterenol pharmacophore with an alexa dye was used to study the β_2-adrenoceptor in living cells using FCS. It had respective log K_D values of -8.88 and -8.22 at β_2 receptors of neurons (hippocampal neuron cells) and A549 cells (human cancer cells) respectively. It was calculated that the association rates were comparable in both cell types.

Baker *et al.*[64] recently published the synthesis and characterisation of high affinity BODIPY labelled ligands for the β-adrenoceptors. Ligands were based on the orthosteric ligands propranolol, alprenolol and pindolol. These ligands had the commercially available BODIPY-

630/650-X fluorophore tethered via a range of straight hydrocarbon or polyethylene glycol linkers. Binding affinities were calculated through radioligand binding experiments with [^{3}H]-4-[3-[(1,1-dimethylethyl)amino]2-hydroxypropoxy]-1,3-dihydro-2*H*-benzimidazol-2-one hydrochloride ([^{3}H]-CGP 12177) and functional reporter gene assays. Confocal microscopy was used to visualise the binding of the fluorescent ligands at the β_2-adrenoceptor in single living cells. It was possible to prevent fluorescent ligand binding via pre-incubation with a non-selective antagonist. The most potent ligand was based on propranolol with a diethylene glycol linker (**12**); displaying log K_D values of -9.53 and -8.46 at the β_2 and β_1 receptor respectively.

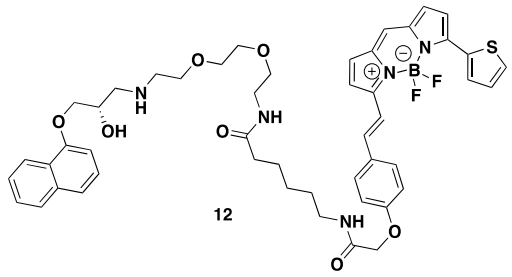

Figure 1.14. Structure of fluorescent β-adrenoceptor ligand

It is clear from the above and other reports in the literature that fluorescently tagged ligands are now becoming a well-established practice for GPCR pharmacology with a range of different targets and different experiments being reported. The majority of fluorescent ligands synthesised have included a commercially available fluorophore attached by either amide bond formation or alkylation.

1.4 Click chemistry

To synthesise a fluorescent ligand, a fluorescent molecule needs to be attached to a biologically active molecule. As previously stated, this has been commonly achieved via either amide bond formation or alkylation reactions. These techniques can be troublesome if protecting groups need to be incorporated when synthesising novel fluorophores or connecting the fluorophore to the pharmacophore. One method to avoid the use of functional group protection to allow conjugation of a fluorescent molecule to an orthosteric ligand is through click chemistry. Bonnet and co-workers successfully achieved this when synthesising muscarinic M_1 ligands.[79] Click chemistry is a term defined by Barry K Sharpless to describe a style of chemistry that

joins small molecules together quickly.[88] There are many types of click chemistry reactions, such as cycloadditions, olefin-based, and nucleophilic opening of rings. One of the most favoured reactions is the alkyne-azide copper (I) catalysed 1,3-cycloaddition which was evolved by the Sharpless and Meldal research groups.[88,89] The original reaction was first developed by Rolf Huisgen with other 1,3-dipolar cycloadditions.[90] It was noted that formation of triazoles from azides and acetylenes was first discovered 60 years earlier by O. Dimroth.[91] This reaction uses an azide functionalised molecule and a molecule with an alkyne functionality to form a five membered ring known as a 1,2,3-triazole shown in scheme 1.1, with the mechanism shown in figure 1.14. The original Huisgen 1,3-cyclo-addition did not use catalysts, and used high temperatures that resulted in a mixture of 1,4 and 1,5-adducts while the work of Sharpless and Meldal ultilised copper catalysis to optimise the regio-isomerism. The reaction time was decreased without the need for high temperatures which was also a reason for mixed isomerism, which is still true with the catalysed reaction.[92] Another catalyst that can be used is a ruthenium metal catalyst, which results in a 1,5-regioisomer.[93]

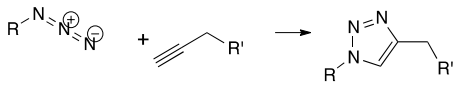

Scheme 1.1. Synthesis of a triazole from an azide and an alkyne using click chemistry.

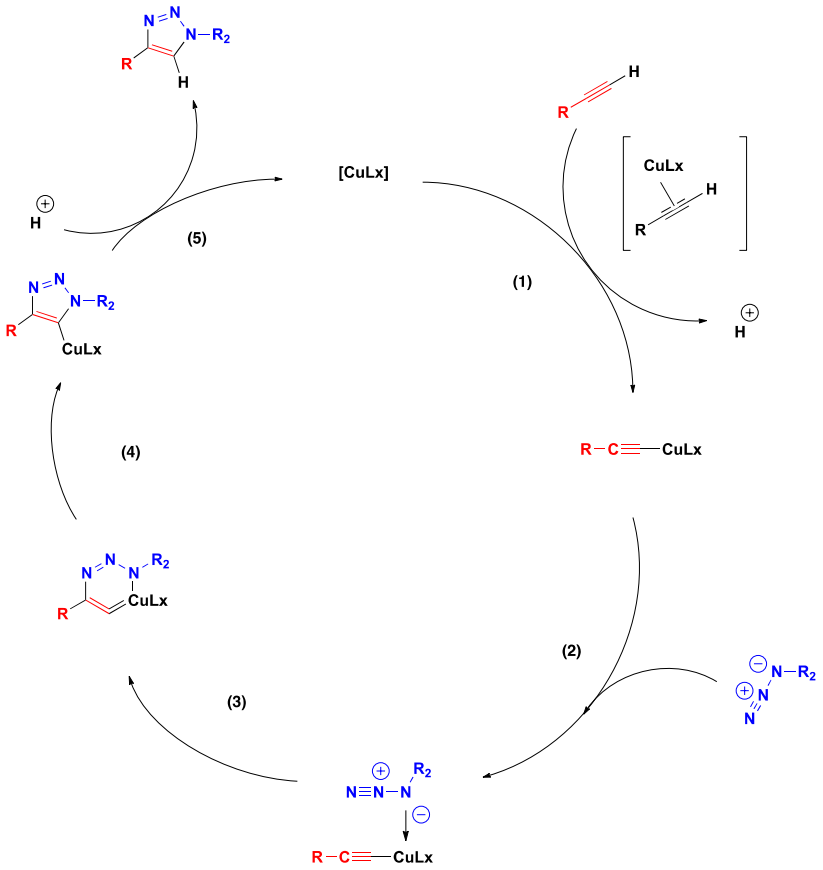

Figure 1.15 Mechanism for the click chemistry 1,3-cycloaddtion.

A mechanism has been proposed for the click reaction using density functional theory calculations and is shown in figure 1.15.[94] The mechanism begins with (1) the alkyne coordinating with the copper (I) species, displacing one ligand from the copper and results in the conversion of the alkyne to an acetylide. The next step (2) involves the replacement of one ligand in the copper complex with the azide. This allows binding to the copper via the nitrogen proximal to the carbon (3). The distal nitrogen in the azide attacks the acetylene carbon forming an unsual six membered copper (III) metallacycle. Step (4) is a ring contraction resulting in the five membered triazolyl-copper derivative and final protonation of the five membered ring releases the 1,2,3-triazole as the product and completing the cycle (5).

It has been noted that both azide and alkyne groups are very convenient functional groups due to the ease with which they can be introduced into a molecule, their stability under a variety of conditions and that they are stable in organic conditions that include molecular oxygen, water and the majority of common reaction conditions employed in modern-day synthesis.[95-97] It is widely accepted that the two functional groups can be attached when needed for convenience and remain unaffected through a number of transformations unlike other reactive groups that

could be used to couple fluorophores to pharmacophores such as amines, carboxylic acids, alcohols and halides. When using azides and alkynes, side group modifications can be made without the need for protecting groups and this is also true when coupling the azide and alkyne together. Thus making the click chemistry reaction highly reliable, with the reaction being experimentally straightforward.[98] Whilst the reaction (to form the 1,4 adduct) can be performed using commercial sources of copper (I) such as cuprous bromide or iodide, it has also been reported that the reaction works much better using a mixture of copper (II) usually in the form of copper (II) sulfate and a reducing agent with common agents being sodium ascorbate or copper wire; which produces Cu (I) *in situ*.[79] The reaction can be performed in a range of solvents and a mixture of solvents are common, usually water and a partially miscible organic solvent such as acetone, methanol, ethanol and acetonitrile. In many cases, the product can be simply be filtered from the solution.[99]

1.5 Research aims

Fluorescent ligands have found numerous applications for studying the interactions of drug molecules and probes with biological systems.[74] For a large proportion of these applications the use of fluorescently labelled molecules offers potential for a unique insight into following the course of cellular processes, or a more efficient and safer alternative to radio-labelled derivatives for routine applications such as for those used in ligand binding assays. The aims of this research are to identify an efficient and broadly applicable route to fluorescently labelled ligands and then demonstrate their effectiveness in a pharmacological setting.

For this approach to be suitable for a range of applications it requires chemistry that is widely applicable, from readily available starting materials, that proceeds in a reliable and efficient manner and that is tolerant of a wide range of functionality, ideally without the need for protecting groups.

The aims are to establish the chemistry to produce key fluorescently-labelled synthons for use in a click chemistry labelling step and then to explore their introduction into pharmacophores.

In addition these ligands will be investigated in a pharmacological manner at the receptor target through a number of processes.

2. Design and synthesis of fluorescent beta-adrenoceptor ligands

2.1 Adrenoceptors

One GPCR receptor subtype that is of interest is the adrenoceptor family. These receptors have been the target for numerous drug discovery projects and have been established as key therapeutic targets for cardiovascular and respiratory diseases.[64] There are two types of adrenoceptor: α and β. The α-adrenoceptors are subdivided into α_1 and α_2; the β-adrenoceptors (βAR) are subdivided into β_1, β_2 and β_3. Generally, when activated α_1-adrenoceptors cause relaxation of smooth muscle in the gut, glycogen breakdown in the liver and vasoconstriction.[1] α_2-Adrenoceptors can pre-synaptically inhibit the release of neurotransmitters, affect platelet aggregation and inhibit the release of insulin.[1] β_1-Adrenoceptors (β_1AR) are primarily located in the heart and their activation results in an increase in the heart rate and force of contraction. β_1-AR are also found in the kidneys where activation can lead to an increase in blood pressure by activation of the renin-angiotensin-aldosterone system. β_2-Adrenoceptors (β_2AR) are primarly found in the airways and in blood vessels. Activation of β_2AR can result in vasodilation and also leads to more rapid contraction of skeletal muscle and an increased rate of glycogenolysis in the liver.[1] β_3-adrenoceptors (β_3AR) are predominantly found in adipose tissue and are involved in thermogenesis and lipolysis.[1]

2.1.1 β –Adrenoceptor

The β-adrenoceptors are primarly found in the heart (β_1AR), airways and blood vessels (β_2AR). All β-adrenoceptors signal through the G_s G-protein. On activation the α_s-subunit and βγ-subunit can activate separate signaling pathways. The α_s-subunit causes activation of adenylyl cyclase, resulting in coversion of adenosine triphosphate (ATP) to cyclic adenosine monophosphate (cAMP).[100] Amplification of the signal can arise from multiple molecules of cAMP being produced by each adenylyl cyclase. The secondary messenger cAMP has a range of diverse signaling targets that include cyclic nucleotide-gated ion channels, protein kinase A and exchange protein activated directly by cAMP.[100] It has been noted that the βγ-subunit can

initiate intracellular signaling pathways independent of the Gα subunit.

2.1.1.1 β –Adrenoceptor structure

Adrenoceptors are grouped into family A of the GPCRs, in which they all share a common structure with that of rhodopsin,[101] and that of all GPCRs. The TM helices are grouped to form the ligand-binding site in the centre of the receptor. β_1AR is a 477 residue 7-TM protein, β_2AR is a 413 residue 7-TM while β_3AR is a 408 amino acid protein.[102,103] The are similarities in the sequences of β_1AR and β_2AR: they share 48.9% homology while β_3AR has 50.7% homology with β_1AR and 45.5% homology with β_2AR.[104]

Figure 2.1. Representation of family A of the GPCRs. The seven TM helices are labelled 1-7 and ligand shown in green. **Source:** Congreve et al. *J Med Chem*, 2011, 54, 4283-4311.[4]

2.2 β –Adrenoceptors as drug targets

Many adrenergic compounds are currently in widespread clinical use to treat a range of disorders, including; hypertension, asthma and *angina pectoris.*

2.2.1 Cardiovascular targets

Targeting β-adrenoceptors in the treatment of cardiovascular disease have been used since the first β –blockers propranolol and pronethalol, were demonstrated to reduce blood pressure and have beneficial effects for the treatment of angina.[105] Now antagonists are available for the targeting of β_1AR in the treatment of hypertension, coronary heart disease, arrhythmia and myocardial infarction, for example.[106]

2.2.1.1 Hypertension

Hypertension is chronic cardiac condition in which the systemic blood pressure is elevated.[1] Causes include stress, obesity, smoking and potassium deficiency.[107-109] A range of treatments are available for hypertension, including weight loss, dietary changes, calcium channel blockers, angiotensin-converting enzyme inhibitors and β-blockers.[110-112] Antagonists of β_1AR diminish the effect of adrenaline and other stress hormomes. Antagonists that are used for hypertension are propranolol (**13**), metoprolol (**14**) and nadolol (**15**).

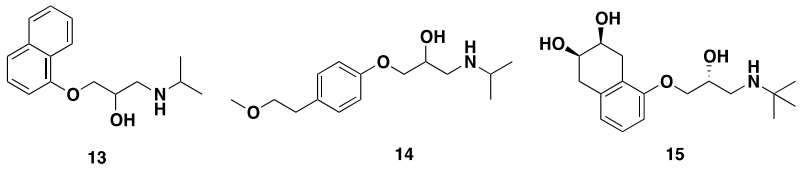

Figure 2.2. Structures of propranolol, metoprolol and nadolol.

2.2.1.2 Angina pectoris

Angina pectoris occurs when the oxygen supply to the cardiac muscle is insufficient for its needs, often resulting in severe pain for the patient.[1] The pain has a characteristic distribution in the chest, arm and neck and is usually brought on by exertion or excitement. There are three types of *angina pectoris*: stable angina, unstable angina and microvascular angina.[1] Stable angina is characterised by predictable pain on exertion. It is produced by an increased demand on the heart and is caused by the fixed narrowing of the coronary artery. Unstable angina is characterised by pain with less exertion, cumulating in pain at rest. Microvascular angina is characterised by angina-like chest pain but has different causes.[113] Contributory factors associated with *angina pectoris* are smoking, diabetes, hypertension and obesity. The range of treatments for *angina pectoris* include nitroglycerin, a potent vasodilator that reduces blood pressure in the arteries and dilates the veins. Calcium blockers and β-blockers are used to decrease the workload of the cardiac muscle. β_1AR antagonists that are currently used therapeutically include; bisoprolol (**16**), metoprolol (**14**), carvedilol (**17**) and nebivolol (**18**).[114]

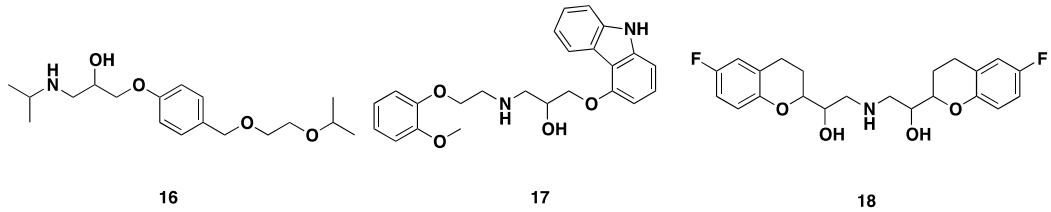

Figure 2.3. Structures of bisoprolol, carvedilol and nebivolol.

2.2.1.3 Myocardial infarction

Myocardial infarction, more commonly known as a heart attack, results in the interruption of the blood supply to a part of the heart, which causes heart cells to die. The most common cause of myocardial infarction is the occlusion of a coronary artery following the disturbance of an atherosclerotic plaque.[1] It is accepted that the risks associated with atherosclerosis are generally the same as those for myocardial infarction and these are age, high blood pressure, obesity, prolonged exposure to high quantities of alcohol and smoking.[115,116] β-blocker therapy is used in the prevention of myocardial infarction and has been demonstrated to be beneficial in high-risk patients. β_1AR antagonists such as metoprolol and carvedilol have been successfully used clinically to prevent the reoccurrence of myocardial infarction.[117]

2.2.1.4 Arrhythmia

Arrhythmia also known as cardiac dysrhythmia, is the name given to the large group of conditions related to the abnormal electric activity of the heart. This involves an increased or decreased heart rate, and can be a regular or irregular heart beat. The most common heart arrhythmia is heart palpitations. The classification of arrhythmia is related to the site of the abnormality and whether there is an increase (tachycardia) or decrease (bradycardia) in the heart rate.[1]

Anti-arrhythmic agents include fast inward sodium channel blockers (quinidine), slow channel blockers (verapamil) and β-blockers. The β_1AR agents used include atenolol, esmolol and propranolol. Using antagonists decreases myocardial infarction mortality and prevents recurrence of tachyarrhythmia.[118]

2.2.2 Respiratory targets

Many adrenergic compounds are currently in widespread clinical use to treat asthma and chronic obstructive pulmonary disease.[106]

2.2.2.1 Asthma

Asthma is an inflammatory disorder in which there is a recurrent reversible obstruction of the airflow in the airways in response to stimuli that themselves are not noxious and do not effect non asthmatics.[1] Asthma is thought to be caused by a combination of genetic and environmental factors.[119] Asthma can be acute or chronic. In chronic asthma, the sufferer has intermittent attacks of dyspnoea, wheezing and coughing, which can be reduced by drug treatment. Acute asthma, also known as s*tatus asthmaticus*, is not easily reversed by medication, can be fatal and requires prompt treatment.[1] Two types of β_2AR agonists are commonly used for the treatment of asthma: short acting and long acting. Short acting agonists include salbutamol (**19**), levosalbutamol (**20**) and terbutaline (**21**).[120]

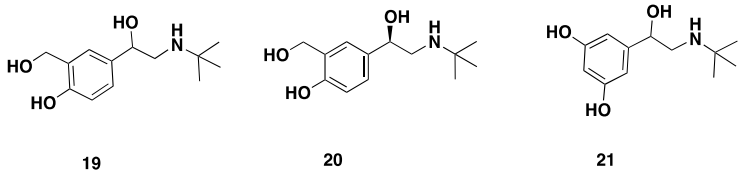

Figure 2.4. Structures of salbutamol, levosalbutamol and terbutaline.

The long-acting agonists include salmeterol (**22**), formoterol (**23**) and bambuterol (**24**), are used for moderate to persistant asthma.

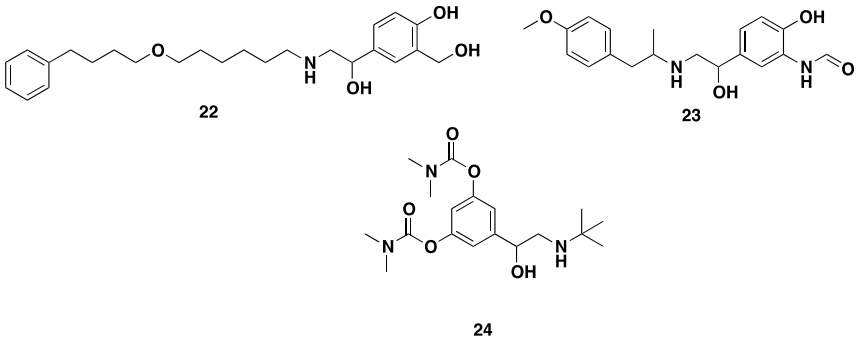

Figure 2.5. Structures of salmeterol, formoterol and bambuterol.

2.2.2.2 Chronic obstructive pulmonary disease

Chronic obstructive pulmonary disease (COPD) is the co-occurrence of chronic bronchitis and emphysema, which results in the narrowing of the airways in the lung. Chronic bronchitis is the inflammation of the bronchi and bronchioles. Emphysema is distention and damage of the lung beyond the respiratory bronchioles and it supervenes after years of coughing. This

combination results in limited airflow to the lungs, causing shortness of breath.[1] Causes of COPD include smoking, occupational exposure, air pollution and genetics.[121,122] There is currently no cure for COPD, however COPD is a preventable and treatable disease. Treatments include anticholinergics, corticosteroids and bronchodilators such as β_2AR agonists, e.g. salbutamol and an ultra-long-acting agonist, indacaterol (**25**).[123]

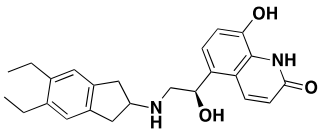

25

Figure 2.6. Structure of indacaterol

2.2.3 Aims

This chapter describes the design, synthesis and pharmacological evaluation of a series of fluorescent ligands, which bind to β-adrenoceptors. The aim of this work was to synthesise a range of fluorescently labelled β-adrenergic antagonists to use as tools to study ligand-receptor interactions through radioligand binding assays, confocal imaging and kinetic experiments. The technique that was used to conjugate a fluorescent probe to the orthosteric ligand was click chemistry. This was utilised to remove the need for functional group protection and deprotection steps that are commonly required for other conjugation methods.

2.3. Design and synthesis of fluorescent ligands

The design of novel fluorescent ligands for β-adrenoceptors required an active pharmacophore for the receptor and the connection of a fluorescent molecule. The addition of this fluorophore cannot compromise the functional groups essential to receptor binding. The addition of a linker bearing a terminal group that can be utilised in a copper (I) catalysed azide-alkyne cycloaddition could prove a quick and convenient way of tethering a fluorescent molecule to an active pharmacophore.

Two known pharmacologically active and therapeutically used ligands, propranolol, a non-selective antagonist, and metoprolol a β_1 inverse agonist, were chosen as the orthosteric ligands.[124] It was found that almost all of the hydrophobic regions of the 7-TMs influence the binding with agonists, while antagonist-binding specificity is mainly controlled by TMs six

and seven.[125] It was proposed that there are three major interactions that are critical for binding between the endogenous ligand and receptor. The first is the amine, which has an ionic reaction to the receptor. The second is hydrogen bonding with the hydroxyl and catechol hydroxyl groups, and finally, an aromatic-aromatic interaction with the catechol ring (figure 2.7). The aromatic portion is important with interactions with the Phe-290 residue in the TM6 helices by van der Waals interactions. These functional groups must not be interfered with when adding a linker and fluorophore. Figure 2.8 shows the structure of cyanopindolol and the key binding interactions with the B_1AR.[126-128]

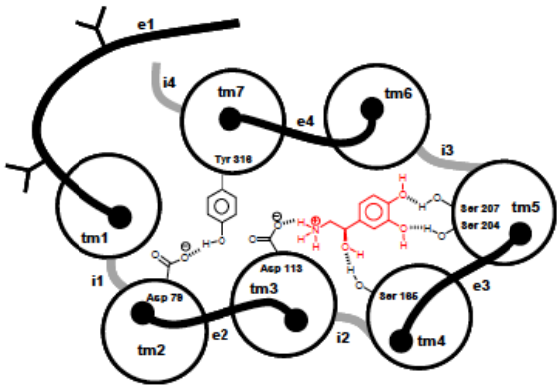

Figure 2.7. Interaction of the agonist noradrenaline with the β_2AR. **Source:** Strosberg *Protein Science* 1993, *2*, 1198-1209.[102]

e1; extracellular N-terminal domain; e2-4; extracellular loops; i1-3; intracellular loops; i4; intracellular C-terminal domain; tm1-7 transmembrane regions.

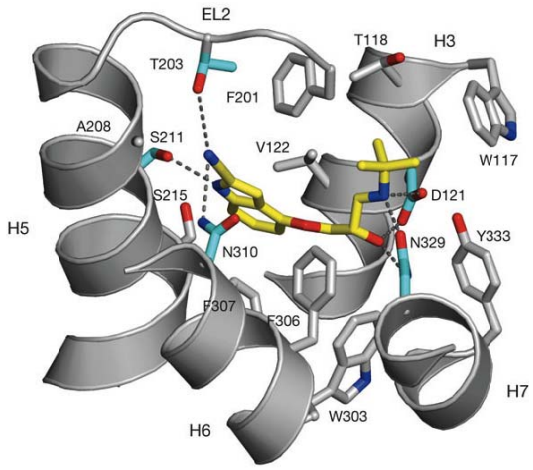

Figure 2.8. Amino acid residues of a β_1AR that interact with the ligand cyanopindolol (yellow) by polar interactions (aquamarine) or non-polar interactions (grey). **Source:** Warne *et al, Nature* 2008, *454*, 486-491.[125]

The incorporation of a linker for fluorophore attachment can be tolerated beyond the amine group. It is known that branching and extension from the amine can be tolerated. Previous work within the group has also attached fluorescent moieties through linkers adjacent to the amine and they have been well tolerated.[64,86]

For initial investigations into the copper (I) catalysed azide-alkyne cycloaddition between a fluorophore and pharmacophore, the synthesis of a non-commercially available fluorophore afforded many potential benefits such as individual functionalisation and individual fluorescent properties. Fluorophores based on boron-dipyrromethene (BODIPY) dyes were chosen (figure 2.9), due to their excellent properties of high quantum yields with sharp excitation and emission spectra. BODIPY dyes have the ability to be individually functionalised for the required emission and excitation characteristics and functional groups for attachment.[129] Previous work within the group has utilised BODIPY dyes to great success. [45,82,86,130]

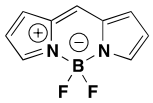

Figure 2.9. BODIPY core structure

2.3.1. Retrosynthesis of fluorescent ligands

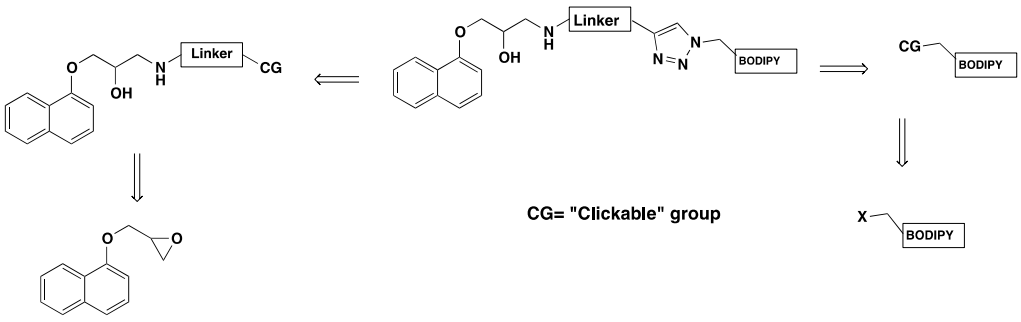

Scheme 2.1. Retrosynthetic analysis of β-adrenoceptor fluorescent ligand based on propranolol

As described above, the alcohol and amine group are essential for pharmacological activity; thus, extension of the molecule adjacent to this motif was required. Incorporation of the linker into the secondary amine would extend the molecule and enable connection of the fluorophore. This allowed investigation to whether the triazole can be tolerated in the binding site or if it

would have an effect on binding. Synthesis of the fluorescent ligands would be separated into two parts, pharmacophore/linker synthesis and fluorophore/linker synthesis. The two synthons would then be conjugated together by click chemistry to yield the final fluorescent ligand.

2.3.2 Synthesis of pharmacophore and linker

Syntheses of the two orthosteric headgroups were initiated with the deprotonation of the requiste phenol with sodium hydride in DMF, and addition of racemic epichlorohydrin (**26**), which after stirring at room temperature, yielded the epoxides **27a** and **27b** after column chromatography (83 and 64% yield) as confirmed by mass spectroscopy and nuclear magnetic resonance spectroscopy (NMR).

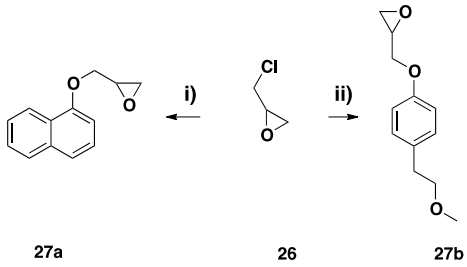

Scheme 2.2. i) NaH, 1-napthol, DMF, 16 hr (83%). ii) NaH, 4-(2-methoxyethyl)phenol DMF, 16 hr (64%).

Synthesis of a short azide linker was achieved by refluxing 2-bromoethylamine hydrobromide (**28**) with sodium azide to yield the azido-amine (**29**) as a free base after treatment with KOH (94% yield). Infra red spectroscopy (IR) was used to confirm the substitution with the azide with a peak at 2098 cm^{-1}. This value is typical for a compound with azide functionality and there is usually an intense peak at ~2100 cm^{-1}.[131]

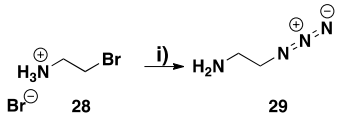

Scheme 2.3. i) NaN_3, H_2O, KOH, 21 hr (94%).

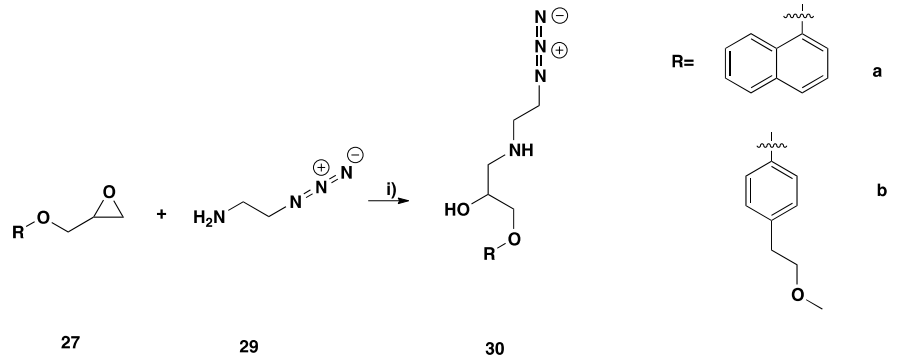

Scheme 2.4. i) isopropanol, 18 hr, reflux (32-41%).

Treatment of the epoxides **27a** and **27b** with the primary amine **29** yielded the secondary amines **30a** and **30b**.

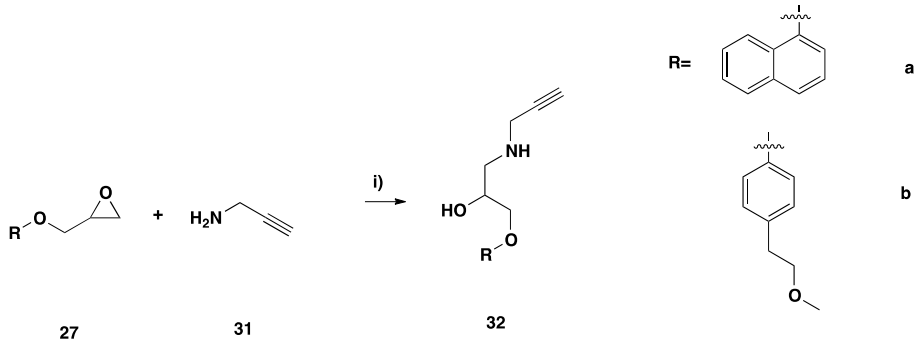

Scheme 2.5. i) isopropanol, reflux, 18 hr, (37-77%).

An alkyne-functionalised pharmacophore was synthesised from commercially available propargylamine **31**. The secondary amine was heated to reflux in isopropanol with the two separate epoxides **27a-b** to yield alkyne-functionalised pharmacophores **32a** and **32b** in yields ranging from 37 to 77% after purification by column chromatography.

The regiochemistry of the ethanolamines was confirmed by ^{1}H NMR, ^{13}C NMR and ^{1}H-^{13}C HSQC NMR spectroscopy. Epoxide opening occurred from the least hindered side, which is to be expected when the reaction is carried out in neutral or basic conditions. [132] Evidence for regioselective opening can be taken from ^{1}H-^{13}C HSQC NMR experiment of **30a** for example (figure 2.10). The 'C' proton at 2.88-3.0ppm displays a chemical shift that is too low to be adjacent to an oxygen. The ^{13}C experiment also supports this with a peak at 51.44. In addition,

it would be expected that protons 'C' and 'D' would have similar shifts in signals in both ^{1}H and ^{13}C experiments, as shown in figure 2.10. Overlay of the linker with the product also helped determine regioselective opening. This configuration of the aryloxypropanolamines is present in all pharmacophores **30a-b** and **32a-b**.

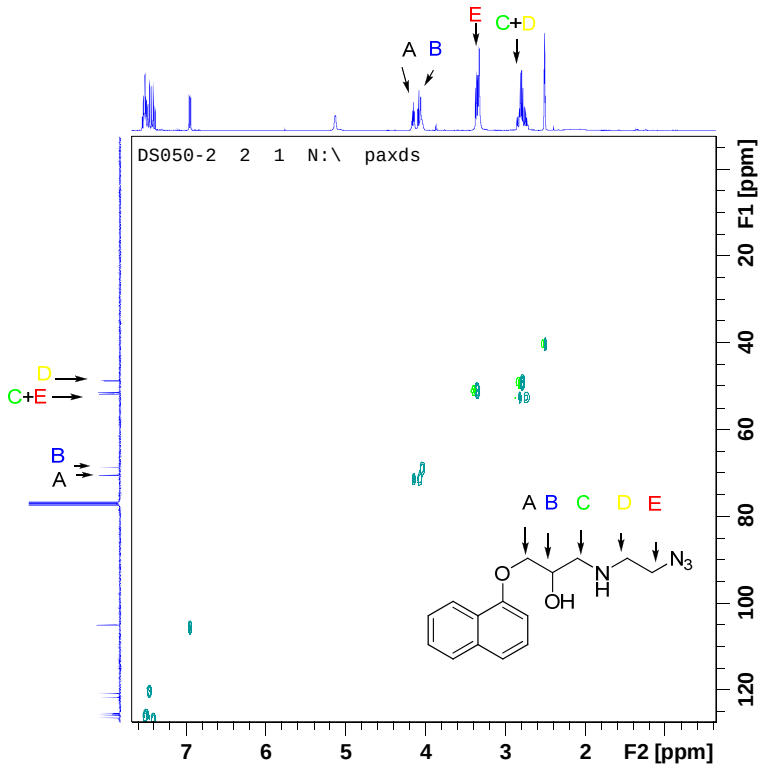

Figure 2.10. ^{1}H-^{13}C HSQC NMR of **30a** in $CDCl_3$. Spectral assignment using ^{1}H-^{13}C HSQC experiment. The relevant ^{1}H proton and ^{13}C carbon experiments are displayed on the x and y axis.

2.3.3 Fluorophore synthesis

Fluorophores were synthesised with terminal alkynes and azides to allow the desired copper (I) catalysed alkyne-azide cycloaddition with the linkers.

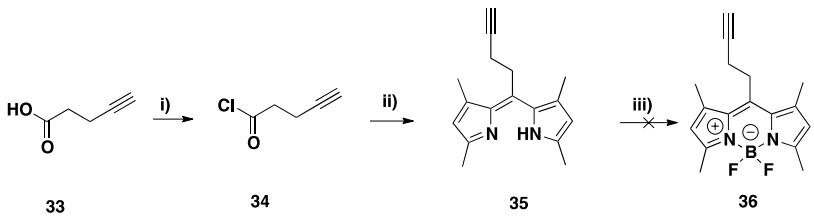

Scheme 2.6. i) $SOCl_2$, toluene, DMF, 4 hr. ii) DCE, 2,4-dimethylpyrrole, 3 hr. iii) $BF_3.OEt_2$, DIPEA, 12 hr.

Synthesis of the acetylene-functionalised fluorophore began with the conversion of carboxylic acid (**33**) to its corresponding acid chloride (**34**) in quantitative yield confirmed by thin layer chromatography (TLC). Coupling of acid chloride **34** to 2,4-dimethylpyrrole at room temperature afforded the dipyrrin species **35**, as comfirmed by TLC and mass spectroscopy. Due to the dipyrrin being unstable and difficult to isolate,[129] both boron trifluoride diethyl etherate and *N,N,*-diisopropylethylamine (DIPEA) were added to the reaction mixture but this did not yield the desired fluorophore **36**. TLC showed a number of fluorescent spots but unfortunately due to the large mixture of compounds in the crude, purification was not attempted and a similar synthesis was attempted to synthesise an azide-functionalised fluorophore.

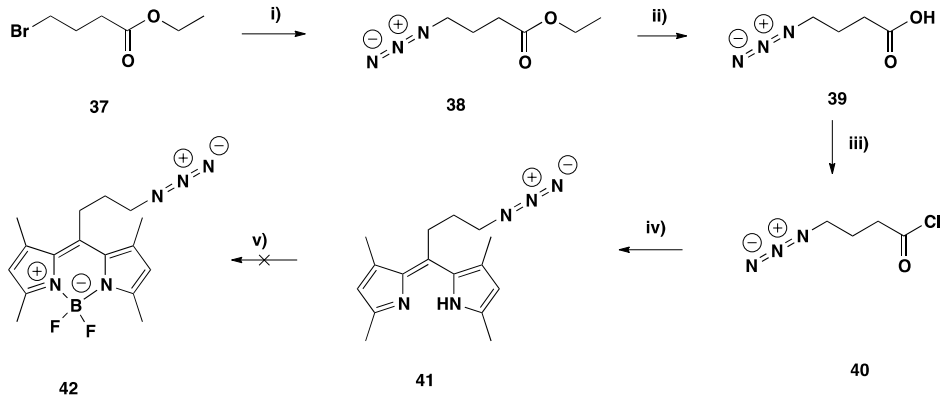

Scheme 2.7. i) NaN_3, acetone/H_2O, 60 °C, 7 hr (85%). ii) KOH, MeOH/H_2O, 6 hr, (80%). iii) $SOCl_2$, DMF, Toluene, 4 hr. iv) 2,4-dimethylpyrrole, DCE, 3 hr. v) $BF_3.OEt_2$, DIPEA, RT, 12 hr.

The synthesis commenced with an azide substitution of the bromo ester **37** in 85% yield. The hydrolysis of ester **38** with aqueous KOH yielded the carboxylic acid **39**. This was confirmed by NMR with the loss of two peaks in the proton NMR corresponding to the ethyl group. The carboxylic acid **39** was converted to the acid chloride **40**, which was used *in-situ* and coupled to 2,4-dimethylpyrrole at room temperature in quantitative yield as confirmed by TLC. Boron trifluoride diethyl etherate and DIPEA were added to the reaction mixture but the desired fluorophore was not purified from the reaction mixture due to the large amount of byproducts, which made column chromatography extremely difficult. As this reaction failed with two types of precursor (azide and alkyne), a different synthetic scheme was undertaken. BODIPY dyes have been synthesised from benzaldehydes in the prescene of trifluoroacetic acid (TFA) and 2,3-dichoro-5,6-dicyano-1,4-benzoquinone (DDQ),[98] therefore this was attempted.

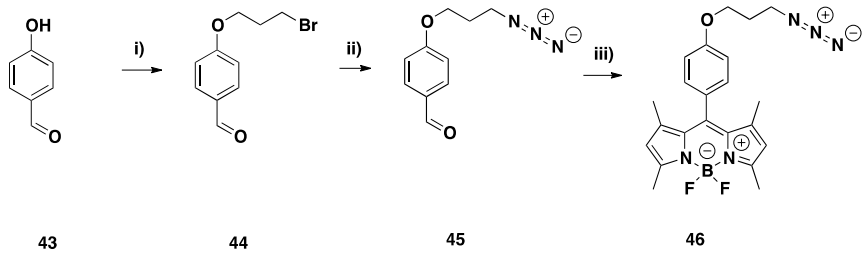

Scheme 2.8. i) Bromopropanol, DIAD, PPh_3, THF, DCM, 12 hr (62%). ii) NaN_3, DMF, 100 °C, 12 hr, (44%). iii) 2,4-dimethylpyrrole, DCM, TFA, DDQ, Et_3N, $BF_3.OEt_2$, RT, 16 hr, (17%).

The synthesis of an azide-functionalised fluorophore required a Mitsunobu reaction between 4-hydroxybenzaldehyde (**43**) and 1-bromo-3-propanol to yield the ether **44**.

There is still debate over the exact intermediates of the Mitsunobu reaction; however, the widely accepted mechanism is shown in figure 2.11.[133]

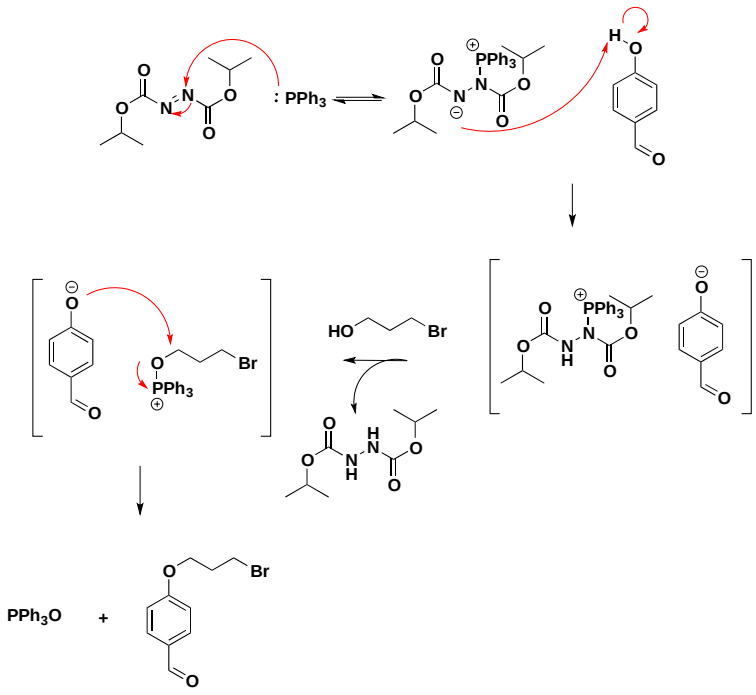

Figure 2.11. Mechanism of the Mitsunobu reaction between **43** and 1-bromo-3-propanol.

The bromo-ether was heated to reflux with sodium azide to create 4-(3-azidopropoxy)benzaldehyde (**45**) without the need for purification. The azide was confirmed by IR spectroscopy and movement of a triplet signified the substitution. The azide-functionalised benzaldehyde was coupled to 2,4-dimethylpyrrole with a catalytical amount of TFA, and finally reacted with boron trifluoride diethyl etherate, and triethylamine after being

oxidised by DDQ. The final step gave the azide-functionalised fluorophore **46** in 17% yield after purification. A similar literature procedure had a yield of 27%.[98]

The alkyne derived fluorophore (**48)** followed the literature procedure of Li *et al*.[134] starting with the commercially available 4-ethynylbenzaldehyde (**47**).

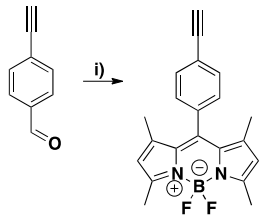

47 48

Scheme 2.9. i) 2,4-dimethylpyrrole, DCM, TFA, DDQ, Et_3N, $BF_3.OEt_2$, 16 hr (28%).

2.3.4 Fluorescent spectroscopy

With two fluorophores synthesised it was necessary to determine the excitation and emission profile of both. This would enable the correct filters and lasers to be employed when using and imaging the fluorescent ligands. As the fluorophores are similar in structure to BODIPY FL,[135] an approximate value of the emission was known. This was used to determine the excitation profile.

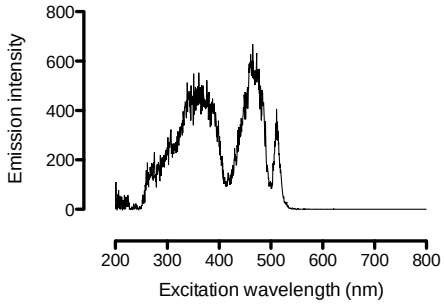

Figure 2.12. Excitation profile with emission intensity measured at 515 nm.

From the excitation scan, (Figure 2.12) both fluorophores were shown to have two main excitation wavelengths; one at 350 nm and the other at 480 nm. Both fluorophores were excited at each wavelength to give an accurate emission for the fluorophores and not a value based on BODIPY FL.

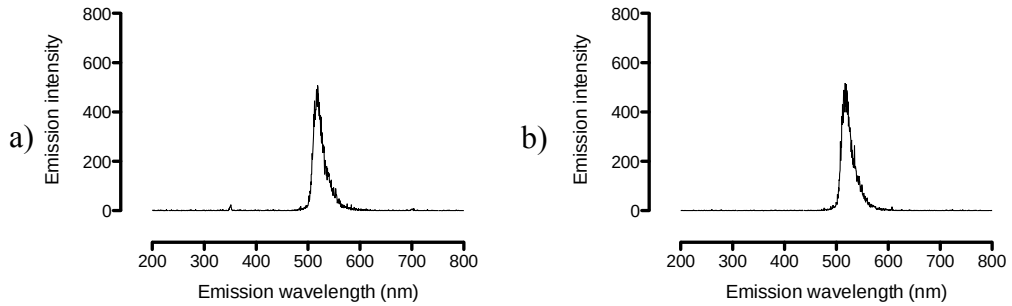

Figure 2.13. Excitation emission profiles when the fluorescent molecule was excited at a) 350 nm and b) 480 nm.

The excitation at 350 and 480 nm showed a single emission at 517 nm. There was no difference between the two fluorophores as the conjugation within both fluorophores was very similar.

2.3.5 Final pharmacophore fluorophore coupling reaction

The final step in synthesising the fluorescent ligand was to form the five membered 1,2,3-triazole ring by copper (I) catalysed 1,3-dipolar cycloaddition. Review of the relevant literature showed that the cycloaddition could be performed in many different solvent systems such as water/*tert*-butanol, water/acetonitrile and water/DCM.[50,79,88,136,137] The cycloaddition can be achieved at room temperature or reflux and even with microwave irradiation.[50,88,138,139]

The results of trial reactions between ethynylbenzene (**49**) and ethyl 4-azidobutanoate (**38**) with a range of different conditions are summarised in tables 2.1. and 2.2. Trial reactions established that water/DMF was the best solvent system.

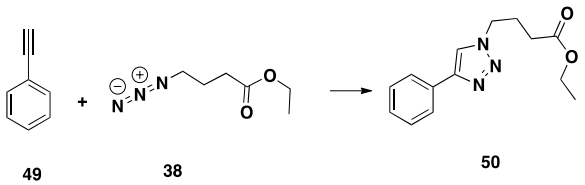

Scheme 2.10. Trial reaction for click chemistry

Procedures included different solvents systems; water/DCM, water/DMF, water/*tert* – butanol and water/acetonitrile. Different catalysts were also trialed, including copper wire/copper sulfate pentahydrate, and copper sulfate pentahydrate/sodium ascorbate. Sodium ascorbate and copper sulfate pentahydrate were found to be the best catalysts for the reaction.

Solvent	Temperature	Yield (%)
H_2O/*tert*-butanol	RT	80
H_2O/*tert*-butanol	60 °C	83
H_2O/acetonitrile	RT	68
H_2O/acetonitrile	60 °C	72
H_2O/DMF	RT	83
H_2O/DMF	60 °C	89
H_2O/DCM	RT	55
H_2O/DCM	60 °C	59

Table 2.1. Trial click reactions. Reaction between ethynylbenzene and ethyl 4-azidobutanoate in the presence of copper wire and $CuSO_4.5H_2O$ over 24 hr.

Solvent	Temperature	Yield (%)
H_2O /*tert*-butanol	RT	89
H_2O/*tert*-butanol	60 °C	92
H_2O/acetonitrile	RT	74
H_2O/acetonitrile	60 °C	77
H_2O/DMF	RT	88
H_2O/DMF	60 °C	93
H_2O/DCM	RT	44
H_2O/DCM	60 °C	44

Table 2.2. Trial click reactions. Reaction between ethynylbenzene and ethyl 4-azidobutanoate in the presence of sodium ascorbate and $CuSO_4.5H_2O$ over 24 hr.

Microwave (MW) irradiation provided high yields and low reaction times compared with room temperature reactions when actual fluorophores and pharmacophores were reacted compared with the trial reagents. The reaction temperature were kept low to avoid the possible formation of the undesired 1,5- adduct as well as the 1,4-adduct. NMR confirmed there was not a mixture

of adducts by the presence of only one proton peak for the triazole. The final click reactions gave four final compounds with yields in the range of 24-70% after high performance liquid chromatography (HPLC) purification with an isocratic eluent of 40% water, 60% acetonitrile over 16 minutes. The crude and purified HPLC trace for **51a** is shown in figure 2.15.

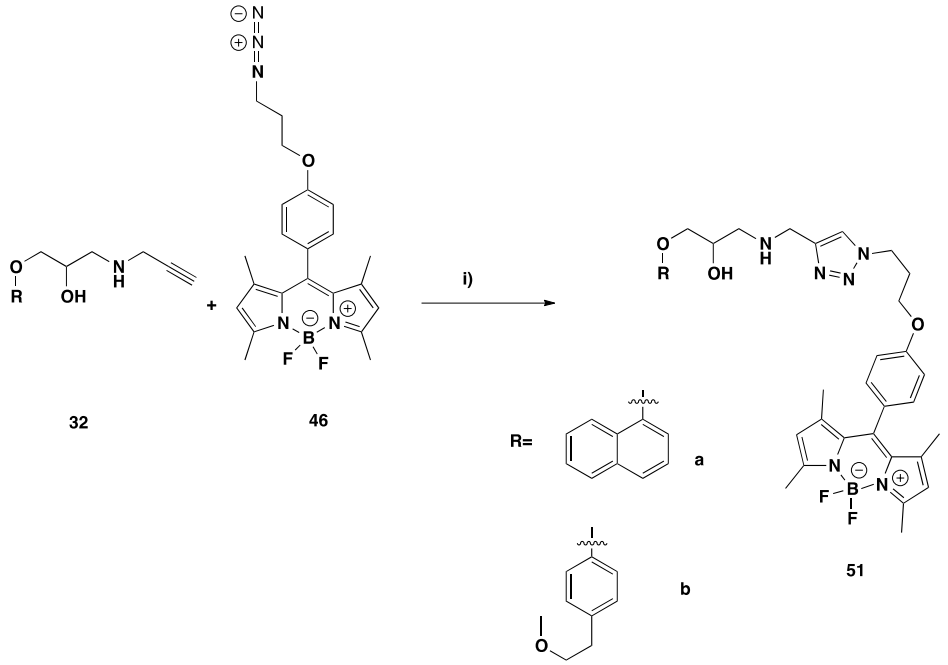

Scheme 2.11. i) DMF/H_2O, $CuSO_4.5H_2O$, sodium ascorbate, MW, 80 min, 80 °C, 40 W, (24-56%).

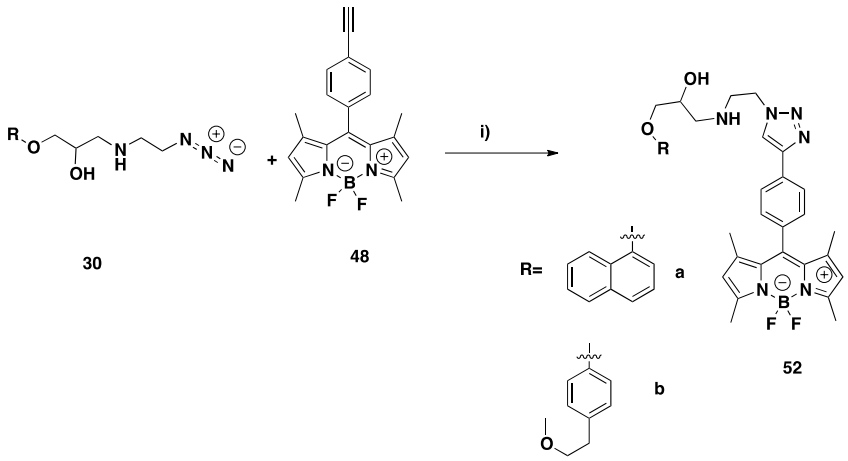

Scheme 2.12. i) DMF/H_2O, $CuSO_4.5H_2O$, sodium ascorbate, MW, 80 min, 80 °C, 40 W ,(46-70%).

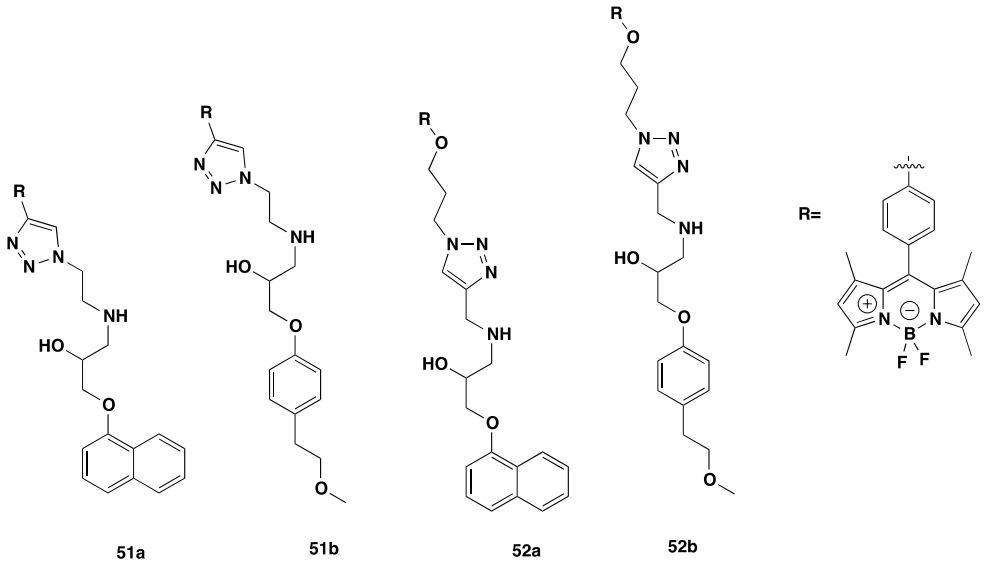

Figure 2.14. Structures of first-generation ligands

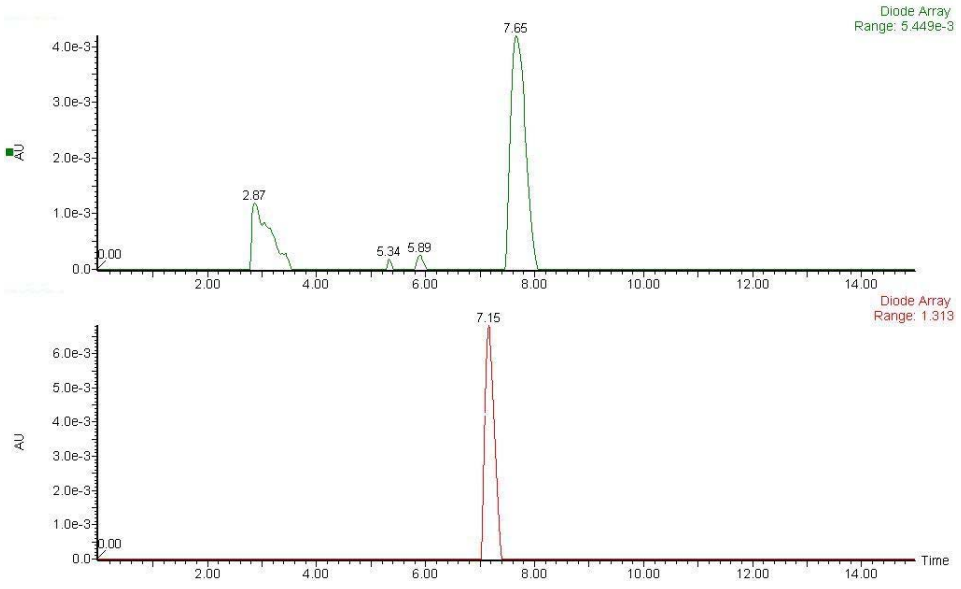

Figure 2.15. HPLC traces of crude (green) and purified (red) compound **51a**. The HPLC method used: Kromasil reverse-phase C18 column (250 x 4.6 mm), a flow rate of 1.00 mL/min and UV detection at 254 and 366 nm. Linear gradient 5% - 95% solvent B over 16 min. Solvent A: 0.06% TFA in water; solvent B: 0.06% TFA in MeCN.

2.3.6 Pharmacology

The pharmacological activity of the fluorescent ligands was assessed by radioligand binding assays (RLB). Competitive radioligand binding was used to ascertain the binding affinity of the ligands. The affinity was determined by competitive displacement of the radioligand, [^{3}H]-CGP 12177 from chinese hamster ovary (CHO) cells expressing either β_1- or β_2-adrenoceptors. Radioligand binding was performed as previously described by Baker.[106] At least three

different experiments were conducted for each ligand in triplicate and the binding affinities of two standards, ICI 118,551 a β_1-antagonist and CGP 12177 a β_2-antagonist, were run in each experiment. The assays were run with a range of final concentrations from 1×10^{-4} M to 1×10^{-10} M to produce the required dose-response curves. It was occasionally not possible to start at 1×10^{-4} M due to the low solubility of the ligands. In addition at higher concentrations, the percentage of DMSO in the media would exceed 0.1% and this may harm the cells due to the toxicity of DMSO.[140] Each ligand was diluted to 10^{-2} M using DMSO and the stock solution was stored at -20 °C until the ligand was tested.

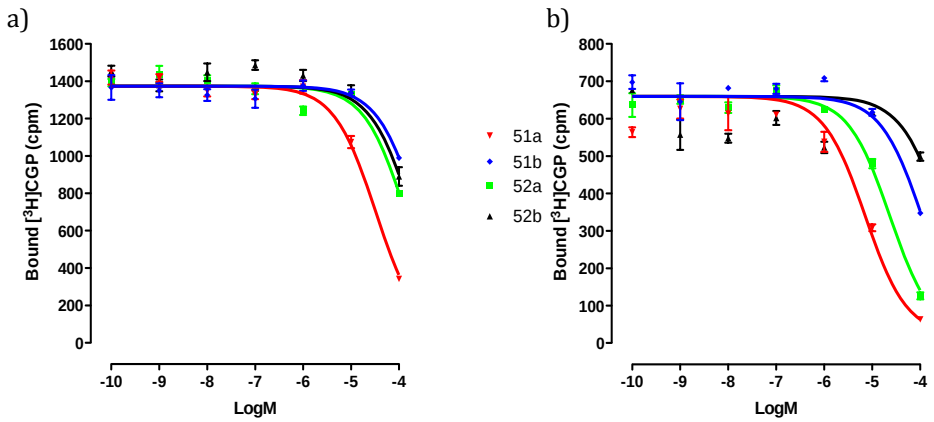

Figure 2.16. Fluorescent ligand displacement of [^{3}H]-CGP 12177 specific binding at the human β-AR in whole CHO cells. Inhibition of [^{3}H]-CGP 12177 specific binding to whole cells by compounds 51a, 51b, 52a and 52b in a) β_1 cells and b) β_2 cells. Nonspecific binding was determined by 10 μM propranolol. A concentration of 1 nM of [^{3}H] CGP 12177 was used in each experiment. Data points are a mean ± s.e.m of triplicate determinations. These single experiments are a representative of a minimum of three different experiments.

Compound	β_1 Log K_i (n)	β_2 Log K_i (n)
51a	-4.85 ± 0.01 (4)	-4.86 ± 0.01 (4)
51b	-4.27 ± 0.01 (4)	- 4.64 ± 0.06 (4)
52a	-4.27 ± 0.10 (4)	-5.13 ± 0.05 (4)
52b	-4.24 ± 0.02 (3)	-4.21 ± 0.13 (4)
Propranolol	-8.21 ± 0.12 (4)	-8.93 ± 0.07 (4)

Table 2.3. Log K_i values were obtained from [^{3}H]-CGP12177 binding in whole cells expressing either the human β_1 or β_2-AR. Values are mean ± s.e.m from n number of experiments. K_i refers to the equilibrium dissociation constant and the values were calculated from the IC_{50} values.

Data from radio-ligand binding assays were used to calculate the IC_{50} values of the fluorescent conjugates. These values were used to calculate the respective binding affinities, K_i, using the Cheng-Prushoff equation.[141]

$$K_i = \frac{IC_{50}}{1 + \frac{[radioligand]}{K_D}}$$

Where [radioligand] = the concentration of free radioligand used in the assay, and K_D = the dissociation constant of the radioligand for the receptor. IC_{50} is the concentration of the ligand that displaces 50% of the specific binding of the radioligand.

The radioligand binding assays of the fluorescent ligands show that is it possible to synthesise a biologically fluorescent ligand with the alkyne-azide copper (I) catalysed cycloaddition. It is clear that the binding affinities are not comparable to that of propranolol or metoprolol. Ligand affinity values ranged from -4.24 to -5.13 and these values are significantly lower than those of the fluorescent ligands synthesised by Baker *et al*.[64] The ligands synthesised by this group can be directly compared. All 14 ligands that Baker *et al.* synthesised had affinities greater than 6.06 ± 0.07 for β_1AR and -7.33 ± 0.09 for β_2AR. The ligand with the lowest affinity synthesised by Baker *et al*. **53** is shown in figure 2.16.

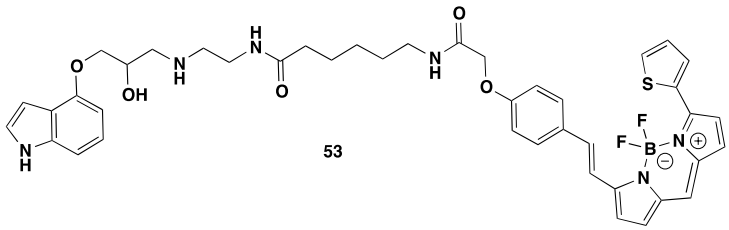

Figure 2.17. Structure of weakest adrenoceptor agonist synthesised by Baker *et al*.[64]

The main differences between **53** and the ligands synthesised in this thesis excluding the pharmacophore, are the linker length and type as well as the fluorophore used. The fluorophore in **53** is BODIPY 630/650 X, a commercially available fluorophore that has a large linker attached. The fluorophore attached to ligands **51a-b** and **52a-b** has a BODIPY FL type fluorophore that does not come with such an extended linker. This could be one of the possible reasons that ligands **51a-b** and **52a-b** have poor affinity. The incorporation of a triazole into the linker is present in the ligands synthesised while ligand **53** does not. This triazole could

reduce the binding affinity due to steric interaction. The movement of the triazole away from the pharmacophore could increase binding affinity.

2.4 Synthesis of second-generation ligands

Due to the poor binding affinity of each compound, the ligands required a second round of design and synthesis to improve receptor binding before any further receptor-ligand interactions could be investigated. Extension of the 1,2,3-triazole away from pharmacophore may achieve increased binding affinities as steric interactions from the triazole and fluorophore could be reduced. A second generation of ligands was designed with a longer linker between the pharmacophore and triazole, moving the triazole away from the amine and alcohol which are key for binding.

This approach will increase the linker atom by atom to give more detail about the SAR of the molecules. The movement of the fluorophore away from the triazole was synthesised for a different approach of moving the fluorophore away from the triazole and the pharmacophore. The fluorescent ligands would be based on the propranolol pharmacophore due to the increased binding affinity over the metoprolol-based pharmacophore. The binding data suggest that the alkyne attached to the pharmacophore shows increased binding affinity over the azide functionalised pharmacophore. The second-generation ligands will have this orientation wih the fluorophore attached to the sp^3-hybridised nitrogen of the 1,2,3-triazole.

2.4.1 Linker synthesis

Synthesis of the second-generation ligands started with the linker. Linkers varied in length from a two-carbon linker up to a four-carbon linker between the amine and the triazole. With the pharmacology results showing that alkyne-functionlised orthosteric ligands producing more potent fluorescent ligands, this orientation was kept.

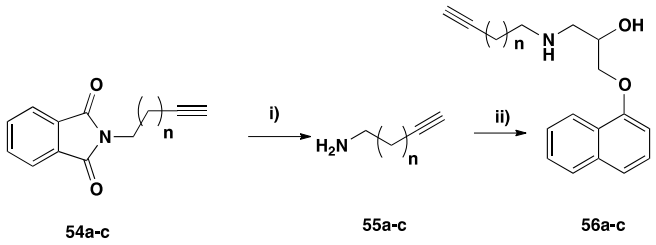

Scheme 2.13. i) Hydrazine monohydrate, isopropanol, sealed tube, 70 °C, 2 hr. ii) 1-(2,3-Epoxypropoxy)- naphthalene, isopropanol, sealed tube, 90 °C, 12 hr (25-31%), n=1 (a), n=2 (b), n=3 (c).

Alkyne functional phthalamides were commercially available with literature procedures for the deprotection of these phthalamides to yield the amino-alkynes.[142,143] Literature procedures for the deprotection were attempted but did not result in the required product. After aqueous workup, it was found that the resulting amine was extremely volatile. Attempts were made to make the hydrochloride salt but these were not successful. An alternative approach was developed to achieve the required linkers. The phthalamide-protected amines were deprotected in the presence of hydrazine monohydrate at 70 °C in a sealed tube for 2 hours, the vessel was cooled and the epoxide **27a** added. The vessel was sealed and heated to 90 °C. An excess of starting phthalimide was needed over the hydrazide monohydrate to stop any excess hydrazine reacting with the epoxide. This resulted in yields of 25% to 31% after purification. The mechanism for the phthalimide deprotection is shown in figure 2.18.

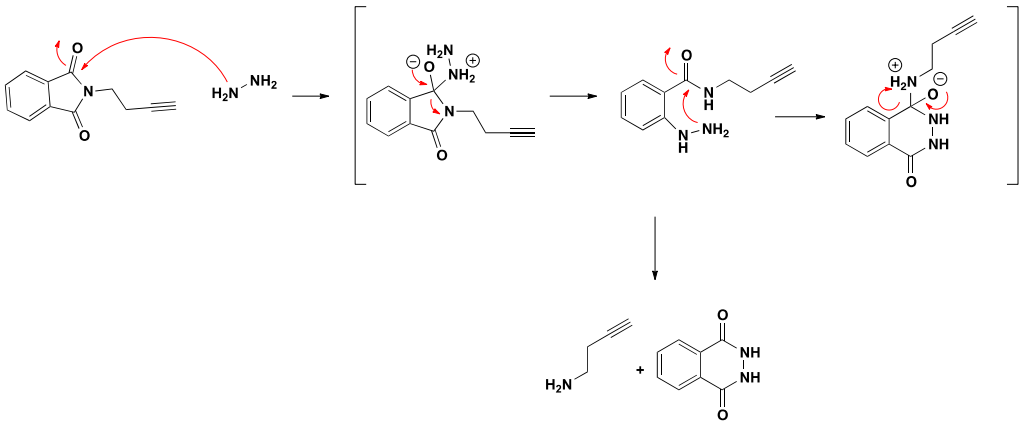

Figure 2.18. Phthalimide protecting group cleavage mechanism

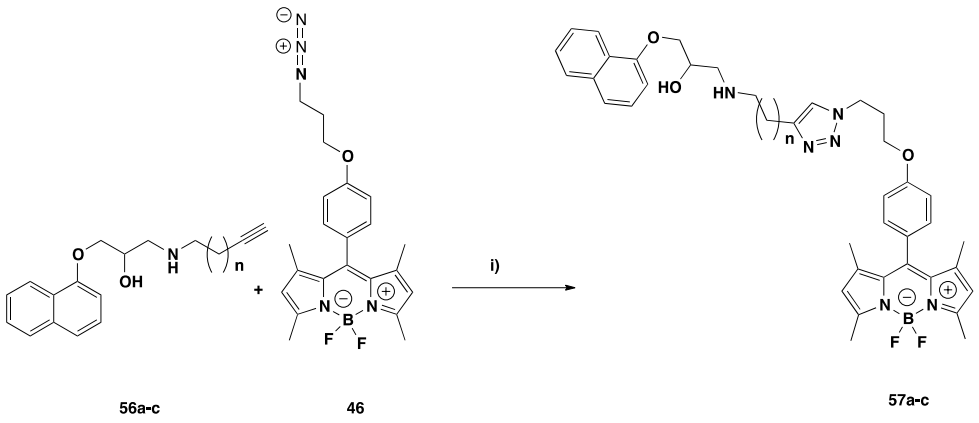

Scheme 2.14. i) DMF/H_2O, $CuSO_4.5H_2O$, sodium ascorbate, MW, 80 min, 80 °C, 40 W, (44-54%),

n=1 (a), n=2 (b), n=3 (c).

Three novel alkyne functionalised orthosteric ligands **56a-c** were synthesised and coupled to **46**.

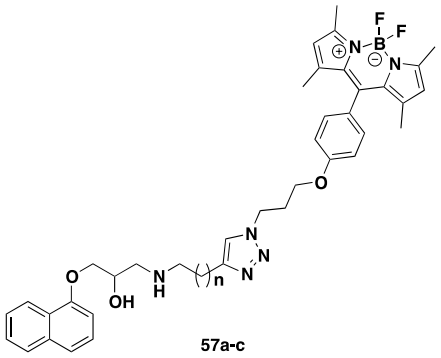

Figure 2.19. Structures of second-generation fluorescent adrenoceptor ligands (n=1 57a, n=2 57b, n=3 57c).

Extending the linker between the triazole and the fluorophore was attempted. Two new fluorophores were synthesised, one with a straight six-carbon chain and the other contained an ether linkage.

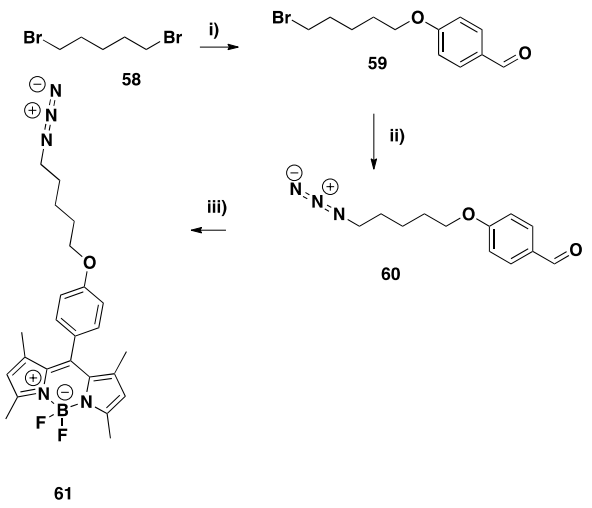

Scheme 2.15. i) K_2CO_3, DMF, 4-hydroxybenzaldehyde 12 hr (59%) ii) NaN_3, DMF, reflux, 16 hr (89%). iii) DCM, 2,4-Dimethylpyrrole, TFA, DDQ, Et_3N,$BF_3.OEt_2$, 16 hr, (16%).

The synthesis for longer linker attached to the fluorophore starting with a Williamson ether synthesis of 1,5-dibromopetane (**58**) and 4-hydoxybenzaldehye in the presence of potassium carbonate. Slow addition and controlled stochiometry reduced disubstitution. The benzaldehyde **59** was heated under reflux with sodium azide to form the terminal azide. This was confirmed by IR spectroscopy with the characteristic peak at 2100 cm^{-1}. The azide-substituted benzaldehyde **60** was coupled to 2,4-dimethylpyrrole with the addition of boron trifluoride diethyl etherate and triethylamine to yield fluorophore **61** in 16% yield. NMR and IR confirmed the fluorophore had been synthesised and held azide functionality.

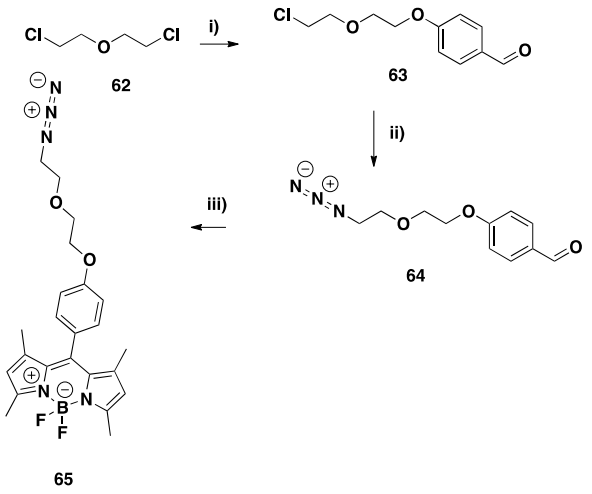

Scheme 2.16. i) K_2CO_3, DMF, 4-hydroxybenzaldehyde 12 hr (67%) ii) NaN_3, DMF, reflux, 16 hr (74%) iii) DCM, 2,4-Dimethylpyrrole, TFA, DDQ, Et_3N, $BF_3.OEt_2$, 16 hr, (39%).

The second fluorophore to be synthesised included an ether linkage. Synthesis began with 1-chloro-2-(2-chloroethoxy)ethane (**62**) and 4-hydroxybenzaldehyde in the presence of potassium carbonate to yield 4-(2-(2-chloroethoxy)ethoxy)benzaldehyde (**63**). Then benzaldehyde **63** was heated to 100 ºC with sodium azide to yield **64** which was confirmed with IR spectroscopy. The azide-functionalised benzaldehyde was finally reacted with 2,4-dimethylpyrrole, and boron trifluoride diethyl etherate in the presence of TFA, DDQ and triethylamine to yield the ether-linked fluorphore 65 in 39% yield after column chromatography eluted in DCM.

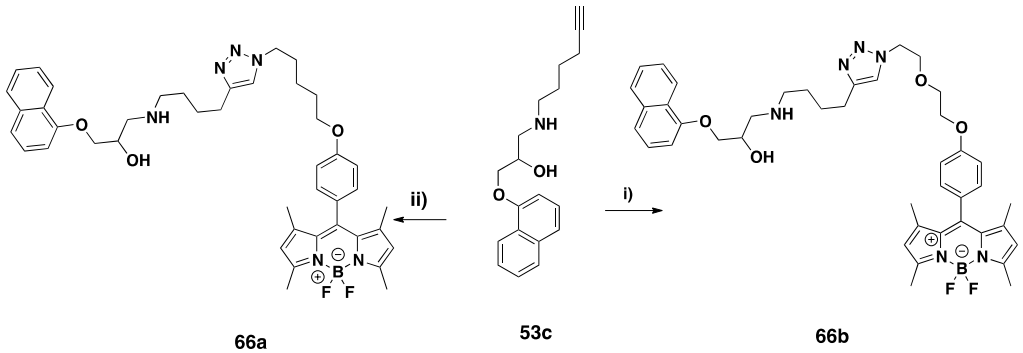

Scheme 2.17. i) **65**, DMF/H_2O, $CuSO_4.5H_2O$, sodium ascorbate, MW 80min, 80 °C, 40 W (48%). ii) **61**, DMF/H_2O, $CuSO_4.5H_2O$, sodium ascorbate, MW 80min, 80 °C, 40 W (14%).

The two new fluorophores **61** and **65** were conjugated to **53c** to form two new fluorescent ligands **66a-b** in yields ranging between 14% and 48% with microwave irritation after HPLC purification.

2.4.2 Pharmacology of second-generation ligands

The second-generation fluorescent ligands and pharmacophores were profiled with radioligand binding competition assays in the same format as the first-generation ligands.

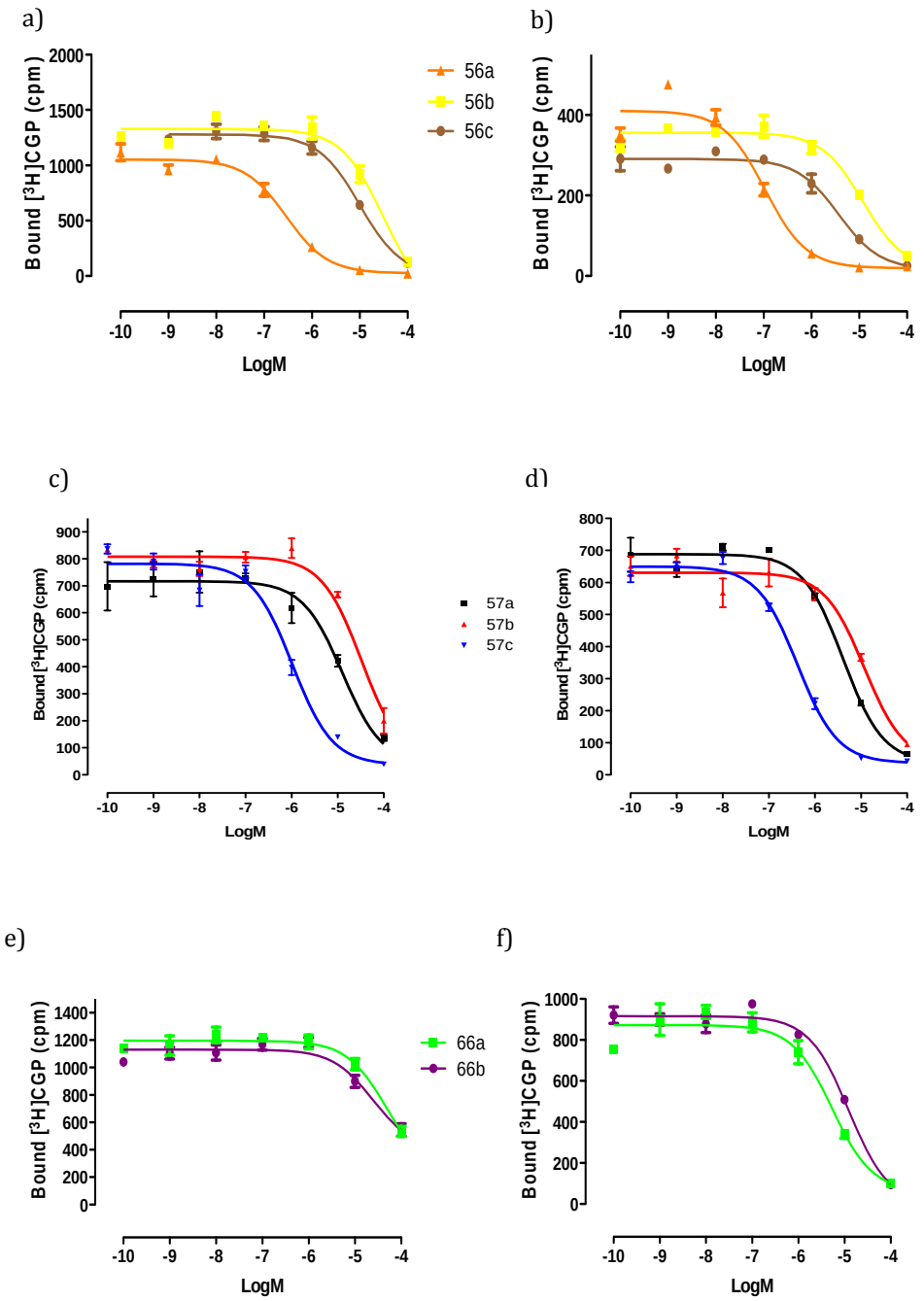

Figure 2.20. Fluorescent ligand displacement of [^{3}H]-CGP 12177 specific binding at the human β-AR in whole CHO cells. Inhibition of [^{3}H]-CGP 12177 specific binding to whole cells in a) β_1 by compounds 56a, 56b and 56c and b) β_2 by compouds 56a, 56b and 56c. Inhibition of [^{3}H]-CGP 12177 specific binding to whole cells in c) β_1 by compounds 57a, 57b and 57c and d) β_2 by compounds by 57a, 57b and 57c. Inhibition of [^{3}H]-CGP 12177 specific binding to whole cells in e) β_1 by compounds 66a and 66b and f) β_2 by compounds 66a and 66b in whole cells. Nonspecific binding was determined by 10 μM propranolol. A concentration of 1 nM of [^{3}H] CGP 12177 was used in each experiment. Data points are a mean ± s.e.m of triplicate determinations. These single experiments are representative of a minimum of three different experiments

Compound	β_1 Log K_i (n)	β_2 Log K_i (n)
56a	-6.60 ± 0.01 (4)	-7.60 ± 0.01 (4)
56b	-4.45 ± 0.20 (4)	-5.36 ± 0.06 (4)
56c	- 5.30 ± 0.05 (4)	-5.84 ± 0.20 (4)
57a	-5.77 ± 0.12 (4)	-6.27 ± 0.10 (4)
57b	-5.00 ± 0.06 (4)	-5.66 ± 0.16 (3)
57c	-6.77 ± 0.20 (8)	-7.32 ± 0.05 (8)
66a	-4.61 ± 0.09 (8)	-5.77 ± 0.10 (8)
66b	-4.65 ± 0.12 (4)	-5.36 ± 0.09 (4)

Table 2.4. Log K_i values were obtained from [^{3}H]-CGP12177 binding in whole cells expressing either the human β_1 or β_2-AR. Values are mean ± s.e.m from n number of experiments. K_i refers to the equilibrium dissociation constant and the values were calculated from the IC_{50} values.

The results of the second-generation ligands and alkyne-linked pharmacophores, showed that no pharmacophore had an affinity close to that of propranolol. This result may suggest that a terminal alkyne is not tolerated to the level of an isopropyl group of propranolol.

The binding affinities of the pharmacophores compared with their fluorescent counterparts do not show a signification change in binding affinity that would be expected. When tethering a large bulky fluorophore onto a known biologically active ligand, it would not be unreasonable to anticipate a decrease in the overall affinity. This result suggests that a triazole could be tolerated more than a terminal alkyne. This tolerance maybe due to more hydrogen bond donor/acceptors in a triazole compared with in the alkyne. The addition of a fluorophore does not seem to have affected the binding affinities relative to the terminal alkyne pharmacophores. This may be due to the fluorophore being positioned in an orientation that allows it to sit in the extracellular media and not interfere with binding.

The fluorescent ligands have improved binding affinities compared with the previous best ligands. **52a** had an affinity of -4.27 (± 0.10) at the β_1 receptor while **51a** had the best affinity at β_2 with an affinity of -4.86 (± 0.01). The binding affinities have been improved with **57c** having affinities of -6.77 (± 0.20) and -7.32 (±0.05) for β_1 and β_2 respectively. This

improvement shows that moving the triazole away from the biologically active portion of the ligand improves the binding affinity. This was clearly observed across for second-generation ligands compared with the first-generation ligands. This ligand has binding affinities that are comparable to those of the weaker ligands synthesised by Baker *et al*.[64]

Results from those compounds bearing an increased linker after the triazole did not show improved binding affinities. Affinities of the extended fluorophores dropped by 2 log units allowing the conclusion that this extention is not favoured.

2.4.3 Confocal imaging studies

Confocal imaging was used to study the fluorescent ligands. The use of confocal microscopy allowed the visualisation of ligands at the single cell level in order to determine whether they bind to the receptor, bind to the cell membrane, internalise or remain in the surrounding solution. A concentration of 100 nM was used initially for each ligand. All ligands were incubated with CHO cells expressing the human β_2 receptor and the experiments were conducted at 37 °C (experimental section) The second-generation ligands had improved affinities to low micromolar and nanomolar. These ligands had affinities low enough to warrant confocal experiments to be carried out. Confocal imaging was used to investigate ligand-receptor interactions. Imaging was carried out in 8-well plates with cells being seeded 24 hours before experiments. During each experiment for a separate antagonist, wells were washed with Hank's buffered saline solution (HBSS) before antagonist addition. Individual antagonists were added to separate wells and confocal images were captured with the aim to visualise specific receptor binding.

The results from the confocal microscopy experiments showed rapid intracellular accumulation which is the movement of a molecule into the cytoplasm of the cell. This is disappointing as the fluorescent antagonist should bind to receptors on the cell membrane and not enter the cytoplasm. Unfortunately it is not possible to distinguish between cytoplasmic ligand and receptor bound-ligand. Experiments reducing the concentration of antagonist were performed, but this did not stop the intracellular accumulation.

As the antagonists contain a hydrocarbon linker and a bulky organic fluorophore, it was believed that the increased lipophilicity of the molecule caused the intracellular accumulation

by allowing the drug to pass through the cell membrane's lipid bilayer into the cytoplasm.

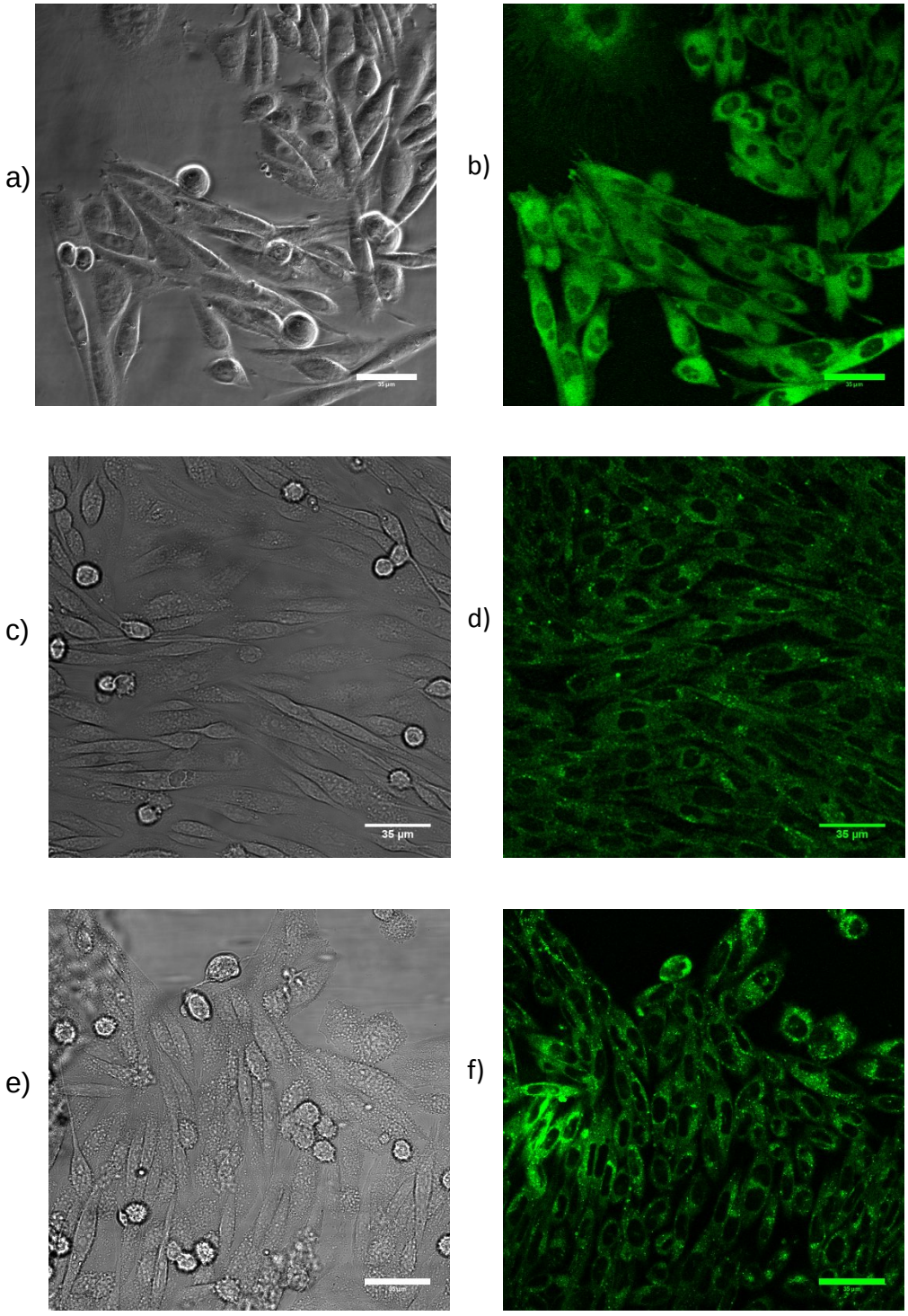

Figure 2.21. Confocal visualisation of fluorescent antagonists (100 nM) binding to CHO β_2 cells. a) Transmitted light image taken at 0 min before the addition of 57a and b) appearance of 57a 10 min after addition. c) Transmitted light image taken at 0 min before the addition of 57b and d) appearance of 57b 10 min after addition. e) Transmitted light image taken at 0 min before the addition of 57c and f) appearance of 57c 10 min after addition. Images of cells were undertaken in the continued presence of fluorescent the ligand.

2.4.4 Lipophilicity evaluation of fluorescent ligands

The second-generation fluorescent ligands clearly accumulated inside the cells when viewed under a confocal microscope. This could be due to the increased lipophilicity of the ligands caused by the addition of the fluorescent moiety.

The lipophilic nature of the ligands was assessed using HPLC techniques. One method that is becoming routinely used in drug discovery programmes, is the chromatographic hydrophobicity index (CHI).[144] This HPLC method allows the characterisation of the interactions of drugs with an immobilised artificial membrane (IAM). With a set of standards, the gradient retention times at pH 7.4 can be converted to CHI values referring to IAM chromatography ($CHI_{IAM\ 7.4}$) that approximates an acetonitrile concentration with which an equal distribution of compound can be achieved between the mobile phase and IAM. The longer the retention time the greater the interaction with the artificial membrane.

Compound	Retention time	$CHI_{IAM\ 7.4}$
Propranolol	N/A	55.50
56a	6.39	49.30
56b	6.48	50.41
56c	6.50	50.65
57a	7.71	66.17
57b	7.71	66.17
57c	5.14*	68.26
66a	4.52*	55.44
66b	N/A	N/A

Table 2.5. Retention times and $CHI_{IAM\ 7.4}$ values of second-generation ligands calculated from HPLC methods using a Regis IAM PC 12 µm column (100 x 4.6mm), a flow rate of 1.00 mL/min and UV detection at 230 and 366 nm. Linear gradient 0 % - 100% solvent A over 7 min. Solvent A: 100% MeCN. Solvent B: water with 50 mM ammonium acetate. * Faster gradient used.

The $CHI_{IAM\ 7.4}$ values of all the second-generation ligands gave insight into the interaction of the molecule with an artificial immobilised column. Propranolol data were acquired through

partnership with Novartis, which allowed comparison of propranolol to the second-generation ligands. The $CHI_{IAM\ 7.4}$ data suggest that there is not a considerable difference between the fluorescent ligand congeners and propranolol, but when a fluorophore is attached the $CHI_{IAM\ 7.4}$ value changes dramatically. Clearly this will have an effect on how the molecule interacts with the receptor and the media. Modifications must be made to the ligands to try and mimic the properties of propranolol itself. Unfortunately it was not possible to obtain data for **66b** due to low quantity of ligand available.

Another HPLC method used to determine the lipophilic properties of the ligands was HPLC LogD analysis. This technique is described by Kerns *et al.*[145] as a quick HPLC method for estimating the logarithm of the octanol-water partition coefficient at pH 7.4. A calibration graph is plotted with retention time vs Log$D_{7.4}$ (literature). In the publication this calibration graph was used to determine Log$D_{7.4}$ (HPLC) for 60 structurally diverse drugs and the correlation with Log$D_{7.4}$ (literature) was determined as $r^2 = 0.89$.

Compound	Retention time	Log$D_{7.4}$
Propranolol	N/A	1.09
56a	2.68	1.97
56b	2.49	1.17
56c	2.67	1.91
57a	3.18	3.96
57b	3.18	3.96
57c	3.11	3.70
66a	3.75	6.28
66b	3.45	5.07

Table 2.6. Second-generation ligand Log$D_{7.4}$ and retention times calculated by HPLC methods using a Polaris C_{18} 5 µm HPLC column (50 x 4.6mm). A flow rate of 1.00 mL/min and UV detection at 230 and 366 nm. Linear gradient 0 % - 95% solvent A over 4 min. Solvent A: 100% MeCN. Solvent B: water with 50 mM ammonium acetate.

The log$D_{7.4}$ values confirm what was observed with the CHI_{IAM} data. An increase of Log$D_{7.4}$ values are observed in the pharmacophores with an acetylene moiety compared to that of

propranolol. A large change was observed with the introduction of the fluorescent moiety and there was a noticeable increase when a longer linker was inserted after the triazole. Due to an increase in membrane interaction and LogD $_{7.4}$ values, modifications to the fluorescent ligands were important and reducing both values to a similar value of propranolol could be beneficial.

A new series of fluorescent antagonists required synthesis with a polar linker in order to investigate whether this would eliminate or reduce the intracellular accumulation of the antagonist and the lipophilic nature of the ligand.

2.5. Amide linked ligands

To stop or reduce the intracellular accumulation of the fluorescent ligands, the insertion of an amide group into the linker may reduce the lipophilicity of the compound by increasing the amount of hydrogen bond donors and acceptors into the molecule. The linker would contain four atoms, the same as the most potent fluorescent ligand to allow comparison of affinity and membrane binding over the previous best ligand. It was acknowledged that such a small change in linker type may not reduce the lipophilicity of the molecule, but extensive change to the molecule may reduce the binding affinity to levels of the first generation ligands. Another approach to this would be to exchange to fluorophore for a smaller more polar fluorophore. This approach was not chosen due to the excellent properties that a BODIPY fluorophore has over the other possible fluorophores that could be used such as NBD, such as limited fluorescence in the aqueous media and high quantum yield when bound to the receptor.

2.5.1 Amide linker synthesis

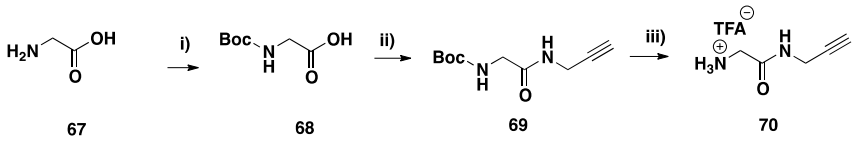

67 68 69 70

Scheme 2.18. i) $BocO_2$, 0 °C, H_2O/dioxane, 12 hr. ii) DCM, HBTU, DIPEA, propargylamine, 5 hr. iii) TFA/DCM, 30 min, (44%).

The synthesis began with boc-protecting glycine (**67**) in water/dioxane. The protected amine **68** was coupled to propargylamine (**31**) with *O*-(benzotriazol-1-yl)-*N,N,N′,N′*-tetramethyluronium hexafluorophosphate (HBTU) as a coupling agent in the presence of

DIPEA. The product was then deprotected in the presence of TFA/DCM to yield the TFA salt **70** in 44% yield overall.

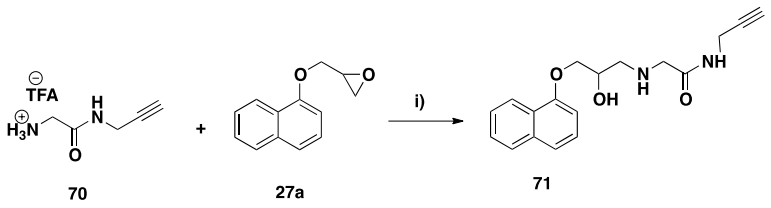

Scheme 2.19. i) Isopropanol, DIPEA, reflux, 16hr (51%).

The amide linker was reacted with the epoxide **27a** to form the amide-linker pharmacophore **71**. This was achieved by reflux in isopropanol in the presence of (DIPEA) in 51% yield after column chromatography.

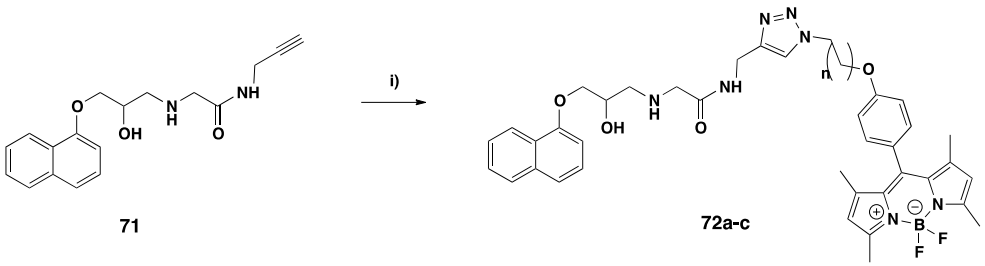

Scheme 2.20. i) 46 or 61 or 65, DMF/H_2O, $CuSO_4.5H_2O$, sodium ascorbate, MW 80 min, 80 °C, 40 W. n= $(CH_2)_2$, a, n= $(CH_2)_4$ b, n= $(CH_2)_2O(CH_2)_2$ c. (24-90%).

The alkyne-functionalised orthosteric ligand **71** was conjugated to the three previously used fluorophores **46**, **61** and **65** with conditions used for other click reactions.

2.5.2 Amide linker pharmacology

The fluorescent ligands and the pharmacophore binding affinities were investigated using radio-ligand binding assay to determine the pharmacological properties of the ligands. As **72b** had solubility issues in media, data was obtained over a concentration range of 1×10^{-11} M to 1×10^{-5} M.

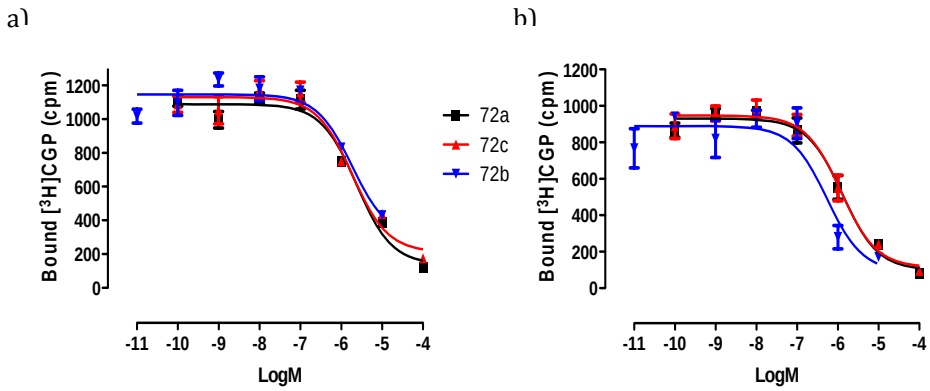

Figure 2.20. Fluorescent ligand displacement of [^{3}H]-CGP 12177 specific binding at the human β-AR in whole CHO cells. Inhibition of [^{3}H]-CGP 12177 specific binding to whole cells in a) β_1 by compounds 72a, 72b and 72c and b) β_2 by compounds 72a, 72b and 72c. Nonspecific binding was determined by 10 μM propranolol. A concentration of 1 nM of [^{3}H] CGP 12177 was used in each experiment. Data points are a mean ± s.e.m of triplicate determinations. These single experiments are a representative a minimum of three different experiments

Compound	β_1 Log K_i (n)	β_2 Log K_i (n)
72a	-5.92 ± 0.07 (4)	-6.36 ± 0.09 (4)
72b	-6.39 ± 0.09 (4)	-6.58 ± 0.14 (4)
72c	-5.95 ± 0.07 (4)	-6.11 ± 0.10 (4)

Table 2.7. Log K_i values were obtained from [^{3}H]-CGP12177 binding in whole cells expressing either the human β_1 or β_2-AR. Values are mean ± s.e.m from n number of experiments. K_i refers to the equilibrium dissociation constant and the values were calculated from the IC_{50} values.

The radioligand binding experiments for the amide-linked fluorescent ligands show low micromolar affinity to receptors. These affinities are comparable to those of previous ligands. Direct comparison between **57c** and **72a** shows that the amide-linker is not tolerated as well as the straight-carbon chained linker. The amide linked ligands lipophilic nature was examined with $LogD_{7.4}$ and $CHI_{IAM\ 7.4}$ analysis to determine if the polar group did make and effect. If there was an effect the ligands would be forwarded for confocal imaging to investigate whether the polar linker would reduce intracellular uptake.

2.5.3 Lipophilic study of amide linker fluorescent ligands

The amide linker pharmacophore and amide-linked fluorophores were analysed with regard to their membrane interaction and lipophilic properties using the previous HPLC methods.

Compound	$CHI_{IAM\ 7.4}$	Log*D* $_{7.4}$
Propranolol	55.50	1.09
71	38.08	1.89
72a	53.19	4.09
72b	54.83	4.50
72c	52.25	3.94

Table 2.8. Retention times and $CHI_{IAM\ 7.4}$ values of second generation ligands calculated from HPLC methods using a Regis IAM PC 12 µm column (100 x 4.6mm), a flow rate of 1.00 mL/min and UV detection at 230 and 366 nm. Linear gradient 0 % - 100% solvent A over 7 min. Solvent A: 100% MeCN. Solvent B: water with 50 mM ammonium acetate. Log*D* $_{7.4}$ values calculated by HPLC methods using a Polaris C_{18} 5 µm HPLC column (50 x 4.6mm). A flow rate of 1.00 mL/min and UV detection at 230 and 366 nm. Linear gradient 0 % - 95% solvent A over 4 min. Solvent A: 100% MeCN. Solvent B: water with 50 mM ammonium acetate

$CHI_{IAM\ 7.4}$ values of the amide linker pharmacophore show a reduced membrane interaction compared with propranolol. This is possibly due to the nature of the linker as there are additional polar groups attached. The amide must be reducing the interaction between the membrane and the pharmacophore. The Log*D* $_{7.4}$ is slightly elevated compared with that of propranolol. This possibly is the effect of the terminal alkyne. It could be assumed that the polar amide in the linker would reduce the Log*D* $_{7.4}$ value. Increased values of both Log*D* $_{7.4}$ and $CHI_{IAM\ 7.4}$ are observed with the attachment of the fluorophore which is comparable to previously synthesised ligands. $CHI_{IAM\ 7.4}$ values are reduced compared with the previous fluorescent ligands **57a-c** and **66a**, with the largest reduction being 68.26 to 52.25. This is a very significant drop in Log*D* $_{7.4}$ values. The ether linkage in **72c** clearly had an additional effect on the amide linker. Interestingly the short-chained fluorophore with amide linker **72a** did not have a reduction of Log*D* $_{7.4}$.

2.5.4 Amide linker confocal imaging

With the slight loss of binding affinity, but improved Log$D_{7.4}$ and $CHI_{IAM\ 7.4}$ values, the fluorescent ligands **72a-c** were imaged by the confocal microscopy. Unfortunately the addition of the polar linker did not change the properties enough to stop intracellular accumulation. The insertion of a polar linker clearly did not reduce intracellular accumulation that was expected from the HPLC data. The large organic fluorophore clearly still has a major effect on the molecule even though there is a reduction in $CHI_{IAM\ 7.4}$ and Log$D_{7.4}$ value. With the understanding of the fluorophore having such a major effect on the ligand, a different fluorescent tag would to be attached to the pharmacophore. From research within the group, it is known that longer wavelength fluorophores are less prone to intracellular accumulation but have the drawback that they are difficult to synthesise and give low yields. Investigation into clicking red-shifted fluorophores to the pharmacophores would allow this previous work to be confirmed.

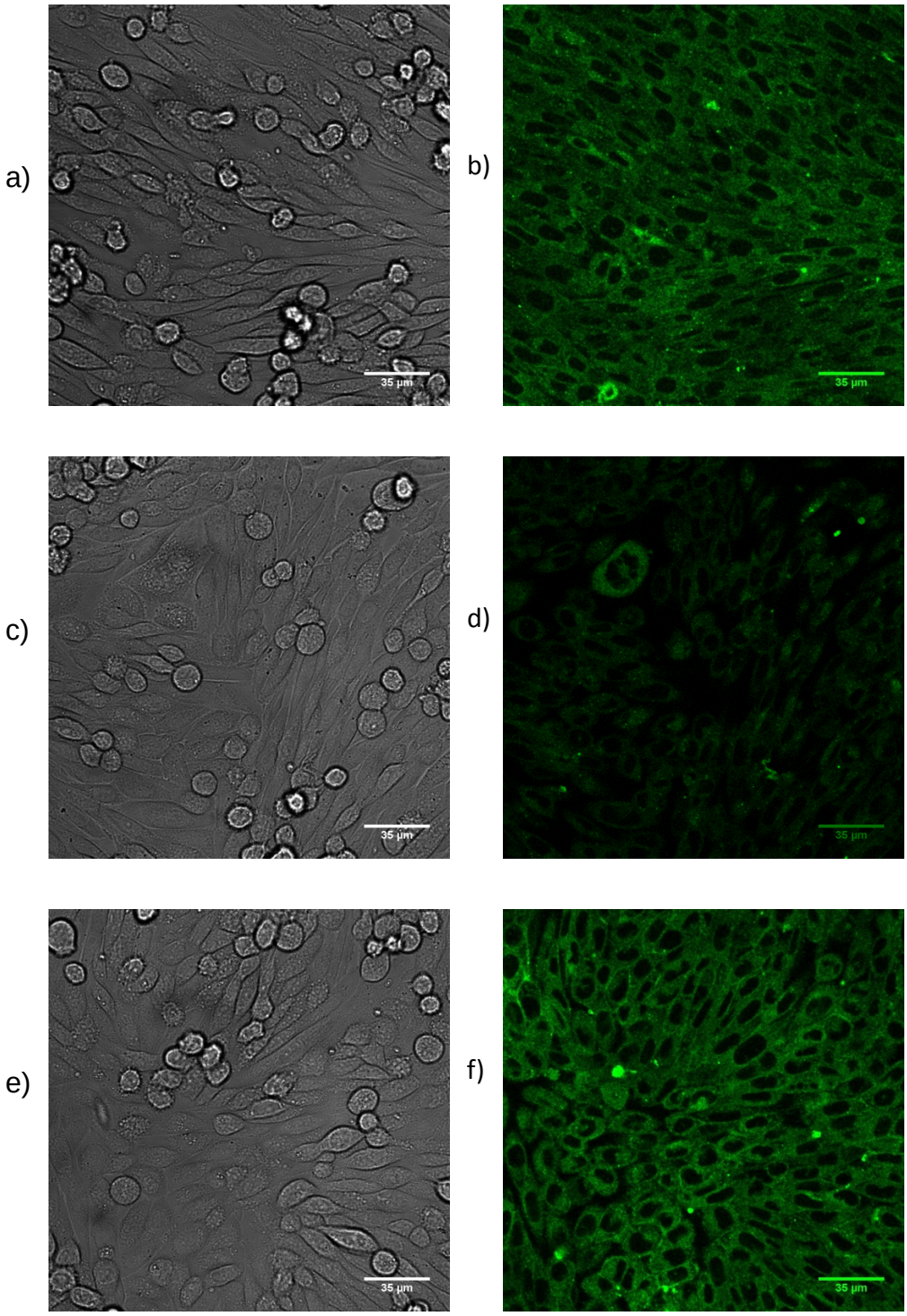

Figure 2.23. Visualisation of fluorescent antagonists (100 nM) on CHO β_2 cells. a) Transmitted light image taken at 0 min before the addition of 72a and b) appearance of 72a 10 min after addition. c) Transmitted light image taken at 0 min before the addition of 72b and d) appearance of 72b 10 min after addition, e) Transmitted light image taken at 0 min before the addition of 72c, f) image taken 10 min after the addition of 72c.

2.6 Longer wavelength fluorophores

Previous fluorophores that were synthesised have been of short excitation wavelength and there are some disadvantages of using shorter wavelength fluorophores, such as lower molecular brightness and a high incidence of background fluorescence,[146] and less intracellular accumulation when confocaly imaged. Changing to a longer wavelength dye, i.e. a red-shifted dye, these disadvantages are overcome and cell and tissue auto-fluorescence are observed less. Another advantage of using a red-shifted dye is the reduction in background fluorescence that ultimately achieves improved sensitivity. Previous work within the group has also shown that red-shifted BODIPY fluorophores tethered to beta adrenoceptor ligands do not internalise like the short wavelength fluorophores.[64] Utilising a longer wavelength fluorophore may improve the ligands behavior in the view of less internalisation and better confocal microscope imaging.

Longer wavelengths BODIPY fluorophores usually contain an increased amount of conjugation within the structure. This increased amount of conjugation could give an increased amount of lipophilicity which contradicts the process that was tried with the amide linker, but as previously mentioned, previous work within the group shows that longer wavelength fluorophores achieve better results when imaged under the confocal microscope.

2.6.1 Longer wavelength fluorescence ligand synthesis

Long wavelength fluorophores are on occasions difficult to synthesis due to long synthetic procedures and low-yielding reactions but a commercially available red-shifted azide functionalised dye was available from Cambridge research biochemicals **73**. As it was azide functionalised, it could be clicked to a chosen pharmacophore with no need for any synthetic modification. It has been noted that the commercially available fluorophore has a long linker between the azide and the fluorophore that has previously been shown to reduce binding affinity in the previously ligands synthesised.

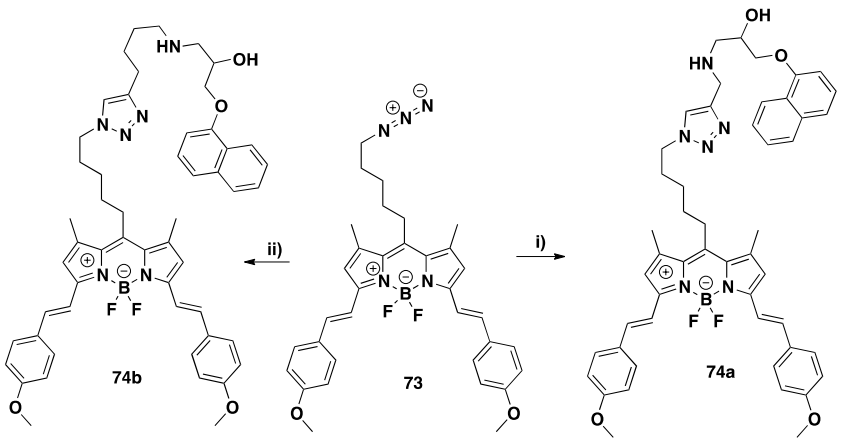

Scheme 2.21. i) 1-(naphthalen-8-yloxy)-3-(prop-2-ynylamino)propan-2-ol, DMF/H_2O, $CuSO_4.5H_2O$, sodium ascorbate, MW 80 min, 80 °C, 40 W,(14%). ii) 1-(hex-5-ynylamino)-3-(naphthalen-1-yloxy)propan-2-ol, DMF/H_2O, $CuSO_4.5H_2O$, sodium ascorbate, MW 80 min, 80 °C, 40 W, (22%).

This reaction used previously described conditions in this chapter. Fluorophore **73** was clicked to pharmacophore **30a** and pharmacophore **53c**.

2.6.2 Red-shifted fluorescent ligand pharmacology

The two long wavelength fluorescent ligands were examined under radio-ligand competition assays.

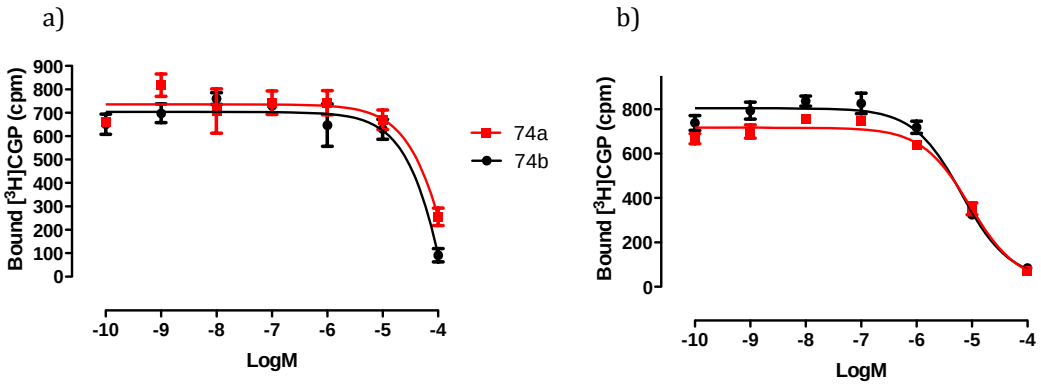

Figure 2.24. Fluorescent ligand displacement of [^{3}H]-CGP 12177 specific binding at the human β-AR in whole CHO cells. Inhibition of [^{3}H]-CGP 12177 specific binding to whole cells in a) β_1 by compounds 74a, 74b and b) β_2 by compouds 74a, 74b. Nonspecific binding was determined by 10 µM propranolol. A concentration of 1 nM of [^{3}H] CGP 12177 was used in each experiment. Data points are a mean ± s.e.m of triplicate determinations. These single experiments are a representative a minimum of three different experiments

Compound	β_1 Log K_i (n)	β_2 Log K_i (n)
74a	-5.02 ± 0.08 (4)	-5.89 ± 0.15 (4)
74b	-4.27 ± 0.10 (4)	-5.48 ± 0.12 (3)

Table 2.9. Log K_i values were obtained from [^{3}H]-CGP12177 binding in whole cells expressing either the human β_1 or β_2-AR. Values are mean ± s.e.m from n number of experiments. K_i refers to the equilibrium dissociation constant and the values were calculated from the IC_{50} values.

74a was based on the initial one carbon linked pharmacophore, in comparison there is an improvement in binding affinity. Compound **74b** was based on the pharmacophore which when tethered to a fluorescent moiety had the greatest binding affinity **57c**. Unfortunately there was no improvement in binding affinity, which could be due to the extended linker between the triazole and fluorophore. Extension of this linker has not been beneficial when linker extension was trialed with previous ligands **66a** and **66b**. The red shifted fluorophore is also bulkier, with side groups adjacent to the pyrrole rings.

Both ligands were taken forward for analysis with the HPLC methods to establish the Log*D* $_{7.4}$ and $CHI_{IAM\ 7.4}$ values to determine if the introduction of a red-shifted fluorophore has a reduction in membrane interaction and lower lipophilicity resulting in the overall desired effect of reduced intracellular accumulation.

2.6.3 Lipophilic study of longer wavelength fluorescent ligands

The red shifted fluorescent ligands were analysed with regard to their membrane interaction and lipophilic properties using the previous HPLC methods.

Compound	$CHI_{IAM\ 7.4}$	Log*D* $_{7.4}$
Propranolol	55.50	1.09
74a	69.17	5.79
74b	67.04	5.08

Table 2.10 . $CHI_{IAM\ 7.4}$ values of longer wavelength ligands calculated from HPLC methods using a Regis IAM PC 12 µm column (100 x 4.6mm), a flow rate of 1.00 mL/min and UV detection at 230 and 366 nm. Linear gradient 0 % - 100% solvent A over 7 min. Solvent A: 100% MeCN. Solvent B: water with 50 mM ammonium acetate. LogD $_{7.4}$ values calculated by HPLC methods using a Polaris C_{18} 5 µm HPLC column (50 x 4.6mm). A flow rate of 1.00 mL/min and UV detection at 230 and 366 nm. Linear gradient 0 % - 95% solvent A over 4 min. Solvent A: 100% MeCN. Solvent B: water with 50 mM ammonium acetate.

The longer wavelength fluorescent ligands showed unfavorable properties when analytical Log$D_{7.4}$ and $CHI_{IAM\ 7.4}$ values were determined. In comparison to Propranolol there is a noticeable change in both values. The Log$D_{7.4}$ of both red shifted fluorophores show that the ligands are highly lipophilic, the values are similar to the previous ligand **57c** which showed unwanted characteristics when imaged. The $CHI_{IAM\ 7.4}$ data shows high levels of membrane interaction and again is similar to **57c**, which had a value of 68.26, compared to **74a** that had a value of 69.18 and **74b** of 67.04. The ligands were taken forward for confocal imaging, even in the light of poor $CHI_{IAM\ 7.4}$ and Log$D_{7.4}$, as the previous work within the group showing red-shifted ligands did not accumulate in the cytoplasm.

2.6.4 Long wavelength fluorescent ligand confocal imaging

Both ligands were imaged by confocal microscopy to see if the longer wavelength fluorophore would make a difference to intracellular accumulation but unfortunately intracellular accumulation was still present. The antagonists were used at a range of concentrations but this did not reduce the amount of intracellular accumulation. It was noted that this commercially available dye **73** did not react as successfully as the previous dyes **46**, **61** and **65**, the yields being much lower than those of the green shifted dye. Binding affinities were not improved and from the confocal imaging results showing intracellular accumulation, the fluorophore was discarded and the synthesis of a red-shifted dye was initiated.

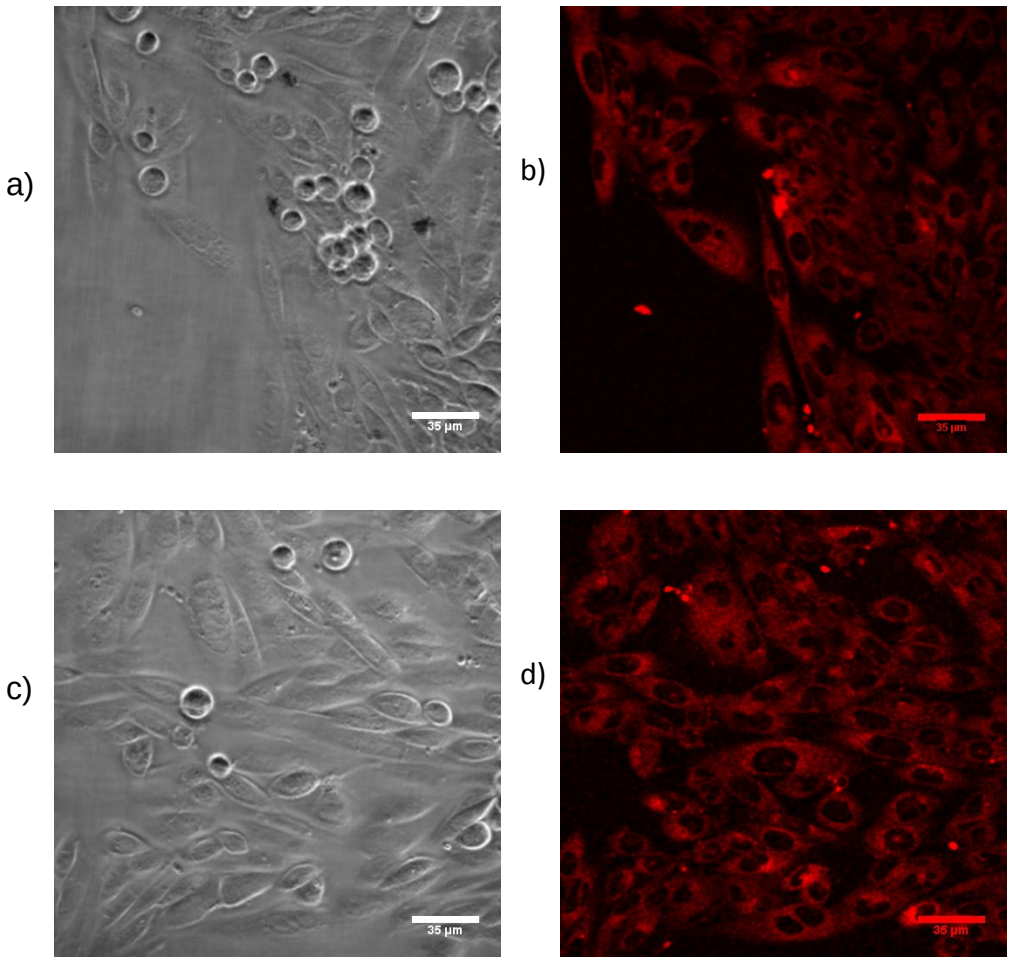

Figure 2.25. Visualisation of fluorescent antagonists (100 nM) on CHO β_2 cells. a) Transmitted light image taken at 0 min before the addition of 74a and b) appearance of 74a 10 min after addition. c) Transmitted light image taken at 0 min before the addition of 74b and d) appearance of 74b 10 min after addition.

2.7 Synthesis of longer wavelength fluorophore

As the commercially available red fluorophore when coupled to the orthosteric ligand had poor binding affinity and the confocal imaging showed intracellular accumulation, synthesis of a longer wavelength fluorophore was necessary. Previous work within the group has suggested that fluorophores similar in structure to BODIPY 630/650 internalise to a lesser extent than other available fluorophores. This fluorophore needed azide functionality to allow an alkyne-azide copper (I) catalysed cycloaddition with the alkyne-functionalised pharmacophore. This fluorophore would possibly be less lipophilic in comparison to the previous fluorophore **73**,

with the benefit of the amide bond within the linker. With only one phenyl extension would also help to reduce the lipophilicity of the ligand and may stop the internalisation. Previous work by Baker *et al*.[64] had success with an extremely similar fluorophore with an amide bond for tethering the fluorophore attached to an adrenergic ligand with brilliant confocal imaging and displacement of the fluorescent ligang was possible when the cells were pre-incubated with a known antagonist.

2.7.1 Retrosynthesis of a long wavelength fluorophore

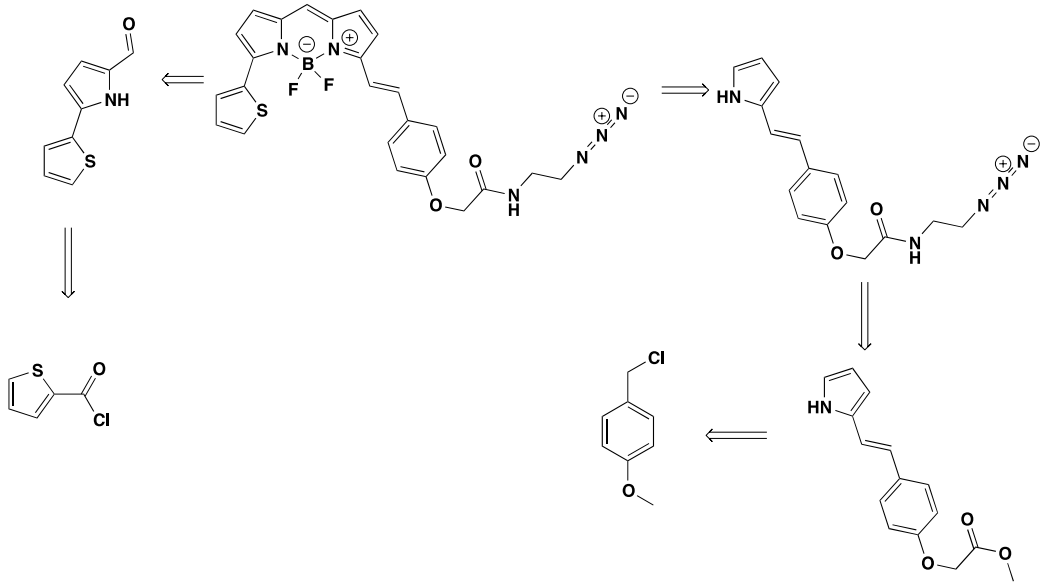

Scheme 2.22. Retrosynthesis of BODIPY azide

2.7.1.1 Synthesis of red shifted ligands

Synthesis of the BODIPY azide would be separated into forming two pyrrole rings substituted differently then combining the two in the final step.

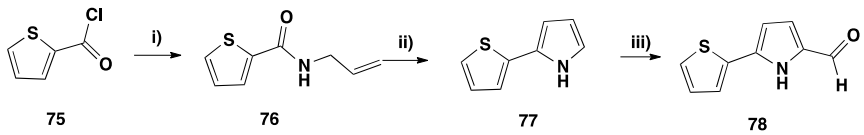

Scheme 2.23. i) allylamine, pyridine, DCM, 4 hr (85%) ii) a- phosgene, DMF, 16 hr; b- KO^{t}Bu, 0 °C, 10min, (34%) iii) $POCl_3$, DMF, DCE, 2 hr (45%).

The synthesis began with the acylation of allyamine with 2-thiophenecarbonyl chloride (**75**) to afford the amide **76** in 85% yield.[147] Synthesis of **77** was achieved in a one-pot, two-step reaction. Starting with the amide **76** and a solution of phosgene in toluene to afford the iminoyl chloride. This was treated with potassium *tert*-butoxide without further purification. The resulting nitrogen ylide formed by the elimination of HCl undergoes a 1,5-dipolar ring closure and subsequent isomerisation to yield **77**. Formylation of pyrrole **77** was achieved using a Vilsmeier reagent formed from DMF and $POCl_3$ in 1,2-dichloroethane. The mechanism for the Vilsmeier formylation is shown in figure 2.26.

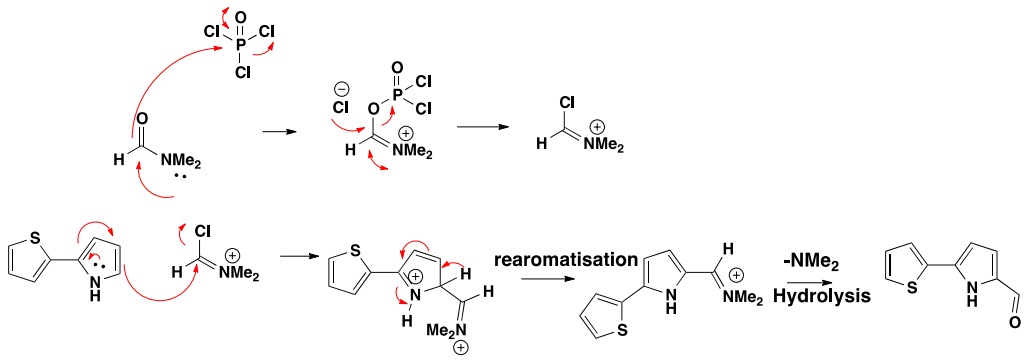

Figure 2.26. Mechanism for the Vilsmeier formylation of **77**.

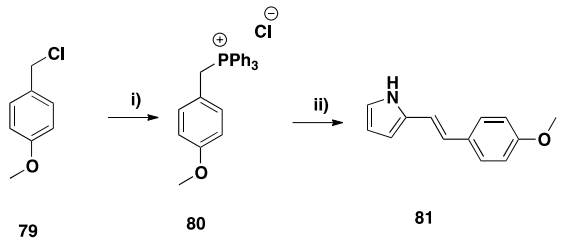

Scheme 2.24. i) PPh_3, benzene, reflux, 22 hr (85%) ii) 2-Pyrrole-carboxaldehyde NaH, toluene, reflux 16 hr, (5%).

The second pyrrole to be coupled for the formation of the longer wavelength fluorophore requires a phenolic ring bonded to the pyrrole through a carbon-carbon double bond. This was achieved through a Wittig reaction. This required the synthesis of the ylid. 4-Methoxybenzyl chloride (**79**) was reacted with triphenylphosphine to afford the phosphoium salt (**80**) in 85% yield. The ylid was reacted with pyrrole-2-carboxaldehye to produce the desired product **81**. ^{1}H NMR confirmed that the product was of the *E*-isomer (*J* 16Hz). This reaction proceeded with a very low yield (5%) possibly due to the acidity of the amine of the pyrrole. Once deprotonated,

the pyrrole nitrogen would be an extremely good nucleophile and could lead to possible side reactions.

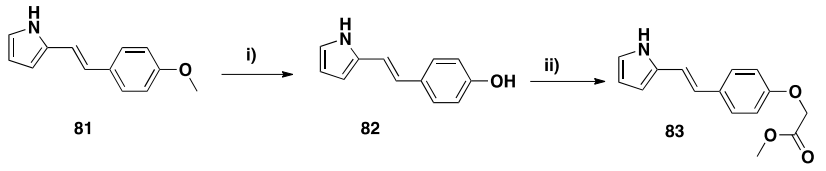

Scheme 2.25. i) Sodium ethanthiolate, reflux, 5 days ii) NaH, methyl bromoacetate, THF, 5 hr (48%).

The next stage of synthesis required the demethylation of the methyl ether **81** and the addition of an acetate group. The initial synthesis, was a one-pot two-step synthesis with sodium ethanthiolate, reflux in DMF, then addition of methylbromoacetate. It was found that this reaction did not have a high yield. It was therefore decided to try a two-step, two-pot reaction forming the phenol first, then deprotonation with sodium hydride in THF and the addition of methyl bromoacetate. This resulted **83** in higher yield (48%).

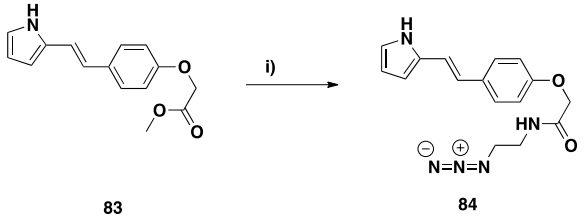

Scheme 2.26. i) 2-azidoethanamine, MeOH, reflux, 3 days (95%).

The last step for the synthesis was the conjugation of 83 with the previously used linker **29**, the reaction was heated at reflux for 3 days to yield the azido-amine motif **84**.

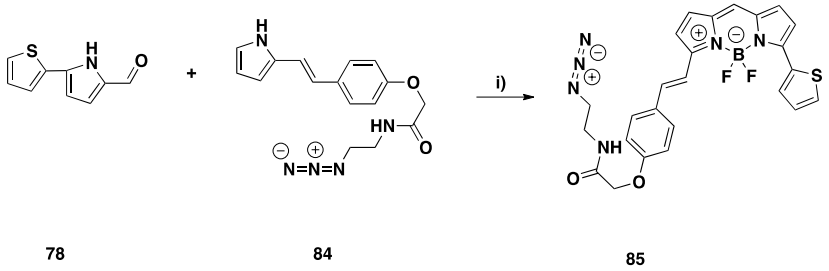

Scheme 2.27. i) a) $POCl_3$, DCM:MeOH (1:1), 18 h b). Et_3N, $BF_3.OEt_2$, DCM, 12 h, (34%).

The final reaction was the coupling and subsequent mediated cyclicisation of pyrrole **78** and pyrrole **84** to generate the azide functionalised BODIPY dye **85**. There are several one-pot

reactions that have been reported.[148,149] The reaction is a one-pot, two-step reaction which afforded the desired red-shifted dye in reasonable yield. The first step involved the coupling of the two components **78** and **84** in the presence of $POCl_3$ followed by the introduction of the BF_2 group through boron trifluoride diethyl etherate in the presence of triethylamine to yield **85** in 34% yield.

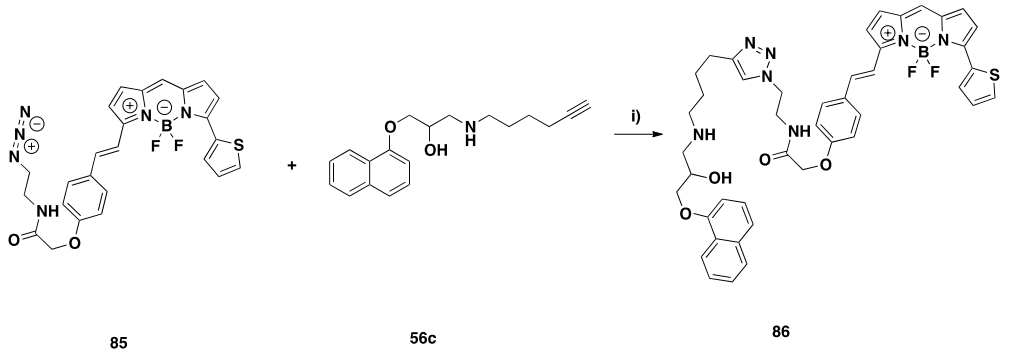

85 56c 86

Scheme 2.28. i) DMF/H_2O, $CuSO_4.5H_2O$, sodium ascorbate, MW 80 min, 80 °C, 40 W.

The long wavelength fluorophore **85** was then conjugated to the previous best pharmacophore **56c** through the click reaction conditions used throughout. This yielded the desired product **86**. Regrettably, the desired product had surprisingly poor solubility in all solvents including DMSO, DMF, methanol and water. Due to the insolubility of the ligand, binding affinities could not be calculated.

As **86** was unusable, the amide-linked pharmacophore **71** was clicked to the in-house red shifted dye **85**. Previous cycloaddition conditions were used to yield the fluorescent antagonist **87**.

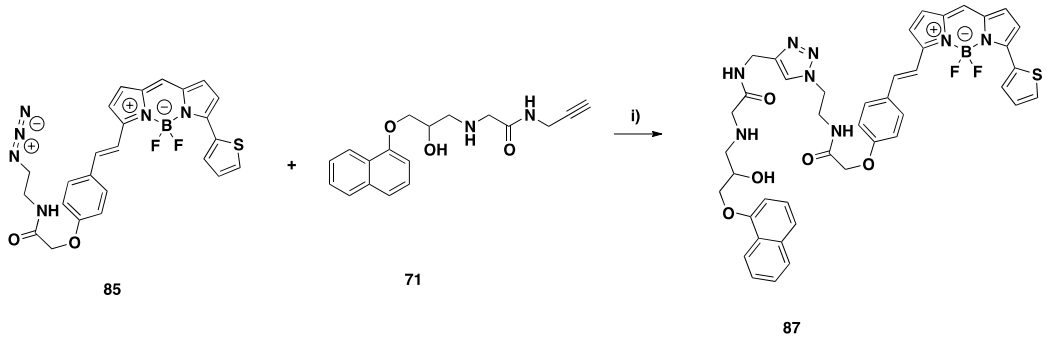

85 71 87

Scheme 2.29. i) DMF/H_2O, $CuSO_4.5H_2O$, sodium ascorbate, MW 80 min, 80 °C, 40 W,(45%).

2.7.1.2 Pharmacology of long wavelength fluorescent ligand

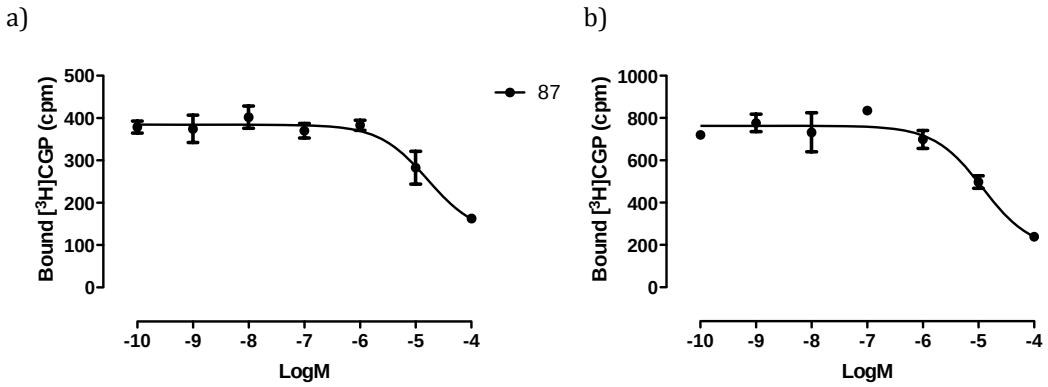

Figure 2.27. Fluorescent ligand displacement of [^{3}H]-CGP 12177 specific binding at the human β-AR in whole CHO cells. Inhibition of [^{3}H]-CGP 12177 specific binding to whole cells in a) β_1 by compounds 87 b) β_2 by compound 87. Nonspecific binding was determined by 10 µM propranolol. A concentration of 1 nM of [^{3}H] CGP 12177 was used in each experiment. Data points are a mean ± s.e.m of triplicate determinations. These single experiments are a representative a minimum of four different experiments

Compound	β_1 Log K_i (n)	β_2 Log K_i (n)
87	-5.16 ± 0.06 (4)	-5.96 ± 0.20 (4)

Table 2.9. Log K_i values were obtained from [^{3}H]-CGP12177 binding in whole cells expressing either the human β_1 or β_2-AR. Values are mean ± s.e.m from n number of experiments. K_i refers to the equilibrium dissociation constant and the values were calculated from the IC_{50} values.

Ligand **87** had improved binding affinities when compared with ligands **74a** and **74b**, the two previous red-shifted dyes. The binding affinities were lower than **57c**, but had very comparable affinities to other amide linker ligands **72a-c**. There is a slight loss of activity at the β_1 receptor. This result shows interesting SARs. The fluorophore is orientated differently to the shorter wavelength fluorophore as the linker is conjugated to the pyrrole ring and not in the *meso* position of the core. This could possibly result in a slightly different orientation to that of the ligands **74a-b** and the shorter wavelength ligands. The ligand was imaged by confocal imaging to gauge if this conjugate would not internalise like previously synthesised ligands.

2.7.2.1 Confocal imaging of red-shifted ligands

The main area of interest with this ligand was the confocal imaging and with the previous knowledge of reduced intracellular accumulation diminished with a fluorophore of this type imaging was highly important.

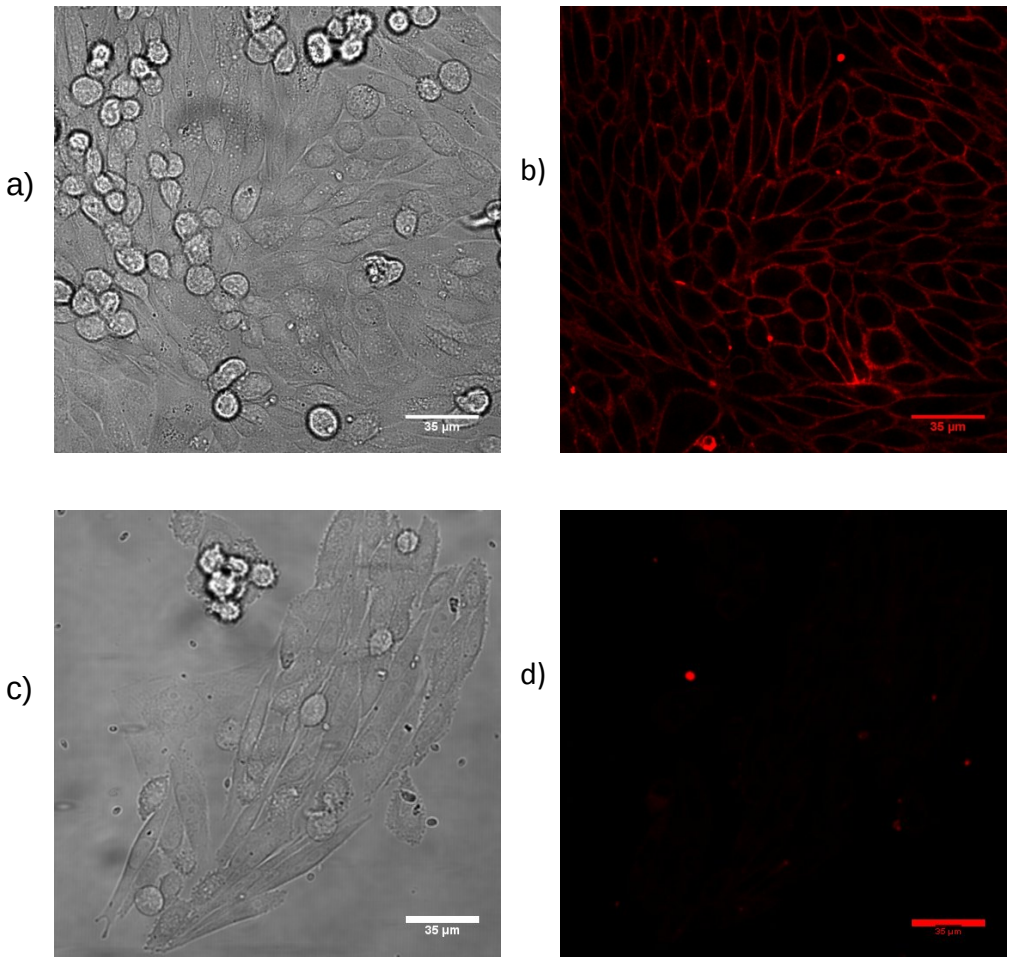

Figure 2.28. Visualisation of fluorescent antagonists (100 nM) on CHO β_2 cells. a) Transmitted light image taken at 0 min before the addition of 87 and b) appearance of 87 10 min after addition. c) Transmitted light image taken at 0 min before the addition of 87 after preincubation with ICI 118551 (100 nM) and d) appearance of 87 10 min after addition.

Confocal imaging of **87** clearly showed membrane binding of the fluorescent ligand and no internalisation of the ligand is shown. As membrane binding can be seen, experiments were carried out to determine if the ligand has receptor binding or non-specific binding. From the RLB experiments it could be assumed that it had receptor binding but to confirm, cells were pre-incubated with 1µM ICI 118551, a selective β_2 antagonist that would block all available binding sites. This occupation of the receptors does not allow the fluorescent ligand to bind to the receptor. Figure 2.28 shows no receptor binding and minimal non-specific binding.

Unfortunately the quantity of **87** synthesised and lack of time did not allow lipophilic characterisation to be carried out. This data would potentially have afforded excellent analytical data towards the understanding of internalisation of fluorescent molecules.

2.8 Triazole bearing fluorophores and pharmacophores

Attachment and incorporation of the triazole and fluorophore to a known orthosteric ligand has an effect on the binding affinities shown in the study. To quantify this, triazole bearing fluorophores and triazole-tethered pharmacophores were investigated to determine the extent of this, to whether the triazole-fluorophore had any specific binding or whether the triazole had a beneficial effect on binding when attached to the orthosteric ligand. This investigation required triazole bearing pharmacophore and triazole bearing fluorophores to be synthesised and tested assessed by radioligand binding competition assays.

2.8.1 Capped molecule synthesis

The fluorophores were conjugated with azide-functionalised amines to form simple 1,2,3-triazoles that the azide would not interfere with binding. These molecules would mimic the fluorophore-triazole structure observed in the final ligand.

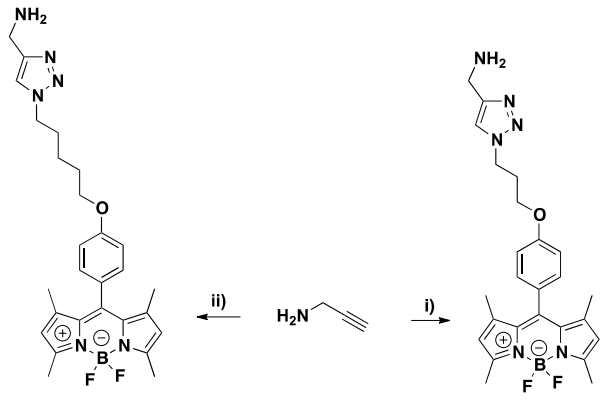

Scheme 2.30. i), 4,4-Difluoro-8-(4-(3-azidopropoxy))phenyl-2,6-dimethyl-4-bora-3a,4adiaza-s-indacene, DMF/H_2O, $CuSO_4.5H_2O$, sodium ascorbate, MW 80 min, 80 °C, 40 W (60%). ii) ,4-Difluoro-8-(4-(5-azidopentyl))phenyl-2,6-dimethyl-4-bora-3a,4adiaza-s-indacene DMF/H_2O, $CuSO_4.5H_2O$, sodium ascorbate, MW 80 min, 80 °C, 40 W. (76%).

The fluorophores were capped with propargylamine to form the triazole with a terminal amine. Two capped fluorophores **88a-b** were synthesised in reasonable yield.

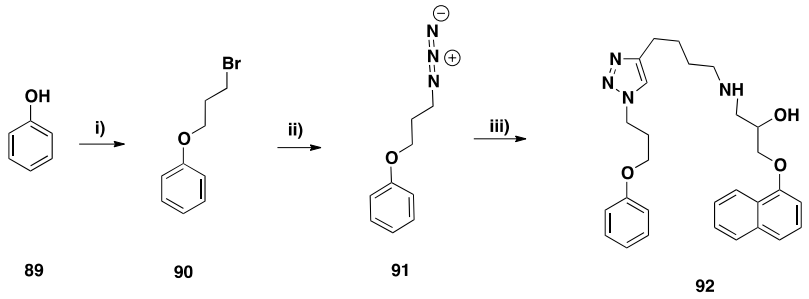

Scheme 2.31. i) 1,3-dibromopropane, K_2CO_3 12hr, (69%). ii) Sodium azide, DMF, 16hr, (80%). iii) 1-(hex-5-ynylamino)-3-(naphthalen-1-yloxy)propan-2-ol, DMF/H_2O, $CuSO_4.5H_2O$ sodium ascorbate, MW 80 min, 80 °C, 40 W (62%).

To get an understanding of the influence of the triazole on the pharmacophore **56c**, a simple azide was coupled to the pharmacophore. This azide included the linker from the fluorophore resulting in a terminal phenol.

The synthesis of the fluorophore linker began with 1,3 dibromopropane and phenol (**89**) stirrred at room temperature in the presence of K_2CO_3 to yield (3-azidopropoxy) benzene (**90**). This was clicked to the alkyne **56c** to yield **92**.

2.8.2 Pharmacology of triazole pharmacophores and capped fluorophores

Binding affinities of the capped molecules were calculated by radio ligands binding assays.

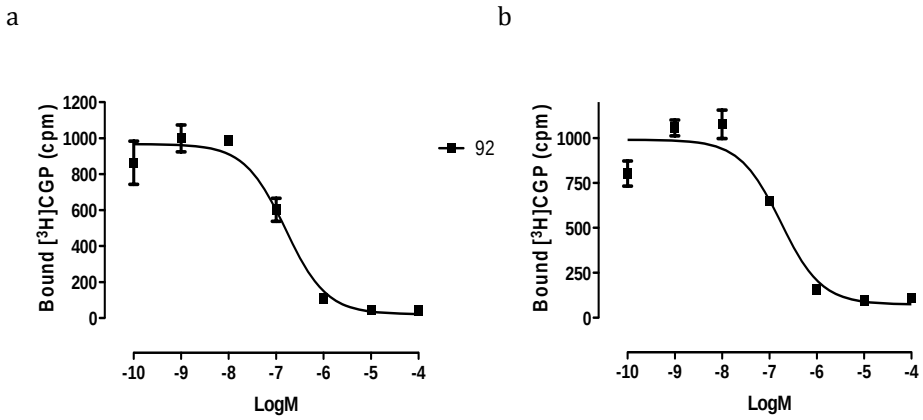

Figure 2.27. Fluorescent ligand displacement of [^{3}H]-CGP 12177 specific binding at the human β-AR in whole CHO cells. Inhibition of [^{3}H]-CGP 12177 specific binding to whole cells in a) β_1 by compound 92 and b) β_2 by compounds 92. Nonspecific binding was determined by 10 μM propranolol. A concentration of 1 nM of [^{3}H] CGP 12177 was used in each experiment. Data points are a mean ± s.e.m of triplicate determinations. These single experiments are a representative a minimum of four different experiments.

Compound	β_1 Log K_i (n)	β_2 Log K_i (n)
92	-7.21 ± 0.01 (4)	-7.33 +0.09 (4)
88a	> -4.00* (4)	> -4.00* (4)
88b	> -4.00* (4)	> -4.00* (4)

Table 2.10. Log K_i values were obtained from [^{3}H]-CGP12177 binding in whole cells expressing either the human β_1 or β_2-AR. Values are mean ± s.e.m from n number of experiments. K_i refers to the equilibrium dissociation constant and the values were calculated from the IC_{50} values. *No displacement at the concentrations tested.

The fluorophores do not displace the radioligand and they have no affinity to the receptor at the concentrations tested (binding curves not shown).

Ligand **92** showed nano-molar affinity it has the best binding affinities of the non-fluorescent ligands tested. There is a large improvement on binding compared to alkyne-functionalised pharmacophores. This result again points towards the triazole being accommodated in the binding pocket. Comparison between the best fluorescent ligand **57c**, which had log K_i values of -6.77 and -7.32 respectively at β_1 and β_2 and **92** there is no significant difference between the two at the β_2 receptor. This shows addition of the fluorophore onto **92** is not having an effect on binding at the β_2 receptor. Interestingly there is an effect on the β_1 receptor. Activity drops from -7.21 to -6.77 Log K_i possibly showing receptor selectivity.

2.8.3 Stability assays

Stability assays were performed to determine whether the fluorescent ligands degraded in cell media. If the ligands decomposed in the media while incubating with the cells, this could result in a false positive or negative result.

Antagonists were diluted from DMSO stock solution to 10^{-4} M concentration in serum free media and incubated for a maximum of six hours. The maximum incubation time was six hours as this would be beyond the time length for which the antagonists would be in solution. HPLC analytical traces were performed with 20 μL of antagonist/serum free media and were injected at 0, 0.5, 1, 2, 3, and 6 hours in order to observe if the media had caused any decomposition of the ligands. Results showed that there was no decomposition of any adrenoceptor antagonists.

2.9 Conclusions and future work

A range of fluorescent β-adrenoceptor ligands were synthesised successfully using the alkyne-azide copper (I) cycloaddition "click" reaction. 15 novel fluorescent beta adrenoceptor ligands were synthesised with a range of binding affinities, physicochemical propterties and confocal microscopy characteristics.

The three main components of a fluorescent ligand are the pharmacophore, linker and fluorophore. Each component of the fluorescent conjugate can affect the ligand greatly. In this study a range of linkers and fluorophores were used in an attempt to synthesise a fluorescent ligand with high binding affinity and properties that were close to the parent ligand and could be used in a range of assays. Unfortunately not one fluorescent ligand had all these characteristics.

2.9.1. Effect of hydrocarbon linker length on binding affinity

Linker length was investigated in two separate ways, length between the pharmacophore and triazole and the linker between the fluorophore and the triazole. Non branched hydrocarbon linkers were investigated.

Generally, it appeared that the longer the linker between the pharmacophore and triazole the greater the binding affinity of the ligand. There was a difference of over two log units in difference between the shortest linker synthesised, a one carbon linker **52a** (log K_i -4.27 ± 0.10 β_1 and β_2 -5.13 ± 0.05) to the longest linker, a four carbon linker, **57c** (log K_i -6.77 ± 0.20 β_1, and -7.32 ± 0.05 β_2). Interestingly the two carbon linker gave better affinity then the one carbon linker and three carbon linker but not as good as the four carbon linker.

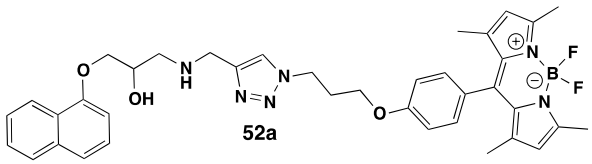

52a

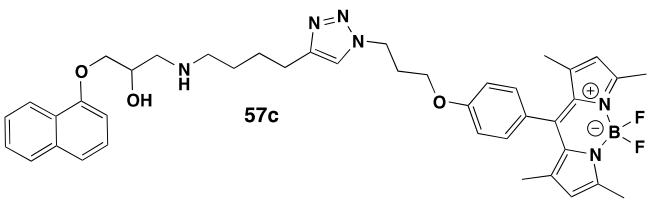

57c

Figure 2.28. Structures of ligands **52a** and **57c**.

Increasing the linker between the triazole and the fluorophore had the opposite effect to binding affinity. Affinity reduced by over two log units when the most potent fluorescent ligand, a three carbon linker, **57c** (log K_i -6.77 ± 0.20 β_1, and -7.32 ± 0.05 β_2 was altered to include a longer, five carbon linker between the triazole and fluorophore, **66a** (log K_i -4.61 ± 0.12 β_1, and -5.36 ± 0.09 β_2.)

Figure 2.28 shows a representation of a fluorescent ligand. In general it was found that when linker A is longer, binding affinity increases while an increase in linker B causes a reduction in binding affinity.

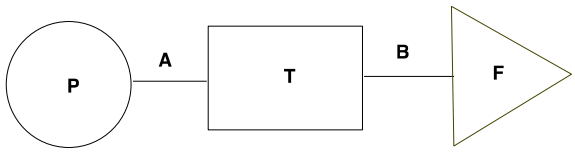

Figure 2.28. Representation of a fluorescent ligand. P = Pharmacophore, T = triazole, F = fluorophore, A is a linker and B is a linker.

Effect of linker type on binding affinity

Fluorescent ligands were synthesised with an amide bond containing linker between the triazole and the pharmacophore, this was synthesised to reduce the lipophilicity of the fluorescent ligands to counter internalisation of the fluorescent ligands when imaged with a confocal microscope. This incorporation of an amide bond into the linker had an effect on the binding affinity of the ligand (**72a**) with roughly a 10-fold decrease in binding affinity at both receptors compared to the equivalent straight carbon linked fluorescent ligand (**57c**).

An ethoxyethane linker between the triazole and fluorophore was synthesised and compared with longest triazole-fluorophore linker. This change in linker did not have a significant change in binding affinity over the equivalent straight hydrocarbon linker.

Effect of the fluorophore on binding affinity

A range of fluorophores were attached to the pharmacophore, with each fluorophore having an effect on physiochemical properties and binding. One short wave fluorophore was used as well as two long wavelength fluorophores. The shorter wavelength fluorophore (**46**) when tethered

to a pharmacophore gave better binding affinities than that of the longer wavelength fluorophores (**73** and **85**) with a minimum of a 10-fold reduction in binding affinity.

Log D, CHI $_{AIM}$ and confocal microscopy

Log D and CHI $_{AIM}$ values were calculated for all fluorescent ligands in an aim to assess the properties of the fluorescent ligand and allow comparison to the orthosteric ligand it was based on. The attachment of a fluorophore had a large impact on the physicochemical properties of the ligand, with a general large increase in both log D and CHI $_{AIM}$ values, signifying a large increase in lipophilicity. Amide bond linkers did improve these values. Longer wavelength ligands that were assessed had increased values than the shorter wavelength ligands.

Confocal imaging of the ligands synthesised resulted in intracellular accumulation. When a polar linker was inserted into the ligand, no improvement was shown, and moving to a commercially available, azide functionalised longer wavelength fluorophore (**73**) intracellular accumulation still occurred. Only when the attachment of a BODIPY 630/650 fluorophore tethered to the amide linked pharmacophore, did intracellular accumulation stop and receptor binding was imaged. This binding could be stopped by pre-incubation with a known antagonist.

Future work would include the synthesis of variations of both **57c** and **87**. As both of these ligands had excellent individual properties, merging the two together resulting in a ligand that has good affinity and images well would result in an excellent tool for fluorescent GPCR studies. One synthetic idea would be to incorporate the fluorophore (**119** from chapter 3) onto the 4 carbon chained linker **56c**. This may help reduce the lipophilicity of the ligand, which is shown in chapter 3 on a different ligand and receptor. Changes to improve **87** by coupling the dye to the three-carbon linker pharmacophore **56b** could help improve affinity, as previous work with the four-carbon chained linker when clicked resulting in a non-soluble ligand. Investigation to longer linkers to determine if there is a more potent ligand available and whether there is a cut off to when a linker becomes too long and affinity is reduced.

3. Design and synthesis of fluorescent Muscarinic M_3 antagonists

3.1 Muscarinic receptors

Another GPCR that is of interest for synthesising fluorescent ligands is the family of muscarinic receptors. There are three different muscarinic receptors expressed in the human airway, M_1–M_3.[150] It is known that acetylcholine is involved in airway smooth muscle contraction and narrowing, which can be targeted for COPD treatment.[151-153]

There are five subtypes of muscarinic receptor, M_1–M_5, and they are members of the metabotropic GPCR family.[1] Muscarinic M_1 receptors are found primarily in the central nervous system (CNS), peripheral neurons and gastric parietal cells, and mediate excitatory postsynaptical potential.[154] Muscarinic M_2 receptors are predominately found within the heart. Activation of M_2 receptors reduces the heart rate and reduces the contractile force of the atrium.[1] Muscarinic M_3 receptors are found in the lungs, smooth muscle, and endocrine and exocrine glands. Activation of M_3 receptors results in the contraction of visceral muscle, an increase in exo- and endocrine secretion, and increases intracellular calcium in the vascular endothelium.[155] The muscarinic M_4 and M_5 receptors are implicated in complex CNS responses, such as memory, arousal, attention and analgesia.[1]

3.1.1 Muscarinic receptor structure

The muscarinic receptor structure is similar to that of the adrenoceptors, with the orthosteric binding pocket being located in a similar position, namely in the middle of the TM helices.[101] Muscarinic receptors M_1–M_5 share a high degree of sequence homology and analysis of the sequences divides the receptors into two classes: $G_{i/o}$ coupled and $G_{q/11}$ coupled.[156,157] It has been noted that the orthosteric binding pocket is formed by amino acids that are identical in all receptor subtypes.[158] Recently, Kruse *et al*.[159] published the crystal structure of an M_3 receptor of *Rattus norvegicus* with a T4L lysozyme for stability and the ligand tiotropium bound, as shown in figure 3.1. Haga *et al*.[158] published the crystal structure of the human M_2 receptor, which also had a T4L lysozyme incorporated into the structure. The inverse agonist

3-quinuclidinyl-benzilate (QNB) was bound to the receptor, as shown in figure 3.2.

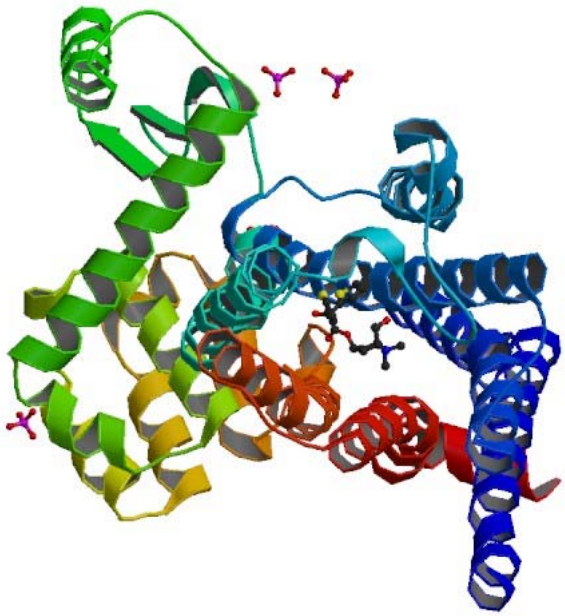

Figure 3.1. Crystal structure of the *rattus norvegicus* M_3 receptor with Tiotropium bound. **Source:** Kruse *et al*, *Nature* 2012, *482*, 552-556.[159]

Figure 3.2. Crystal structure of the human M_2 receptor with ligand QNB bound. **Source**: Haga *et al*, Nature 2012, advance online publication [158]

3.1.2 Muscarinic M_3 receptor

Muscarinic M_3 receptors, as previously stated, can be found in smooth muscle in numerous locations, including most glands, the stomach, iris and bronchi, with activation leading to iris

muscular constriction, increased motility in the stomach, increased glandular secretion and constriction of the bronchi, respectively.[1]

M_3 receptors signal through the $G_{q/11}$ G-protein. On activation, the α_q-subunit causes activation of membrane-bound phospholipase C. This hydrolyses phosphatidylinositol 4,5-bisphosphate into 1,2-diacylgylcerol and inositol 1,4,5-triphosphate (IP_3). IP_3 promotes Ca^{2+} release from specialised intracellular compartments[43] and flux from voltage-dependent Ca^{2+} channels. 1,2-diacylgylcerol promotes the activation of protein kinase C isoforms that phosphorylate numerous cellular enzymes involved in the regulation of diverse signaling events and cellular functions.

3.2 Muscarinic M_3 receptor as drug targets

As the muscarinic M_3 receptor is located in a range of cells throughout the human body, there is an assortment of uses for agonists and antagonists of the receptor.

3.2.1 Glaucoma

Glaucoma is a disorder of the eye in which the optic nerve suffers damage. This damage alters vision and if left untreated can lead to blindness. The damage to the nerve involves loss of ganglion cells. There are two types of glaucoma, closed angle and open angle. Open-angle glaucoma has a slow onset glaucoma and vision deteriorates over time.[1] Closed-angle glaucoma has a sudden onset and vision can be lost quickly; it is usually accompanied by sudden pain. Glaucoma is commonly caused by an increase in ocular pressure. It has been noted that glaucoma can be steroid induced or diabetic induced.[160] Treatments for glaucoma include surgery, prostaglandin analogues, topical β_2AR agonists and M_3 agonists, such as pilocarpine (**93**) and aceclidine (**94**).[161]

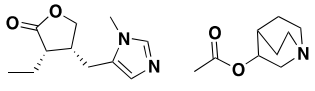

93 **94**

Figure 3.3. Structures of pilocarpine and aceclidine.

3.2.2 Urinary incontinence

Urinary incontinence is a commonly reported problem caused by a range of factors. Causes include polyuria, enlarged prostate and caffeine/cola beverages that stimulate the bladder. There is a range of types of urinary incontinence relating to stress, urge, overflow structural, functional and transient. Treatment can range from behaviour management, dietary change, medication and surgery.[162] Medications commonly used include solifenacin (**95**), tolterodine (**96**) and darifenacin (**97**), which target the M_3 receptor in the bladder antagonistically. This reduces the contractions within the bladder and therefore reduces the urgency to urinate.[163]

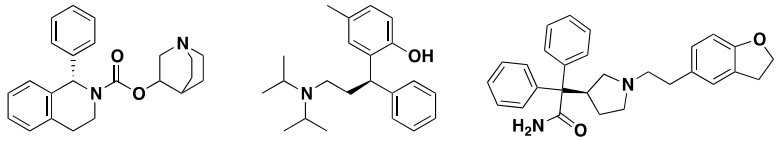

95 96 97

Figure 3.4. Structures of solifenacin, tolterodine and darifenacin

3.2.3 Chronic obstructive pulmonary disease

An area of growing research is the use of the M_3 receptor as a target in COPD treatment.[85,123,164-167] The World Health Organisation predicts that COPD will become the fourth most common cause of death by 2030 and the third most common cause of chronic disability by 2030.[168,169] COPD is the co-occurrence of chronic bronchitis and emphysema, which results in the narrowing of the airways in the lung. Chronic bronchitis is the inflammation of the bronchi and bronchioles. Emphysema is distention and damage of the lung beyond the respiratory bronchioles, and it supervenes after years of coughing. This combination results in limited airflow to the lungs, causing shortness of breath.[1] Causes of COPD include smoking, occupational exposure, air pollution and genetics.[121,122] There is currently no cure for COPD; however, COPD is a preventable and treatable disease. Anticholinergics that have been recently developed for COPD include ipratropium bromide (**98**) (a short-term agent) and tiotropium bromide (**99**) (a long-term agent).[165]

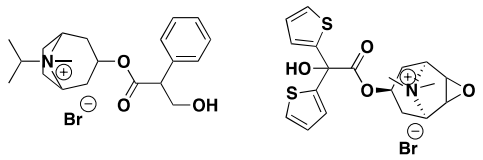

98 99

Figure 3.5. Structure of ipratropium bromide and tiotropium bromide.

3.2.4 Aim

This chapter describes the design, synthesis and pharmacological evaluation of fluorescent ligands active at the muscarinic M_3 receptor. The main aims of this chapter are to use the knowledge gained in the previous chapter and incorporate this into the design and synthesis of synthons for the synthesis of novel fluorescent M_3 ligands utilising click chemistry. Once this has been achieved, investigation into the physiochemical properties, ligand interaction by receptor binding assays, confocal microscopy and receptor kinetics will allow full characterisation and profiling of the novel fluorescent ligands.

3.3 Design and synthesis of fluorescent M_3 Ligands

With the previous success of using the alkyne-azide copper (I) cycloaddition to conjugate a fluorophore to a known pharmacologically active orthosteric ligand, this methodology was revisited in order to synthesise novel fluorescent muscarinic receptor ligands, initially targeting the M_3 subtype. The pharmacophore chosen for the M_3 antagonist was a tiotropium bromide analogue (**100**) recently exemplified by Prat *et al*.[165] Tiotropium bromide (**99**) is a long-acting 24-hour bronchodilator used for the treatment of COPD.[164]

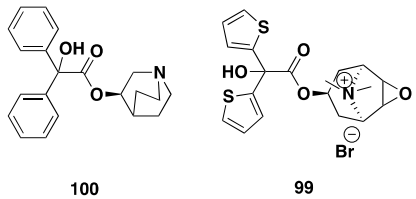

100 99

Figure 3.6. Structures of pharmacophore and tiotropium bromide.

It is known that some functional groups are key for interaction with the receptor. The nitrogen species is essential for binding and binding is improved when it is positively charged. The nitrogen has a strong interaction with the anionic side group of an aspartic acid residue. The

ester is also key for binding with interaction with asparagine 507 on the TM6.[159,170] Figure 3.7 shows the X-ray crystal structure with tiotropium bound in the orthosteric binding site.

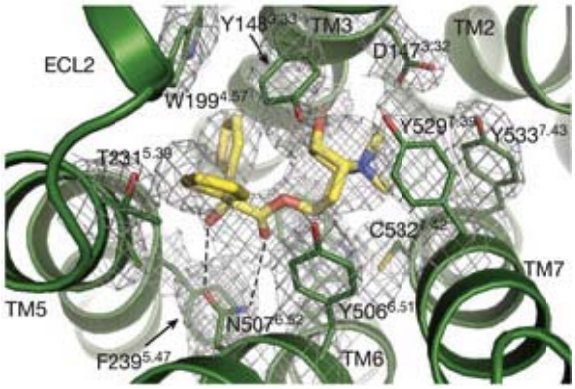

Figure 3.7. Tiotropium binding site in the M_3 receptor. M_3 receptor shown in green and tiotropium shown in yellow. **Source:** Kruse *et al*, *Nature* 2012, *482*, 552-556.[159]

The pharmacophore **100** was chosen as it displayed good affinity for the receptor, was expeditious to synthesise and alkylation of the nitrogen would allow linker attachment whilst concomitantly installing a charged nitrogen species, possibly improving binding affinities. The alkylation of the nitrogen improved binding with various moieties that showed potential for the addition of a fluorophore.[165] Compound **100** was noted as having a log IC_{50} value of −9.04 while alkylation of the nitrogen with a phenoxypropyl, which formed the quaternised nitrogen, resulted in improved Log IC_{50} values of −9.21.

3.3.1 Retrosynthetic analysis

A retrosynthetic analysis was carried out in similar fashion to the β-adrenergic ligands. The coupling of a pharmacophore to a fluorophore would be the final step through an alkyne-azide copper (I) cycloaddition. The fluorophores from chapter 2 would be utilised for the fluorescent ligands. As the fluorophores had a terminal azide, the congener required a linker with a terminal alkyne.

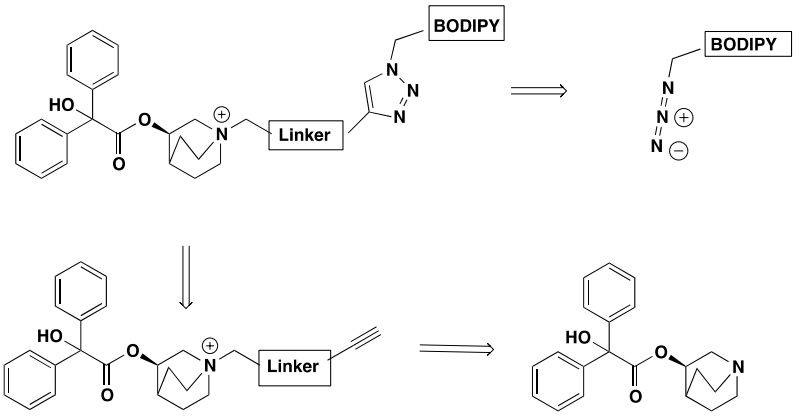

Scheme 3.1. Retrosynthetic scheme for muscarinic M_3 antagonists.

3.3.2 Synthesis of pharmacophore and linker

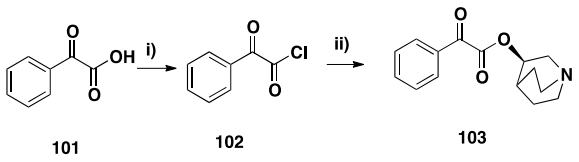

Scheme 3.2. i) Oxalyl chloride, DMF, $CHCl_3$, 90 min. ii) (3*R*)- quinuclidinol, K_2CO_3, $CHCl_3$, 4 hr (96%).

Synthesis of the pharmacophore started from phenylglyoxylic acid (**101**), which was converted into the acid chloride **102** by treatment with Oxalyl chloride and DMF. The acid chloride was then reacted with (3*R*)-quinuclidinol to form the ester **103** in a yield of 96%.

The final step required was a nucleophilic addition to the carbonyl. **103** was treated with phenyllithium at − 42°C to produce the diphenyl. This was achieved in 66% yield. ^{1}H NMR confirmed that addition of a second phenyl group and the formation of an alcohol with a broad peak at 5.19 ppm.

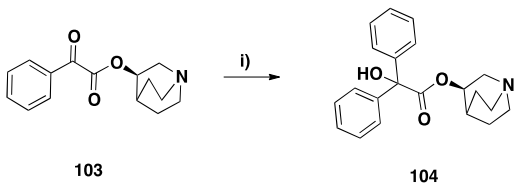

Scheme 3.3. PhLi (1.8M in dibutyl ether), THF, - 42 °C to RT, 2 hr, (66%).

The next step was to attach a linker by alkylation of the tertiary amine. The same strategy was applied to linker length from chapter 2 (section 2.3). Linkers ranged from a single-atom linker to a four-carbon linker. An amide linker was also synthesised similar to pharmacophore **71**. The straight carbon-chained linkers were commercially available, but the amide linker required synthesis.

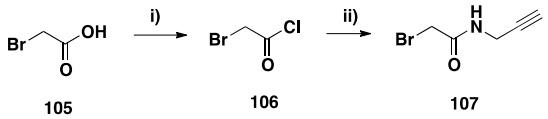

105 106 107

Scheme 3.4. i) Oxalyl chloride, DMF, $CHCl_3$, 2 hr. ii) progargylamine, $CHCl_3$, K_2CO_3, 4 hr, (52%).

Synthesis began with the conversion of bromoacetic acid (**105**) to its corresponding acid chloride **106** using oxalyl chloride. The product **106** was reacted *in situ* with progargylamine to generate 2-bromo-*N*-(prop-2-ynyl)acetamide (**107**) in 52% yield.

The second linker synthesised was a phenolic derivative. The literature suggests that inclusion of a phenoxypropyl moiety bound to the nitrogen increases activity;[165] therefore, this linker was incorporated with the starting material 3-ethynylphenol (**109**), allowing a terminal alkyne to be attached.

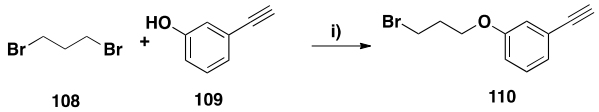

108 109 110

scheme 3.5. i) Acetone, K_2CO_3, 12 hr, (46%).

This linker was synthesised by a Williamson ether synthesis between 1,3-dibromopropane (**108**) and phenol (**109**) to produce the alkynyl ether (**110**) in 46% yield.

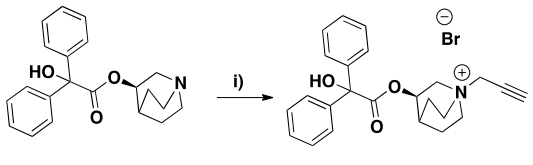

104 111a

Scheme 3.6. Propargyl bromide, MeCN:$CHCl_3$ (6:4), reflux, 12 hr, (45%).

Attachment of the linker to the orthosteric head-group was achieved *via* alkylation of the tertiary amine. The ester **104** was refluxed with six separate linkers in acetonitrile:chloroform (6:4) to afford six different alkyne-functionalised congeners **111a–f**. One example is shown in scheme 3.6.

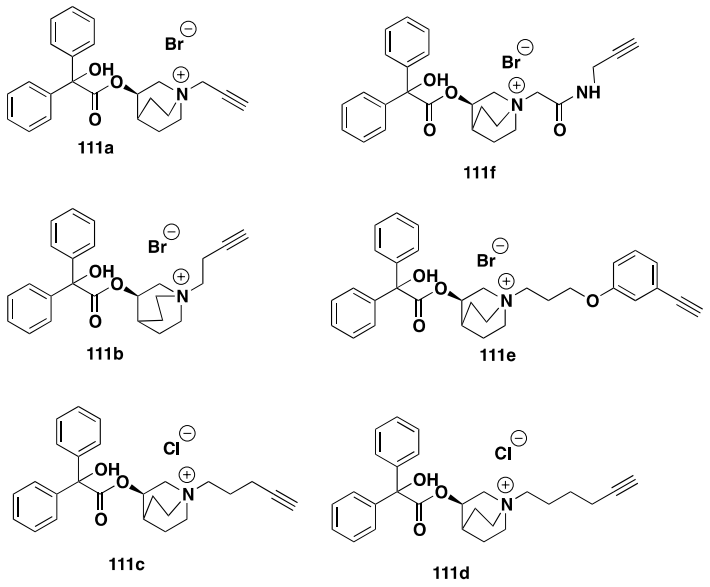

Figure 3.2. Structures of M_3 alkyne functionalised pharmacophores.

3.3.3 Synthesis of fluorescent ligands

Conjugation of the orthosteric ligand to the fluorophore was achieved by click chemistry. The congeners were coupled to four different fluorophores utilising the optimised conditions previously described in chapter 2, to synthesis a range of novel fluorescent M_3 antagonists. An example of this reaction is illustrated in scheme 3.7. The structures of the fluorescent ligands are show in figure 3.2 and table 3.1.

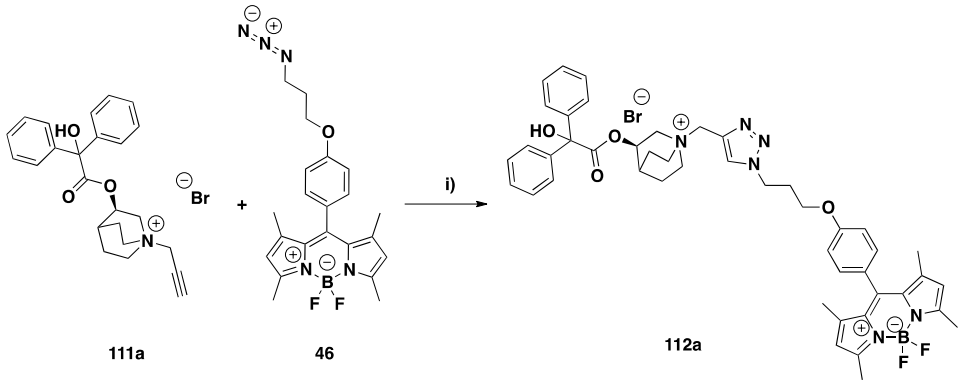

Scheme 3.7. i) DMF/H_2O, $CuSO_4.5H_2O$, sodium ascorbate, MW 80 min, 80 °C, 40 W, (50%).

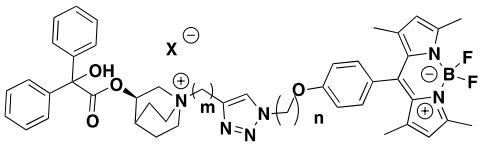

Figure 3.2. General structure of 517 nm emitting ligands.

(m)	$(CH_2)_3$	(n) $(CH_2)_5$	$(CH_2)_2O(CH_2)_2$	Counter-ion (X)
CH_2	**112a**	**112b**	**112c**	Br
$(CH2)_2$	**113a**	**113b**	**113c**	Br
$(CH2)_3$	**114a**	**114b**	**NS**	Cl
$(CH2)_4$	**115a**	**115b**	**115c**	Cl
$CH_2CONHCH_2$	**116a**	**116b**	**116c**	Br
***p*-$(CH_2)_3O$-Ph**	**117a**	**117b**	**117c**	Br

Table 3.1. Structures of different M_3 fluorescent antagonists synthesised. NS = not synthesised.

Two red-shifted ligands were synthesised using pharmacophores **111b** and **111f** and coupled to the previous long-wavelength fluorophore **85**.

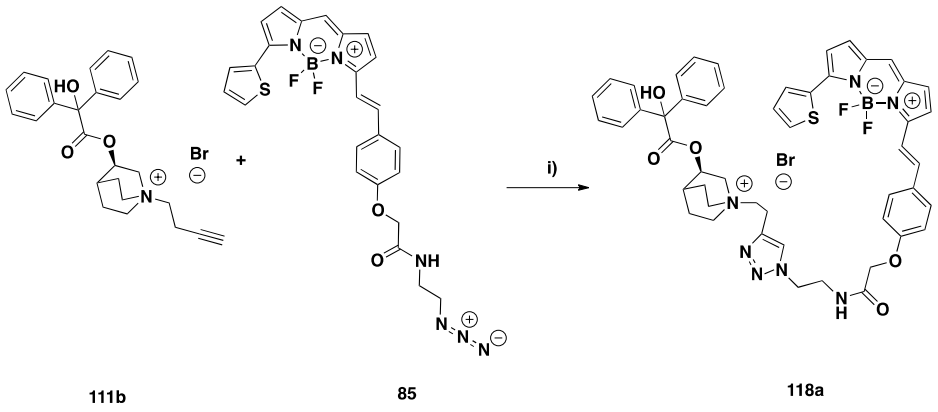

Scheme 3.8.i) DMF/H_2O, $CuSO_4.5H_2O$, sodium ascorbate, MW 80 min, 80 °C, 40 W, (35%).

Two fluorescent ligands with 650 nm emission were synthesised and are list in table 3.2.

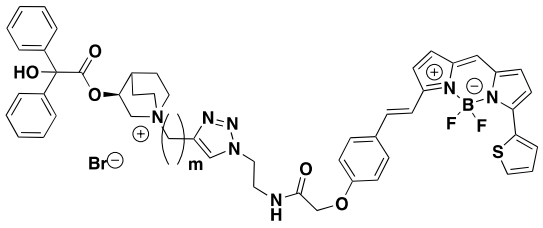

Figure 3.3. General structure of 650 nm emitting ligands

(m)	Compound number
$(CH2)_2$	118a
p-$(CH_2)_3OPh$	118b

Table 3.2. Structures of 650 nm emitting fluorescent M_3 antagonists

3.4 Muscarinic antagonist pharmacology

3.4.1 Antagonist confirmation and initial screen

The pharmacology of the M_3 ligands was assessed by intracellular calcium mobilisation assays. When M_3 agonists activate their respective receptor, one series of downstream signaling processes results in a release of Ca^{2+} from specialised intracellular compartments. This calcium can be monitored by an intracellular fluorescent dye, 2-[5-[bis[(acetoxymethoxy-oxomethyl)methyl]amino]-4-[2-[2-[bis[(acetoxymethoxy-oxo-methyl)methyl]amino]-5-methylphenoxy]ethoxy]benzofuran-2-yl]oxazole-5-carboxylate (fura-2). When this fluorescent dye detects calcium, a change in the fluorescence was detected by the change of spectral properties when calcium is bound to the fluorescent calcium detector and the signal can be monitored. The fluorescence excitation wavelegnth is dependent on the amount of calcium within the cell as the ratio between the excitation is calculated. The more calcium bound to fura-2, the greater the lower excitation (330 nm) is over the base-level excitation (380 nm). If there is no activation of receptor, there will be no change or increase in the fluorescent properties. This allows competitive binding experiments to calculate the IC_{50} and K_i values. The affinities are determined by competitive displacement of carbachol from CHO cells expressing M_3 receptors. Three separate experiments were performed in triplicate. Each ligand

was diluted to 10^{-2} M concentration using DMSO and solutions were stored at −20°C until the ligand was tested.

3.4.1.1 Counteracting extracellular fluorescence

One major effect on the assay was the fluorescence from the extracellular media. As this assay uses a fluorescent molecule to bind to the intracellular calcium produced, and as the ligands are also fluorescent, there was a requirement to quench the extracellular fluorescence. Brilliant black is an extracellular fluorescence quencher and was trialed against no quencher.

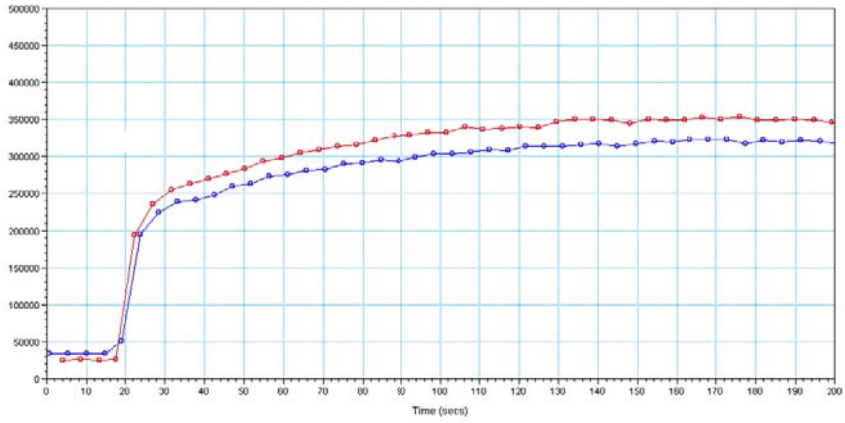

Figure 3.8. Typical signal obtained from a fura-2 loaded cell when fluorescent antagonist is added at 20 seconds without extracellular fluorescence quencher. Y axis represents fluorescence intensity and x axis is time.

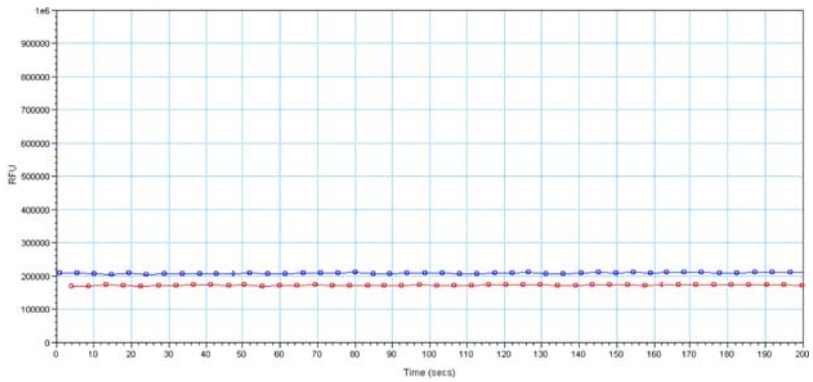

Figure 3.9. Typical signal obtained from a fura-2 loaded cell when fluorescent antagonist is added at 20 seconds with extracellular fluorescence quencher brilliant black. Y axis represents fluoresce intensity and x axis is time.

Figures 3.8 and 3.9 show antagonist addition with brilliant black and no brilliant black. The fluorescent antagonist was added at 20 seconds. Figure 3.8 reveals that without brilliant black there is a large response due to the fluorescent nature of the ligand and not to the receptor

response. The increase in fluorescent activity was above the expected threshold for calcium production and must be due to the fluorescent ligands. While figure 3.9 shows antagonist addition following pre-incubation with brilliant black, this clearly showed no fluorescent activity either due to extracellular ligand or calcium production.

An initial investigation was carried out to determine if the fluorescent ligands had agonist activity. The experimental conditions were repeated with brilliant black and all ligands that were tested showed no agonist activity in three separate experiments in triplicate. Responses were identical to that shown in figure 3.5, when the fluorescent ligand was preincubated and carbachol was added at 20 seconds.

3.4.2 Percentage inhibition assay

After this initial antagonist screening process, a competition assay was conducted on all fluorescent ligands and congeners within a calcium assay to assess which ligands had the greatest activity. This assay was a single-point concentration experiment using 1 μM fluorescent antagonist and 0.1 μM carbachol. This assay allowed the measurement of the percentage inhibition.

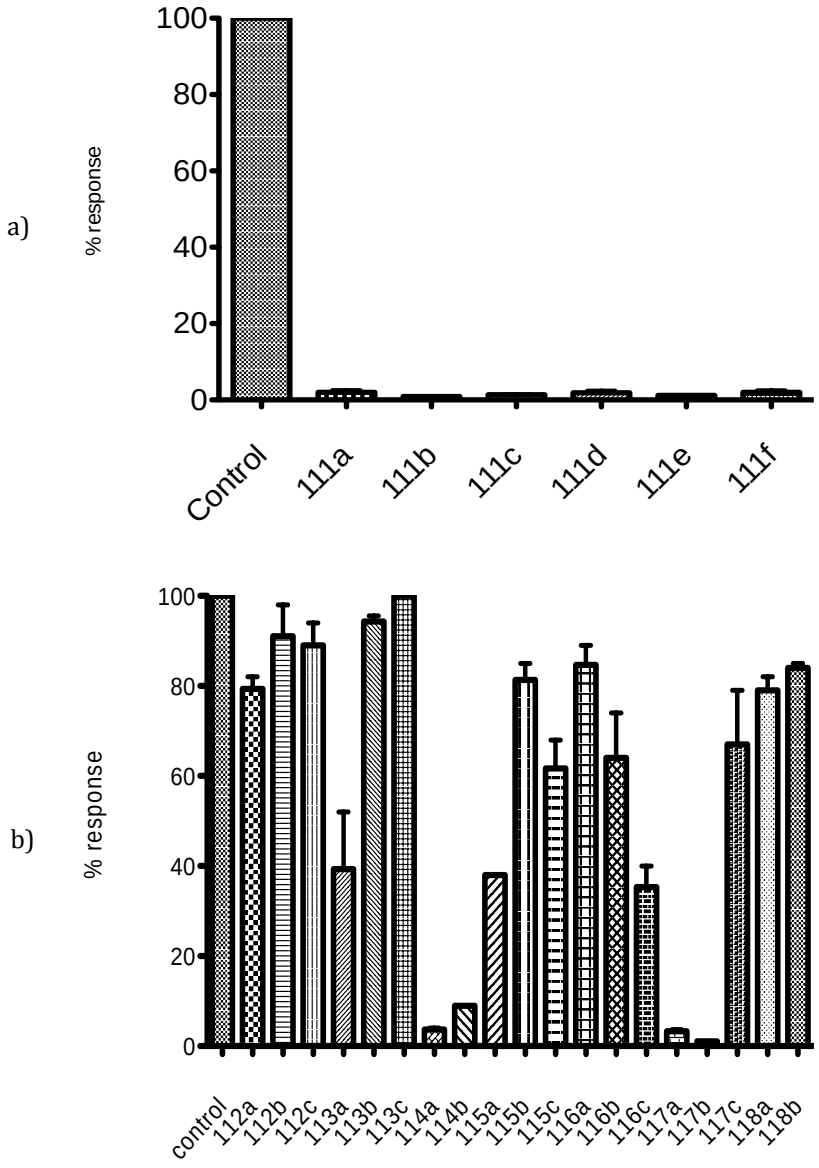

Figure 3.10. Histograms showing relative calcium production, when antagonist a) pharmacophores 111a-f and b) fluorescent ligands 112a-c, 113a-c, 114a-b, 115a-c, 116a-c, 117a-c and 118a-b at 1 μM concentration in competition against carbachol at 0.1 μM concentration on CHO cells expressing the human M_3 receptor. Experiments were repeated three times and all compounds were tested in triplicate in each experiment.

The results of this initial assay clearly show that all pharmacophores (**111a–f**) completely inhibit carbachol at this concentration. There is a range of inhibition profiles from the fluorescently tagged antagonists, ranging from minimal inhibition to complete inhibition.

The initial assay showed that four fluorescent ligands (**114a, 114b, 117a and 117b**) greatly inhibited carbachol. All four of these fluorescent ligands had major similarities, one being the type of linker attached to the pharmacophore and the second being the linker attached to the

fluorophore. The fluorophore was the short wavelength fluorophore in all fluorescent ligands and the linkers attached to the pharmacophore were of two types; either a three carbon linker or the phenyl derived linker. The short linkers were not favoured with one carbon and two carbon linkers giving little inhibition. This was also the case for the longer wavelength fluorophore and the four carbon linkers gave a varying inhibition response dependent to which fluorophore was attached.

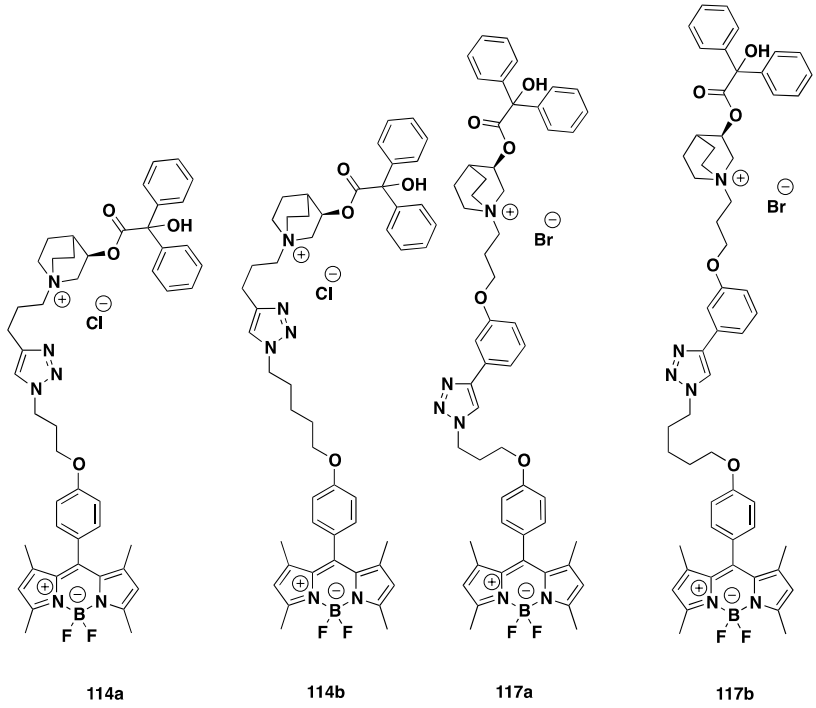

Figure 3.11. Structures of most potent fluorescent ligands.

3.4.3 Dose response competition assays

From the initial screening assay, the most promising ligands **114a–b** and **117a–b** were taken forward for further study. An intracellular calcium assay was again used, with a range of concentrations of antagonist and one concentration of agonist per experiment. The varying response of the antagonist would allow a dose–response curve to be produced, giving an IC_{50} value that then could be used to produce a K_b value by using the Schild equation:[171]

$$DR = 1 + \frac{[A]}{K_b}$$

where DR (dose ratio) is the ratio of the concentrations of agonist required to produce an identical response in the presence and absence of antagonist, [A] is the concentration of antagonist and K_b is the antagonist inhibitory constant.

This assay used concentrations of carbachol ranging from 0.1 µM. The range of antagonist concentration was from 1×10^{-10} to 1×10^{-5} M. An example curve from each fluorescent ligand and non-fluorescent ligand is shown in figure 3.12.

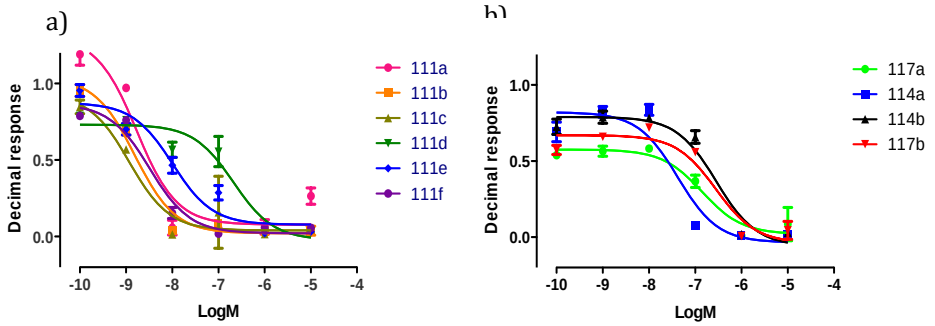

Figure 3.12. Inhibition of Carbachol binding to whole CHO expressing the human M_3 cells by a) pharmacophores 111a-f and b) fluorescent antagonists 114a-b and 117a-b. Data points are mean ± s.e.m (triplicate determinations) from a single experiment which is representative of 3 separate experiments for each ligand. A concentration of 0.1 µM of Carbachol was used in each experiment.

Compound	Log IC_{50} (n=)	Log K_b (n=)
111a	-7.16 ± 0.02 (3)	-9.44 ± 0.23 (3)
111b	-7.85 ± 0.03 (3)	-10.00 ± 0.13 (3)
111c	-9.02 ± 0.18 (3)	-10.29 ± 0.10 (3)
111d	-7.96 ± 0.20 (3)	-6.68 ± 0.19 (3)
111e	-8.85 ± 0.11 (3)	-10.15 ± 0.01 (3)
111f	-8.58 ± 0.15 (3)	-9.72 ± 0.19 (3)
114a	-7.62 ± 0.20 (3)	-8.89 ± 0.11 (3)
114b	-6.73 ± 0.20 (3)	-8.02 ± 0.09 (3)
117a	-7.16 ± 0.24 (3)	-8.42 ± 0.16 (3)
117b	-6.69 ± 0.16 (3)	-7.97 ± 0.07 (3)

Table 3.3. Inhibition of carbachol binding to CHO cells expressing the human M_3 receptor induced by antagonists 111a-f, 114a-b and 117a-b. K_i refers to the equilibrium dissociation constant and the values were calculated from the IC_{50} values. All values are expressed as mean value ± s.e.m of different experiments (n).

The binding data from competition assays gave very promising information. First, the pharmacophores were of a similar standard to the compounds published in the literature.[165] The non-quaternised pharmacophore (**104**, figure 3.1) had a Log IC_{50} of −9.05 in radioligand binding studies and the phenoxypropyl-functionalised ligand had a Log IC_{50} of −9.21. The synthesised congeners had a similar IC_{50} to these ligands, with the best ligand having a Log IC_{50} of −9.02 with a binding affinity of −10.29 (Log K_b). It is noteworthy that the congener **111f** based upon the best compound in the literature did not give the highest affinity.[165] The best congener was **111c**, which contained a three-carbon linker. This congener also afforded the best fluorescent ligand, **114a**, with a binding affinity of −8.89 ± 0.11 (Log K_b). Of the fluorescent ligands, those with greater binding affinity possessed the shorter linker after the triazole to the fluorophore and not the extended six-atom linker. These data also agree with those from earlier studies whereby the extended linker was not tolerated to the same extent as the shorter linker. All ligands had low nanomolar affinity, which was a relative improvement of binding affinity for the desired receptor in comparison to the β-adrenoceptor ligands synthesised in chapter 2.

3.4.4 Confocal imaging

The ligands were assessed by confocal microscopy for visualisation at the single-cell level. A concentration of 100 nM was used initially for each ligand as this was greater than the K_b and would allow for good imaging. All ligands were incubated with CHO cells expressing the human M_3 receptor. All experiments were conducted at 37°C (experimental section). Imaging was carried out in 8-well plates, with cells being seeded 24 hours before experimentation. The wells were washed and HBSS added before antagonist addition. The antagonists were added to the wells and confocal images were produced with the aim to see specific receptor binding.

The initial confocal imaging of the fluorescent ligands did not produce the anticipated results. The images suggested that the ligand was binding to the glass and not to the membrane. After two separate washes the fluorescent ligand was not removed and was still bound to the glass. This binding to the glass is likely to be due to the positive charge of the ligand while the glass has a slight negative charge, which is common to silica and silicate glassware. To combat this

problem, the cover slips were pre-treated with poly-L-lysine. This changes the contact charge of the glass from negative to positive and minimise binding to the glass and allow receptor-binding visualisation.

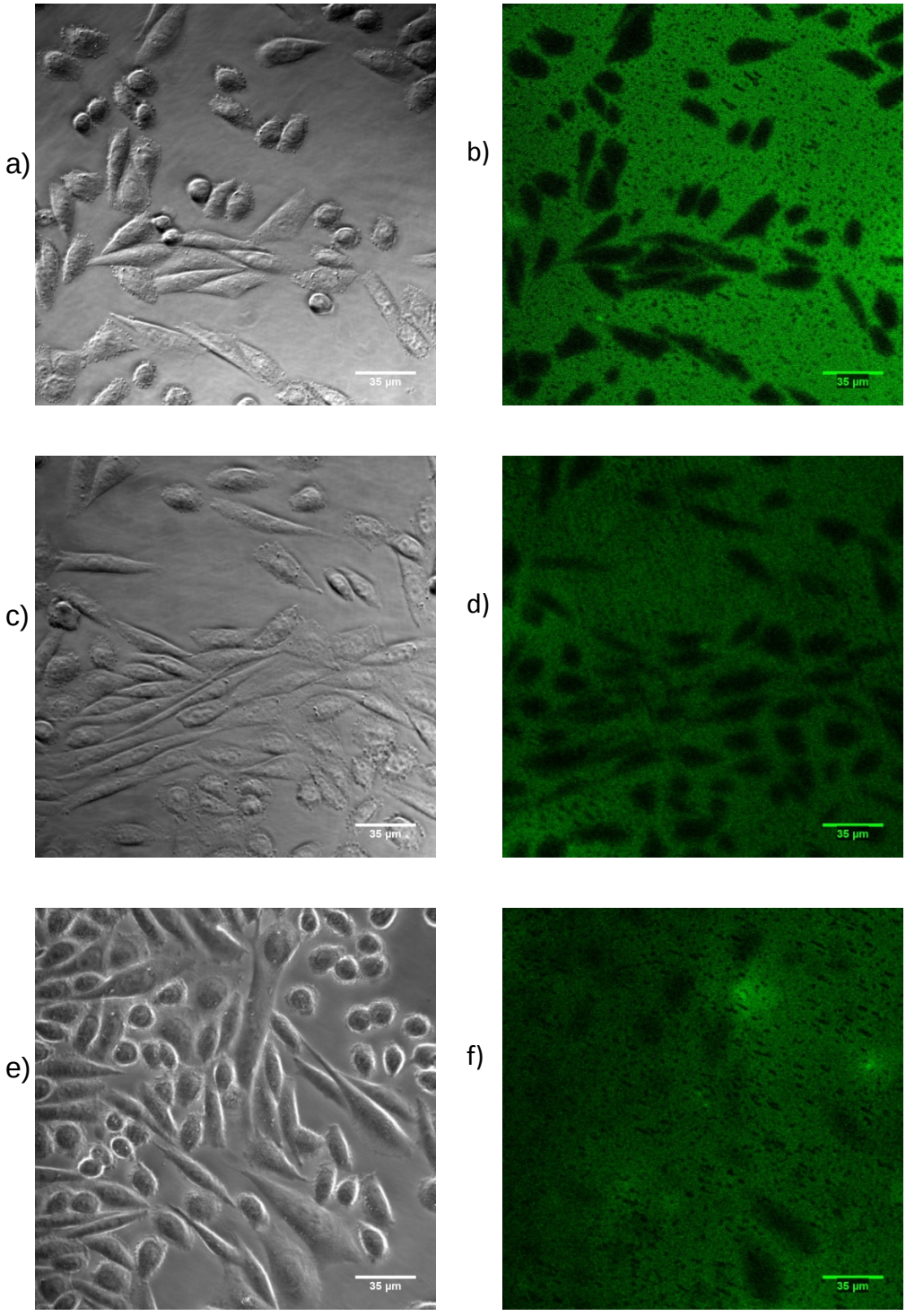

Figure 3.13. Visualisation of fluorescent antagonists (100 nM) on CHO M_3 cells. a) Transmitted light image taken at 0mins before the addition of 114a and b) appearance of 114a 10 min after addition. c) Transmitted light image taken at 0 min before the addition of 114a and d) appearance after well washed with HBSS. e) Transmitted light image taken at 0min before the addition of 114a and f) appearance after multiple washings.

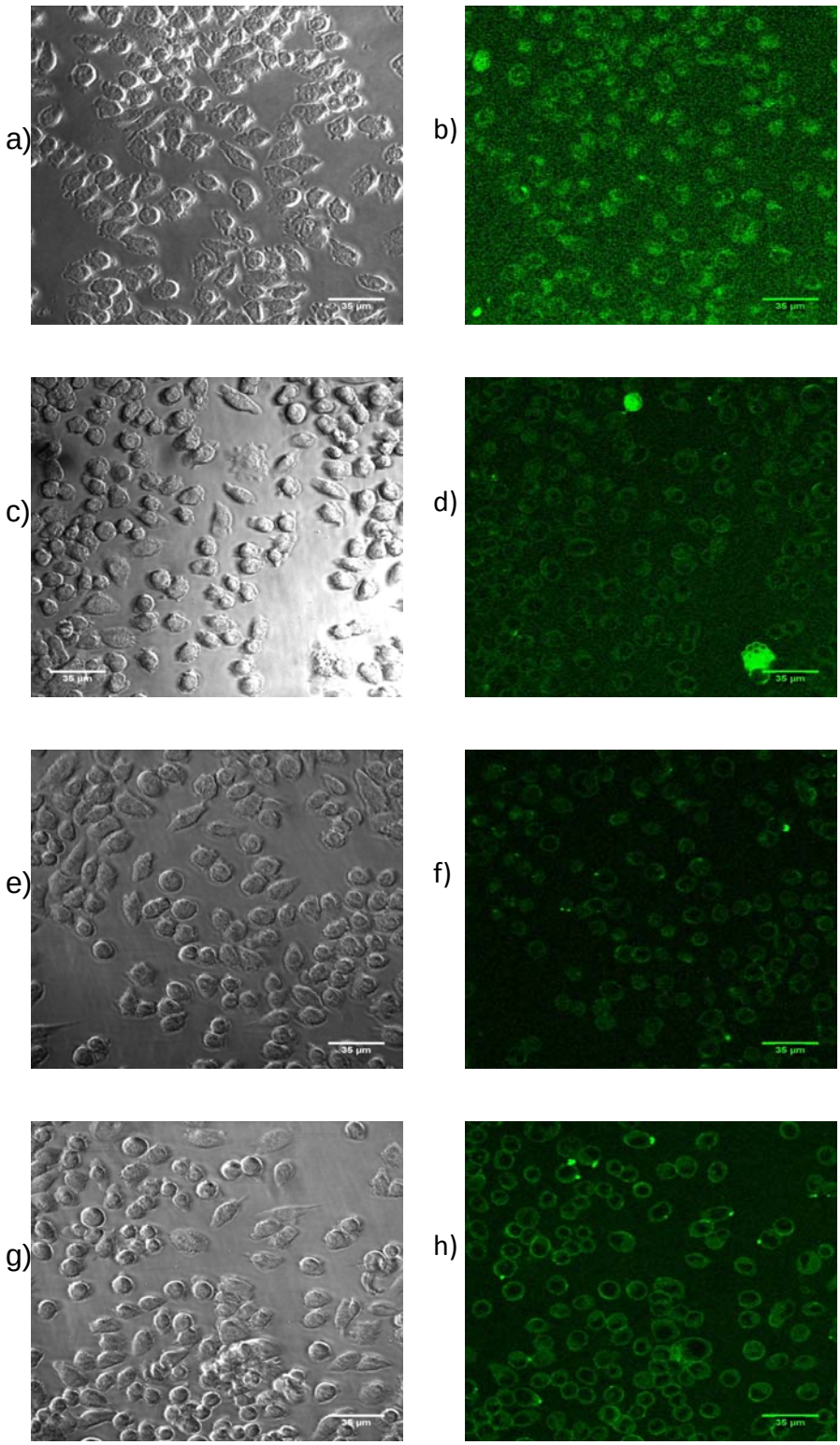

Figure 3.14. Visualisation of fluorescent antagonists (100 nM) on CHO M_3 cells and wells preincubated with poly-L-lysine. a) Transmitted light image taken at 0 min before the addition of 117a and b) appearance of 117a 10 min after addition. c) Transmitted light image taken at 0 min before the addition of 114b and d) appearance of 114b 10 min after addition. e) Transmitted light image taken at 0 min before the addition of 117b and f) appearance of 117b 10 min after addition. g) Transmitted light image taken at 0 min before the a addition of 114a and h) appearance of 114a 10 min after addition.

With wells being pre-incubated with poly-L-lysine, the ligand binding to the glass has dramatically reduced allowing the ligand membrane binding to be captured. Figure 3.14b. displays cell membrane binding of all fluorescent ligands. **117a** still showed binding of ligand to the glass but it is still possible to see membrane binding. Ligands were then administered with cells being pre-incubated with atropine, an known antagonist to the muscarinic acetylcholine receptor.[172] Pre-treatment with atropine will help distinguish between specific and non-specific receptor binding. The pre-incubation of atropine would saturate the receptor not allowing the fluorescent ligand to bind.

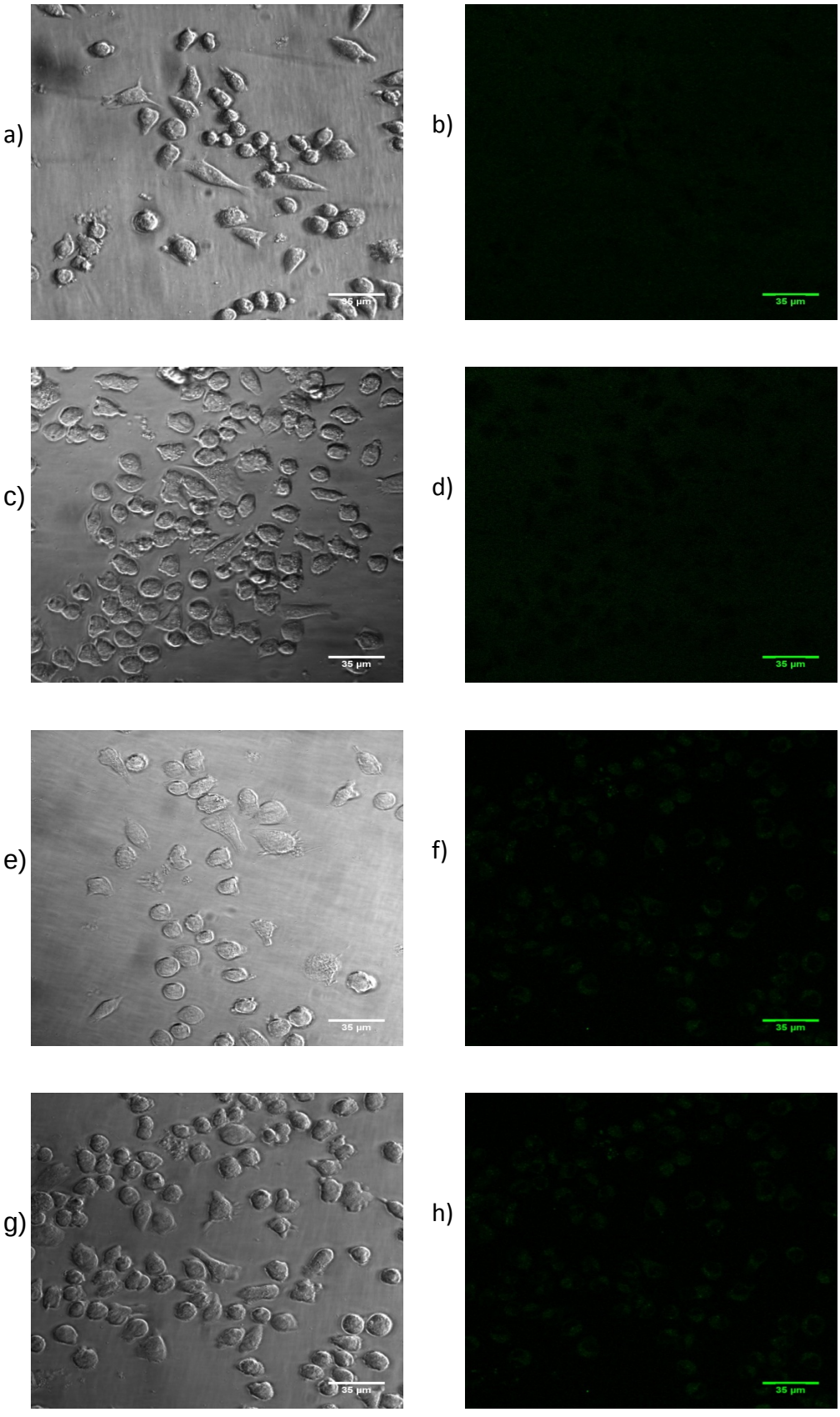

Figure 3.15. Visualisation of fluorescent antagonists (100 nM) on CHO M_3 cells and wells preincubated with poly-L-lysine and atropine (100 nM). a) Transmitted light image taken at 0 min before the addition of 114a and b) appearance of 114a 10 min after addition. c) Transmitted light image taken at 0 min before the addition of 114b and d) appearance of 114b 10 min after addition. e) Transmitted light image taken at 0 min before the addition of 117a and f) appearance of 117a 10 min after addition. g) Transmitted light image taken at 0 min before the addition of 117b and h) appearance of 117b 10 min after addition.

The confocal images in figure 3.15 show no fluorescent ligand binding when atropine is administered to the cells. Thus showing specific receptor binding by all fluorescent ligands and no internalisation is present either. These ligands show specific membrane binding with low nanomolar affinity.

3.4.5. Lipophilicity evaluation of fluorescent ligands

The fluorescent ligands are clearly binding to the receptors when viewed using confocal microscopy. Previous ligands **57a–c** with shorter wavelength fluorophores showed cytoplasmic accumulation when imaged. One possible reason for this was the lipophilic nature of the ligand. Investigation into the lipophilic nature of the M_3 ligands was conducted using $CHI_{IAM\ 7.4}$ and Log*D* $_{7.4}$ HPLC methods, as used in chapter 2.[144,145] This would allow comparisons to be made with regard to the possible intracellular accumulation and lipophilicity of the ligands synthesised in chapter 2.

Compound	$CHI_{IAM\ 7.4}$	Log*D* $_{7.4}$
111a	45.72	1.16
111b	46.16	1.48
111c	46.92	1.67
111d	48.22	1.89
111e	48.42	1.37
111f	53.94	2.55
114a	60.11	3.59
114b	61.76	3.92
117a	61.65	4.06
117b	62.87	4.55

Table 3.4. $CHI_{IAM\ 7.4}$ values of M_3 ligands wavelength ligands calculated from HPLC methods using a Regis IAM PC 12 µm column (100 x 4.6mm), a flow rate of 1.00 mL/min and UV detection at 230 and 366 nm. Linear gradient 0 % - 100% solvent A over 7 min. Solvent A: 100% MeCN. Solvent B: Water with 50 mM ammonium acetate. LogD $_{7.4}$ values calculated by HPLC methods using a Polaris C_{18} 5 µm HPLC column (50 x 4.6mm). A flow rate of 1.00 mL/min and UV detection at 230 and 366 nm. Linear gradient 0 % - 95% solvent A over 4 min. Solvent A: 100% MeCN. Solvent B: Water with 50 mM ammonium acetate.

The $CHI_{IAM\ 7.4}$ and Log$D_{\ 7.4}$ values are consistent with those observed for previously synthesised ligands, e.g. ligand **57c** had a $CHI_{IAM\ 7.4}$ of 68.26 and a Log$D_{\ 7.4}$ of 3.70. The addition of a fluorophore greatly increases the Log$D_{\ 7.4}$ and $CHI_{IAM\ 7.4}$ values compared with those of the pharmacophore alone. The $CHI_{IAM\ 7.4}$ values are lower than those for the shorter wavelength ligands for the β-adrenoceptors, possibly due to the quaternised nitrogen, but the Log$D_{\ 7.4}$ values are larger than those for the majority of the previously tested ligands. This result showed that the ligands have a reduced interaction with the membrane but are more lipophilic. Once again, the attachment of the fluorophore is impacting on the molecule overall with regard to the physicochemical properties. Investigation to whether a more polar fluorophore would improve the lipophilic nature of the fluorescent ligands.

3.5. Polar fluorophore synthesis

The pattern of lipophilicity and the incorporation of a fluorophore into a muscarinic fluorescent ligand followed the same observations to that of ligands synthesised in chapter two. Incorporation of a fluorophore dramatically increases the lipophilicity. This increase changes the physicochemical properties of the fluorescent ligand from the parent ligand that it was based on. The possible incorporation of a more polar fluorophore into a ligand may imbue properties similar to that of the parent drug. This could be achieved by the addition of a sulfonic acid group onto the fluorophore, as this would introduce a charged group. Sulfonation of BODIPY dyes has been previously described[173] and this route was followed for the synthesis of a novel azide-functionalised fluorophore. Another route to more polar dyes would be to insert a polar side chain within the linker between the triazole and fluorophore. This side chain with a terminal carboxylic acid could be coupled to a number of amines or amino acids to allow fine adjustment to the fluorophore. One major benefit of both concepts is that the spectral properties of the fluorophores would be extremely similar to those of previously synthesised fluorophores.

3.5.1 Synthesis of polar fluorophores

Synthesis of the sulfonated dye (**119**) started with the previously synthesised fluorophore **46**. This fluorophore was treated with chlorosulfonic acid for 10 minutes at −40 °C and then warmed to room temperature for 30 minutes and purified by HPLC in 62% yield. This was

confirmed by mass spectroscopy and NMR spectroscopy. The ^{1}H NMR spectra showed that the molecule did not have symmetry and the terminal methyl groups were not equivalent. The starting material showed two singlet peaks, integrating for six protons each, while fluorophore **46** showed four singlets all integrating to three protons each. Mass spectroscopy also confirmed monosulfonation.

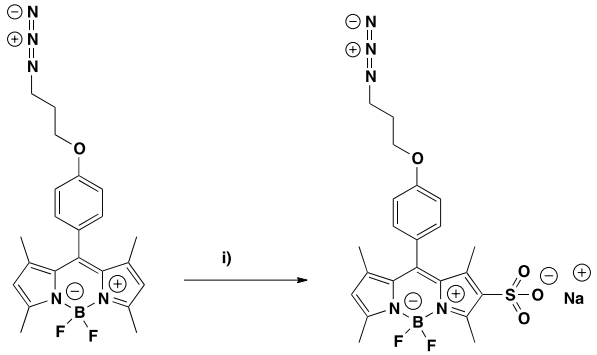

Scheme 3.9.i) Chlorosulfonic acid, DCM, -40 °C to RT, 30 min, (62%).

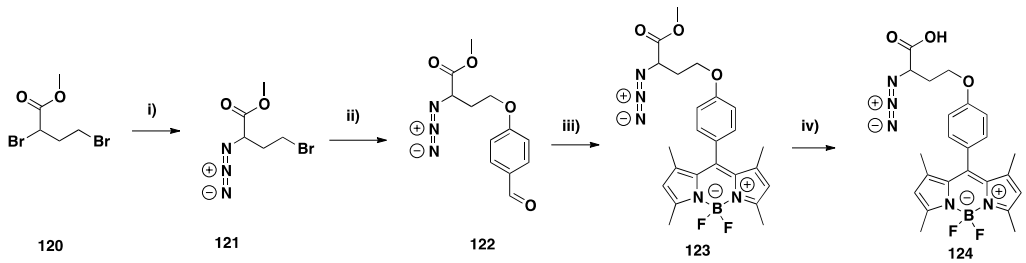

Scheme 3.10.i) NaN_3, DMF, reflux, 3 hr, (91%). ii) 4-Hydroxybenzaldehyde, K_2CO_3, 60 °C, 3 hr, (58%). iii) 2,4-Dimethylpyrrole, TFA, DCM, DDQ, $BF_3.OEt_2$, Et_3N, 36 hr, (23%). iv) LiOH, $MeOH/H_2O$, 3 hr,(98%).

Synthesis of the polar side-chained fluorophore began with an azide substitution of methyl 2,4-dibromobutanoate (**120**) in DMF. Methyl 2-azido-4-bromobutanoate (**121**) was then coupled to 4-hydroxybenzaldehyde with a Williamson ether synthesis in the presence of potassium carbonate in 58% yield. Benzaldehyde **122** was then coupled to 2,4-dimethylpyrrole and then boron trifluoride diethyl etherate to yield the methyl ester-protected fluorophore **123**. The final step was to deprotect the methyl ester in the presence of LiOH to yield the free carboxylic acid **124**, primed for further modification.

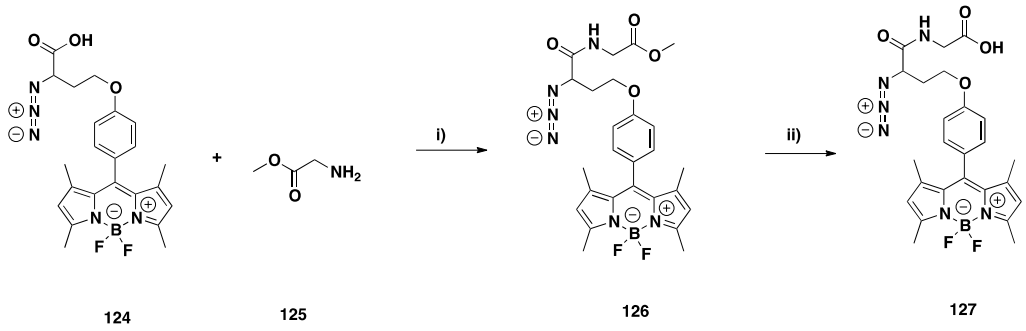

Scheme 3.11. i) DCM, HBTU, DIPEA, 3 hr. ii) LiOH, MeOH/H_2O, 12hr (95%).

The synthesis of a fluorophore with a terminal glycine residue began with the coupling of glycine methyl ester (**125**) to the fluorophore **124** in the presence of HBTU and DIPEA and then deprotected by aqueous LiOH in methanol to yield the carboxylic acid **127**.

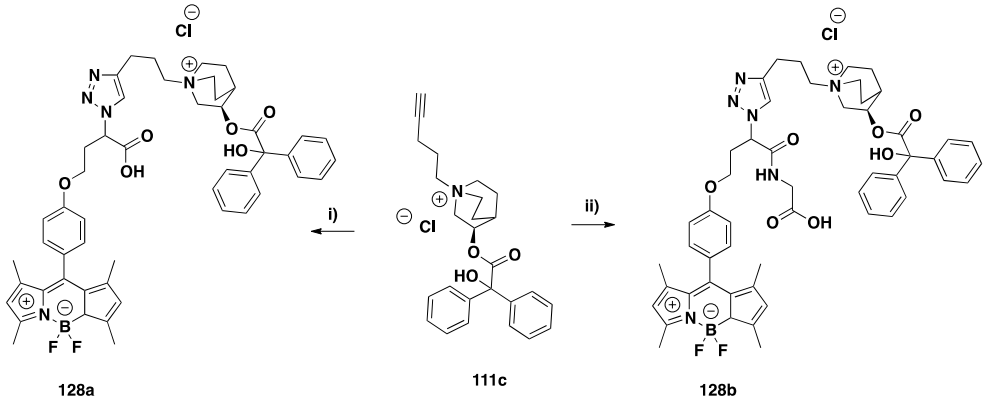

Scheme 3.12. i) 4,4-difluoro-8-(4-(2-azido-4-(4-formyl)phenoxy))phenyl-2,6-dimethyl-4-bora-3a,4-adiaza-s-indacene DMF/H_2O, $CuSO_4.5H_2O$, sodium ascorbate, MW 80 min, 80 °C, 40 W, (57%). ii) 4,4-difluoro-8-(4-(2-(2-azido-4-(4-formyl)phenoxy)butanamido))phenyl-2,6-dimethyl-4-bora-3a,4-adiaza-s-indacene, DMF/H_2O, $CuSO_4.5H_2O$, sodium ascorbate, MW, 80 min, 80 °C, 40 W, (47%).

The three polar fluorophores were coupled to **111c** to yield three novel fluorescent ligands.

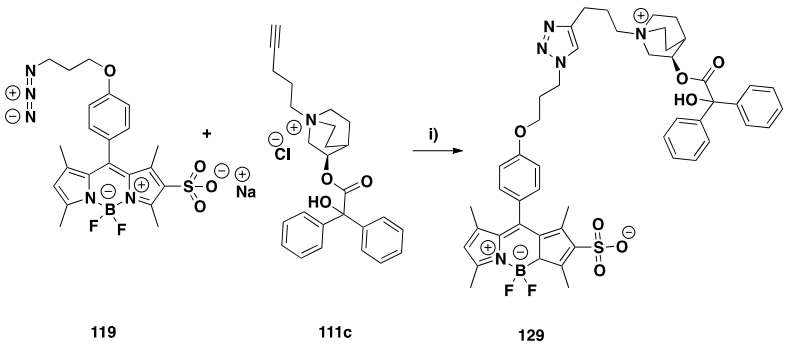

Scheme 3.13. i) DMF/H_2O, $CuSO_4.5H_2O$, sodium ascorbate, MW, 80 min, 80 °C, 40 W, (42%).

3.5.2 Pharmacology of polar ligands

The binding affinities of the three ligands with polar fluorophores were investigated to determine whether changes in the fluorophore's properties affects the receptor interaction.

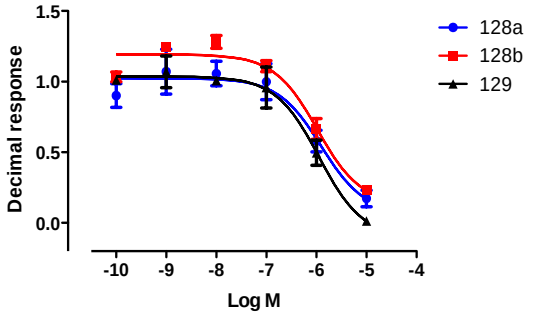

Figure 3.16. Inhibition of carbachol binding to whole CHO cells expressing the human M_3 cells by antagonists 128a-b and 129. Data points are mean ± s.e.m (triplicate determinations) from a single experiment which is representative of 3 separate experiments for each ligand. A concentration of 0.1 μM of carbachol was used in each experiment.

Compound	Log K_b (n=)
128a	-7.36 ± 0.12 (3)
128b	-7.04 ± 0.14 (3)
129	-7.26 ± 0.03 (3)

Table 3.5. Inhibition of carbachol binding to whole CHO cells expressing the human M_3 receptor induced by antagonists 128a-b and 129. K_i refers to the equilibrium dissociation constant and the values were calculated from the IC_{50} values. All values are expressed as mean value ± s.e.m of different experiments (n).

The introduction of a sulfonic acid group onto the fluorophore, making the compound neutral overall, resulted in some loss of activity. A reduction from −8.89 to −7.26 (Log K_b) suggests

that the overall positive charge of the compound is important for receptor interaction. With the insertion of a polar side chain, affinity is also reduced compared with the equivalent non-polar side chain ligand **108a**. These affinities are respectable for fluorescent ligands.

3.5.3. Confocal imaging of polar ligands

Ligands **128a-b** and **129** were evaluated by confocal microscopy. As ligand **129** has an overall neutral charge, pre-incubation with poly-L-lysine was not required.

Confocal images of **129** without the addition of poly-L-lysine show membrane specific binding. Figure 3.17 also shows that the binding is receptor specific as there is no fluorescence present when atropine is administered prior to antagonist addition.

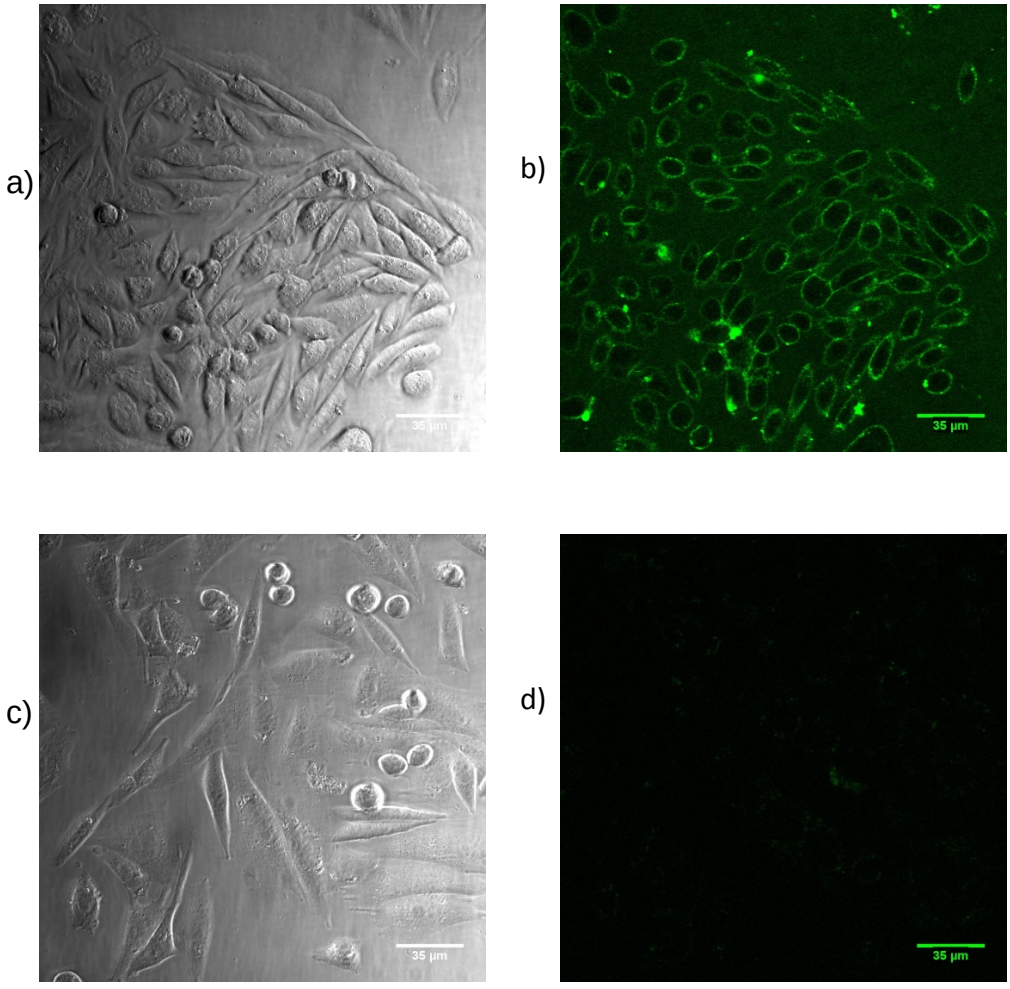

Figure 3.17. Visualisation of fluorescent antagonists (100 nM) on CHO M_3 cells. a) Transmitted light image taken at 0 min before the addition of 129 and b) appearance of 129 10 min after addition. c) CHO cells Preincubated with atropine (100 nM). Transmitted light image taken at 0 min before the addition of 129 and d) appearance of 129 10 min after addition with CHO cells preincubated with atropine (100 nM).

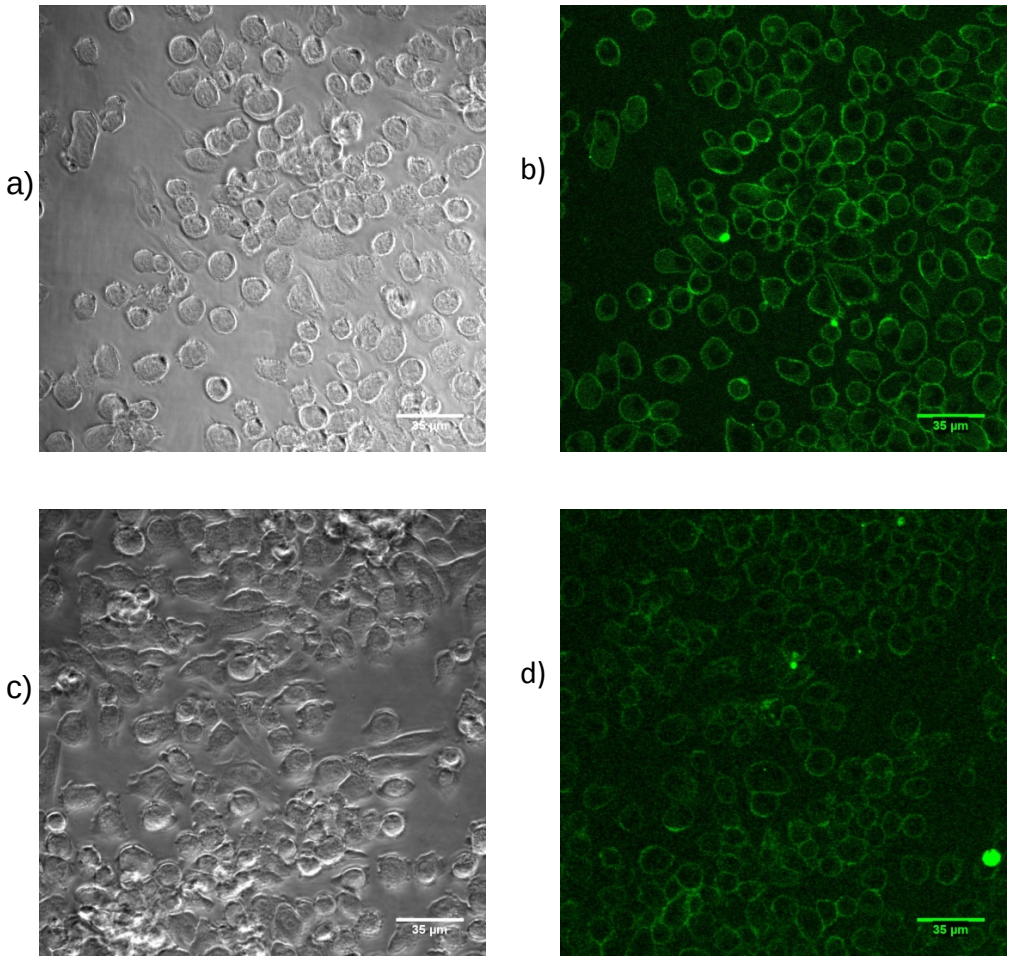

Figure 3.18. Visualisation of fluorescent antagonists (100 nM) on CHO M_3 cells preincubated with poly-L-lysine. a) Transmitted light image taken at 0 min before the addition of 128a and b) appearance of 128a 10 min after addition. c) Transmitted light image taken at 0 min before the addition of 128b and d) appearance of 128b 10 min after addition.

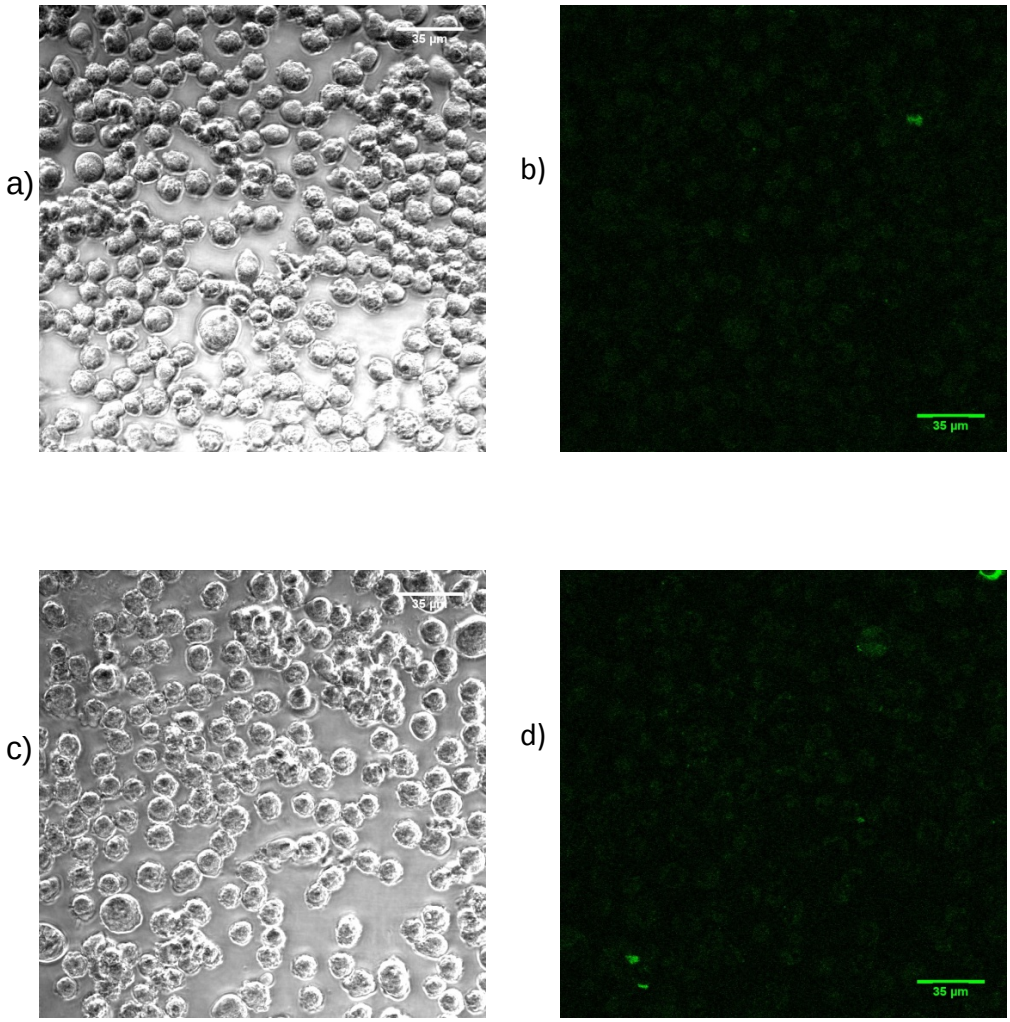

Figure 3.19. Visualization of fluorescent antagonists (100 nM) on CHO M_3 cells preincubated with poly-L-lysine and atropine (100 nM). a) Transmitted light image taken at 0 min before the addition of 128a and b) appearance of 128a 10 min after addition. c) Transmitted light image taken at 0 min before the addition of 128b and d) appearance of 128b 10 min after addition.

The polar-tailed ligands show good membrane binding in figure 3.18. Ligand **128b** showed minor background fluorescence, which is due to poor treatment of the glass with poly-L-lysine. Both ligands cannot be seen at the receptor when atropine has been administered prior to antagonist addition. Thus clearly showing that ligands **128a** and **128b** are receptor specific and not non-specific binding, identical to the ligands **114a–b** and **117a–b**.

3.5.4 Physicochemical properties of Polar ligands

The addition of a sulfonic acid, glycine residue or just a terminal carboxylic acid to the ligand will have an effect on the physicochemical properties of the ligand. All three ligands, **128a–b** and **123**, were investigated for changes in $CHI_{IAM\ 7.4}$ values.

Compound	$CHI_{IAM\ 7.4}$
111c	46.92
114a	60.11
128a	46.76
128b	47.09
129	44.04

Table 3.6. $CHI_{IAM\ 7.4}$ values of polar M_3 ligands, 111c, 114c, 128a-b and 129 calculated from HPLC methods using a Regis IAM PC 12 µm column (100 x 4.6mm), a flow rate of 1.00 mL/min and UV detection at 230 and 366 nm. Linear gradient 0 % - 100% solvent A over 7 min. Solvent A: 100% MeCN. Solvent B: Water with 50 mM ammonium acetate. $LogD_{7.4}$ values calculated by HPLC methods using a Polaris C_{18} 5 µm HPLC column (50 x 4.6mm). A flow rate of 1.00 mL/min and UV detection at 230 and 366 nm. Linear gradient 0 % - 95% solvent A over 4 min. Solvent A: 100% MeCN. Solvent B: Water with 50 mM ammonium acetate.

It is clear that with the addition of polar and charged groups to the fluorophore, $CHI_{IAM\ 7.4}$ values are improved and closer to the value of the parent ligand. With the charged sulfonic acid group attached to the ligand, the $CHI_{IAM\ 7.4}$ is reduced to below the value of the parent ligand, indicating less interaction with the membrane relative to the parent ligand. This result showed that it is possible to modify a ligand to have characteristics similar to the parent ligand, but unfortunately reduces the binding affinity of the ligand.

3.6 Receptor kinetics

With a range of novel high-affinity fluorescent M_3 ligands successfully synthesised, imaged and investigated at the physicochemical level, further investigation into the receptor kinetics could determine if association and dissociation rates are comparable to those of the parent ligand. This would give a greater profile of the fluorescent ligands synthesised to give a greater understanding of the introduction of a fluorophore and linker. Receptor association and disassociation rates are usually determined by either direct radiolabelling of the specific ligand of interest or in a competition-style assay with a radioligand specific for that receptor. Slow receptor dissociation kinetics have been implicated in the long clinical duration of action of some drugs.[166,167] Therefore, calculating the kinetic parameters of new ligands early in the drug discovery process may be beneficial to improved SAR information and drug action.

Investigation into whether the fluorescent ligands retain the kinetic properties of the parent ligand would be of interest in the development of fluorescent ligands.

3.6.1 Binding affinities for M_3 membranes

First, new IC_{50} and binding affinity values were calculated, as the binding kinetic studies are carried out on cell membranes and not whole cells. The affinities were determined by competitive displacement of the radioligand [^{3}H]-*N*-methyl scopolamine ([^{3}H]-NMS) from CHO membranes expressing the human M_3 receptor. Radioligand binding was performed as previously described by Dowling *et al.*[166] and cell membrane preparation was performed as previously described by Skyes *et al.*[37] At least three different experiments were conducted for each ligand in triplicate. The assays were run with a range of concentrations from 1×10^{-5} to 1×10^{-10} M for the fluorescent ligands and from 1×10^{-8} to 1×10^{-12} M for the parent ligand **104**, to produce dose–response curves. Each ligand was diluted to 10^{-2} M using DMSO and the stock solution was stored at −20°C until the ligand was tested.

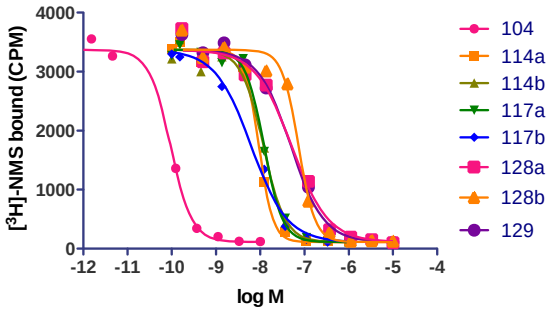

Figure 3.20. Inhibition of [^{3}H]-NMS binding to CHO membranes expressing the human M_3 receptor by antagonists 104, 114a-b, 117a-b, 128a-b and 129. Data points are mean ± s.e.m (triplicate determinations) from a single experiment which is representative of 3 separate experiments for each ligand. [^{3}H]-NMS was used at a concentration of 1 nM.

Compound	Log K_i (n=)
104	-11.36 ± 0.13 (3)
114a	-8.36 ± 0.04 (3)
114b	-8.32 ± 0 .04 (3)
117a	-8.12 ± 0.05 (3)
117b	-8.34 ± 0.06 (3)
128a	-7.26 ± 0.11 (3)
128b	-7.58 ± 0.08 (3)
129	-7.20 ± 0.18 (3)

Table 3.7. Inhibition of [^{3}H]-NMS binding to CHO membranes expressing M_3 receptors induced by antagonists 104, 114a-b, 117a-b, 128a-b and 129. K_i refers to the equilibrium dissociation constant and the values were calculated from the IC_{50} values. All values are expressed as mean value ± s.e.m of different experiments (n). [^{3}H]-NMS was used at a concentration of 1 nM.

Data from radioligand binding assays were used to calculate the IC_{50} values of the pharmacophores. These values were then used to calculate the binding affinities, K_i, using the Cheng–Prushoff equation:[141]

$$K_i = \frac{IC_{50}}{1 + \frac{[radioligand]}{K_D}}$$

where [radioligand] is the concentration of the free radioligand used in the assay and K_D is the dissociation constant of the radioligand for the receptor. IC_{50} is the concentration of the ligand that displaces 50% of the specific binding of the radioligand.

The binding affinities calculated from the radioligand binding experiments on cell membranes are similar to those calculated on whole cells by the intracellular calcium. The radioligand binding experiments are more accurate due to the longer incubation time of the antagonist, membrane and radioligand (3 hours). In the intracellular calcium assay, the antagonist was incubated with the cells and the agonist was added with a reading straight away not allowing for equilibrium to be reached.

Compound	Membrane Log K_i (n=)	Whole cell LogK_b (n=)
104	-11.36 ± 0.13(3)	Not tested
114a	-8.36 ± 0.04 (3)	8.89 ± 0.09 (3)
114b	-8.32 ± 0 .04 (3)	-8.02 ± 0.09 (3)
117a	-8.12 ± 0.05 (3)	-8.42 + 0.16 (3)
117b	-8.34 ± 0.06 (3)	-7.97 ± 0.07 (3)
128a	-7.26 ± 0.11 (3)	-7.36 ± 0.12 (3)
128b	-7.58 ± 0.08 (3)	-7.04 ± 0.14 (3)
129	-7.20 ± 0.18 (3)	-7.26 ± 0.03 (3)

Table 3.8. Comparision of binding affinities of antagonists 104, 114a-b, 117a-b, 128a-b and 129. All values are expressed as mean value ± s.e.m of different experiments (n).

3.5.2 Receptor Kinetic experiments

With the IC_{50} values calculated, it was possible to calculate the association and disassociation rates. First, the observed dissociation rate (k_{off}) of radioligand [^{3}H]-NMS was required and then the association rate (k_{on}) of the radioligand [^{3}H]-NMS was calculated. Finally, the kinetics of the unlabelled antagonist were investigated. Kinetic experiments were carried out on seven fluorescent ligands and the parent ligand in table 3.14. Kinetic experiments of unlabelled antagonists and radiolabelled [^{3}H]-NMS were performed as previously described by Dowling *et al.*[166] Approximately 1 nM [^{3}H]-NMS was added with fluorescent ligand (at t = 0) to CHO M_3 membranes in 500 mL of assay buffer and then membrane was added at each time point in separate wells. The degree of [^{3}H]-NMS bound to the receptor was assessed at multiple time points by filtration harvesting and liquid scintillation counting. Three different concentrations of fluorescent ligand were tested to ensure the rate parameters calculated were independent of ligand concentration. All compounds were tested at 3-, 10- and 30-fold of the K_i. Data were interpreted according to Sykes *et al.*[37]

First, the $t_{½}$ was calculated for [^{3}H]-NMS. In one half-life, half of the radioligand will have dissociated from the receptor, whereas in two half-lives, three-quarters of the radioligand will have dissociated, etc. Dissociation data were fitted to a single-phase exponential decay function and the $t_{½}$ value obtained was transformed into a k_{off} rate using the following

equation:

$$k_{off} = \frac{0.963}{t_{\frac{1}{2}}}$$

It was found that [^{3}H]-NMS had a k_{off} equal to 0.015 ± 0.0004 min^{-1}. It was possible to calculate the k_{on} as the observed association rate of a ligand is dependent upon its concentration, k_{on} and k_{off} values. This was possible by constructing a family of association curves using a range of radioligand concentrations. [^{3}H]-NMS association data were fitted to a single-phase exponential association function to calculate an observed rate constant, k_{ob}. The association rate constant, k_{on}, was calculated using the following equation, as described originally by Hill:[174]

$$k_{on} = \frac{(k_{ob} - k_{off})}{[Radioligand]}$$

where the k_{off} value used was predetermined from dissociation rate experiments.

K_i could be calculated by the following equation:

$$K_i = \frac{k_{off}}{k_{on}}$$

The association (k_3) and disassociation rate (k_4) for the fluorescent ligands were calculated in line with Sykes *et al.*[37]

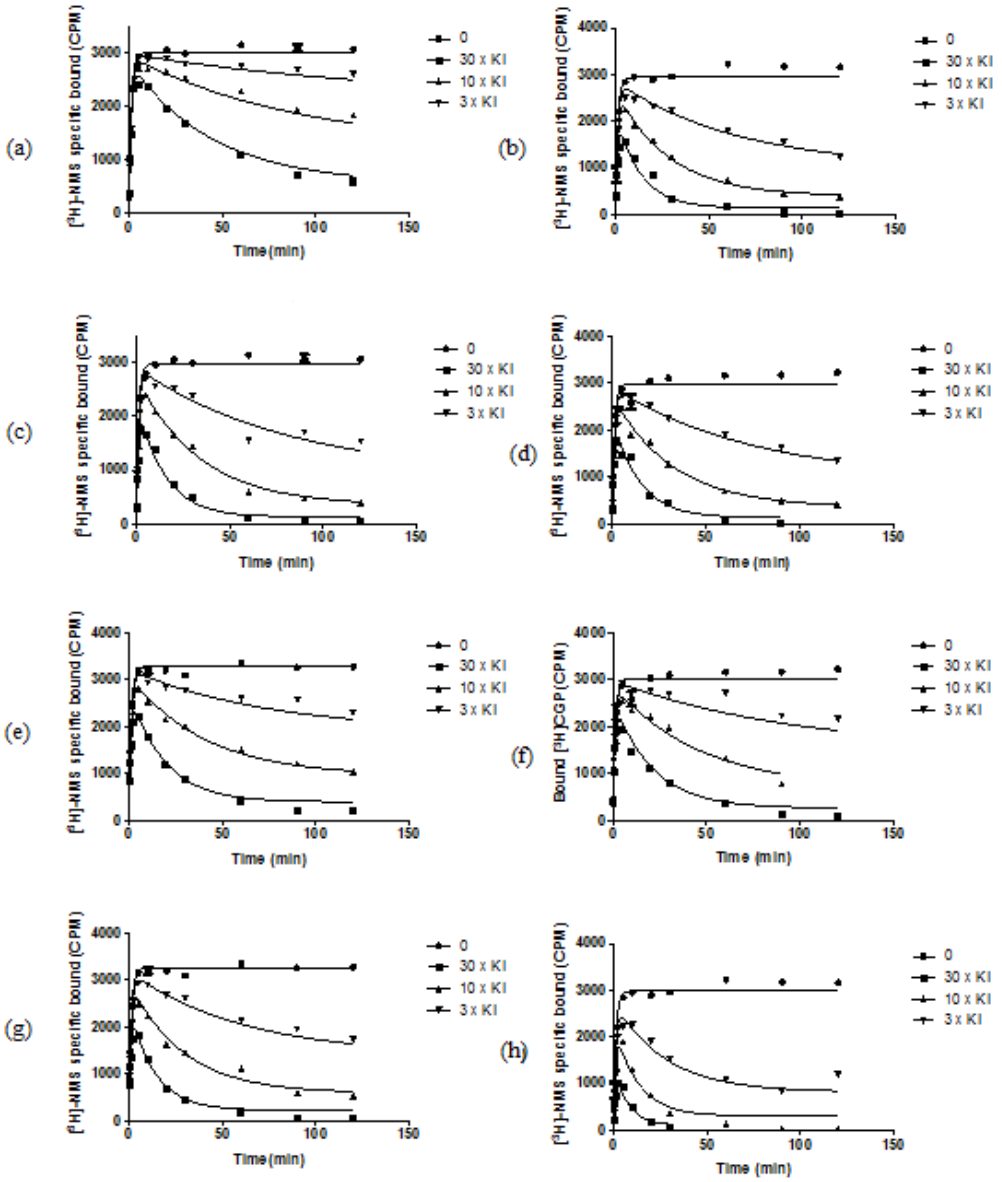

Figure 3.21. [^{3}H]-NMS Competition kinetics curves in the presence of 104 (a), 117a (b), 114a (c), 128a (d), 114b (e), 128b (f), 117a (g) and 129 (h). CHO-M_3 cell membranes were incubated with ~1 nM [^{3}H]-NMS and either 0, 3-fold Ki, 10-fold Ki or 30-fold Ki. Plates were incubated at room temperature for the indicated time points and non specific binding levels determined in the presence of 5 μM atropine from a single experiment, which is representative of 3 separate experiments for each ligand.

Ligand	K_{on} $M^{-1}min^{-1}$ (k_3)	K_{off} min^{-1} (k_4)	Kinetic K_i (n=)	Competition K_i (n=)
104	9.86 ± 1.7 x 10^6	0.0017 ± 0.0004	-11.33 ± 0.02 (3)	-11.36 ± 0.06 (3)
114a	2.67 ± 27 x 10^6	0.0052 ± 0.0014	-8.72 ± 0.07 (3)	-8.36 ± 0.04 (3)
114b	1.69 ± 19 x 10^6	0.0060± 0.0014	-8.45 ± 0.07 (3)	-8.22 ± 0.04 (3)
117a	1.22 ± 11x 10^6	0.0062 ± 0.0021	-8.31 ± 0.10 (3)	-8.12 ± 0.05 (3)
117b	2.33 ± 21 x 10^6	0.0061 ± 0.0021	-8.62 ± 0.01 (3)	-8.43 ± 0.06 (3)
128a	2.19 ± 0.5 x 10^5	0.0068 ± 0.0019	-7.50 ± 0.06 (3)	-7.20 ± 0.18 (3)
128b	1.28 ± 16 x 10^5	0.0045 ± 0.0020	-7.49 ± 0.14 (3)	-7.26 ± 0.12 (3)
129	3.28 ± 51 x 10^5	0.0021 ± 0.0004	-7.72 ± 0.09 (3)	-7.58 ± 0.07 (3)

Table 3.9. Binding affinity values and kinetically derived parameters for M_3 antagonists.

From the kinetic experiments, the association and dissociation rates were calculated for seven fluorescent M_3 ligands and the parent ligand. The kinetic data also give a K_d value, which in comparison to the competition assay K_i are extremely similar. An excellent correlation was observed ($R^2 = 0.99$).

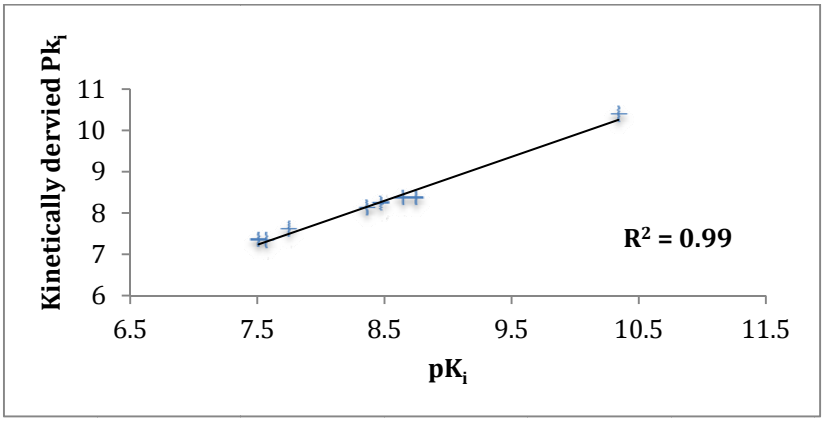

Figure 3.22. Correlation between competition calculated K_i and kinetically derived K_D for the eight test antagonists. K_i values were taken from [^{3}H]-NMS competition binding experiments at equilibrium. The values comprising the kinetically derived K_D (k_{off}/k_{on}).

The association rates are slightly slower than that of the parent ligand, which is believed to be due to steric interaction of the fluorescent moiety inhibiting the movement of the ligand. Interestingly, the change in lipophilicity has an effect on the association rates. The ligands that

can be directly compared are **114a**, **114b**, **128a**, **128b** and **129**. These ligands contain the same pharmacophore and different fluorophores based on a similar BODIPY core. Comparison of the two types of fluorophore, fluorophores with the polar tailed fluorophore and non-polar tailed fluorophore. Between these two types there is a shift of one log unit in association rates. The ligands containing a polar-tailed dye have a lower CHI $AIM_{7.4}$ in comparison to the ligands without the polar tail and the reduced association rate is believed to be dependent on local concentration modulation. Ligands with larger CHI $AIM_{7.4}$ values will be located around the membrane, causing a higher concentration around the receptor, which will result in a faster association rate.

The dissociation rates of the ligands are similar throughout the antagonists tested, including the parent ligand. This result could be because the fluorescent ligand has the same binding interaction to the receptor and that the fluorescent group is not interacting with the binding site or interfering with binding. If this is the case, it could be expected that the dissociation rates would be faster than for the parent ligand, due to weaker interactions. Comparison of the novel fluorescent ligand association and dissociation rates to known and therapeutically used M_3 antagonists, the fluorescent ligands dissociate much slower than atropine (0.27 min^{-1}), *N*-methyl scopolamine (0.017 min^{-1}) and ipratropium (0.07 min^{-1}).[166] Tiotropium is a long-duration, slow-dissociation muscarinic M_3 antagonist[167] with a k_4 value of 0.0015 min^{-1}, which is very similar to the fluorescent ligands shown in figure 3.21.[166] The association rates of the fluorescent ligands in figure 3.15 are slower than those of atropine (1.5×10^{-9} $M^{-1}min^{-1}$), tiotropium (1.58×10^{-8} $M^{-1}min^{-1}$) and the parent ligand.

3.7 Conclusions

A range of novel fluorescent M_3 antagonists have been successfully synthesised utilising the alkyne-azide copper (I) cycloaddition "click" reaction. 19 fluorescent were assessed with a single point concentration inhibition study. From this result four fluorescent ligands were deemed to be of interest after an initial screening process and these ligands were studied pharmacologically.

From the initial screen, there was a wide variety of inhibition from the fluorescent ligands. It was apparent that the longer wavelength fluorophores did not result in high affinity ligands.

Small chained linkers were not favoured, both one carbon and two carbon linkers gave poor inhibition responses, the best one carbon chain fluorescent ligand gave 20% inhibition while the best two carbon chain linker gave 60%. The amide linker was not favoured with an average inhibition of 40% and four carbon linkers were reasonable with an average of 50% inhibiton. The most favoured linkers to use were the non branched three carbon linker and the para-phenyl linkers with over 90% inhibition in four of the ligands, two with each linker.

Four ligands had IC_{50} values and binding affinities calculated giving a range of log K_b values from -7.97 ±0.16 to -8.89 ± 0.11 calculated by the functional calcium assay.

During this investigation, three ligands based on the highest affinity ligand (**114a**, log K_b -8.89) were synthesised to include either a polar side chain or a sulfonic acid group on the fluorohpore for investigation into lipophilicity. The binding affinity values decreased by at least 10-fold to give a range of log K_b values from -7.04 ± 0.14 to -7.36 ± 0.12.

The physicochemical properties of all the ligands synthesised were assessed by log D and CHI $_{AIM}$ HPLC analysis. Attachement of the fluorophore to the pharmacophore had the same effect that was shown in chatper 2. An increase in both CHI AIM values and log D values were significant. A change from 46.92 to 60.11 in CHI AIM for the most potent fluorescent ligand and its alkyne functionalised pharmacophore. A change in log D from 1.67 to 3.59 was also observed and all fluorescet ligands followed this trend with similar values. The insertion of a sulfonate group to the fluorophore (ligand **129**) or a polar side chain in the fluorophore linker (ligands **128a** and **128b**) did reduce the CHI $_{AIM}$ values back to the original pharmacophore profile (46.92) with values of 44.04 for **129**, and 47.09 and 46.76 for the polar side chain fluorophores. Thus showing it is possible to have a fluorescent ligand with the similar physicochemical properties of the parent ligand.

The seven ligands with binding affinity values and physicochemical properties profiled were imaged confocally. The confocal images showed membrane specific binding that could be inhibited by pre-incubation with atropine.

The association and dissociation rates of the ligands were investigated. It was shown that the fluorescent ligands had a slower association rate in comparison to the parent ligand. Within the

fluorescent ligands, the polar-tailed ligands had a lower association rate, which is believed to be due to modulation of the local concentration due to lipophilicity of the ligands. The dissociation rates of the ligands were comparable to that of the parent ligand and tiotropium, which is a long-duration, slow-dissociation muscarinic M_3 antagonist. With dissocation rate of the fluorescent ligands similar to that of the parent ligand, this shows that the fluorescent ligand has similar binding interactions of that parent pharmacophore and the properties of the fluorescent molecules are comparable to that of congener.

This chapter has shown that it is possible to synthesise fluorescent ligands that have properties highly comparable to those of the parent ligand without a major effect on the binding and receptor interaction.

3.7.1 Future Work

With several fluorescent antagonists for the M_3 receptor being synthesised and highly characterised, future work could consist of developing fluorescent-based assays using the ligands. Assays that could be developed would include fluorescent polarisation, fluorescent competition binding assays and kinetic assays using fluorescent ligands instead of radioligands.

Other future work could consist of developing ligands for another GPCR receptor type. Utilising the results from the two chapters to build ligands and use them in protocols that could eventually be used in a medium-throughput environment.

Since this research has been carried out, a crystal structure of the muscarinic M_3 receptor from *rattus norvegicus*. has been published.[159] This receptor has the known antagonist tiotropium bound and gives insight into the binding position of this ligand, and could result in a better fluorescent ligand to be synthesised. Comparisons could be made with between the bound ligand and the fluorescent ligands evaluated in this chapter.

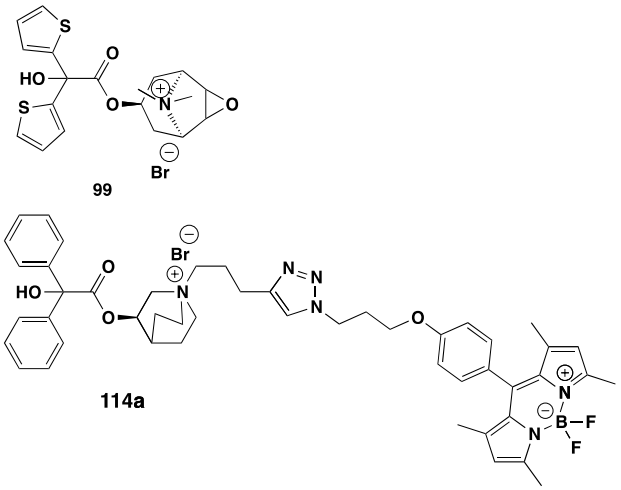

Figure 3.24 Structure of tiotropium bromide (**99**) and fluorescent ligand **114a**

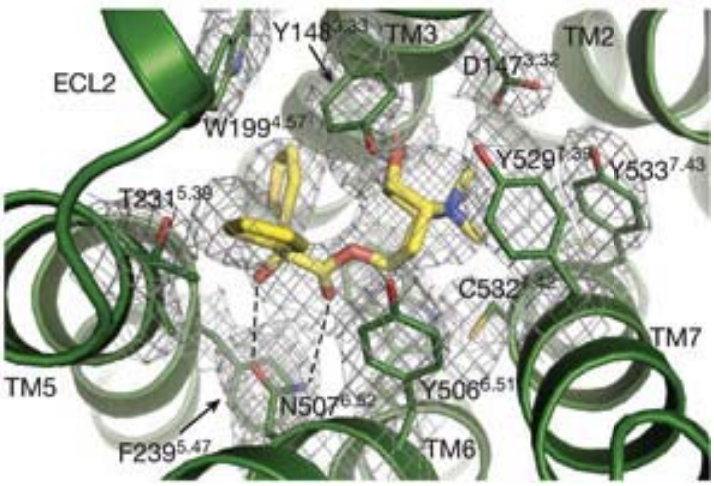

Figure 3.25 Crystal structure of the *rattus norvegicus* M_3 receptor with Tiotropium bound. **Source:** Kruse *et al*, *Nature* 2012, *482*, 552-556.[159]

The x-ray crystal structure shown in figure 3.25 shows that tiotropium, **99**, is bound within a tightly closed pocket formed from TM2, TM3 and TM7. If the binding model shown in the x-ray crystal structure is applicable to the fluorescent ligands described in this chapter the fluorophore and linker are directed into the closed pocket. The surface projection in figure 3.26. shows that there is little space within the pocket to accommodate the fluorophore and linker.

It may be possible to increase the binding affinity by moving the connection between the fuorophore and pharmacophore from the quaternary nitrogen to the primary alcohol. This may allow the pharmacophore portion of the ligand to adopt a more favourable orientation within the active site of receptor, as the current linker position would not allow the pharmacophore to bind in a similar manor to tiotropium.

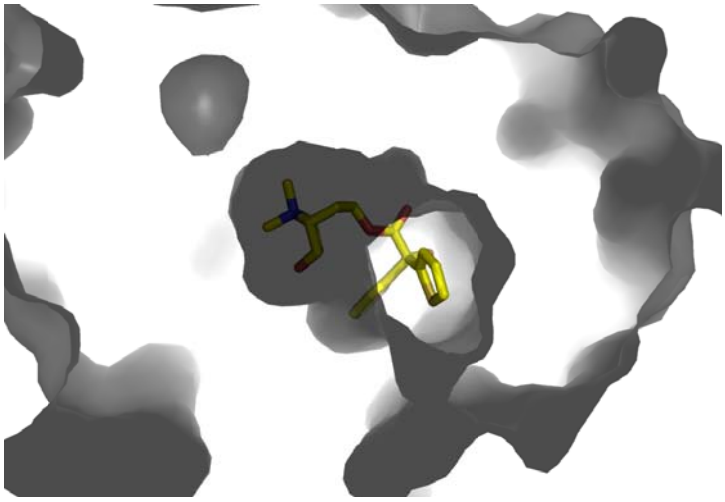

Figure 3.26. X ray crystal structure of tiotropium bound into the active site of the Muscarinic M_3 receptor. Protein surface projection is shown in grey and tiotropium shown in yellow. **Source:** Kruse *et al*, *Nature* 2012, *482*, 552-556.[159]

It is clear that there is a small channel leading to the binding site that could accommodate the fluorescent moiety and linker of the ligand. This is shown in figure 3.26 and 3.27.

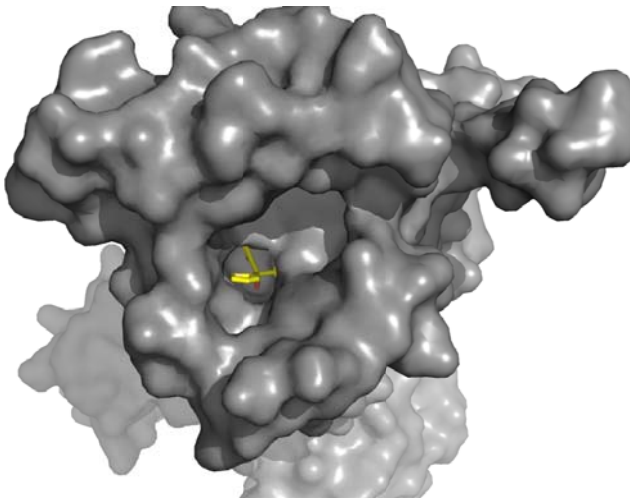

Figure 3.27. X ray crystal structure of tiotropium bound into the active site of the Muscarinic M_3 receptor. Protein surface projection is shown in grey and tiotropium shown in yellow. **Source:** Kruse *et al*, *Nature* 2012, *482*, 552-556.[159]

This pocket could allow the fluorescent moiety and linker to sit out of the active site and improve binding interaction of the fluorescent ligand. Future work could include molecular modeling to assess this hypothesis of the binding interactions of the fluorescent ligand. Further synthesis of a new fluorescent ligand, such as ligand **130**, would give experimental data to whether a different orientation of the fluorophore and linker is favoured.

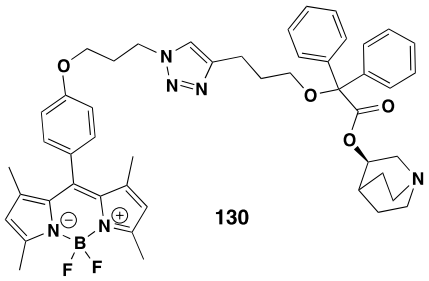

130

Figure 3.28. Structure of a possible fluorescent ligand with an alternative fluorophore orientation.

4. Conclusion and Future work

This chapter is not intended to replace the individual conclusions within each chapter, but to complement them by pulling findings together from each chapter. It will also set out plans for future work.

4.1. Click Chemistry

Fluorescently tagging a biologically active molecule through alkyne-azide copper (I) cycloaddition click reaction was successful at both receptor types. It is widely accepted that click reactions require the reaction to have certain properties: give very high yields, isolation by non-chromatographic methods and use a solvent that is easily removed for example.[88] Clearly these properties are not shown in this work but in the context of this thesis, properties of this reaction were exploited to yield a final step reaction that was quick, reproducible and direct. The alkyne-azide copper (I) cycloaddition has yielded a range of fluorescent ligands with fluorophores that can be connected to other alkyne or azide functionalised molecules which do not need protecting groups being removed or added for tethering.

4.2 Linker Length

At both receptor types linker length before and after the triazole had a large impact on the binding affinities of the ligand, primarily due to steric interactions. At both receptor types a short linker between the pharmacophore and triazole were not tolerated and longer linkers between the fluorophore and triazole not well tolerated either. Combining both gives a narrow region for incorporating the triazole in between the fluorophore and pharmacophore. A range of 11 to 13 atoms between the pharmacophore and fluorophore has given the best ligands with the triazole situation in the middle containing atoms 5-7 for both receptor types.

4.3 Fluorophore Selection

A range of fluorophores (**46**, **48**, **61**, **65**, **85**, **119**, **124** and **127**) were synthesised and coupled to the pharmacophores. These fluorophores had different influences on each ligand on a whole with a range of effect on receptor interaction and physicochemical properties. With the beta-adrenoceptors the shorter wavelength fluorophores (**46**, **48**, **61** and **65**) gave ligands with good

affinity but when examined under confocal microscopy intracellular accumulation was detected. Beta-adrenoceptors with the longer wavelength fluorophore (**85**) resulted in reduced affinity and no intracellular accumulation when examined with confocal microscopy. On the other hand the M_3 ligands with the shorter wavelength fluorophores were well tolerated in confocal microscopy with no internalisation and producing the greater binding affinities while the red shifted dye had poor interaction with the receptor with no investigation with confocal microscopy.

The fluorophore clearly has an effect on the physicochemical properties of the ligand and selection of a fluorophore is extremely important when designing a fluorescent ligand. Using software that predicts $Clog_P$ values could be beneficial when designing a fluorescent ligand to reduce the lipophilic nature of the ligand. The benefit of azide or alkyne functionalised fluorophores, incorporating them onto a drug is a simple one step reaction while other fluorophores use amide bonds for tethering, protecting groups would be needed if coupling the polar tailed fluorophores.

4.4 Future Work

Firstly future work would include the development of the beta-adrenoceptor fluorescent ligands with the coupling of pharmacophore **56c** with the polar tailed fluorophores **124** and **127** and the sulfonic acid fluorophore **119** to investigate whether this would stop intracellular accumulation. An improved synthetic scheme for the red shifted fluorophore **85** would be addresses as this synthesis was capricious. Some steps would be poor yielding or would not yield product. Once this is addressed physicochemical analysis could be carried out and help determine how the red shifed dye **85** does not become internalised unlike all the other beta adrenoceptor ligands.

Assay development using the M_3 fluorescent ligands synthesised in chapter 3 as they have shown great potential to be used in a range of assays that could include competition binding assays and FP assays. Utilising these ligands in a routine drug discovery programme would highlight the benefits to fluorescent ligands in replacement of radioligands.

Finally developing the technique used through this work to develop a range of fluorescent ligands at another GPCR to validate the method and to provide a basic protocol for synthesising fluorescent ligands for GPCRs on a whole. Such protocols could give a basic linker length and fluorophore as a starting point for fluorescent ligand synthesis with only small modifications need to get a usable fluorescent ligand.

5. Experimental

All chemicals and solvents were obtained from commercial suppliers and used without further purification. Thin-layer chromatography (TLC) was done using precoated aluminium backed plates (Silica gel 60F 254 plates) purchased from Merck. Flash Chromatography was performed using E. Merck Kieselgel silica gel 60 (230-440 mesh, 0.040-0.063 mm). TLC plate visualisations were examined under UV light (256 & 366 nm). General staining carried out with ninhydrin and potassium permanganate. All organic extracts after aqueous work-up procedures were dried with Na_2SO_4 before gravity filtering and evaporation to dryness. Organic solvents were evaporated under reduced pressure at ≤ 40°C (water bath temperature). Melting point was recorded on a Reichert 7905 apparatus. Mass spectra (TOF ES +/-) were recorded on a waters 2795 separation module/micromass LCT platform. Avatar 360 Nicolet FT-IR spectrometer was used to record FT-IR spectra on KBr discs and NaCl plates in the range of 4000-500 cm^{-1}. ^{1}H-NMR spectra were recorded on a Bruker-AV 400 at 400.13 MHz and ^{13}C-NMR was recorded at 101.62 MHz. Chemical shifts (δ) were obtained in ppm with reference to the chemical shift of the deuterated solvent. Coupling constants (*J*) are recorded in Hz and the significant multiplicities described by singlet (s), doublet (d), triplet (t), quartet (q), multiplet (m), doublet of doublets (dd), and broad (br). Unless otherwise stated all spectra were recorded in $CDCl_3$.

Analytical HPLC was performed using system 1 and system 2 to confirm purity. All retention times (Rt) are quoted inminutes.

System 1: YMC reverse phase C8 column (150 x 4.6mm), a flow rate of 1.00 mL/min and UV detection at 254 and 366 nm. Linear gradient 5% - 95% solvent B over 16 min. Solvent A: 0.06% TFA in water; solvent B: 0.06% TFA in MeCN.

System 2: Kromasil reverse phase C18 column (250 x 4.6 mm), a flow rate of 1.00 mL/min and UV detection at 254 and 366 nm. Linear gradient 5% - 95% solvent B over 16 min. Solvent A: 0.06% TFA in water; solvent B: 0.06% TFA in MeCN.

System 3: YMC reverse phase C8 column (150 x 4.6mm), a flow rate of 1.00 mL/min and UV detection at 254 nm and 366 nm. Samples were run in isocratic 40% solvent A - 60% solvent B over 16 min. Solvent A: 0.06% TFA in water; solvent B: 0.06% TFA in MeCN.

System 4: YMC reverse phase C8 column (150 x 4.6mm), a flow rate of 1.00 mL/min and UV detection at 254 nm and 366 nm. Samples were run Linear gradient 20% - 95% solvent B over 25 min. Solvent A: 0.06% TFA in water; solvent B: 0.06% TFA in MeCN.

Preparative HPLC was performed using system 5 and 6. All retention times (Rt) are quoted in minutes.

System 5: Luma reverse phase C8 column (150 x 30 mm), a flow rate of 20.00 mL/min and UV detection at 254 nm and 366 nm. Samples were run in 5% - 95% solvent B over 16 min. Solvent A: 0.06% TFA in water; solvent B: 0.06% TFA in MeCN.

System 6: YMC reverse phase C8 column (150 x 10 mm), a flow rate of 3.00 mL/min and UV detection at 254 nm and 366 nm. Samples were ran in 40% solvent A 60% solvent B isocratic over 20 min. Solvent A: 0.06% TFA in water; solvent B: 0.06% TFA in MeCN.

CHI IAM $_{7.4}$ HPLC method: Regis IAM PC 12 μm column (100 x 4.6mm), a flow rate of 1.00 mL/min and UV detection at 230 and 366nm. Linear gradient 0 % - 100% solvent A over 7 min. Solvent A: 100% MeCN. Solvent B: Water with 50 mM ammonium acetate.

Log D $_{7.4}$ HPLC method: Polaris C_{18} 5 μm HPLC column (50 x 4.6mm). A flow rate of 1.00 mL/min and UV detection at 230 and 366nm. Linear gradient 0 % - 95% solvent A over 4 min. Solvent A: 100% MeCN. Solvent B: Water with 50 mM ammonium acetate.

General procedure 1, alkyne-azide copper (I) catalysed cycloaddition

Azide functionalised compound (1 equiv) and alkyne functionalised compound (1eq) were dissolved in DMF (2 mL). Sodium ascorbate (0.1 eq) dissolved in water (1 mL) and copper sulfate pentahydrate (0.05 eq) dissolved in water (1 mL) was added to the DMF. The resulting mixture was microwaved for 80 minutes at 80 °C and 40 watts. When the reaction was complete, the solvents were evaporated under vacuum and the residue was dissolved in DCM. This was washed with water, filtered, dried and concentrated. The product was purified using reverse phase HPLC using either system 3 or 4.

General procedure 2, alkylation of (3*R*)-1-azabicyclo[2.2.2]oct-3-yl hydroxy(diphenyl)acetate

(3*R*)-1-azabicyclo[2.2.2]oct-3-yl hydroxy(diphenyl)acetate was dissolved in acetonitrile:chloroform (4:6). Linkers were added in 10 equivalents and refluxed overnight. When the reaction was complete the solvents were evaporated. The residue was suspended in ether (20 mL) and extracted with water (3 × 10 mL). The aqueous layer was evaporated to yield the alkyne-linked pharmacophores.

Synthesis of 1-(2,3-epoxypropoxy)- naphthalene[64] 27a

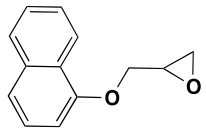

Sodium hydride (60% dispersion in mineral oil) (308 mg 12.7 mmol) was suspended in anhydrous DMF (7 mL) and stirred under an environment of nitrogen for five minutes. A solution of 1-naphthol (1.0 g, 6.9 mmol) and anhydrous DMF (7mL) was added to the sodium hydride drop wise in an ice bath and stirred for 20minutes. Epichlorohydrin **26** (1.8 mL, 23.3 mmol) was added dropwise into the solution and was stirred overnight at ambient temperature. The solution was quenched cautiously with methanol and partitioned between a large excess of water (60 mL) and was extracted with diethyl ether (3 × 30 mL). The organic layer was washed with 2M sodium hydroxide, dried and concentrated.

A silica plug was performed with ethyl acetate: petroleum ether (1:9) for purification to yield the product as a clear oil (760 mg, 83%).

^{1}H NMR: δ 2.86 (1H, dd, *J* 2.5, 5.0, epoxide CH_2), 2.97 (1H dd, *J* 4.0, 4.5, epoxide CH_2), 3.50 (1H, m, Epoxide CH), 4.16 (1H, dd, *J* 5.5, 11.0, OCH_2), 4.40 (1H, dd, *J* 3.0, 11.0, OCH_2), 6.82 (1H, d, *J* 7.5, ArH), δ 7.36 (1H, t, *J* 7.5, ArH), δ 7.44-7.52 (3H, m, ArH), δ 7.8 (1H, m, ArH), δ 8.31 (1H, m, ArH).

^{13}C NMR: 44.78 (Epoxide CH_2), 50.30 (Epoxide CH), 69.05 ($ArOCH_2$), 105.11 (naphthyl C), 120.93 (naphthyl C), 122.10 (naphthyl C), 125.39 (naphthyl C), 125.39 (naphthyl C), 125.58 (naphthyl C) 126.57 (naphthyl C), 127.52 (naphthyl C), 134.61 (naphthyl C), 154.58 (naphthyl C).

FT-IR: (NaCl) 3053 (Epoxide CH), 2925, 2871, 1594, 1509 (aryl str), 1240 (epoxide C-O, str) 1099 (C-O-C).

Synthesis of 2-((4-(2-methoxyethyl)phenoxy)methyl)oxirane[175] 27b

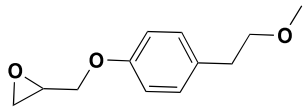

Sodium hydride (60% dispersion in mineral oil) (693 mg, 28.7 mmol) in anhydrous DMF (25 mL) was stirred under nitrogen for five minutes. To this solution 4-(2-methoxyethyl)phenol (3.5 g, 21 mmol) in anhydrous DMF (20 mL) was added. This was left to stir in an ice bath for 20minutes. Epichlorohydrin **26**, (18 mL, 233.1 mmol) was added dropwise and the solution was left to stir overnight at ambient temperature. The solution was the quenched with methanol. Water (50 mL) and diethyl ether (50 mL) was added to and the organic layer was separated and extracted three times with diethyl ether (50 mL). The organic layer was washed with 2M sodium hydroxide, dried and concentrated. The product was then washed through a silica plug in DCM:MeOH (9:1) yielding a yellow oil (2.81 g, 64%).

^{1}H NMR: δ 2.74 (1H, dd, *J* 2.5, 5.0, Epoxide CH_2), 2.82 (2H, t, *J* 7.0, $OCH_2\underline{CH_2}$), 2.89 (1H, dd, *J* 4.5, 5.0, Epoxide CH_2), 3.31 (3H, s, OCH_3), 3.34 (1H, m, epoxide CH), 3.63 (2H, t, *J* 7.0, OCH_2), 3.94 (1H, dd, *J* 5.5, 10.5, OCH_2), 4.21 (1H, dd, *J* 3.0, 10.5, OCH_2) 6.85 (2H, d, J 8.5, ArH), 7.13 (2H, d, J 9.01, ArH).

^{13}C NMR: δ 35.33 ($\underline{CH_2}CH_2O$), 44.71 (Epoxide CH_2), 50.24 (OCH), 58.74 (OCH_3), 68.80 ($OC\underline{H_2}CH$), 73.86 ($\underline{CH_2}OCH_3$), 114.62 (ArCH), 129.82 (ArCH), 131.70 (ArC), 157.03 ($\underline{ArC}O$).

FT-IR: (NaCl) (Epoxide CH), 2597, 1722, 1512 (aryl str), 1242 (epoxide C-O, str) 1112 (C-O-C).

Synthesis of 2-azidoethanamine 29 [176]

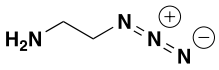

2-Bromoethylamine hydrobromide **28**, (2.5 g,12.3 mmol) and sodium azide (2.38 g, 36.6 mmol) were dissolved in water (10 mL), the reaction mixture was stirred at reflux for 21 hours.

The solution was cooled to 0 °C and diethyl ether (10 mL) and potassium hydroxide (4 g, 71.1 mmol) was added. The organic phase was separated with diethyl ether (3 × 20 mL), dried and concentrated to yield a clear oil (0.97 g, 94%). The product was used without further purification.

^{1}H NMR: δ 1.38 (2H, s, Br, NH_2), 2.82, (2H, t, *J* 5.5, CH_2N_3), 3.36 (2H, t, *J* 5.5, CH_3NH_2).

^{13}C NMR: δ 41.41 (CH_2NH_2), 54.73 (CH_2N_3).

FT-IR: (NaCl) 3476 (br NH stretch), 2077 (N_3) 1599, 1446 1282.

Synthesis of 1-(2-azidoethylamino)-3-(naphthalen-5-yloxy)propan-2-ol 30a

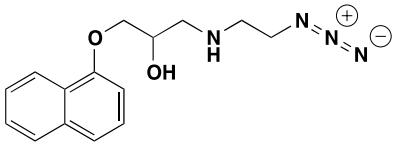

1-(2,3-Epoxypropoxy)- naphthalene **27a** (200 mg, 1 mmol) and 2-azidoethanamine **29** (516 mg, 6 mmol) were dissolved in isopropanol (10 mL) and refluxed for 12 hours at 60 °C. The reaction mixture was cooled to room temperature and concentrated. The residue was purified by column chromatography with MeOH: DCM (5:95) to yield a yellow solid (92 mg, 32%).

^{1}H NMR: δ 2.28 (1H, Br S, NH), 2.88-3.0 (4H, m, $\underline{CH_2}NHCH_2\underline{CH_2}N_3$), 3.45 (2H, t, *J* 5.5 $CH_2NH\underline{CH_2}$), 4.19 (3H, m, $O\underline{CH_2}\underline{CH}OH$), 6.84 (1H, d, *J* 7.5, ArH), 7.36 (1H, t, *J* 7.5, ArH), 7.44-7.52 (3H, m, ArH), 7.80 (1H, m, ArH), 8.30 (1H, m, ArH).

^{13}C: NMR δ 48.68 (CH_2N_3), 51.44 (CH_2NH), 51.79 ($NHCH_2$), 68.6 (CHOH), 70.51 (OCH_2), 104.99 (Naphthyl C2), 120.75 (naphthyl C), 121.75 (naphthyl C), 125.31 (naphthyl C) 125.54 (naphthyl C), 125.82 (naphthyl C), 126.47 (naphthyl C), 127.57 (naphthyl C), 134.53 (naphthyl C), 154.25 (naphthyl C).

Mpt: 135-136 °C.

FT-IR: (KBr) 3067(NH str), 2926 (OCH_2 sym str), 2127 (N_3), 1580, 1397.

ES-MS MH+ calc. For $C_{15}H_{19}N_40_2$ 287.1503 found 287.0657.

Synthesis of 1-(2-azidoethylamino)-3-(4-(2-methoxyethyl)phenoxy)propan-2-ol 30b

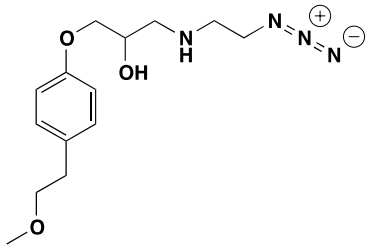

2-Azidoethanamine (992 mg, 11.52 mmol) **29** and 2-((4-(2-methoxyethyl) phenoxy) methyl) oxirane **27b** (400 mg, 1.92 mmol) were dissolved in isopropanol (20 mL). This reaction mixture was refluxed overnight. When reaction was complete, the product was concentrated and purified by column chromatography eluted with MeOH:DCM (1:9) to yield a clear oil (233 mg, 41%).

^{1}H NMR: δ 2.80 (6H, m, $\underline{CH_2}N_3$, $\underline{CH_2}CH_2O$, CHOH$\underline{CH_2}$), 3.30 (3H, s, OCH_3), 4.05 (1H, m, $\underline{CH}$OH), 3.56 (2H, t, *J* 7.0, OCH_2), 3.42 (2H, t, J 5.8, NH$\underline{CH_2}$), 3.94 (2H, d, *J* 5.16, O$\underline{CH_2}$CHOH), 6.84 (2H, d, J 8.6, ArH), 7.13 (2H, d, J 8.7, ArH).

^{13}C NMR: δ 35.22 ($\underline{CH_2}CH_2O$), 48.5 ($\underline{CH_2}N_3$), 51.2 (CHOH$\underline{CH_2}$), 51.6 (NH$\underline{CH_2}$), 58.7 (O$\underline{CH_3}$), 68.7 (CHOH), 70.5 (O$\underline{CH_2}$CHOH), 73.8 ($CH_2\underline{CH_2}O$), 114.6 (ArC), 129.8 (ArH), 131.4 (ArCq), 157.1 (ArCq).

Mpt: 138-140 °C.

ES-MS MH+ calc. For $C_{14}H_{23}N_40_3$ 295.1765 found 295.0803.

FT-IR: (KBr) 3031 (NH str), 2934 (O-CH_2 str), 2100 (N_3), 1612, 1515, 1245.

Synthesis of 1-(naphthalen-8-yloxy)-3-(prop-2-ynylamino)propan-2-ol 32a

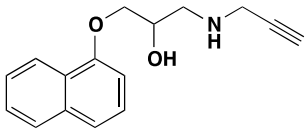

1-(2,3-Epoxypropoxy)- naphthalene **27a** (400 mg, 2 mmol) and propargylamine **31** (0.68 mL, 12 mmol) were dissolved in isopropanol (20 mL) and refluxed overnight. The reaction mixture was cooled to room temperature and concentrated. The residue was purified by column chromatography with NH_4OH:MeOH: DCM (1:9:90) to yield a yellow solid (391 mg, 77%).

^{1}H NMR: δ 2.25 (1H, t, *J* 2.4, CCH), 2.97 (1H, dd, *J* 7.30, 5.0, $COH_2\underline{CH_2}NH$), 3.11 (1H, dd, *J* 3.6, 8.5, $COH_2\underline{CH_2}NH$), 3.51 (2H, d, 2.3, $NH\underline{CH_2}$), 4.22 (3H, m, $\underline{CH_2}\underline{CH}OH$), 6.83 (1H, d, *J* 7.5, ArH), 7.36 (1H, t, *J* 7.5, ArH), 7.44-7.51 (3H, m, ArH), 7.80(1H, m, ArH), 8.24 (1H, m, ArH).

^{13}C NMR: δ 38.27 ($\underline{CH_2}CCH$), 51.03 ($\underline{CH_2}NH$), 68.60 (CHOH), 70.60 ($O\underline{CH_2}$), 71.8 ($C\underline{CH}$), 81.77($\underline{C}CH$) 105.11 (naphthyl C), δ 120.93 (naphthyl C), δ 122.10 (naphthyl C), δ 125.39 (naphthyl C), δ 125.39 (naphthyl C), 125.58 (naphthyl C), δ 126.57 (naphthyl C), δ 127.52 (naphthyl C), δ 134.61 (naphthyl C), δ 154.58 (naphthyl C).

Mpt: 134-135 °C.

FT-IR: (KBr) 3301 (OH str), 3050 (NH str), 1593, 1508, 1269.

ES-MS MH+ calc. For $C_{16}H_{18}N0_2$ 256.1332 found 256.0943.

Synthesis of 1-(4-(2-methoxyethyl)phenoxy)-3-(prop-2-ynylamino)propan-2-ol 32b

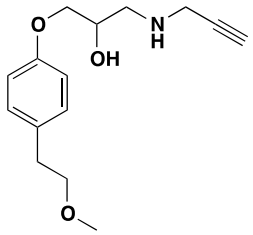

Propargylamine **31** (476 mg, 5.76 mmol) and 2-((4-(2-methoxyethyl)phenoxy)methyl)oxirane **27b** (200 mg, 0.96 mmol) were dissolved in isopropanol (10 mL). This reaction mixture was refluxed overnight. When reaction was complete, the product was concentrated and purified by flash column chromatography eluted with MeOH: DCM (5:95) to yield a yellow solid (86 mg, 39%).

^{1}H NMR: δ 2.23 (1H, t, *J* 2.40 CH), 2.83 (3H, m, $\underline{CH_2}CH_2O$ and $\underline{CH_2}NH$), 2.97 (1H, dd, *J* 3.8, 8.2, $\underline{CH_2}NH$), 3.34 (3H, s, OCH_3), 3.48 (2H, d, *J* 2.4, $\underline{CH_2}CCH$)3.56 (2H, t, *J* 7.08, $CH_2\underline{CH_2}O$), 3.98 (2H, m, $O\underline{CH_2}CHOH$), 4.06 (1H, m, $\underline{CH}OH$), 6.84, (2H, d, *J* 8.8, ArH), 7.13 (2H, d, *J* 8.50, ArH).

^{13}C NMR: δ 35.43 ($\underline{CH_2}CH_2O$), 38.38 ($\underline{CH_2}CCH$), 50.87 ($CHOH\underline{CH_2}$), 58.79 ($O\underline{CH_3}$), 68.74 (CHOH), 70.59 ($O\underline{CH_2}CHOH$), 71.81 (CCH), 73.97 ($CH_2\underline{CH_2}O$), 81.97 ($CH_2C\underline{CH}$), 114.68 (ArC), 129.95 (ArH), δ131.71 (ArCq), 157.26 (ArCq).

Mpt:137-140° C.

FT-IR: (KBr) 3278 (OH str), 3031 (NH str), 1612, 1515, 1245.

ES-MS MH+ calc. For $C_{14}H_{19}NO_3$ 264.3395 found 264.1117.

Synthesis of 4-azidobutyric acid ethyl ester 38 [177]

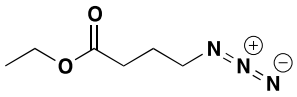

4-Bromobutyric acid ethyl ester **37** (2.21 mL, 15.4 mmol) was dissolved in acetone/water (22.5 mL/ 7.5 mL). Sodium azide (2.0 g, 30.8 mmol) was added to the reaction mixture which was refluxed for seven hours. The acetone was removed and the water was partitioned with DCM (10 mL). The organic layer was removed and the aqueous layer was washed with DCM (3 x 10 mL). The product was dried and concentrated to yield a yellow oil (2.05 g, 85%). The product was used without further purification.

^{1}H NMR: δ 1.26 (3H, t, *J* 7.1, CH_3), 1.88-1.96 (2H, m, $N_3CH_2\underline{CH_2}$), 2.40 (2H,t, *J* 7.0, $COCH_2$), 3.35 (2H, t, *J* 7.1, CH_2N_3), 4.15(2H, q, *J* 7.0, 7.4, $CH_3\underline{CH_2}O$).

^{13}C NMR: δ 14.20 (CH_3), 24.27 ($CH_2\underline{CH_2}CH_2$), 31.19 ($CO\underline{CH_2}$), 50.66 ($\underline{CH_2}N_3$), 60.56 (CH_2CH_3), 172.50 (C=O).

FT-IR: (NaCl) 3546 (CO stretch), 2980 (O-CH_2 str), 2098 (N_3), 1731, 1447.

Synthesis of 4-azidobutyric acid 39 [177]

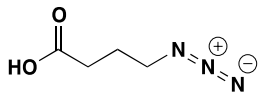

4-Azidobutyric acid ethyl ester **38** (11.2 g, 73.0 mmol) was dissolved in MeOH/water (174/ 141 mL). Potassium hydroxide (20.44 g, 365 mmol) was added to the reaction mixture while in an ice bath. The reaction mixture was stirred overnight at room temperature. The solvent was evaporated and the residue was partioned between DCM and water. The aqueous layer was extracted and acidified to pH 1 with 1M HCl. The product was then extracted several times in diethyl ether, dried and concentrated to afford the product as a yellow oil. (7.55 g, 80%).

^{1}H NMR: δ 1.89-1.96 (2H, m, $\underline{CH_2}CH_2N_3$), 2.48 (2H, t, *J* 7.2, CH_2CO), 3.38 (2H, t, *J* 6.7, CH_2N_3), 8.86 (1H, s, OH).

^{13}C NMR: δ 178.67 (CO), 50.59 (CH_2N_3), 30.95 ($COCH_2$), 23.96 ($CH_2\underline{CH_2}CH_2$).

FT-IR: (NaCl) 2939 (COOH), 2100 (N_3), 1710 (C=O stretch), 1413.

Synthesis of 4-(3-bromopropoxy) Benzaldehyde 44 [178]

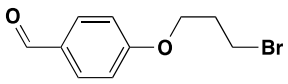

A solution of bromopropanol (1.32 mL, 14.4 mmol), 4-hydroxybenzaldehyde **43** (1.46 mg, 12 mmol), triphenyphosphine (3.76 g, 14.4 mmol) and THF (60 mL) were stirred for fiveminutes, to which DIAD (2.84 mL in 15 mL DCM) was added drop wise to the solution over an ice bath. The solution was stirred overnight at room temperature. The reaction mixture was concentrated to residue and dissolved in diethyl ether (60 mL) and the mixture was sonicated. Petroleum ether (30 mL) was added and sonicated further. The precipitate was filtered and the filtrate was washed with sodium hydroxide (2M), and brine. The organic layer was dried and concentrated.

The residue was purified by column chromatography eluted with ethyl acetate: petroleum ether (10:90) to yield a pale yellow oil (1.79 mg, 62%).

^{1}H NMR: δ 2.32- 2.38 (2H, m, $CH_2\underline{CH_2}CH_2$), 3.60 (2H, t, *J* 6.5, CH_2Br), 4.19 (2H, t, *J* 5.8, OCH_2), 7.01 (2H, d, *J* 9.0 ArH), 7.83 (2H, d, *J* 8.5, ArH), 9.88 (1H, s, OH).

^{13}C NMR: δ 28.71 ($BrCH_2$), δ 48.15 ($OCH_2\underline{CH_2}$), 65.01 (OCH_2), 114.86 (ArCH), 132.11 (ArCH), 63.79 (ArCO), 190.88 (COOH).

FT-IR: (NaCl) 2936, 2827 (C=O str), 2739, 1691, 1577, 1508.

Synthesis of 4-(3-azidopropoxy) Benzaldehyde 45 [98]

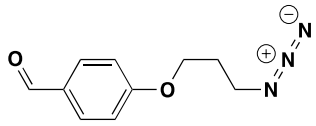

A solution of 4-(3-bromopropoxy)benzaldehyde **44** (410 mg, 1.7 mmol) and sodium azide (276 mg, 4.25 mmol) in DMF (6 mL) was refluxed over night at 100 °C. The reaction mixture was cooled and added to a large excess of water. The product was extracted several times into chloroform, dried and concentrated to yield the azido-benzaldehyde as a dark yellow oil. (150 mg, 44%). This product was used without further purification.

^{1}H NMR: δ 2.08 (2H,m, $CH_2\underline{CH_2}CH_2$), 3.52 (2H, t, *J* 6.5, CH_2N_3), 4.13 (2H, t, *J* 6.0 OCH_2), 6.98 (2H, d, *J* 9.0 ArH), 7.83 (2H, d, *J* 8.5, ArH), 9.88 (1H, s, OH).

^{13}C NMR δ 28.73 ($\underline{CH_2}CH_2N_3$), 48.17 ($\underline{CH_2}N_3$), 65.02 (OCH_2), 114.88 (ArC), 130.27 (ArC), 132.13 (ArC), 163.79 (ArCO), 190.89 (C=O).

FT-IR: (NaCl) 3492, 2929 (C=O str), 2098 (N_3), 1678, 1600, 1505, 1256.

Synthesis of 4,4-difluoro-8-(4-(3-azidopropoxy))phenyl-2,6-dimethyl-4-bora-3a,4adiaza-s-indacene 46

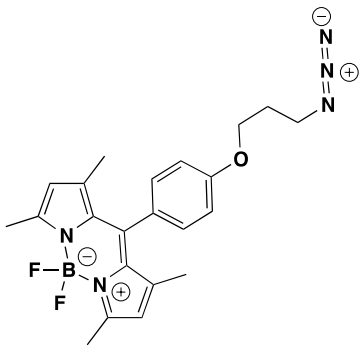

2,4-Dimethylpyrrole (0.2 mL, 1.47 mmol) and 4-(3-azidopropoxy)benzaldehyde **45** (150 mg, 0.73 mmol) were dissolved in anhydrous DCM (200 mL) and was stirred under an atmosphere of nitrogen. TFA (one drop) was added and the reaction mixture was stirred for 4 hours. DDQ

(180 mg, 0.73 mmol) was added and the reaction mixture was stirred further for 30 minutes. Triethylamine (1 mL, 0.73 mmol) and boron trifluoride diethyl etherate, (1 mL, 0.94 mmol) were added to the reaction mixture and it was stirred overnight.

The reaction mixture was then washed with water (3 × 100 mL), dried and concentrated. The residue was purified by column chromatography eluted in chloroform to yield a red solid (51 mg, 17% yield).

^{1}H NMR: δ 1.42 (6H, s, CH_3), 2.09-2.12 (2H, m, $CH_2\underline{CH_2}CH_2N_3$), 2.53 (6H, s, CH_3), 3.55 (2H, t, *J* 6.5, $CH_2CH_2\underline{CH_2}N_3$), 4.09 (2H, t, *J* 6.0, $CH_2CH_2\underline{CH_2}N_3$), 5.96 (2H, s, CH), 7.00 (2H, d, *J* 8.5, ArH), 7.15 (2H, d, *J* 8.45, ArH).

^{13}C NMR: δ 14.72 (CH_3), 28.94 ($\underline{CH_2}CH_2N_3$), 48.36 ($\underline{CH_2}N_3$), 64.79 (OCH_2), 115.21 (phenyl CH), 121.27 (pyrrole CH), 127.51 (Phenyl C), 129.44 ($N\underline{C}CCH_3$), 131.98 (Phenyl CH), 141.88 ($CH_3C\underline{C}$), 143.28 (PhenylC-$\underline{C}$), 155.46 ($N\underline{C}CH_3$), 159.40 (Phenyl CO).

FT-IR: 3431 (br, pyrrole ring), 2933, 2737, 2676, 2092 (N_3), 1607(conjugated C=N).

Mpt: 141-143 °C.

Synthesis of 4,4-difluoro-8-(1-acetylene)phenyl-2,6-dimethyl-4-bora-3a,4a-diaza-s-indacene 48 [134]

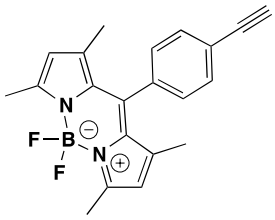

2,4-Dimethylpyrrole (182mg, 0.2mL, 1.47mmol) and 4-ethynylbenzaldehyde **47** (100 mg, 0.74 mmol) were dissolved in anhydrous DCM (200 mL) under a nitrogen environment. TFA (one drop) was added and the reaction mixture was stirred for four hours. DDQ (180 mg, 0.74

mmol) was added in DCM (15 mL) and was stirred for 30minutes. Triethylamine (1 mL, 0.73 mmol) and Boron trifluoride diethyl etherate (1 mL, 0.94 mmol) were added and the reaction mixture was left to stir overnight.

The reaction mixture was washed several times with water, dried and concentrated. The residue was purified by column chromatography eluted in ethyl acetate: petroleum ether (2:8) to yield a pink solid (72 mg, 28%).

^{1}H NMR: δ 1.39 (6H, s, CH_3), δ 2.55 (6H, s, CH_3), δ 3.17 (1H, s, CCH), δ 5.98 (2H, s, $CCH_3\underline{CH}$), δ 7.26 (2H, d, *J* 7.7, ArH), δ 7.62 (2H, d, *J* 8.3, ArH).

^{13}C: NMR δ 14.71 (CH_3), 76.69 (C<u>CH</u> alkyene), 83.02 (<u>C</u>CH), 121.54 (Pyrrole CH), 123.10 (<u>Phenyl C</u>-C), 128.37 (phenyl CH), 133.01 (Phenyl CH), 135.74 (Pyrrole <u>C</u>-CH_3), 140.70 (N<u>C</u>CCH_3), 143.12 (Phenyl C-<u>C</u>), 155.99 (N<u>C</u>CH_3).

Mpt: 251-253 °C.

FT-IR: (KBr) 3444 (br, pyrrole ring), 2912, 2747, 2676, 1607(conjugated C=N).

Synthesis of 1-(((4,4-difluoro-8-(4-propoxy)phenyl-2,6-dimethyl-4-bora-3a,4adiaza-s-indacene -1*H*-1,2,3-triazol-4-yl)methyl)amino)-3-(naphthalen-1-yloxy)propan-2-ol 51a

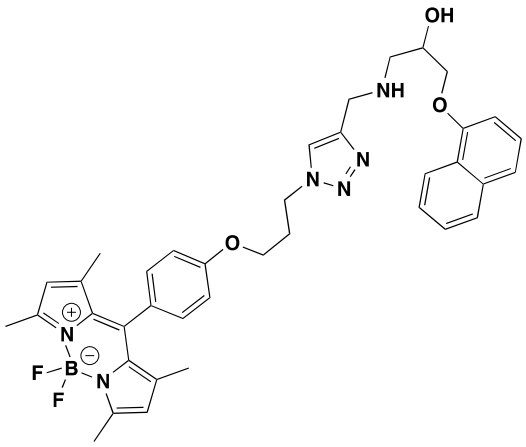

Using general procedure 1 starting with 4,4-difluoro-8-(4-(3-azidopropoxy))phenyl-2,6-dimethyl-4-bora-3a,4adiaza-s-indacene **46** and 1-(naphthalen-8-yloxy)-3-(prop-2-ynylamino)propan-2-ol **32a** yielded a red solid (1.2mg, 46%).

HPLC Rt: 8.73 (System 3).

ES-MS MH+ calc. For $C_{38}H_{42}BF_2N_60_3$ 679.3374 found 679.1365.

Synthesis of 1-((2-(4,4-difluoro-8-(4-propoxy)phenyl-2,6-dimethyl-4-bora-3a,4adiaza-s-indacene -1*H*-1,2,3-triazol-1-yl)ethyl)amino)-3-(4-(2-methoxyethyl)phenoxy)propan-2-ol 51b

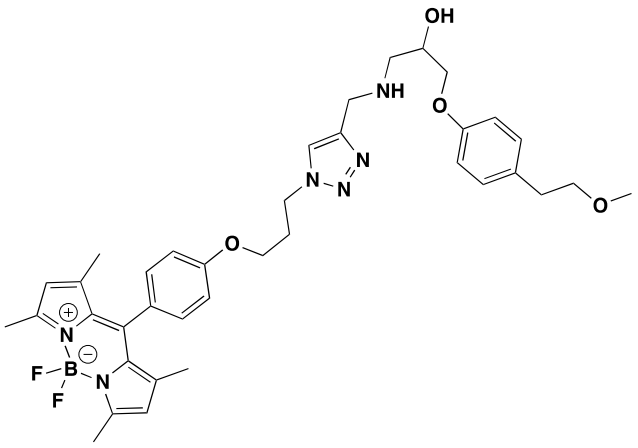

Using general procedure 1 starting with 4,4-difluoro-8-(4-(3-azidopropoxy))phenyl-2,6-dimethyl-4-bora-3a,4adiaza-s-indacene **46** and 1-(naphthalen-8-yloxy)-3-(prop-2-ynylamino)propan-2-ol **32b** yielded a red solid (1.8 mg, 70%).

HPLC Rt: 5.80 (System 3).

ES-MS MH+ calc. For $C_{38}H_{42}BF_2N_60_3$ 687.3636 found 687.1597.

Synthesis of 1-((2-(4,4-difluoro-8-phenyl-2,6-dimethyl-4-bora-3a,4a-diaza-s-indacene -1*H*-1,2,3-triazol-1-yl)ethyl)amino)-3-(naphthalen-1-yloxy)propan-2-ol (52a)

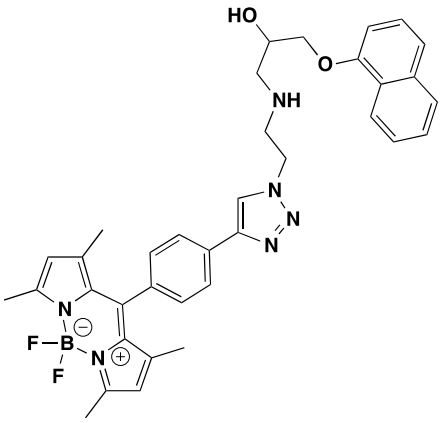

Using general procedure 1 starting with 4,4-difluoro-8-(1-acetylene)phenyl-2,6-dimethyl-4-bora-3a,4a-diaza-s-indacene **48** and 1-(2-azidoethylamino)-3-(naphthalen-5-yloxy)propan-2-ol **30a** yielded a red solid (1.9 mg, 24%).

HPLC Rt: 9.35 (System 3).

ES-MS MH+ calc. For $C_{36}H_{38}BF_2N_60_2$ 635.3112 found 635.1654.

Synthesis 1-((2-(4,4-difluoro-8-phenyl-2,6-dimethyl-4-bora-3a,4a-diaza-s-indacene -1*H*-1,2,3-triazol-1-yl)ethyl)amino)-3-(4-(2-methoxyethyl)phenoxy)propan-2-ol 52b

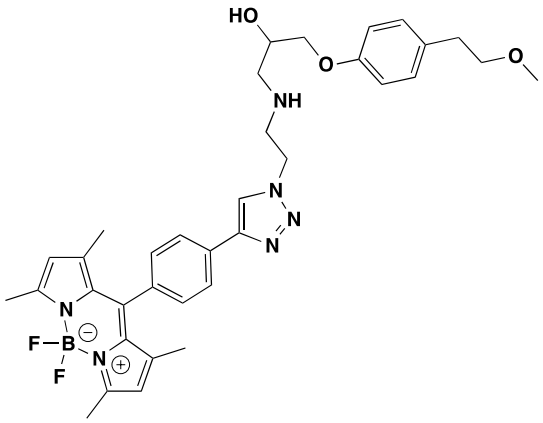

Using general procedure 1 starting 4,4-difluoro-8-(1-acetylene)phenyl-2,6-dimethyl-4-bora-3a,4a-diaza-s-indacene **46** and 1-(2-azidoethylamino)-3-(4-(2-methoxyethyl)phenoxy)propan-2-ol **30b** to yield a red solid (3.4 mg, 56%).

HPLC Rt: 7.65 (System 3).

ES-MS MH+ calc. For $C_{35}H_{41}BF_2N_60_3$ 643.3374 found 643.1825.

Synthesis of but-3-yn-1-yl[2-hydroxy-3-(naphthalen-1-yloxy)propyl]amine 56a

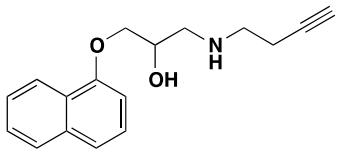

N-(3-butynyl)-phthalimide **54a** (2.5 g, 12.5 mmol) and hydrazine monohydrate (0.57 mL, 11.87 mmol) were dissolved in isopropanol (60 mL) and heated in a sealed tube at 70 °C for two hours. Once reaction was complete (formation of precipitate), the reaction mixture was cooled to room temperature. To the mixture 1-(2,3-epoxypropoxy)- naphthalene **27a** (778 mg, 3.88 mmol) was added. The vessel was sealed and heated to 90 °C overnight. Reaction was then cooled to room temperature and the reaction mixture was concentrated. The residue was redissolved in DCM (20 mL). The organic later was washed with water (3 × 20 mL), dried and

evaporated. The residue was purified by column chromatography eluted in MeOH:DCM (5:95) to yield a brown oil (26 3mg, 25%).

^{1}H NMR: δ 2.06 (1H, t, *J* 2.68, CCH) 2.42- 2.46 (2H, m, CH_2CCH) 2.82 – 2.91 (3H, m, CH_2NHCH_2), 2.95 - 2.99, (1H, m, COHCH_2) 4.10-4.20 (2H, m, OCH_2), 4.24 - 4.28 (1H, m, CHOH), 6.83 (1H, d, *J* 7.5, ArH), δ 7.36 (1H, t, *J* 7.5, ArH), δ 7.44-7.51 (3H, m, ArH), δ 7.82 – 7.85(1H, m, ArH), δ 8.30-8.34 (1H, m, ArH).

^{13}C NMR: δ 19.43 (NHCH$_2$$CH_2$), 47.77 (NH$CH_2$), 51.87 ($CH_2$NH), 68.30 ($OCH_2$CHOH), 69.95 (CCH), 70.57 (OCH_2), 82.12 (CCH), 105.11 (naphthyl C), 120.93 (naphthyl C), 122.10 (naphthyl C), 125.39 (naphthyl C), 125.39 (naphthyl C), 125.58 (naphthyl C), 126.57 (naphthyl C), 127.52 (naphthyl C), 134.61 (naphthyl C), 154.58 (naphthyl C).

Mpt: 141-143°C

FT-IR (KBr) 3301 (OH str), 3050 (NH str), 1593, 1508, 1269.

ES-MS MH+ calc. For $C_{17}H_{19}N0_2$ 270.1488 found 270.1250.

Synthesis of 1-(naphthalen-1-yloxy)-3-(pent-4-ynylamino)propan-2-ol 56b

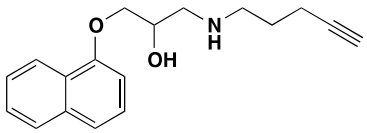

N-(4-pentynyl)-phthalimide **54b** (2.5 g, 11.0 mmol) and hydrazine monohydrate (0.55 mL, 10.0 mmol) were dissolved in isopropanol (40 mL) and heated in a sealed tube at 70 °C for two hours. Once reaction was complete (formation of precipitate), the reaction mixture was cooled to room temperature. To the mixture 1-(2,3-epoxypropoxy)- naphthalene **27a** (205 mg, 3.14 mmol) was added. The vessel was sealed and heated to 90 °C overnight. Reaction was then cooled to room temperature and concentrated. The residue was redissolved in DCM (20 mL). The organic later was washed with water (3 × 20 mL), dried and evaporated. The crude was purified by column chromatography eluted in MeOH:DCM (1:9) to yield a brown/yellow solid (500 mg, 31%).

^{1}H NMR: δ 1.95 (1H, t, *J* 2.6, CCH), 2.19-2.23 (2H, m, $\underline{CH_2}CCH$), 2.69-2.72 (3H, m, $\underline{CH_2}N\underline{CH_2}$), 2.86-3.1 (3H, m, $\underline{CH_2}N\underline{CH_2}$), 4.10-4.27 (3H, m, $O\underline{CH_2}\underline{CH}OH$), 6.82 (1H, d, *J* 7.5, ArH), δ 7.37 (1H, t, *J* 7.5, ArH), δ 7.42-7.49 (3H, m, ArH), δ 7.80(1H, m, ArH), δ 8.24 (1H, m, ArH).

^{13}C NMR: δ 18.20 ($\underline{CH_2}CCH$), 26.05 ($\underline{CH_2}CH_2CCH$), 28.91 ($\underline{CH_2}$), 49.91 ($NH\underline{CH_2}$), 50.71 ($\underline{CH_2}NH$), 68.22 ($OCH_2\underline{CHOH}$), 69.81 ($C\underline{C}H$), 70.65 ($O\underline{CH_2}$), 84.20 ($\underline{C}CH$), 105.11 (naphthyl C2), δ 120.66 (naphthyl C), δ 121.80 (naphthyl C), δ 125.28 (naphthyl C), δ 125.39 (naphthyl C), 125.58 (naphthyl C), δ 126.57 (naphthyl C), δ 127.52 (naphthyl C), δ 134.61 (naphthyl C), δ 154.58 (naphthyl C).

Mpt: 140-142 °C.

FT-IR: (KBr) 3319 (OH str), 3049 (NH str), 1592, 1508, 1279.

ES-MS MH+ calc. For $C_{18}H_{22}N0_2$ 284.1645 found 284.1364

Synthesis of 1-(hex-5-ynylamino)-3-(naphthalen-1-yloxy)propan-2-ol 56c

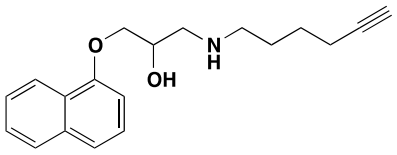

N-(5-hexynyl)-phthalimide **54c** (1.5 g, 6.6 mmol) and hydrazine monohydrate (0.3 mL, 6.27 mmol) were dissolved in isopropanol (60 mL) and heated in a sealed tube at 70 °C for two hours. Once reaction was complete (formation of precipitate), the reaction mixture was cooled to room temperature. To the mixture 1-(2,3-epoxypropoxy)- naphthalene **27a** (1.1 g, 5.7 mmol) was added. The vessel was sealed and heated to 90 °C overnight. Reaction was then cooled to room temperature and concentrated. The residue was redissolved in DCM (20 mL). The organic later was washed with water (3 × 20 mL), dried and evaporated. The crude was purified by column chromatography eluted in MeOH:DCM (1:9) to yield a brown solid (289 mg, 31%).

^{1}H NMR: δ 1.93 (1H, t, *J* 2.6, 5.2, C<u>CH</u>), 2.19-2.23 (2H, m), 2.68-2.74 (3H, m), 2.90-2.97 (3H, m), 4.12-4.20 (4H, m), 6.82 (1H, d, *J* 7.5, ArH), δ 7.33 (1H, t, *J* 7.5, ArH), δ 7.42-7.49 (3H, m, ArH), δ 7.78-7.80(1H, m, ArH), δ 8.22-8.25 (1H, m, ArH).

^{13}C NMR: 18.29 (<u>CH_2</u>CCH), 26.08 (<u>CH_2</u>CH_2CCH), 28.99 (<u>CH_2</u>), 49.28 (NH<u>CH_2</u>), 50.74 (<u>CH_2</u>NH), 52.04 (CH_2), 68.28 (OCH_2<u>CHOH</u>), 68.58 (C<u>CH</u>), 70.62 (O<u>CH_2</u>), 84.20 (<u>C</u>CH), 104.93 (naphthyl C2), δ 120.66 (naphthyl C), δ 121.80 (naphthyl C), δ 125.23 (naphthyl C), δ 125.83 (naphthyl C), 126.45 (naphthyl C), δ 127.55 (naphthyl C), δ 143.50 (naphthyl C), δ 138.59 (naphthyl C), δ 154.29 (naphthyl C).

Mpt: 141-143 °C.

FT-IR: (KBr) 3300 (OH str), 3050 (NH str), 1560, 1512, 1269

ES-MS MH+ calc For $C_{19}H_{24}NO_2$ 298.1802 found 298.1308.

Synthesis of 1-((2-(4,4-difluoro-8-(4-propoxy)phenyl-2,6-dimethyl-4-bora-3a,4adiaza-s-indacene -1*H*-1,2,3-triazol-4-yl)ethyl)amino)-3-(naphthalen-1-yloxy)propan-2-ol 57a

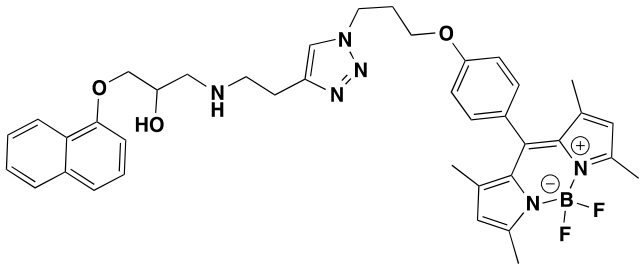

Using general procedure 1 starting with but-3-yn-1-yl[2-hydroxy-3-(naphthalen-1-yloxy)propyl]amine **56a** and 4,4-difluoro-8-(4-(3-azidopropoxy))phenyl-2,6-dimethyl-4-bora-3a,4adiaza-s-indacene **46** yielded a red solid (2 mg, 52%).

HPLC Rt: 12.42 (System 1), 14.55 (System 2).

ES-MS MH+ Calc. for $C_{39}H_{44}BF_2N_6O_3$ 693.3531 found 693.3589.

Synthesis of 1-((3-(4,4-difluoro-8-(4-propoxy)phenyl-2,6-dimethyl-4-bora-3a,4adiaza-s-indacene

-1*H*-1,2,3-triazol-4-yl)propyl)amino)-3-(naphthalen-1-yloxy)propan-2-ol 57b

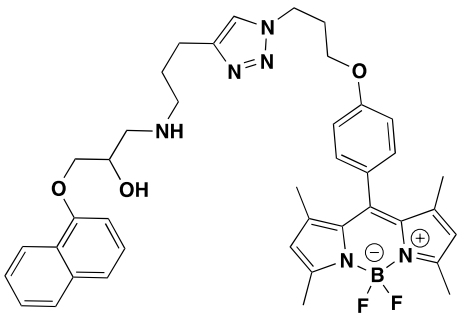

Using general procedure 1 starting with 1-(naphthalen-1-yloxy)-3-(pent-4-ynylamino)propan-2-ol **56b** and 4,4-difluoro-8-(4-(3-azidopropoxy))phenyl-2,6-dimethyl-4-bora-3a,4adiaza-s-indacene **46** yielded a red solid (2 mg, 54%).

HPLC Rt: 12.42 (System 1), 14.53 (System 2).

ES-MS MH+ Calc. for $C_{40}H_{46}BF_2N_6O_3$ 707.3687 found 707.3749.

Synthesis of 1-((4-(4,4-difluoro-8-(4-propoxy)phenyl-2,6-dimethyl-4-bora-3a,4adiaza-s-indacene -1*H*-1,2,3-triazol-4-yl)butyl)amino)-3-(naphthalen-1-yloxy)propan-2-ol 57c

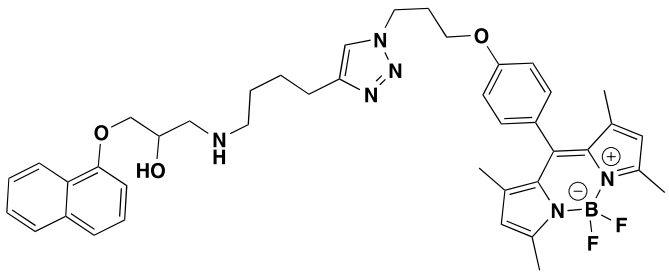

Using general procedure 1 starting with 1-(hex-5-ynylamino)-3-(naphthalen-1-yloxy)propan-2-ol **56c** and 4,4-difluoro-8-(4-(3-azidopropoxy))phenyl-2,6-dimethyl-4-bora-3a,4adiaza-s-indacene **46** yielded a red solid (1.7 mg, 44%).

HPLC Rt: 12.47 (System 1), 14.55 (System 2).

ES-MS MH+ Calc. for $C_{41}H_{48}BF_2N_6O_3$ 721.3844 found 721.3900.

Synthesis of 4-(5-bromopentyloxy)Benzaldehyde[179] 59

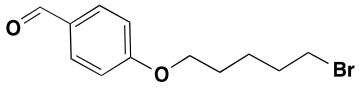

1,5-Dibromopentane **58** (2.08 mL, 15.2 mmol) and K_2CO_3 (3.8 g, 27.6 mmol) was dissolved in DMF (50 mL). 4-Hydroxybenzaldehyde (1.69 g, 13.84 mmol) dissolved in DMF (50 mL) was added dropwise and stirred for 15 hours. The reaction mixture was poured into toluene and washed with water. The organics were extracted in toluene (3 × 25 mL), dried and concentrated. The residue was purified by column chromatography eluted in chloroform to yield a clear oil (1.7 g, 54%).

^{1}H NMR: δ 1.66-1.76 (2H, m, CH_2), 1.81-1.95 (4H, m, CH_2's), 3.38-3.46 (2H, m, CH_2), 4.02-4.08 (2H, m, CH_2), 6.95-6.99 (2H, m, ArCH), 7.79-7.83 (2H, m, ArCH), 9.86 (1H, s, COH).

^{13}C NMR: δ 24.74 (CH_2), 28.25 (CH_2), 31.86 (CH_2), 33.32 (CH_2), 67.98 (OCH_2), 114.74 (phenyl CH), 129.87 (Phenyl C), 131.99 (Phenyl C), 164.40 (phenyl C), 190.77 (CO).

FT-IR: (NaCl) 2945, 2882, 2832, 1679 (C=O str), 1602, 1463 (C-O str), 1162.

Synthesis of 4-(5-azidopentyloxy)benzaldehyde 60

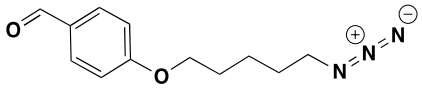

4-(5-Bromopentyloxy)benzaldehyde **59** (3 g, 11.1 mmol) and sodium azide (1.8 g, 27.75 mmol) were refluxed in DMF (75 mL) at 100 °C for five hours. Once complete the reaction mixture was poured into water and extracted with ethyl acetate and evaporated to yield a clear oil (2.32 g, 89%).

The product was used without further purification

^{1}H NMR: δ 1.47-1.63 (4H, m, $\underline{CH_2}CH_2\underline{CH_2}N_3$), 1.74-1.88 (2H, m, $CH_2\underline{CH_2}CH_2N_3$) 3.19-3.26 (2H, m, $\underline{CH_2}N_3$), 3.96-4.06 (2H, m, $O\underline{CH_2}$), 6.90 (2H, dd, *J* 2.2, 8.8 ArCH), 7.75 (2H, dd, *J* 2.2, 8.8, Ar<u>CH</u>CO), 9.79 (1H, s, COH)

^{13}C NMR: δ 23.25 (CH_2), 28.53 (CH_2), 28.71 (CH_2), 51.22 (CH_2N_3), 67.94 (OCH_2), 114.60 (phenyl CH), 129.80 (Phenyl C), 131.90 (Phenyl C), 162.44 (phenyl C), 190.77 (CO)

FT-IR: (NaCl) 2940, 2880, 2828, 2110 (N_3), 1688 (C=O str), 1600, 1468 (C-O str), 1159.

Synthesis of 4,4-difluoro-8-(4-(5-azidopentyl))phenyl-2,6-dimethyl-4-bora-3a,4adiaza-s-indacene 61

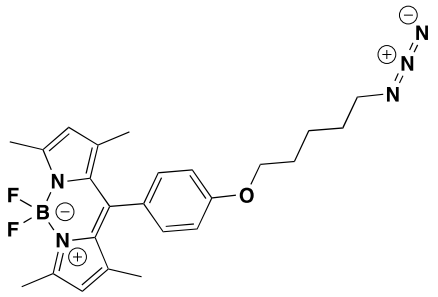

4-(5-Azidopentyloxy)benzaldehyde **60** (1 g, 4.28 mmol) and 2,4-dimethylpyrrole (0.814 g, 0.88 mL, 8.56 mmol) with TFA (5 drops) were dissolved in anhydrous DCM (300 mL) and stirred under N_2 for 12 hours at room temperature. DDQ (1.94 g, 8.56 mmol) was added as a single portion and left to stir for one hour. Then DIPEA (8.5 mL, 48.79 mmol) and BF_3OEt_2 (8.6 mL, 68.48 mmol) were added and the solution stirred for six hours.

The solution was washed with water and extracted in chloroform and concentrated to residue. The residue was purifed with column chromatography eluted in chloroform to yield a red solid (304mg, 16%).

^{1}H NMR: δ 1.42 (6H, s, CH_3), 1.60 (4H, m, $\underline{CH_2}CH_2\underline{CH_2}N_3$), 1.80 (2H, m, $CH_2\underline{CH_2}CH_2N_3$) 2.54 (6H, s, CH_3), 3.31 (2H, m, $\underline{CH_2}N_3$), 4.01 (2H, m, $O\underline{CH_2}$), 5.9 (2H, s, CH), 6.97 (2H, d, *J* 8.3 ArCH), 7.15 (2H, d, *J* 8.3, ArCH)

13C NMR: δ 14.59 (CH_3), 23.45 (CH_2), 28.70 (CH_2), 28.82 (CH_2), 51.4 (CH_2N_3), 67.70 (OCH_2), 115.04 (phenyl CH), 121.10 (pyrrole CH), 126.98 (Phenyl C), 129.20 ($N\underline{C}CCH_3$), 131.85 (Phenyl CH), 141.90 ($CH_3C\underline{C}$), 143.16 (PhenylC-$\underline{C}$), 155.23 ($N\underline{C}CH_3$), 159.55 (Phenyl CO)

Mpt: 148-150 °C.

FT-IR (KBr) 2919, 2086 (N_3), 1609, 1544.

ES-MS MH+ Calc. for $C2_4H_{27}BF_2N_5O$ 452.2428 found 452.2464.

Synthesis of 4-(2-(2-chloroethoxy)ethoxy)benzaldehyde 63

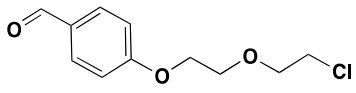

4-Hydroxybenzaldehyde (5.0 g, 40.96 mmol) and K_2CO_3 (11.25 g, 81.69 mmol) were dissolved in DMF (300 mL). Bis-(2-chloroethyl) ether **62** (14.38 mL, 122.9 mmol) and refluxed for 20 hours. the reaction mixture was filter, poured into water (500 mL) and extracted into ethyl acetate (3 x 60 mL). The organic layer was washed with water, dried and evaporated. The residue was precipitated from diethyl ether/water to yield a white solid (6.28 g, 67%).

^{1}H NMR: δ 3.65 (2H, t, *J* 5.8, CH_2), 3.83 (2H, t, *J* 5.5, CH_2), 3.91 (2H, t, *J* 4.7, CH_2), 4.22 (2H, t, *J* 4.7, CH_2), 7.02 (2H, d, *J* 8.6, ArH), 7.83 (2H, d, *J* 8.6, ArH), 9.88 (1H, s, COH).

^{13}C NMR: δ 42.81, 67.80, 69.63, 71.75 (CH_2), 115.00 (ArCH), 130.33 (ArCH), 132.12 (ArC), 163.83 (ArCO), 190.10 (COH).

Mpt: 65-66 °C.

FT-IR: (KBr) 2930, 2780 (C=O str), 2628, 1588, 1500, 1468,1259 (C-O-C str).

Synthesis of 4-(2-(2-azidoethoxy)ethoxy)Benzaldehyde 64

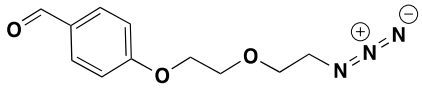

4-(2-(2-Chloroethoxy)ethoxy)benzaldehyde **63** (500 mg, 2.19 mmol) and sodium azide (691 mg, 10.95 mmol) was heated in DMF (50 mL) at 100 °C for 20 hours. The reaction mixture was cooled to room temperature and poured into water (100 mL) and extracted into ethyl acetate (3 × 60 mL). The organics were washed with water (2× 50 mL), dried and evaporated. to yield a clear oil (377mg, 74% yield). The product was used without further purification.

^{1}H NMR: δ 3.40 (2H, t, *J* 5.1, CH_2), 3.74 (2H, t, *J* 4.8, CH_2), 3.88 (2H, t, *J* 4.8, CH_2), 4.21 (2H, t, *J* 4.6, CH_2), 7.02 (2H, d, *J* 8.7, ArH), 7.82 (2H, d, *J* 8.8, ArH), 9.86 (1H, s, CHO).

^{13}C NMR: δ 50.72, 67.81, 69.54, 70.42 (CH_2), 114.96 (ArCH), 130.42 (ArCH), 132.03 (ArC), 163.80 (ArCO), 190.81 (COH).

Mpt: 60-62 °C.

FT-IR: (KBr) 2929, 2789, 2632, 2097 (N_3), 1570, 1512, 1488,1239.

Synthesis of 4,4-difluoro-8-(4-(2-azidoethoxy)ethoxy))phenyl-2,6-dimethyl-4-bora-3a,4adiaza-s-indacene 65

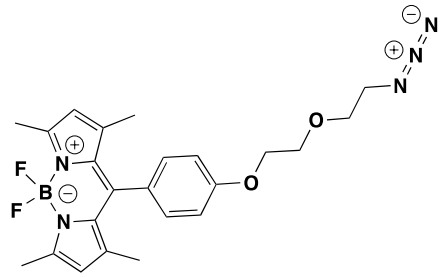

4-(2-(2-Azidoethoxy)ethoxy)benzaldehyde **64** (200 mg, 0.85 mmol) and 2,4-dimethylpyrrole (162 mg, 1.70 mmol) were dissolved in anhydrous DCM (80 mL) with TFA (4 drops) and stirred under a nitrogen environment for 12 hours. DDQ (193 mg, 0.85 mmol) was added in a

single portion and the reaction was stirred for one hour. Triethylamine (0.674 mL, 4.84 mmol) and boron trifluoride diethyl etherate (1.67 mL, 13.6 mmol) was added to the reaction mixture and stirred under a nitrogen environment for 10 hours. The reaction mixture was washed with water (3 × 100 mL) and brine (3 × 50 mL), dried and concentrated. The residue was purified by column chromatography eluted with DCM to yield a red solid (150 mg, 39%).

^{1}H NMR: δ 1.42 (6H, s, CH_3), 2.54 (6H, s, CH_3), 3.39-3.48 (2H, m, CH_2), 3.76-3.82 (2h, m, CH_2), 3.89-3.94 (2H, m, CH_2), 4.18-4.22 (2H, m, CH_2), 5.97 (2H, s, CH), 7.02-7.03 (2H, m, ArCH), 7.15-7.17 (2H, m, ArCH).

^{13}C NMR: δ 14.72 (CH_3), 47.3 (CH_3), 50.80 (CH_2), 67.60 (CH_2), 69.81 (CH_2), 70.44 (CH_2), 115.23 (phenyl CH), 121.24 (pyrrole CH), 127.44 (Phenyl C), 129.30 (N<u>C</u>CCH_3), 131.91 (Phenyl CH), 141.90 (CH_3C<u>C</u>), 143.35 (PhenylC-<u>C</u>), 155.31 (N<u>C</u>CH_3), 159.40 (Phenyl CO).

Mpt: 138-140 °C.

FT-IR: (KBr) 3445, 2801, 2490, 2114 (N_3), 1612 (conjugated C=N).

ES-MS MH+ calc. For $C_{23}H_{26}BF_2N_50_2$ 454.2222 found 454.2230.

Synthesis of 1-((4-(4,4-difluoro-8-(4-pentyl)phenyl-2,6-dimethyl-4-bora-3a,4adiaza-s-indacene -1*H*-1,2,3-triazol-4-yl)butyl)amino)-3-(naphthalen-1-yloxy)propan-2-ol 66a

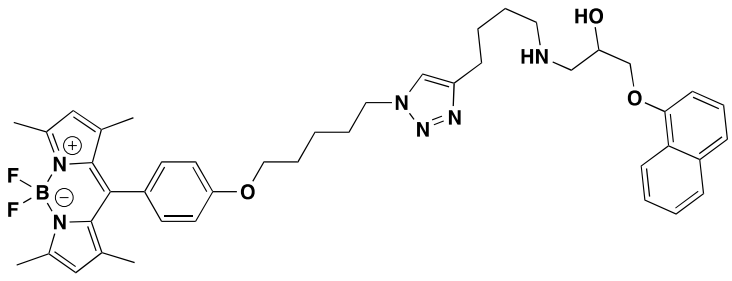

Using general procedure 1 starting with 4,4-difluoro-8-(4-(5-azidopentoxy))phenyl-2,6-dimethyl-4-bora-3a,4adiaza-s-indacene **61** and 1-(hex-5-ynylamino)-3-(naphthalen-1-yloxy)propan-2-ol **53c** yielded a red solid (2.6 mg, 14%).

HPLC Rt: 12.42 (System 1), 14.53 (System 2).

ES-MS MH+ Calc. for $C_{43}H_{52}BF_2N_6O_3$ 749.4157 found 749.3139

Synthesis of 1-((4-(4,4-difluoro-8-(4-(2-ethoxy)ethoxy)phenyl-2,6-dimethyl-4-bora-3a,4adiaza-s-indacene -1*H*-1,2,3-triazol-4-yl)butyl)amino)-3-(naphthalen-1-yloxy)propan-2-ol 66b

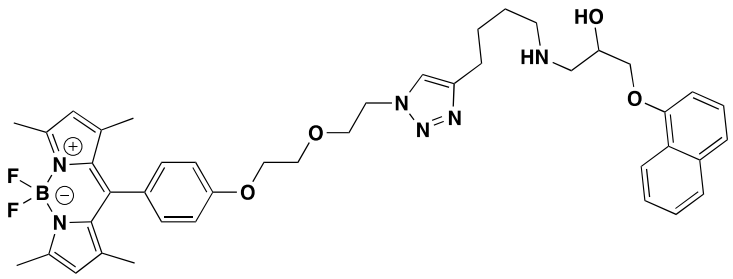

Using general procedure 1 and starting with 1-(hex-5-ynylamino)-3-(naphthalen-1-yloxy)propan-2-ol **53c** and 4,4-difluoro-8-(4-(2-azidoethoxy)ethoxy))phenyl-2,6-dimethyl-4-bora-3a,4adiaza-s-indacene **65** yielded a red solid (2.4 mg, 48%).

HPLC Rt: 19.85 (System 4).

ES-MS MH+ calc. for $C_{42}H_{50}BF_2N_6O_4$ 751.3949 found 751.3956

Synthesis of 2-amino-*N*-(prop-2-ynyl)acetamide[180] (TFA salt) 70

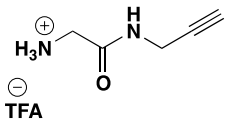

Glycine **67** (4.4 g, 59.2 mmol) was dissolved in water/dioxane (1:1, 80 mL). Sodium hydroxide (2.36 g, 0.06 mmol), was added and cooled to 0 °C BOC anhydride (14.12 g, 64.8 mmmol) was added in three portions to the reaction. The Reaction mixture was stirred at 0 °C for 30minutes then room temperature for 12 hours. The solvent was removed in vacuo and the residue was dissolved in water (200 mL) and washed with ether (3 × 100 mL). The aqueous layer was washed with citric acid to pH 4 and the product was extracted with ether (3 × 75 mL).

The organics were dried and concentrated to yield a white solid (2.9 g) the product was used without further purification.

The product **68** (1.93 g, 13.12 mmol) was dissolved in DCM (15 mL) to which HBTU (4.8 g, 13.12 mmol) was added with DIPEA (2.27 mL, 13.13 mmol). The reaction was stirred for 30 seconds and then propargylamine (662 mg, 12.04 mmol) was added and the reaction mixture was stirred for five hours. The solvent was evaporated and redissolved in ethyl acetate (20 mL) and washed with 1M HCl (10 mL) and 1M NaOH (10 mL) followed by a brine wash (10 mL), dried and concentrated.

The product **69** was dissolved in DCM (10 mL) treated with trifluoroacetic acid (10 mL) and stirred for 30 minutes. The reaction mixture was concentrated, and co-evapourated with petroleum ether (3 x 10 mL) and triturated with diethyl ether. The product was dissolved in water and lyophilised to yield a brown oil (687 mg, 44%).

^{1}H NMR: (DMSO-d_6) δ 3.18-3.19 (1H, t, *J* 2.5, CCH), 3.56 (2H, s, CH_2NH_3), 3.93-3.95 (2H, dd, *J* 2.5, 5.5, $\underline{CH_2}CCH$), 8.07 (3H, br s, NH_3), 8.81 (s, NH).

^{13}C NMR: (DMSO-d_6) δ 28.5 ($\underline{CH_2}CCH$), 40.52 (CH_2NH_3), 74.0 ($\underline{C}CH$), 80.8 ($C\underline{C}H$), 166.2 (C=O).

FT-IR: (NaCl) 2954, 2732, 1672 (C=O str), 1549 (NH Bend), 742.

ES-MS M+ calc for $C_5H_9N_2O$+ 113.070 found 113.0625.

Synthesis of 2-(2-hydroxy-3-(naphthalen-1-yloxy)propylamino)-*N*-(prop-2-ynyl)acetamide 71

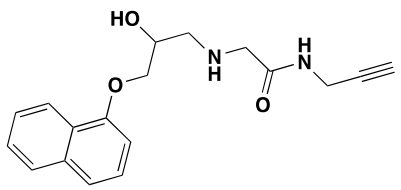

2-Amino-*N*-(prop-2-ynyl)acetamide **70** (687 mg, 3.03 mmol) and 1-(2,3-epoxypropoxy)-naphthalene **27a** (150 mg, 0.75 mmol) were dissolved in isopropanol (10 mL) and DIPEA

(0.527 mL, 3.03 mmol) was added and refluxed for 16 hours. The reaction mixture was evaporated and washed with water. The organic layer was dried and concentrated. The redisue was purified by column chromatography eluted in MeOH:DCM (1:9) to yield a white solid (120 mg, 51% yield).

^{1}H NMR: δ 2.18-2.19 (1H, t, *J* 2.5, CCH), 2.93-2.95 (2H, m, $COH_2\underline{CH_2}NH$), 3.39 (2H, d, *J* 6.5, $CO\underline{CH_2}$), 4.05-4.07 (2H, dd, *J* 2.5,5.5, $\underline{CH_2}CCH$), 4.15- 4.23 (2H, m, $NH\underline{CH_2}CO$), 4.26-4.30 (1H, m, COH<u>H</u>), 6.83 (1H, d, *J* 7.5, ArH), δ 7.36 (1H, t, *J* 7.5, ArH), δ 7.44-7.51 (3H, m, ArH), δ 7.80 (1H, m, ArH), δ 8.21 (1H, m, ArH).

^{13}C NMR: δ 28.71, 52.42, 52.51, 69.39 (CH_2), 70.47 (<u>C</u>CH), 71.46 (C<u>CH</u>), 75.70 (CHOH), 105.11 (naphthyl C), 121.02 (naphthyl C), 121.50 (naphthyl C), 125.51 (naphthyl C), 125.73 (naphthyl C), 125.58 (naphthyl C), 126.57 (naphthyl C), 127.52 (naphthyl C), 134.61 (naphthyl C), 154.58 (naphthyl C), 161.1 (C=O).

Mpt: 141-143 °C.

FT-IR (KBr) 3301 (OH str), 3050 (NH str), 1671 (C=C Ar str), 1593, 1508, 1269.

ES-MS M-TFA+ calc. For $C_{18}H_{19}N_2O_3$+ Calc 313.1547 found 313.1449.

Synthesis of *N*-((4,4-difluoro-8-(4-(3-propoxy))phenyl-2,6-dimethyl-4-bora-3a,4adiaza-s-indacene -1*H*-1,2,3-triazol-4-yl)methyl)-2-((2-hydroxy-3-(naphthalen-1-yloxy)propyl)amino) acetamide 72a

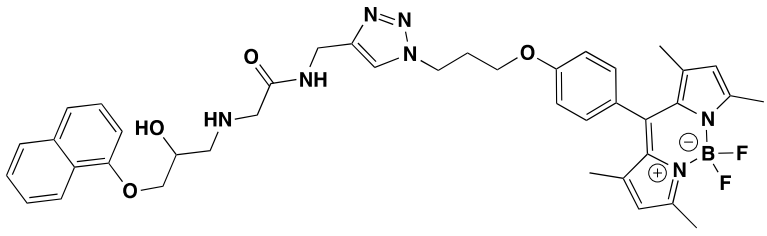

Using general procedure 1 starting with 2-(2-hydroxy-3-(naphthalen-1-yloxy)propylamino)-*N*-(prop-2-ynyl)acetamide **71** and 4,4-difluoro-8-(4-(3-azidopropoxy))phenyl-2,6-dimethyl-4-bora-3a,4adiaza-s-indacene **46** to yield an orange solid (3.4 mg, 90% yield).

HPLC Rt: 16.55 (System 4).

ES-MS M-F+ calc. For $C_{40}H_{43}BFN_7O_4$ Calc 715.3443 found 715.3568.

Synthesis of *N*-((4,4-difluoro-8-(4-(pentyl))phenyl-2,6-dimethyl-4-bora-3a,4adiaza-s-indacene -1*H*-1,2,3-triazol-4-yl)methyl)-2-((2-hydroxy-3-(naphthalen-1-yloxy)propyl)amino)acetamide 72b

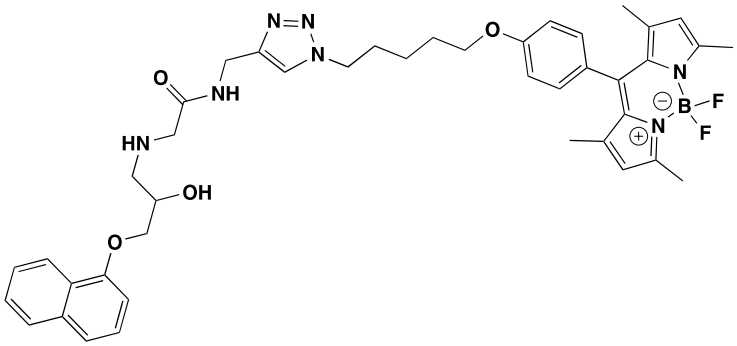

Using general procedure 1 and starting with 2-(2-hydroxy-3-(naphthalen-1-yloxy)propylamino)-*N*-(prop-2-ynyl)acetamide **71** and 4,4-difluoro-8-(4-(5-azidopentyl))phenyl-2,6-dimethyl-4-bora-3a,4adiaza-s-indacene **61** yielded a red solid (3.4 mg, 24%).

HPLC Rt: 17.70 (System 4).

ES-MS M+ calc. For $C_{42}H_{49}BF_2N_7O_4$ 764.3902 found 764.3896.

Synthesis of *N*-((4,4-difluoro-8-(2-ethoxy)ethoxy)phenyl-2,6-dimethyl-4-bora-3a,4adiaza-s-indacene -1*H*-1,2,3-triazol-4-yl)methyl)-2-((2-hydroxy-3-(naphthalen-1-yloxy)propyl)amino) acetamide 72c

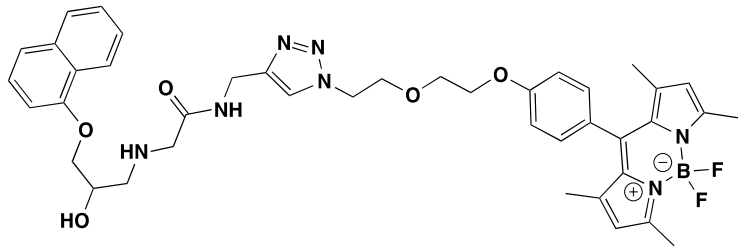

Using general procedure 1 starting with 2-(2-hydroxy-3-(naphthalen-1-yloxy)propylamino)-*N*-(prop-2-ynyl)acetamide **71** and 4,4-difluoro-8-(4-(2-azidoethoxy)ethoxy))phenyl-2,6-dimethyl-4-bora-3a,4adiaza-s-indacene **65** yielded a red solid (1.9 mg, 58%).

HPLC Rt: 19.97 (System 4).

ES-MS M+ calc. For $C_{41}H_{47}BF_2N_7O_5$ Calc 766.3694 found 766.3694.

Synthesis of 1-((2-(4-2-chromis 630 N L5H -1*H*-1,2,3-triazol-1-yl)ethyl)amino)-3-(4-(2-methoxyethyl)phenoxy)propan-2-ol 74a

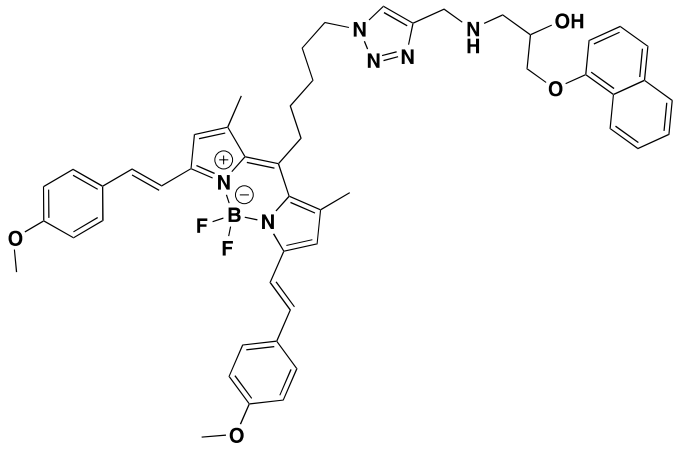

Using general procedure 1 and starting with chromis 630 N L5H azide **73** and 1-(naphthalen-8-yloxy)-3-(prop-2-ynylamino)propan-2-ol **30a** yielded a blue solid (1.4 mg, 14%).

HPLC Rt: 14.64 (System 2).

ES-MS MH+ Calc. for $C_{50}H_{54}BF_2N_6O_4$ 851.4262 found 851.4284.

Synthesis of 1-(2-(1-(2-chromis 630 N L5H -1*H*-1,2,3-triazol-4-yl)butyl)amino)-3-(naphthalen-1-yloxy)propan-2-ol 74b

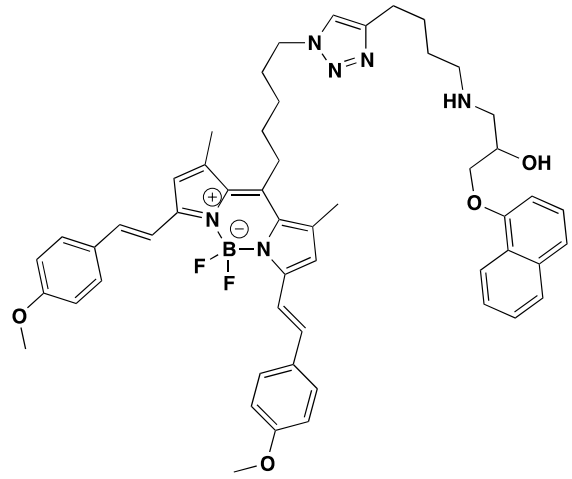

Using general procedure 1 starting with chromis 630 N L5H azide **73** and 1-(hex-5-ynylamino)-3-(naphthalen-1-yloxy)propan-2-ol **53c** yielded a blue solid (2.2 mg, 22%).

HPLC Rt: 23.35 (System 4).

ES-MS MH+ Calc. for $C_{53}H_{60}BF_2N_6O_4$ 893.4732 found 893.4713.

Synthesis of *N*-2-propenyl-2-thiophenecarboxamide 76 [147]

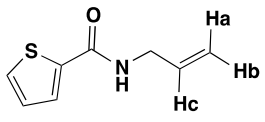

2-Thiophene carbonyl chloride **75** (2.58 mL, 24 mmol) in anhydrous DCM (10 mL) was added drop wise to a mixture of allylamine (1.84 mL, 25 mmol) and pyridine (3.9 mL, 48.4 mmol) in anhydrous DCM (40 mL). The reaction was stirred for four hours under nitrogen. The reaction was diluted with water (25 mL) and the two layers were separated. The organic layer was washed with 2M hydrochloric acid (2 x 10 mL), Brine (2 × 10 mL) and dried. The product was

concentrated to afford a pale yellow solid (3.54 g, 85%). The product was used without further purification.

^{1}H NMR: δ 4.04-4.08 (2H, m, CH_2), 5.18 (1H, dd, *J* 1.5, 10.0, H_b), 5.25- 5.30 (1H, dd, *J* 1.5, 17.0, H_a), 5.89-5.97 (1H, m, H_c), 6.11 (1H, br s, NH), 7.09 (1H, dd, *J* 3.5, 5.0, ArH), 7.47 (1H, dd, *J* 1.1, 5.0, ArH), 7.52 (1H, dd, *J* 1.0, 3.5, ArH).

^{13}C NMR: δ 42.35 (CH_2), 116.78 (=CH_2), 127.61, 128.13, 129.90, 134.01 (3 x ArCH, CH=), 138.81 (4°), 161.78 (C=O).

Mpt: 57-59 °C (Lit 65°C[140]).

FT-IR: (KBr) 3302 (NH str), 1621 (C=O), 1502, 1306, 708.

ES-MS MH+ calc for $C_8H_{10}NOS$ 168.0478 found 168.1099.

Synthesis of 2-(2-thienyl)pyrrole[181] 77

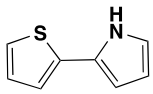

N-2-propenyl-2-thiophenecarboxamide **76** (850 mg, 5.1 mmol) was dissolved in phosgene (20% in toluene) (10 mL) with anhydrous DMF (1 drop). The reaction was stirred at room temperature for 16 hours. Then the solvent was evaporated and the residue was redissolved in anhydrous THF (5 mL). Potassium *tert*-butoxide (1.78 g, 15.8 mmol) was dissolved in anhydrous DMF (10 mL). The THF solution was added dropwise to the DMF solution slowly over an ice bath and stirred for 10minutes. The mixture was poured into ice water (25 mL) and the product was extracted in ether (3 x 15 mL), dried and concentrated. The product was purified by column chromatography eluted in petroleum ether: DCM (1:2) and recrystalised from petroleum ether to yield a yellow solid (262 mg, 34%).

^{1}H NMR: (DMSO-d_6) δ 6.05-6.07 (1H, m, ArH of pyrrole), 6.25-6.27 (1H, m, ArH of pyrrole), 6.78-6.80 (1H, m, ArH of pyrrole), 7.01 (1H, dd, *J* 3.5, 5, ArH of thienyl), 7.18, (1H, dd, *J* 1.2, 3.5, ArH of thienyl), 7.28 (1H, dd *J* 1.2, 5.0, ArH of thienyl), 11.27 (1H, br, s, NH).

^{13}C NMR: (DMSO-d_6) δ 106.34 (ArCH of pyrrole), 109.36 (ArCH of pyrrole), 119.38 (ArCH of pyrrole), 120.92 (ArCH of thienyl), 122.77 (ArCH of thienyl), 126.37 (4 °), 128.17 (ArCH of thienyl), 137.00 (4 °).

Mpt: 73-74 °C (Lit 78°C[172]).

FT-IR: (KBr) 3362 (NH str), 3111 (Ar-H), 726, 686.

Synthesis of 2-formyl-5-(2-thienyl)pyyrole [182] 78

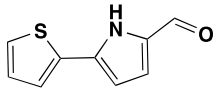

Phosphorus oxychloride (1.34 mL, 14.8 mmol) was added dropwise to anhydrous DMF (1.1 mL, 14.8 mmol) and cooled to 0 °C. The solution was warmed to room temperature and stirred for 15minutes under a N_2 atmosphere. The reaction was cooled to 0 °C and anhydrous 1,2-dichloroethane (25 mL) was added. 2-(2-thienyl) pyrrole **77** (2.0 g, 13.4 mmol) was dissolved in anhydrous 1,2-dichloroethane (66 mL) and added dropwise to the phosphorus oxychloride and refluxed for 90minutes. The reaction was then cooled to room temperature and a solution of sodium acetate (10 g, 27.36 mmol) in water (26 mL) was added and the solution was refluxed for one hour. The solution was cooled to room temperature, the organic layer was collected and the aqueous layer was washed with chloroform (3 × 50 mL). The organic phase was washed with saturated sodium bicarbonate solution (2 × 25 mL), waster (3 × 25 mL) and dried. The organics were concentrated and the residue was purified by column chromatography eluted with petroleum ether: ethyl acetate (3:1) and recrystalised from chloroform and hexane to yield off white crystals (1.07 g, 45%).

^{1}H NMR: δ 6.53 (1H, dd, *J* 1.5, 3.9, ArH of pyrrole), 6.99 (1H, dd, *J*1.2, 3.8, ArH of pyrrole), 7.09 (1H, dd, *J* 3.6,5.0, ArH of thienyl), 7.31 (1H, dd, *J* 1.1, 5.0, ArH of thienyl), 7.39 (1H, dd, *J* 1.1, 3.6, ArH of thienyl), 9.98 1H, br s, NH).

^{13}C NMR: δ 109.56 (ArCH of pyrrole), 123.10 (ArCH of pyrrole), 124.58, 125.94, 128.33 (ArCH of thienyl), 132.99, 133.86, 134.89 (4 □), 178.76 (CHO).

Mpt: 166-167 °C (Lit 167-168[173]).

FT-IR: (KBr) -3170 (NH str), 1646 (C=O), 1481, 1283.

ES-MS MH+ Calc. for C_9H_7NOS 178.0327 found 178.0291.

Synthesis of 4-methoxybenzyl triphenylphosphonium chloride[183,184] 80

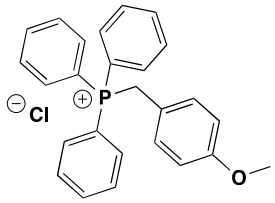

4-Methoxybenzyl chloride **79** (10 g, 63.8 mmol) and triphenylphosphine (16.5 g, 63.8 mmol) were dissolved in anhydrous benzene (30 mL) and refluxed for 22 hours. The solid was then filtered and washed several times with benzene and the product was dried to afford the salt as a white solid (22.8 g, 85%). The product was used without further purification.

^{1}H NMR: (DMSO-d_6) δ 3.69 (3H, s, OMe), 5.08 (2H, m, CH_2), 6.78 (2H, d, *J* 8.5, 2 x ArH), 6.96 (2H, dd, *J* 2.5, 9.0 Hz, 2 x ArH), 7.60-7.76 (15H, m, PPh_3).

^{13}C NMR: (DMSO-d_6) δ 29.88 (CH_2), 55.37 (CH_3), 114.34, 114.37(ArCH), 117.92, 118.77 (4°),

130.14, 130.27, 132.87, 132.92, 134.53, 134.63, 134.91, 134.94, (ArCH).

Mpt: 239-241 °C (Lit 238-240[174]).

FT-IR: (KBr) 2779 (OMe), 1605, 1505, 1438, 1246, 1111.

ES-MS MH+ calc for $C_{26}H_{24}OP$: 383.155 found 383.8857.

Synthesis of 2[(*E*)-methoxyphenyl)ethen-1-yl] pyrrole [149,185] 81

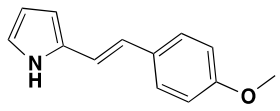

4-Methoxybenzyl triphenyl phosphonium chloride **80** (13.15 g, 31.156 mmol) and sodium hydride (60% dispersion in oil) (1.26 g, 31.56 mmol) were stirred in anhydrous benzene (45 mL) for 30minutes. After this time pyrrole-2-carboxaldehyde (2.5 g, 26.03 mmol) in anhydrous toluene (25 mL) was added by canulla and the reaction was stirred at refluxed for 16 hours.

The reaction mixture was then cooled to room temperature and concentrated. The residue was purified by column chromatography eluted with petroleum ether: ethyl acetate (6:4) and then recrystalised from toluene: petroleum ether to yield a grey solid (260 mg, 5%).

^{1}H NMR: δ 3.82 (1H, s, OCH_3), 6.22-6.24 (1H, m, Pyrrole H), 6.30-6.39 (1H, m, Pyrrole H), 6.60-6.64 (1H, d, *J* 16.5, CH=), 6.79-6.80 (1H, m, Pyrrole H), 6.82-6.86 (1H, d, *J* 16.5, CH=), 6.86-6.88 (2H, d, *J* 8.8, ArH), 7.35-7.37 (2H, d, *J* 8.8, ArH).

^{13}C NMR: δ 55.46 (OCH_3), 108.54 (Pyrrole CH), 110.06 (pyrrole CH), 114.29 (Phenyl CH), 117.26 (Pyrrole CH), 118.78 (alkenyl CH), 123.26 (alkenyl CH), 127.12 (Phenyl CH), 159.89(Phenyl C-O), 130.46 (Pyrrole C), 131.21 (phenyl C).

Mpt: 176-177 °C (169-170°C[142]).

FT-IR: (KBr) 3403 (NH), 1250 (ArC-O), 1602, 1510, 1031, 816.

ES-MS MH+ calc. For $C_{13}H_{14}NO$ 200.1070 found 200.1068.

Synthesis of 2-[(*E*)-2[(4-methoxycarbonylmethoxy)phenyl]ethen-1-yl]pyrrole 83

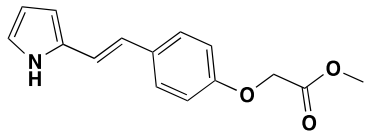

Sodium ethanethiolate (90%, 932 mg, 9.92 mmol), was dissolved in anhydrous DMF (35 mL) at 0 °C. 2-[(*E*)-methoxyphenyl)ethen-1-yl] pyrrole **81** (1 g, 4.96 mmol) was added and refluxed for 3 days under a N_2 environment. The reaction mixture was cooled to room temperature, and washed with water extracted with chloroform. The organics were dried and concentrated. The residue **82** was dissolved in anhydrous THF (20 mL) and treated with Sodium hydride dispersion inmineral oil (60%) (396 mg, 9.92 mmol) and stirred for 5minutes. Methyl bromoacetate (1 mL, 10 mmol) was added to the reaction mixture and stirred for 4 hours under a N_2 environment. The reaction mixture was poured into water (250 mL) and extracted with chloroform (3 x 100 mL). The organics were dried and concentrated. The residue was purified by column chromatography eluted in chloroform to yield a grey solid (610 mg, 48%).

^{1}H NMR: δ 3.81 (3H, s, OMe), 4.64 (2H, s, CH_2), 6.23-6.24 (1H, m, ArH of pyrrole), 6.30-6.32 (1H, m, ArH of pyrrole), 6.59 (1H, dd, *J* 16.4, CH=), 6.78-6.79 (1H, m, ArH of pyrrole), 6.88 (1H, d, *J* 16.4, CH=), 6.9 (2H, 8.7, Phenyl CH), 7.33 (2H, *J*, 8.7, Phenyl CH), 8.3(1H, br s, NH).

^{13}C NMR: δ 52.30 (OMe), 65.41 (CH_2), 108.63, 109.93 (ArCH of pyrrole), 114.90 (Phenyl ArCH), 117.73 (CH=), 118.86 (ArCH of pyrrole), 122.75 (CH=), 127.06 (ArCH of Phenyl) 130.92, 131.50, 156.91 (4°), 169.39 (C=O).

Mpt: 130-132 °C.

FT-IR: (KBr) 3330 (NH), 1748 (C=O), 1222 (ArC-O), 1511, 1178, 731.

ES-MS MH+ calc. For $C_{15}H_{15}N0_3$ 258.1125 found 258.1144.

Synthesis of *N*-(2-azidoethyl)-2-{4-[(*E*)-2 (1*H*-pyrrol-2-yl)ethenyl]phenoxy}acetamide 84

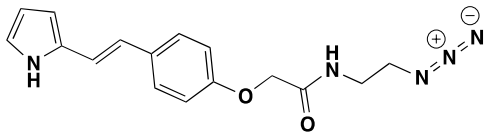

2-[(*E*)-2[(4-Methoxycarbonylmethoxy)phenyl]ethen-1-yl]pyrrole **83** (100 mg, 0.38 mmol) and 2-azidoethanamine (160 mg, 1.9 mmol) were dissolved in methanol (10 mL) and refluxed for 5 days. Reaction was cooled to room temperature and concentrated. The residue was purified by column chromatography eluted in ethyl acetate: hexane (1:1) to yield a grey solid (114 mg, 95%).

^{1}H NMR: δ 3.48-3.56 (4H, m, $\underline{CH_2CH_2}N_3$), 4.51 (2H, s, CH_2), 6.23-6.25 (1H, m, ArH of pyrrole), 6.32-6.34 (1H, m, ArH of pyrrole), 6.59 (1H, dd, *J* 16.4, CH=), 6.80-6.81 (1H, m, ArH of pyrrole), 6.87 (1H, d, *J* 16.4, CH=), 6.9 (2H, 8.7, Phenyl CH), 7.39 (2H, *J*, 8.7, Phenyl CH), 8.30 (1H, br s, NH).

^{13}C NMR; δ 38.40 (CH_2NH), 50.73 (CH_2N_3), 67.42 (CH_2), 108.81, 110.01 (ArCH of pyrrole), 114.93 (Phenyl ArCH), 118.04 (CH=), 118.96 (ArCH of pyrrole), 122.43 (CH=), 127.22 (ArCH of Phenyl) , 130.80, 131.90, 156.11 (4°), 168.52 (C=O).

Mpt: 144-146 °C.

FT-IR: (KBr) 3330 (NH), 1748 (C=O), 1222 (ArC-O), 1432, 1288, 631

ES-MS MH+ calc. For $C_{16}H_{17}N_5O_2$ 312.1455 found 312.1494.

Synthesis of *N*-(((2 azidoethyl)-2-(4,4-difluoro-4,4a-dihydro-5-(thiophenyl)-4-bora-3a,4a-diaza-*s* indacene 3-yl)vinyl)phenoxy)acetamide 85

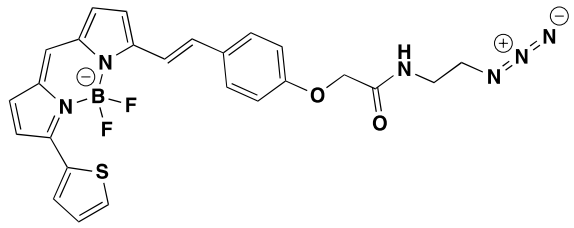

N-(2-azidoethyl)-2-{4-[(*E*)-2 (1*H*-pyrrol-2-yl)ethenyl]phenoxy}acetamide **84** (50 mg, 0.16 mmol) and 2-formyl-5-(2-thienyl)pyrrole **78** (28 mg, 0.16 mmol) were dissolved in MeOH:DCM (1:10, 11 mL). $POCl_3$ (14.8 μL, 0.2 mmol) was added and stirred for 18 hours under a N_2 environment. The reaction mixture was evaporated and the residue was redissolved in DCM (50 mL) Triethylamine (0.1 mL, 0.7 mmol) and $BF_3.OEt_2$ (0.19 mL, 1.5 mmol) added and stirred for 12 hours under a N_2 environment. The mixture was poured into water (150 mL) and washed with brine (3 × 50 mL), dried and concentrated. The residue was purified by preparative layer chromatography eluted in MeOH:DCM (1:9) to yield a blue solid (28 mg, 34%).

^{1}H NMR: δ 3.48-3.56 (4H, m, $\underline{CH_2}\underline{CH_2}N_3$), 4.53 (1H, s, OCH_2), 6.78 (1H, d, *J* 4.1, ArH), 6.84-7.09 (5H, m, ArH), 7.21 (1H, dd, *J* 3.9,5.0, ArH of thienyl), 7.30 (1H, m, CH=), 7.47 (1H, dd, *J* 0.9, 5.0,ArH of thienyl), 7.58-7.63 (3H, m, CH= and 2 × phenyl ArH), 8.20 (1H, dd, *J* 0.9, 3.8, ArH of thienyl)

^{13}C NMR: δ 38.40 ($NHCH_2$), 50.75 (CH_2N_3), 67.22 (CH_2), 115.00, 117.21, 117.74, 119.95, 124.04, 128.23, 128.81, 129.02, 129.55, 129.83, 130.16, (11 × ArCH), 230.6 (ArCH of Thienyl), 134.44, 136.54, 136.82 (3 × 4°) 137.01 (ArCH), 149.34 (4°), 156.33 (4°), 157.95 (4°), 168.21 (C=O).

Mpt: 157-158 °C.

ES-MS MNa+ calc. For $C_{25}H_{21}BF_2N_6O_2S$ 541.1400 found 541.1448.

Synthesis of *N*-((*N*-((ethyl-2-(4,4-difluoro-4,4a-dihydro-5-(thiophenyl)-4-bora-3a,4a-diaza-*s* indacene 3-yl)vinyl)phenoxy)acetamide -1*H*-1,2,3-triazol-4-yl)methyl)-2-((2-hydroxy-3-(naphthalen-1-yloxy)propyl)amino)acetamide 87

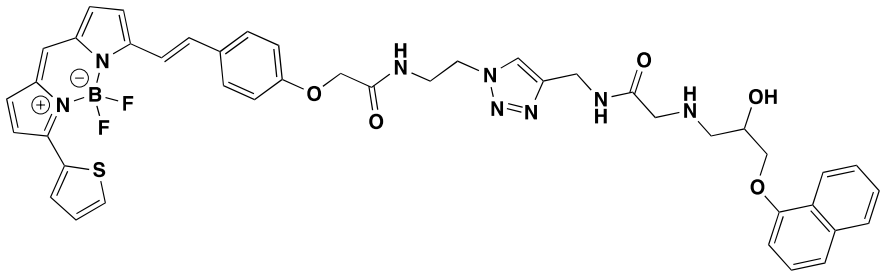

Using general procedure 1 starting with *N*-(2 azidoethyl)-2-(4,4-difluoro-4,4a-dihydro-5-(thiophenyl)-4-bora-3a,4a- diaza-s indacene 3-yl)vinyl)phenoxy)acetamide **85** and 2-(2-hydroxy-3-(naphthalen-1-yloxy)propylamino)-*N*-(prop-2-ynyl)acetamide **71** yielded a blue solid (2 mg, 45%).

HPLC Rt: 23.32 (System 4).

ES-MS MH+ calc. For $C_{43}H_{42}BF_2N_8O_5$ 831.3055 found 831.2963.

Synthesis of capped fluorophores

Synthesis of 4,4-difluoro-8-(4-((1-(2-phenoxypropyl)-1*H*-1,2,3-triazol-4-yl)methanamine))phenyl-2,6-dimethyl-4-bora-3a,4adiaza-s-indacene 88a

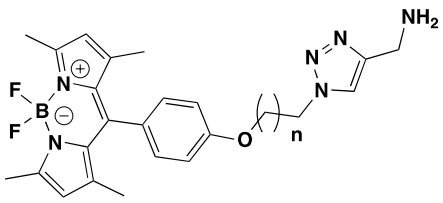

Using general procedure 1 starting with propargylamine and 4,4-difluoro-8-(4-(3-azidopropoxy))phenyl-2,6-dimethyl-4-bora-3a,4adiaza-s-indacene **46** yielded red solid. (6 mg, 60%).

HPLC Rt: 12.37 (System 1), 15.55 (System 2).

ES-MS MH+ calc. For $C_{25}H_{30}BF_2N_60_2$ 479.2537 found 479.2273.

Synthesis of 4,4-difluoro-8-(4-((1-(2-phenoxypentyl)-1*H*-1,2,3-triazol-4-yl)methanamine))phenyl-2,6-dimethyl-4-bora-3a,4adiaza-s-indacene 88b

Using general procedure 1 starting with progargylamine and 4,4-difluoro-8-(4-(5-azidopentyl))phenyl-2,6-dimethyl-4-bora-3a,4adiaza-s-indacene **61** yielded a red solid (3.5 mg, 76%).

HPLC Rt: 15.02 (System 1), 16.85 (System 2).

ES-MS M-FH+ calc. For $C_{27}H_{33}BFN_6O$ 486.2523 found 486.2526.

Synthesis of (3-bromopropoxy) benzene[186] 90

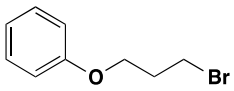

1,5-Dibromopentane (2.08 mL, 15.2 mmol) K_2CO_3 (3.8 g, 27.6 mmol) were stirred in DMF (100 mL). to this, phenol **89** (1.69 g, 13.84 mmol) dissolved in DMF (10 mL) was added dropwise and stirred at room temperature for 15 hours. The reaction mixture was poured into water and extracted with toluene. The organic phase was washed with brine, dried and concentrated. The residue was purifed by column chromatography eluted in MeOH:DCM (1:9) to yield a clear oil (3.7 g, 99% yield).

^{1}H NMR: δ 2.26-2.32 (2H, m, $\underline{CH_2}CH_2Br$), 3.58 (2H, t, *J* 6.4, CH_2Br), 4.08 (2H, t, *J* 5.8 OCH_2) 6.92 (2H, d, *J* 8.8, Ar$\underline{CH}$CO), 6.90-6.97 (1H, m, ArCH), 7.26-7.30, (2H, m, $\underline{ArCH}$CO).

^{13}C NMR: δ 30.09 ($\underline{CH_2}CH_2Br$), 32.43 ($\underline{CH_2}Br$), 65.19 ($O\underline{CH_2}$), 114.53 (ArCH-*p*), 120.94 (ArCH-*m*), 129.52 (ArCH-*o*), 158.69 (ArCO)

FT-IR: (NaCl) 3039, 2928 (C=O str(, 1600, 1498, 1387 (C-O str).

Synthesis of (3-azidopropoxy)benzene 91

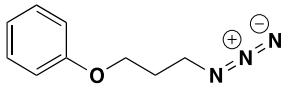

(3-Bromopropoxy) benzene **90** (3 g, 13.9 mmol) and sodium azide (2.26 g, 34.75 mmol) were refluxed in DMF (50 mL) at 100 °C for six hours. The reaction mixture was poured into water and extracted with ethyl acetate, dried and concentrated to yield a clear oil (2.47 g, 80%). This product was used without further purification.

^{1}H NMR: δ 2.02-2.08 (2H, m, $\underline{CH_2}CH_2N_3$), 3.51 (2H, t, *J* 6.5, CH_2N_3), 4.04 (2H, t, *J* 5.9 OCH_2) 6.91 (2H, d, *J* 7.8, Ar$\underline{CH}$CO), 6.94-6.98 (1H, m, ArCH), 7.25-7.31, (2H, m, $\underline{ArCH}$CO).

^{13}C NMR: δ 28.79 ($\underline{CH_2}CH_2N_3$), 48.26 ($\underline{CH_2}N_3$), 64.36 ($O\underline{CH_2}$), 114.46 (ArCH-*p*), 120.90 (ArCH-*m*), 129.42 (ArCH-*o*), 158.64 (ArCO).

FT-IR: (NaCl) 3042, 2916, 2103, 1599, 1492, 1374.

Synthesis of 1-(naphthalen-1-yloxy)-3-((4-(1-(3-phenoxypropyl)-1*H*-1,2,3-triazol-4-yl)butyl)amino)propan-2-ol 92

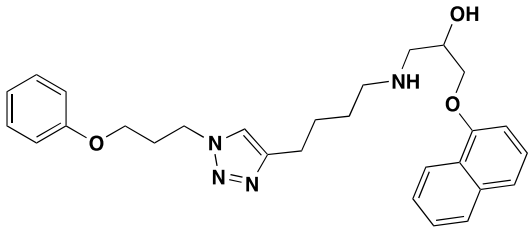

Using general procedure 1 starting with (3-azidopropoxy)benzene **91** and 1-(hex-5-ynylamino)-3-(naphthalen-1-yloxy)propan-2-ol **56c** yielded a brown solid (1.3 mg, 62%).

HPLC Rt: 15.55 (System 1).

ES-MS MH+ calc. For $C_{28}H_{35}N_40_3$ 475.2704 found 475.2794.

Synthesis of (3*R*)-1-azabicyclo[2.2.2]oct-3-yl oxo(phenyl)acetate[165] 103

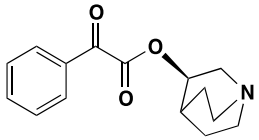

Phenylglyoxylic acid **101** (1 g, 6.6 mmol) dissolved in anhydrous chloroform (22 mL) and cooled to 0 °C. Oxalyl chloride (1 mL, 11.5 mmol) was added with DMF (2 drops). The reaction mixture was warmed to room temperature and stirred for 90minutes.

The solvent was evaporated and co-evaporated with chloroform (2 x 10 mL) and petroleum ether (1 x 15 mL). The residue was redissolved in anhydrous chloroform (10 mL) and added to a solution of (3R)- quinuclidinol (1 g, 7.86 mmol, dissolved in chloroform 15 mL). The reaction was stirred for 4 hours and a solution of K_2CO_3 (10%) was added. The product was extracted with chloroform (3 x 25 mL), dried and concerntrated to yield an off white solid (1.64 g, 96%).

^{1}H NMR: δ 1.40-1.49 (1H, m, CH), 1.59-1.68 (1H, m, CH_2), 1.73-1.76 (1H, m, CH_2), 1.84-1.91 (1H, m,CH_2), 2.72-2.93 (5H, m, CH_2), 3.32-3.39 (1H, m, CH_2), 5.12-5.16 (1H, m, OCH), 7.50-7.45 (m, 2H, ArCH), 7.64-7.69 (1H, m, ArCH), 7.98-8.01 (2H, m, ArCH).

^{13}C NMR: δ 19.29 (CH_2), 24.49 (CH2), 25.26 (CH), 46.47 (CH2), 47.32 (CH2), 55.09 (CH2), 74.00 (OCH), 128.97 (ArCH), 129.96 (ArCH), 132.43 (ArC), 134.97 (ArCH), 163.87 (ArCCO), 186.36 (COOCH).

Mpt: 187-188 °C.

FT-IR (KBr) 2784, 1820, 1726 (ester), 1449, 1020.

ES-MS MH+ calc. For $C_{15}H_{17}N0_3$ 260.1281 found 260.1281.

Synthesis of (3*R*)-1-azabicyclo[2.2.2]oct-3-yl hydroxy(diphenyl)acetate[165] 104

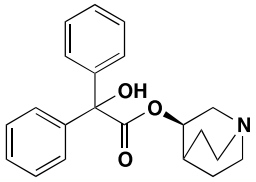

A solution of (3*R*)-1-Azabicyclo[2.2.2]oct-3-yl oxo(phenyl)acetate **103** (1 g, 3.85 mmol) dissolved in anhydrous THF (10 mL) was cooled to -42 °C. Phenyllithium (1.8 M in dibutyl ether, 2.5 mL, 4.24 mmol) was added slowly and the reaction mixture was stirred for 10minutes. The reaction mixture was then warmed to room temperature and stirred for a further 90minutes.

The reaction mixture was then poured into a saturated solution of ammonium chloride and the product was extracted with diethyl ether (3 x 50 mL). The organics were combined, dried and concentrated. The residue was treated with diisopropyl ether and the product was filtered to yield a yellow solid (862 mg, 66%).

^{1}H NMR: δ 1.16 (1H, m, CH), 1.20-1.25 (1H, m, CH_2), 1.29-1.35 (1H, m, CH_2), 1.44-1.54 (1H, m, CH_2), 1.56-1.68 (1H, m, CH_2), 1.96-2.01 (1H, m, CH_2), 2.43-2.51 (2H, m, CH_2), 2.59-2.69 (3H, m, CH_2), 3.08-3.14 (1H, m, CH_2), 4.93-4.95 (1H, m, OCH), 5.19 (s, br, 1H, OH), 7.29-7.39 (6H, m, ArCH), 7.42-7.46 (4H, m, ArCH).

^{13}C NMR: δ 19.16 (CH_2), 24.05 (CH_2), 25.01 (CH), 46.00 (CH_2), 46.84 (CH_2), 54.64 (CH_2), 73.81 (OCH), 77.29 (COH), 127.03 (ArC), 127.45(ArC), 127.80(ArC), 127.95(ArC), 128.00(ArC), 128.06(ArC), 128.24(ArC), 142.33(ArC), 174.16 (CO).

Mpt: 189-191 °C.

FT-IR: (KBr) 3051(OH str), 2784, 1726 (ester), 1449.

HPLC Rt: 12.37 (System 1), 15.55 (System 2).

ES-MS MH+ calc. For $C_{21}H_{24}N0_3$ 338.1751 found 338.1876.

Synthesis of 2-bromo *N*-(prop-2-ynyl) acetamide[187] 107

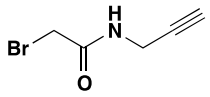

Bromoacetic acid **105** (1 g, 7.2 mmol) was dissolved in anhydrous chloroform (10 mL) and cooled to 0 °C. Oxalyl chloride (0.81 mL, 9.44 mmol) was added to the solution followed by DMF (2 drops). The reaction mixture was warmed to room temperature and stirred for 90minutes. The solvent was evaporated and co-evaporated with chloroform (2 × 10 mL) and petroleum ether (1 × 10 mL). The residue was redissolved in anhydrous chloroform (10 mL) and added to a solution of propargylamine (0.51 mL, 79 mmol) dissolved in anhydrous chloroform (10 mL). The reaction was stirred for 4 hours and a solution of 10% K_2CO_3 was added. The aqueous layer was washed with chloroform. The organics were combined and wash with 1M HCl. The organic phase was washed with brine, dried and concentrated to yield a yellow solid (660 mg, 52%). The product was used without further purification.

^{1}H NMR: δ 2.27 (1H, t, *J* 2.5, C<u>CH</u>), 3.89 (2H, s, NH<u>CH$_2$</u>), 4.07-4.09 (2H, m, Br<u>CH$_2$</u>CO), 6.70 (1H, s, br, NH).

^{13}C NMR: δ 28.6 (NH<u>CH$_2$</u>), 29.96 (Br<u>CH$_2$</u>CO), 72.2 (C<u>CH</u>), 78.5 (<u>C</u>CH)

Mpt: 144-145 °C.

FT-IR: (KBr) 3330 (NH str), 2956, 1672 , 1544.

Synthesis of 1-(3-bromopropoxy)-3-ethynylbenzene 110

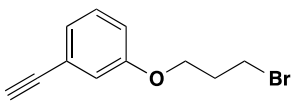

1,3-Dibromopropane **108** (1.88 mL, 18.6 mmol) was dissolved in acetone (100 mL). K_2CO_3 (1.17 g, 8.46 mmol) was added and stirred for 15minutes. 3-Hydroxyphenol acetylene **109** (0.46 mL, 4.23 mmol) was dissolved in acetone (50 mL) and was added dropwise to the reaction mixture over 3 hours and then stirred overnight.The solvent was evaporated and the

residue was redisolved in DCM. The organic was washed with water (3 × 15 mL), dried and concentrated.

The residue was purified by column chromatography eluted with ethyl acetate: hexane (4:6) to yield a clear oil (116 mg, 46%).

^{1}H NMR: δ 1.26 (2H, t, *J* 7.2, CH2), 3.03 (1H, s, CCH), 3.4-3.56, (4H, m, 2x CH2), 6.80-6.85 (1H, m, ArH), 6.94-6.96 (1H, m, ArH), 7.02-7.05 (1H, m, ArH), 7.16 (1H, t, *J* 7.8, ArH).

^{13}C NMR δ 15.1 (CH_2), 60.5 (CH_2), 66.0 (CH_2), 76.9 (CCH), 83.4 (CCH), 116.4 (ArCH), 118.84 (ArCH), 123.14 (ArC), 124,31 (ArCH), 129.56 (ArCH), 155.89 (ArCO).

Synthesis of (*R*)-3-(2-hydroxy-2,2-diphenylacetoxy)-1-(prop-2-yn-1-yl)quinuclidinium bromide 111a

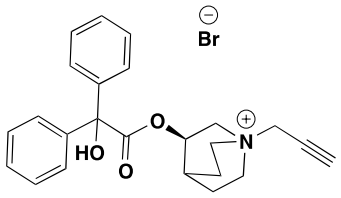

Using general procedure 2 starting with (3*R*)-1-azabicyclo[2.2.2]oct-3-yl hydroxy(diphenyl)acetate **104** (75 mg, 0.22 mmol) and propargyl bromide solution (80% in toluene, 650 mg, 0.474 mL, 0.55 mmol) to yield a white solid (45%).

^{1}H NMR: δ 1.59-1.61 (1H, m), 1.61-1.63 (1H, m), 2.04-2.10 (3H, m), 2.40-2.43 (2H, m), 2.59 (1H, t, *J* 2.6, CCH), 2.72-2.75 (2H, m), 3.07-3.15 (2H, m), 3.35-3.41 (3H, m), 7.35-7.40 (5H, ArCH), 7.45-7.49 (5H, ArCH).

^{13}C NMR: δ 19.16 (CH_2), 24.05 (CH_2), 25.01 (CH), 46.00 (CH_2), 43.12 (CH_2). 46.84 (CH_2), 54.64 (CH_2), 72.25 (CCH), 73.81 (OCH), 77.29 (COH), 78.5 (CCH), 127.03 (ArC), 127.45(ArC), 127.80 (ArC), 127.95 (ArC), 128.00 (ArC), 128.06 (ArC), 128.24 (ArC), 142.33 (ArC), 174.16 (CO).

mp – 175-176 °C

FT-IR 3051(OH str), 2784, 1745 (ester), 1579, 1449

HPLC Rt: 9.03 (System 1), 10.60 (System 2).

ES-MS M-Br+ calc. For $C_{24}H_{26}NO_3$ Calc 376.1907 found 376.1849

Synthesis of (*R*)-1-(but-3-yn-1-yl)-3-(2-hydroxy-2,2-diphenylacetoxy)quinuclidinium bromide 111b

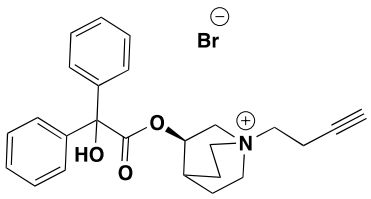

Using general procedure 2 starting with (3*R*)-1-azabicyclo[2.2.2]oct-3-yl hydroxy(diphenyl)acetate **104** (50 mg, 0.14 mmol) and 4-bromo-1-butyne (36 μl, 0.37 mmol) to yield a white solid (16 mg, 25%).

^{1}H NMR: δ 1.59-1.61 (1H, m), 1.61-1.63 (1H, m), 1.79-1.81 (1H,m), 2.00-2.10 (3H, m), 2.40-2.43 (1H, m), 2.60 (1H, t, *J* 2.6, CCH), 2.72-2.75 (2H, m), 3.05-3.12 (2H, m), 3.45-3.51 (3H, m), 5.21-5.30 (2H, m), 7.35-7.40 (5H, ArCH), 7.45-7.49 (5H, ArCH).

^{13}C NMR: δ 19.16 (CH_2), 24.05 (CH_2), 25.01 (CH), 42.11 (CH_2), 43.12 (CH_2), 46.00 (CH_2),. 46.84 (CH_2), 54.64 (CH_2), 72.24 (C<u>CH</u>), 73.81 (OCH), 77.29 (COH), 78.5 (<u>C</u>CH), 127.03 (ArC), 127.45 (ArC), 127.80 (ArC), 127.95 (ArC), 128.00 (ArC), 128.06 (ArC), 128.24 (ArC), 142.33 (ArC), 174.16 (CO).

Mpt: 185-186 °C.

FT-IR: (KBr) 3075(OH), 2884, 1706 (ester), 1449, 1215.

HPLC Rt: 12.37 (System 1), 15.55 (System 2).

ES-MS M-Br+ Calc. For $C_{25}H_{28}N0_3$ 390.2064 found 390.1799.

Synthesis of (*R*)-3-(2-hydroxy-2,2-diphenylacetoxy)-1-(pent-4-yn-1-yl)quinuclidinium chloride 111c

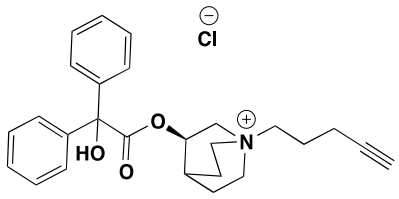

Using general procedure 2 starting with (3*R*)-1-azabicyclo[2.2.2]oct-3-yl hydroxy(diphenyl)acetate **104** (50 mg, 0.14 mmol) and 5-chloro-1-pentyne (0.36 mL, 3.5 mmol) yielded a white solid (40 mg, 66%).

^{1}H NMR: δ 1.59-1.61 (1H, m), 1.65-1.78 (3H, m), 2.05 (1H, t, *J* 2.5, CCH), 2.22-2.25 (2H, m), 2,40 (1H, s), 2.95-3.05 (1H, m), 3.24-3.36 (5H,m), 3.40-3.50 (1H,m), 3.86-2.94 (1H, m), 4.40-4.60 (3H, m), 5.21-5.30 (1H, m), 7.30-7.36 (5H, m, ArCH), 7.39-7.43 (5H, m, ArCH).

^{13}C NMR δ 19.14 (CH_2), 24.05 (CH_2), 25.09 (CH), 35.60 (CH_2), 42.14 (CH_2), 43.12. 46.00 (CH_2), 46.84 (CH_2), 54.64 (CH_2), 60.81 (CH_2) 72.21 (C<u>C</u>H), 73.81 (OCH), 77.29 (COH), 78.5 (<u>C</u>CH), 127.03 (ArC), 127.45 (ArC), 127.80 (ArC), 127.95 (ArC), 128.00 (ArC), 128.06 (ArC), 128.24 (ArC), 142.33 (ArC), 174.16 (CO.)

Mpt: 188-190 °C.

HPLC Rt: 12.37 (System 1), 15.55 (System 2).

FT-IR: (KBr) 3141(OH), 2384, 1940, 1666 (ester), 1310.

ES-MS M-Cl+ Calc. For $C_{26}H_{30}NO_3$ Calc 404.2220 found 404.2230.

Synthesis of (*R*)-1-(hex-5-yn-1-yl)-3-(2-hydroxy-2,2-diphenylacetoxy)quinuclidinium chloride 111d

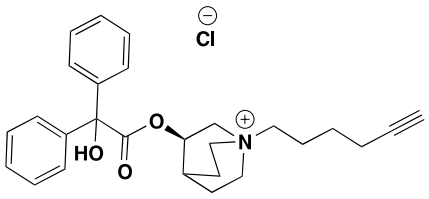

Using general procedure 2 starting with (3*R*)-1-azabicyclo[2.2.2]oct-3-yl hydroxy(diphenyl)acetate **104** (50 mg, 0.14 mmol) and 6-chloro-1-hexyne (0.43 mL, 3.5 mmol) yielded a white solid (34 mg, 53%).

^{1}H NMR: δ 1.52-1.58 (2H, m, CH_2), 1.62-1.8 (4H, m, 2x CH_2), 1.95-2.15 (2H, m, CH_2), 2.28-2.37 (2H, CH_2), 2.42 (1H, s, CCH), 2.90-3.0 (1H, m, CH_2), 3.0-3.5 (7H, m, CH_2), 3.7-3.9 (2H, m, CH), 5.25-5.4 (1H,m, CHO), 7.32-7.49 (10H, m, ArH)

^{13}C NMR: δ, 17.6, 25.7, 35.70, 42.19, 43.12, 46.91, 54.64, 59.8, 60.92 (CH_2), 23.5 (CCH), 23.7 (CCH), 68.4, 68.7 (CH), 142.2 (COHCOO), 127.03 (ArC), 127.45 (ArC), 127.80 (ArC), 127.95 (ArC), 128.00 (ArC), 128.06 (ArC), 128.24 (ArC), 142.33 (ArC), 172.6 (CO).

Mpt: 190-191 °C.

FT-IR: (KBr) 3101 (OH), 2904, 1889, 1712 (ester).

HPLC Rt: 9.72 (System 1), 11.34 (System 2).

ES-MS M-Cl+ Calc. For $C_{27}H_{32}NO_3$+ Calc 418.2378 found 418.2420.

Synthesis of (*R*)-3-(2-hydroxy-2,2-diphenylacetoxy)-1-(2-oxo-2-(prop-2-yn-1-ylamino)ethyl) quinuclidinium bromide 111e

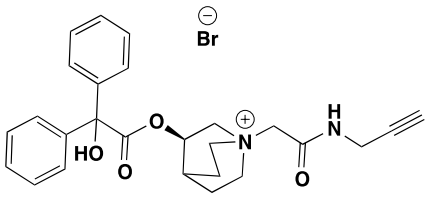

Using general procedure 2 starting with (3*R*)-1-azabicyclo[2.2.2]oct-3-yl hydroxy(diphenyl)acetate **104** (75 mg, 0.22 mmol) and 2-bromo *N*-(prop-2-ynyl) acetamide **107** (97 mg, 0.56 mmol) yielded a white solid (75 mg, 66%).

^{1}H NMR: δ 2.00-2.10 (2H,m), 237-2.43 (1H,m), 3.32-3.33 (1H, m), 3.36-3.44 (1H, m), 3.55-3.65 (2H,m), 3.82-3.86 (2H, m), 3.96-4.02 (5H, m), 5.30-5.35 (1H,m), 4.10-4.14 (1H, m), 7.32-7.48 (10H,m, ArH).

^{13}C NMR: δ 19.16 (CH_2), 24.05 (CH_2), 25.01 (CH), 42.11 (CH_2), 46.00 (CH_2),. 46.84 (CH_2), 56.64 (CH_2), 60.12 (CH_2) 72.24 (C<u>C</u>H), 73.81 (OCH), 77.29 (COH), 78.5 (<u>C</u>CH), 127.03 (ArC), 127.45(ArC), 127.80(ArC), 127.95(ArC), 128.00(ArC), 128.06(ArC), 128.24(ArC), 142.33(ArC), 174.16 (CO).

Mpt: 189-190 °C.

FT-IR: (KBr) 3330, 3051(OH), 2784, 1726 (ester), 1670, 1449.

HPLC Rt: 9.03 (System 1), 10.60 (System 2).

ES-MS M-Br^+ Calc. For $C_{26}H_{29}N_2O_4$+ Calc 433.2122 found 433.2179.

Synthesis of (*R*)-1-(3-(3-ethynylphenoxy)propyl)-3-(2-hydroxy-2,2-diphenylacetoxy) quinuclidinium bromide 111f

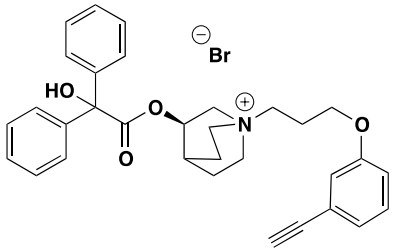

Using general procedure 2 starting with (3*R*)-1-azabicyclo[2.2.2]oct-3-yl hydroxy(diphenyl)acetate **104** (50 mg, 0.14 mmol) and 1-(3-bromopropoxy)-3-ethynylbenzene **110** (83 mg, 3.48 mmol) yielded a white solid (34 mg, 53%).

^{1}H NMR: δ 1.70-1.74 (1H,m), 1.95-2.03 (2H, m), 2.75-2.76 (2H, m), 2.98 (1H, s), 3.40-3.55 (5H, m), 3.72-3.78 (1H,m), 4.04-4.15 (1H, m), 4.37-4.42 (2H, m), 5.20-5.26 (1H, m), 7.29-7.45 (14H, m, ArCH).

^{13}C NMR δ 19.14 (CH_2), 24.05 (CH_2), 25.09 (CH),35.60 (CH_2), 42.14 (CH_2), 43.12 (CH_2), 46.00 (CH_2), 46.84 (CH_2), 54.64 (CH_2), 72.21 (C<u>CH</u>), 73.81 (OCH), 77.29 (COH), 78.5 (<u>C</u>CH),125.51 (ArC), 127.03 (ArC), 127.45 (ArC), 127.80 (ArC), 127.95 (ArC), 128.00 (ArC), 128.06 (ArC), 128.24 (ArC), 1290.33 (ArC), 131.11 (ArCH), 142.33 (ArC), 174.16 (CO).

Mpt: 165-167 °C.

FT-IR: (KBr) 3101 (OH), 2904, 1889, 1712 (ester), 1459, 1201.

HPLC Rt: 11.20 (System 1), 12.95 (System 2).

ES-MS M-Br+ calc. $C_{32}H_{34}NO_4$+ 496.2482 found 496.2449.

Synthesis of (*R*)-1-((4,4-difluoro-8-(4-(3-propoxy))phenyl-2,6-dimethyl-4-bora-3a,4adiaza-s-indacene -1*H*-1,2,3-triazol-4-yl)methyl)-3-(2-hydroxy-2,2-diphenylacetoxy) quinuclidinium bromide 112a

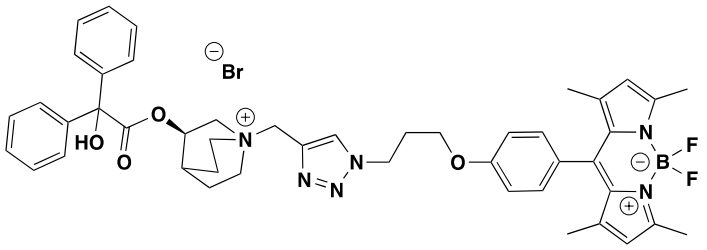

Using general procedure 1 starting with (*R*)-3-(2-hydroxy-2,2-diphenylacetoxy)-1-(prop-2-yn-1-yl)quinuclidinium bromide **111a** and 4,4-difluoro-8-(4-(3-azidopropoxy))phenyl-2,6-dimethyl-4-bora-3a,4adiaza-s-indacene **46** yielded a red solid (1.0 mg, 50%).

HPLC Rt: 12.90 (System 1).

ES-MS M-Br+ calc. For $C_{46}H_{50}BF_2N_6O_4$ 799.3949 found 799.3915.

Synthesis of (*R*)-1-((4,4-difluoro-8-(4-pentyl)phenyl-2,6-dimethyl-4-bora-3a,4adiaza-s-indacene -1*H*-1,2,3-triazol-4-yl)methyl)-3-(2-hydroxy-2,2-diphenylacetoxy)quinuclidinium bromide 112b

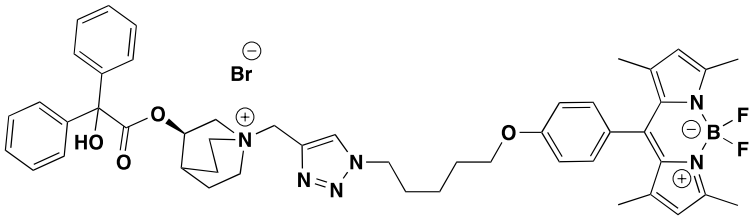

Using general procedure 1 starting with (*R*)-3-(2-hydroxy-2,2-diphenylacetoxy)-1-(prop-2-yn-1-yl)quinuclidinium bromide **111a** and 4,4-difluoro-8-(4-(5-azidopentyl))phenyl-2,6-dimethyl-4-bora-3a,4adiaza-s-indacene **61** yielded a red solid (2.2mg, 40%).

HPLC Rt: 13.46 (System 1), 15.17 (System 2).

ES-MS M-Br+ calc. For $C_{48}H_{54}BF_2N_6O_4$ 827.4262 found 827.4321.

Synthesis of (*R*)-1-((4,4-difluoro-8-(2-ethoxy)ethoxy)phenyl-2,6-dimethyl-4-bora-3a,4adiaza-s-indacene -1*H*-1,2,3-triazol-4-yl)methyl)-3-(2-hydroxy-2,2-diphenylacetoxy)quinuclidinium bromide 112c

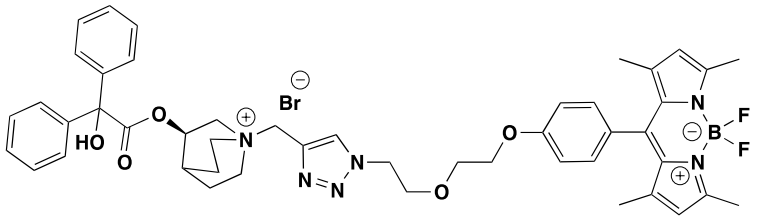

Using general procedure 1 starting with (*R*)-3-(2-hydroxy-2,2-diphenylacetoxy)-1-(prop-2-yn-1-yl)quinuclidinium bromide **111a** and 4,4-difluoro-8-(4-(2-azidoethoxy)ethoxy))phenyl-2,6-dimethyl-4-bora-3a,4adiaza-s-indacene **65** yielded a red solid (3.3 mg, 33%).

HPLC Rt: 12.78 (System 1), 15.00 (System 2).

ES-MS M-Br+ calc. For $C_{47}H_{52}BF_2N_6O_5$ 829.4055 found 829.4056.

Synthesis of (*R*)-1-(2-(4,4-difluoro-8-(4-(3-propoxy))phenyl-2,6-dimethyl-4-bora-3a,4adiaza-s-indacene -1*H*-1,2,3-triazol-4-yl)ethyl)-3-(2-hydroxy-2,2-diphenylacetoxy)quinuclidinium bromide 113a

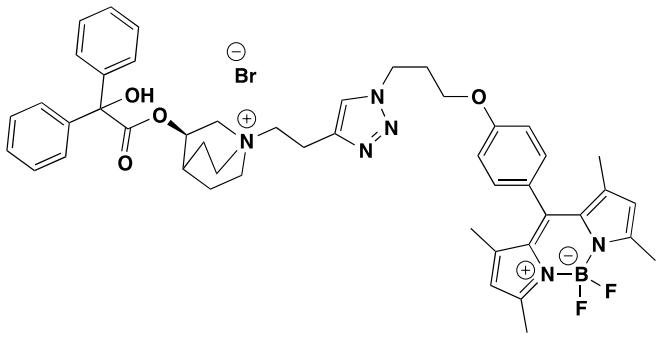

Using general procedure 1 starting with (*R*)-1-(but-3-yn-1-yl)-3-(2-hydroxy-2,2-diphenylacetoxy)quinuclidinium bromide **111b** and 4,4-difluoro-8-(4-(3-

azidopropoxy))phenyl-2,6-dimethyl-4-bora-3a,4adiaza-s-indacene **46** yielded a red solid (0.8mg, 39%).

HPLC Rt: 12.75 (System 1), 15.22 (System 2).

ES-MS M-Br+ calc. For $C_{47}H_{52}BF_2N_6O_4$ 813.4106 found 813.4292.

Synthesis of (*R*)-1-(2-(4,4-difluoro-8-(4-pentyl)phenyl-2,6-dimethyl-4-bora-3a,4adiaza-s-indacene -1*H*-1,2,3-triazol-4-yl)ethyl)-3-(2-hydroxy-2,2-diphenylacetoxy)quinuclidinium bromide 113b

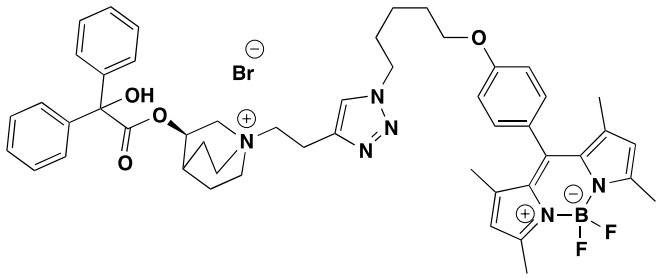

Using general procedure 1 starting with (*R*)-1-(but-3-yn-1-yl)-3-(2-hydroxy-2,2-diphenylacetoxy) quinuclidinium bromide **111b** and 4,4-difluoro-8-(4-(5-azidopentyl))phenyl-2,6-dimethyl-4-bora-3a,4adiaza-s-indacene **61** yielded a red solid (0.4 mg, 20%).

HPLC Rt: 15.80 (System 2).

ES-MS M-Br+ calc. For $C_{49}H_{56}BF_2N_6O_4$ 841.4419 found 841.4412.

Synthesis of (*R*)-1-(2-(4,4-difluoro-8-(2-ethoxy)ethoxy)phenyl-2,6-dimethyl-4-bora-3a,4adiaza-s-indacene -1*H*-1,2,3-triazol-4-yl)ethyl)-3-(2-hydroxy-2,2-diphenylacetoxy)quinuclidinium bromide 113c

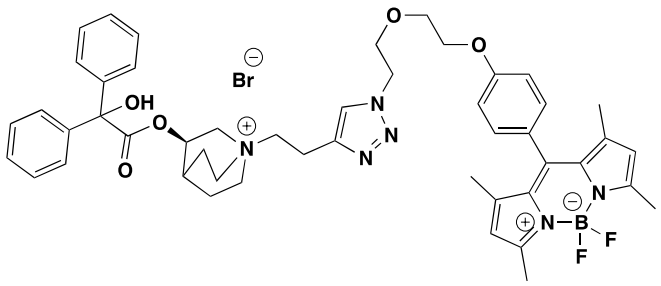

Using general procedure 1 starting with (*R*)-1-(but-3-yn-1-yl)-3-(2-hydroxy-2,2-diphenylacetoxy) quinuclidinium bromide **111b** 4,4-difluoro-8-(4-(2-azidoethoxy)ethoxy))phenyl-2,6-dimethyl-4-bora-3a,4adiaza-s-indacene **65** yielded a red solid (1.3mg, 65%).

HPLC Rt: 12.70 (System 1), 15.07 (System 2).

ES-MS M-Br+ calc. For $C_{48}H_{54}BF_2N_6O_5$ 843.4211 found 843.4338.

Synthesis of (*R*)-1-(3-(4,4-difluoro-8-(4-(3-propoxy))phenyl-2,6-dimethyl-4-bora-3a,4adiaza-s-indacene -1*H*-1,2,3-triazol-4-yl)propyl)-3-(2-hydroxy-2,2-diphenylacetoxy)quinuclidinium chloride 114a

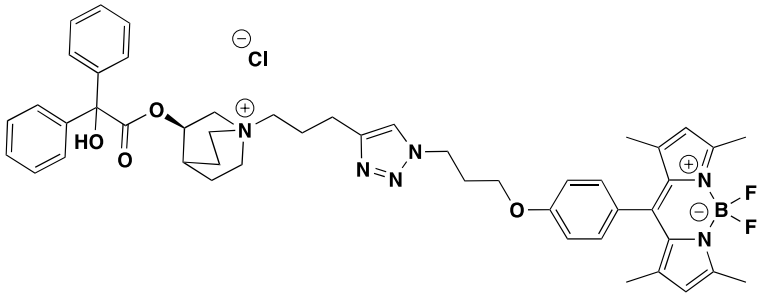

Using general procedure 1 starting with (*R*)-3-(2-hydroxy-2,2-diphenylacetoxy)-1-(pent-4-yn-1-yl)quinuclidinium chloride **111c** and 4,4-difluoro-8-(4-(3-azidopropoxy))phenyl-2,6-dimethyl-4-bora-3a,4adiaza-s-indacene **46** yielded a red solid (1 mg, 50%).

HPLC Rt: 12.80 (System 1), 15.02 (System 2)

ES-MS M-Cl+ calc. For $C_{48}H_{54}BF_2N_6O_4$ 827.4262 found 827.4254.

Synthesis of (*R*)-1-(3-(4,4-difluoro-8-(4-pentyl)phenyl-2,6-dimethyl-4-bora-3a,4adiaza-s-indacene -1*H*-1,2,3-triazol-4-yl)propyl)-3-(2-hydroxy-2,2-diphenylacetoxy)quinuclidinium chloride 114b

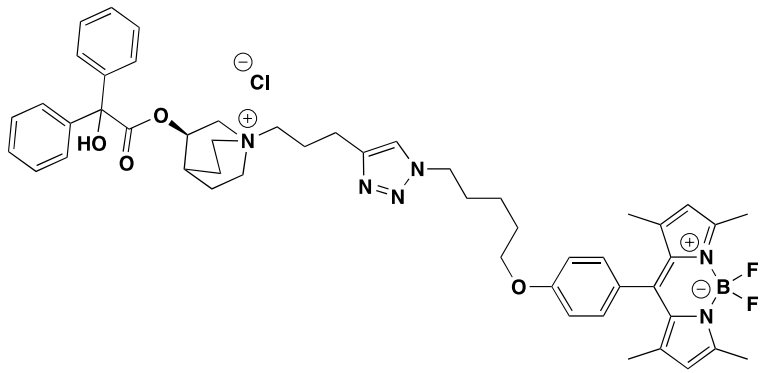

Using general procedure 1 starting with (*R*)-3-(2-hydroxy-2,2-diphenylacetoxy)-1-(pent-4-yn-1-yl)quinuclidinium chloride **111c** and 4,4-difluoro-8-(4-(5-azidopentyl))phenyl-2,6-dimethyl-4-bora-3a,4adiaza-s-indacene **61** yielded a red solid (0.5 mg, 25%).

HPLC Rt: 13.35 (System 1), 15.90 (System 3).

ES-MS M-Cl+ calc. For $C_{50}H_{58}BF_2N_6O_4$ 855.4574 found 855.4575.

Synthesis of (*R*)-1-(4-(4,4-difluoro-8-(4-(3-propoxy))phenyl-2,6-dimethyl-4-bora-3a,4adiaza-s-indacene -1*H*-1,2,3-triazol-4-yl)butyl)-3-(2-hydroxy-2,2-diphenylacetoxy)quinuclidinium chloride 115a

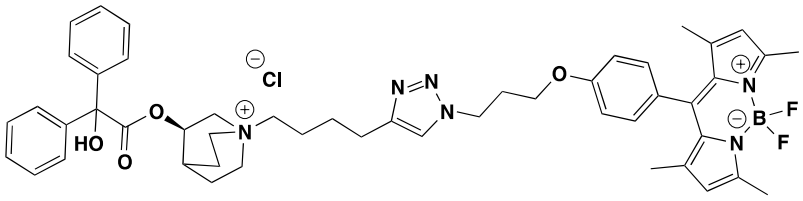

Using general procedure 1 starting with (*R*)-1-(hex-5-yn-1-yl)-3-(2-hydroxy-2,2-diphenylacetoxy)quinuclidinium chloride **111d** and 4,4-difluoro-8-(4-(3-azidopropoxy))phenyl-2,6-dimethyl-4-bora-3a,4adiaza-s-indacene **46** yielded a red solid (1.2 mg, 64%).

HPLC Rt: 12.87 (System 1), 15.53 (System 2).

ES-MS M-Cl+ calc. For $C_{49}H_{56}BF_2N_6O_4$ 841.4419 found 841.4412.

Synthesis of (*R*)-1-(4-(4,4-difluoro-8-(4-pentyl)phenyl-2,6-dimethyl-4-bora-3a,4adiaza-s-indacene -1*H*-1,2,3-triazol-4-yl)butyl)-3-(2-hydroxy-2,2-diphenylacetoxy)quinuclidinium 115b

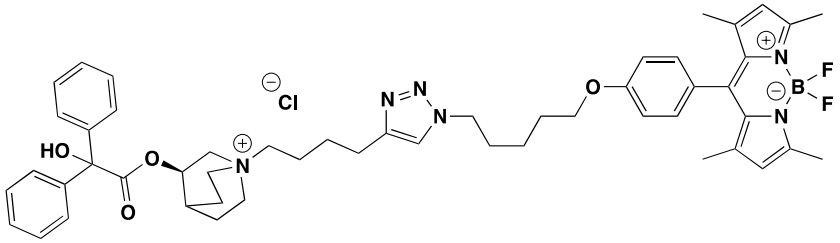

Using general procedure 1 starting with (*R*)-1-(hex-5-yn-1-yl)-3-(2-hydroxy-2,2-diphenylacetoxy)quinuclidinium chloride **111d** and 4,4-difluoro-8-(4-(5-azidopentyl))phenyl-2,6-dimethyl-4-bora-3a,4adiaza-s-indacene **61** yielded a red solid (1.3 mg, 59%).

HPLC Rt: 13.39 (System 1), 15.90 (System 2).

ES-MS M-Cl+ calc. For $C_{51}H_{60}BF_2N_6O_4$ 869.4732 found 869.4749.

Synthesis of (*R*)-1-(4-(4,4-difluoro-8-(2-ethoxy)ethoxy)phenyl-2,6-dimethyl-4-bora-3a,4adiaza-s-indacene -1*H*-1,2,3-triazol-4-yl)butyl)-3-(2-hydroxy-2,2-diphenylacetoxy)quinuclidinium 115c

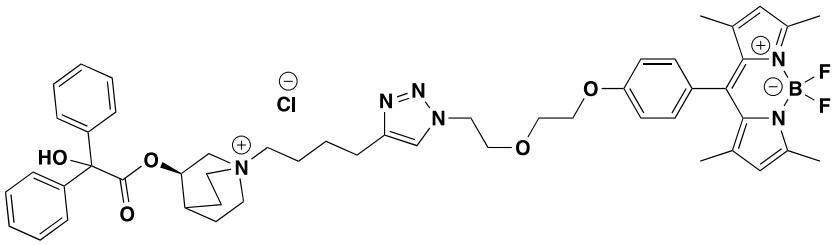

Using general procedure 1 starting with (*R*)-1-(hex-5-yn-1-yl)-3-(2-hydroxy-2,2-diphenylacetoxy)quinuclidinium chloride **111d** and 4,4-difluoro-8-(4-(2-azidoethoxy)ethoxy))phenyl-2,6-dimethyl-4-bora-3a,4adiaza-s-indacene **65** yielded a red solid (0.98 mg, 20%).

HPLC Rt: 12.72 (System 1), 14.98 (System 2).

ES-MS M-Cl+ calc. For $C_{50}H_{58}BF_2N_6O_5$ 871.4524 found 871.4324.

Synthesis of (*R*)-1-((2-(4,4-difluoro-8-(4-(3-propoxy))phenyl-2,6-dimethyl-4-bora-3a,4adiaza-s-indacene -1*H*-1,2,3-triazol-4-yl)methyl)amino)-2-oxoethyl)-3-(2-hydroxy-2,2-diphenylacetoxy) quinuclidinium bromide 116a

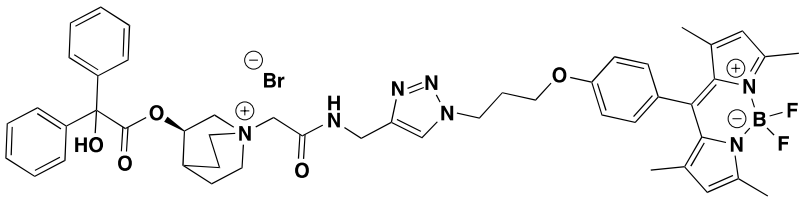

Using general procedure 1 starting with (*R*)-3-(2-hydroxy-2,2-diphenylacetoxy)-1-(2-oxo-2-(prop-2-yn-1-ylamino)ethyl)quinuclidinium bromide **111e** and 4,4-difluoro-8-(4-(3-azidopropoxy))phenyl-2,6-dimethyl-4-bora-3a,4adiaza-s-indacene **46** yielded a red solid (0.7 mg, 35%).

HPLC Rt: 12.60 (System 1), 14.87 (System 2).

ES-MS M-Br+ calc. For $C_{48}H_{53}BF_2N_7O_5$ 856.4164 found 856.4100.

Synthesis of (*R*)-1-((2-(4,4-difluoro-8-(4-pentyl)phenyl-2,6-dimethyl-4-bora-3a,4adiaza-s-indacene -1*H*-1,2,3-triazol-4-yl)methyl)amino)-2-oxoethyl)-3-(2-hydroxy-2,2-diphenylacetoxy) quinuclidinium bromide 116b

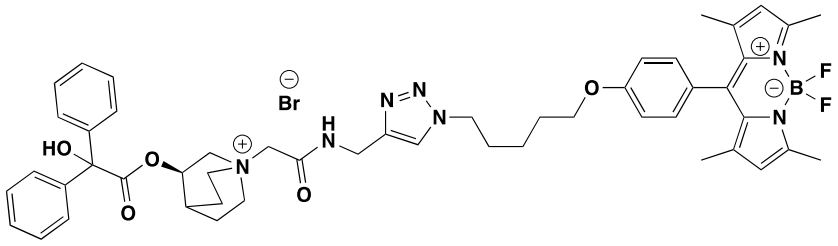

Using general procedure 1 starting with (*R*)-3-(2-hydroxy-2,2-diphenylacetoxy)-1-(2-oxo-2-(prop-2-yn-1-ylamino)ethyl)quinuclidinium bromide **111e** and 4,4-difluoro-8-(4-(5-azidopentyl))phenyl-2,6-dimethyl-4-bora-3a,4adiaza-s-indacene **61** yielded a red solid (0.9 mg, 36%).

HPLC Rt: 13.15 (System 1), 15.60 (System 2).

ES-MS M-Br+ calc. For $C_{50}H_{57}BF_2N_7O_5$ 884.4477 found 884.4481.

Synthesis of (*R*)-1-((2-(4,4-difluoro-8-(2-ethoxy)ethoxy)phenyl-2,6-dimethyl-4-bora-3a,4adiaza-s-indacene -1*H*-1,2,3-triazol-4-yl)methyl)amino)-2-oxoethyl)-3-(2-hydroxy-2,2-diphenylacetoxy) quinuclidinium bromide 116c

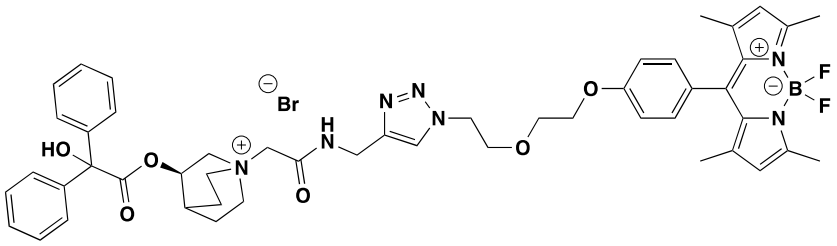

Using general procedure 1 starting with (*R*)-3-(2-hydroxy-2,2-diphenylacetoxy)-1-(2-oxo-2-(prop-2-yn-1-ylamino)ethyl)quinuclidinium bromide **111e** and 4,4-difluoro-8-(4-(2-azidoethoxy)ethoxy))phenyl-2,6-dimethyl-4-bora-3a,4adiaza-s-indacene **65** yielded a red solid (0.94 mg, 47%).

HPLC Rt: 12.47 (System 1), 14.62 (System 2).

ES-MS M-Br+ calc. For $C_{49}H_{55}BF_2N_7O_6$ 886.4269 found 8846.4222.

Synthesis of (*R*)-1-(3-(3-(4,4-difluoro-8-(4-(3-propoxy)phenyl-2,6-dimethyl-4-bora-3a,4adiaza-s-indacene -1*H*-1,2,3-triazol-4-yl)phenoxy)propyl)-3-(2-hydroxy-2,2-diphenylacetoxy) quinuclidinium bromide DS117a

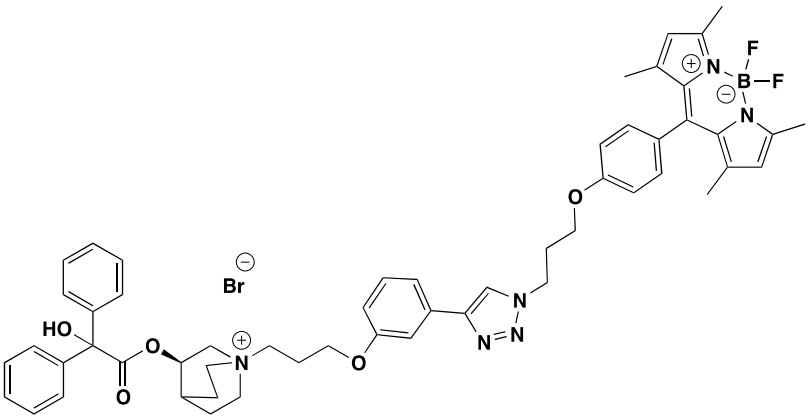

Using general procedure 1 starting with (*R*)-1-(3-(3-ethynylphenoxy)propyl)-3-(2-hydroxy-2,2-diphenylacetoxy)quinuclidin-1-ium bromide **111f** and 4,4-difluoro-8-(4-(3-azidopropoxy)) phenyl-2,6-dimethyl-4-bora-3a,4adiaza-s-indacene **46** yielded a red solid (1.4 mg, 60%).

HPLC Rt: 13.62 (System 1), 15.99 (System 3).

ES-MS M-Br+ calc. For $C_{54}H_{58}BF_2N_6O_5$ 919.4524 found 919.457.

Synthesis of (*R*)-1-(3-(3-(4,4-difluoro-8-(4-pentyl)phenyl-2,6-dimethyl-4-bora-3a,4adiaza-s-indacene -1*H*-1,2,3-triazol-4-yl)phenoxy)propyl)-3-(2-hydroxy-2,2-diphenylacetoxy) quinuclidinium bromide 117b

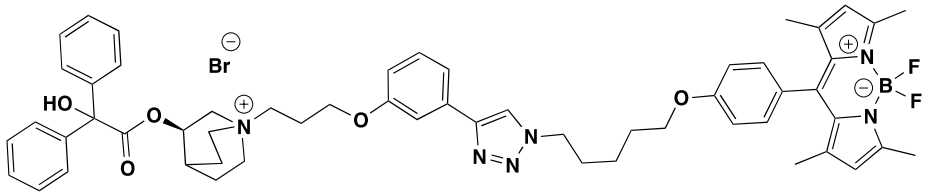

Using general procedure 1 starting with (*R*)-1-(3-(3-ethynylphenoxy)propyl)-3-(2-hydroxy-2,2-diphenylacetoxy)quinuclidin-1-ium bromide **111f** and 4,4-difluoro-8-(4-(5-azidopentyl))phenyl-2,6-dimethyl-4-bora-3a,4adiaza-s-indacene **61** yielded a red solid (1.2 mg, 60%).

HPLC Rt: 14.15 (System 1).

ES-MS M-Br+ calc. For $C_{56}H_{62}BF_2N_6O_5$ 947.4837 found 947.4821.

Synthesis of (*R*)-1-(3-(3-(4,4-difluoro-8-(2-ethoxy)ethoxy)phenyl-2,6-dimethyl-4-bora-3a,4adiaza-s-indacene -1*H*-1,2,3-triazol-4-yl)phenoxy)propyl)-3-(2-hydroxy-2,2-diphenylacetoxy) quinuclidinium bromide 117c

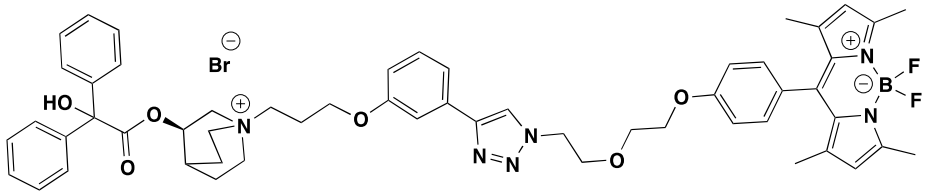

Using general procedure 1 starting with (*R*)-1-(3-(3-ethynylphenoxy)propyl)-3-(2-hydroxy-2,2-diphenylacetoxy)quinuclidin-1-ium bromide **111f** and 4,4-difluoro-8-(4-(2-azidoethoxy)ethoxy))phenyl-2,6-dimethyl-4-bora-3a,4adiaza-s-indacene **65** yielded a red solid (1.1 mg, 40%).

HPLC Rt: 13.34 (System 1), 15.67 (System 2).

ES-MS M-Br+ calc. For $C_{55}H_{60}BF_2N_6O_6$ 949.4630 found 949.4693.

Synthesis of (*R*)-1-(2-((*N*-(2 azidoethyl)-2-(4,4-difluoro-4,4a-dihydro-5-(thiophenyl)-4-bora-3a,4a- diaza-*s* indacene 3-yl)vinyl)phenoxy)acetamide -1*H*-1,2,3-triazol-4-yl)ethyl)-3-(2-hydroxy-2,2-diphenylacetoxy)quinuclidinium bromide 118a

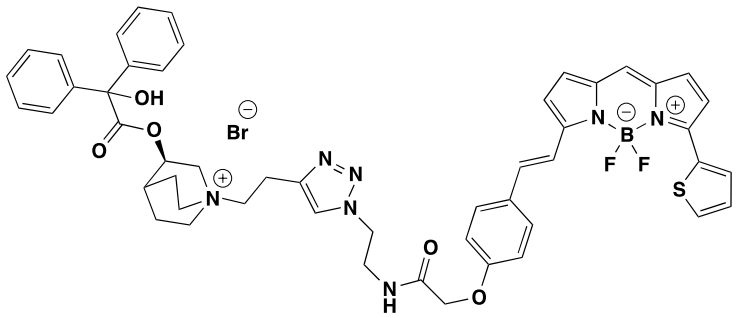

Using general procedure 1 starting with (*R*)-1-(but-3-yn-1-yl)-3-(2-hydroxy-2,2-diphenylacetoxy)quinuclidinium bromide **111b** and *N*-(2 azidoethyl)-2-(4,4-difluoro-4,4a-dihydro-5-(thiophenyl)-4-bora-3a,4a- diaza-s indacene 3-yl)vinyl)phenoxy)acetamide **85** yielded a blue solid (0.7mg, 35%).

HPLC Rt: 12.22 (System 1), 14.62 (System 2).

ES-MS M-Br+ calc. For $C_{50}H_{49}BF_2N_7O_5S$ 908.3572 found 908.3566.

(*R*)-1-(3-(*N*-((2 azidoethyl)-2-(4,4-difluoro-4,4a-dihydro-5-(thiophenyl)-4-bora-3a,4a-diaza-*s* indacene 3-yl)vinyl)phenoxy)acetamide -1*H*-1,2,3-triazol-4-yl)propyl)-3-(2-hydroxy-2,2-diphenylacetoxy)quinuclidinium chloride 118b

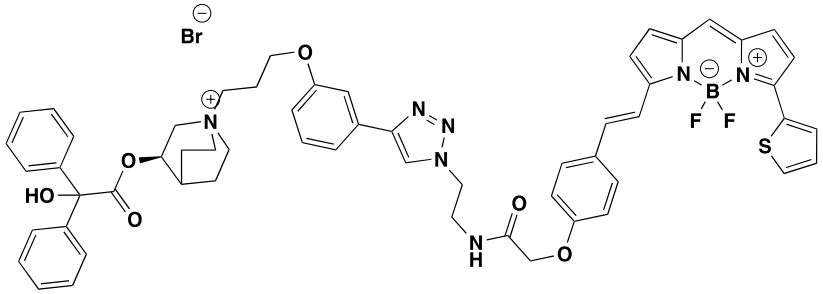

Using general procedure 1 starting with (*R*)-1-(3-(3-ethynylphenoxy)propyl)-3-(2-hydroxy-2,2-diphenylacetoxy)quinuclidin-1-ium bromide **111c** and *N*-(2 azidoethyl)-2-(4,4-difluoro-4,4a-dihydro-5-(thiophenyl)-4-bora-3a,4a- diaza-s indacene 3-yl)vinyl)phenoxy)acetamide **85** yielded a blue solid (0.98 mg, 25%).

HPLC Rt: 12.48 (System 1), 15.28 (System 2).

ES-MS M-Br+ calc. For $C_{57}H_{55}BF_2N_7O_6S$ 1014.3990 found 1014.3925.

Synthesis of Sodium 2-Sulfonate-1,3,5,7-tetramethyl-8-(4-(3-azidopropoxy))phenyl -4,4-difluoro-4-bora-3a, 4a-diaza-s-indacence 119

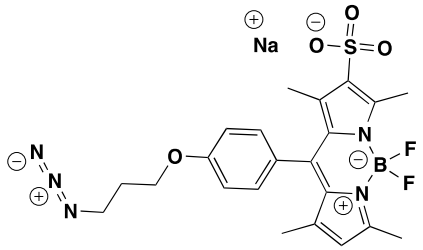

4,4-Difluoro-8-(4-(3-azidopropoxy))phenyl-2,6-dimethyl-4-bora-3a,4adiaza-s-indacene **46** (135 mg, 0.31 mmol) was dissolved in anhydrous DCM (20 mL) and cooled to -40 °C under a nitrogen atmosphere. Chlorosulfonic acid (230 μL, 0.34 mmol) was added dropwise and stirred at -40 °C for tenminutes. The reaction mixture was then warmed to room temperature and stirred for 30minutes. Sodium hydrogen carbonate (310 mg, 0.36 mmol) was added to the

reaction mixture and the organic layer was separated. The aqueous layer was collected and concentrated. The residue was purified by reverse phase HPLC and yielded an orange solid (100 mg, 62%).

^{1}H NMR: δ 1.48 (3H, s, CH_3), 1.72 (3H, s, CH_3) 2.08-2.12 (2H, m, $CH_2\underline{CH_2}CH_2N_3$), 2.53 (2H, s, CH_3), 2.77 (2H, s, CH_3), 3.55 (2H, t, *J* 6.8, $CH_2CH_2\underline{CH_2}N_3$), 4.09 (2H, t, *J* 6.2, $CH_2CH_2\underline{CH_2}N_3$), 5.96 (2H, s, CH), 7.15 (2H, d, *J* 9.0, ArH), 7.25 (2H, d, *J* 9.0, ArH).

^{13}C NMR: δ 14.50, 15.45, 16.43, 17.22 (CH_3), 28.99 ($\underline{CH_2}CH_2N_3$), 48.21 ($\underline{CH_2}N_3$), 64.82 (OCH_2), 115.11 (phenyl CH), 121.27 (pyrrole CH), 127.20 (Phenyl C), 129.21 ($N\underline{C}CCH_3$), 132.44 (Phenyl CH), 141.88 ($CH_3C\underline{C}$), 143.28 (PhenylC-$\underline{C}$), 155.46 ($N\underline{C}CH_3$), 159.40 (Phenyl CO).

Mpt: 156-158 °C.

FT-IR: 3431 (br, pyrrole ring), 2933, 2737, 2676, 2092 (N_3), 1607(conjugated C=N), 1353 (S=O str).

Synthesis of methyl 2-azido-4-bromobutanoate 121

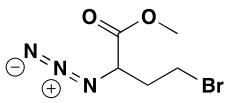

To a solution of methyl 2,4-dibromobutyrate **120** (5 g, 19.3 mmol) in DMF (10 mL), sodium azide (1.32 g, 20.26 mmol) was added at 0 °C and gently warmed to room temperature. The reaction was stirred for three hours was was poured into water (100 mL) and washed with ether (3 x 30mL). The organics were combined, washed with brine, dried and concentrated to yield clear oil (3.9 g, 91%). The product was used without further purification.

^{1}H NMR: δ 2.12-2.20 (1H, m, $CH\underline{CH_2}$), 2.26-2.34 (1H, m, $CH\underline{CH_2}$), 3.40-3.50 (2H, m, CH_2Br), 3.79 (3H, s, OCH_3), 4.18-4.22 (1H, m, CH).

^{13}C NMR: δ 33.94, ($CH\underline{CH_2}$), 28.71 (CH_2Br), 60.21 (OCH_3), 65.82 (CH), 162.52 (CO).

Synthesis of methyl 2-azido-4-(4-formylphenoxy)butanoate 122

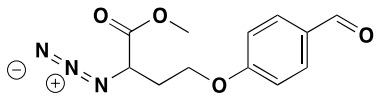

4-Hydroxybenzaldehyde (395 mg, 3.23 mmol) and K_2CO_3 (892 mg, 6.46 mmol) was dissolved in DMF (20 mL) to which methyl 2-azido-4-bromobutanoate **121** (1 g, 4.5 mmol) was added and heated to 60 °C for three hours. The reaction mixture was cooled and poured into water (100mL) The product was extracted with ether (3 x 30mL). The organics were combined, washed with brine, dried and concentrated to yield a clear oil (500 mg, 58%). The product was used without further purification.

^{1}H NMR: δ 2.12-2.20 (1H, m, CH$\underline{CH_2}$), 2.32-2.39 (1H, m, CH$\underline{CH_2}$), 3.40-3.50 (2H, m, OCH_2), 3.76 (3H, s, OCH_3), 4.14-4.18 (2H, m, OCH_2), 4.20-4.26 (1H, m, CH), 6.96 (2H, d, *J* 8.9, ArCH), 7.81 (2H, d, *J* 8.9, ArCH).

^{13}C NMR: δ 33.94, (CH$\underline{CH_2}$), 42.54 (OCH_2), 60.21 (OCH_3), 65.82 (CH), 114.88 (ArC), 130.27 (ArC), 132.13 (ArC), 163.79 (ArCO), 162.52 (CO), 190.89 (Ar-C=O).

Synthesis of 4,4-difluoro-8-(methyl 2-azido-4-(4-formyl))phenyl-2,6-dimethyl-4-bora-3a,4adiaza-s-indacene 123

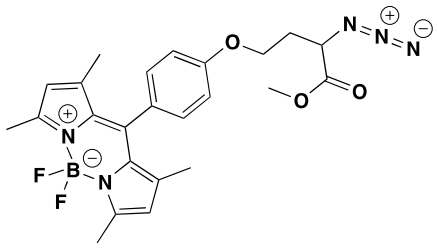

Methyl 2-azido-4-(4-formylphenoxy)butanoate **122** (500 mg, 1.9 mmol) and 2,4-dimethylpyrrole (39 µL, 3.8 mmol) were dissolved in anhydrous DCM (200 mL) under a nitrogen environment. TFA (2 drops) were added and the reaction mixture was stirred overnight. DDQ (431 mg, 1.9 mmol) was added in a single portion and stirred for one hour. Triethylamine (2 mL, 1.46 mmol) and $BF_3.OEt_2$ (2 mL, 1.88 mmol) were added to the reaction

mixture which was stirred for 12 hr. The reaction mixture was poured into water (200 mL) and extracted with DCM (3 x 50mL). The organics were combined and washed with brine, dried and concentrated. The product was purified by reverse phase HPLC to yield a red solid (209 mg, 23%).

^{1}H NMR: δ 1.43 (6H, s, CH_3), 2.12-2.20 (1H, m, CH$\underline{CH_2}$), 2.32-2.39 (1H, m, CH$\underline{CH_2}$), 2.55 (6H, s, CH_3), 3.76 (3H, s, OCH_3), 4.14-4.18 (2H, m, OCH_2), 4.20-4.26 (1H, m, CH), 5.97 (2H, s, 6.96, CH), (2H, d, *J* 8.9, ArCH), 7.81 2H, d, *J* 8.9, ArCH.

Mpt: 144-146 °C.

ES-MS MH+ calc. For $C_{24}H_{27}BF_2N_5O_3$ 482.2170 found 482.2175

Synthesis of 4,4-difluoro-8-(4-(2-azido-4-(4-formyl)phenoxy))phenyl-2,6-dimethyl-4-bora-3a,4adiaza-s-indacene 124

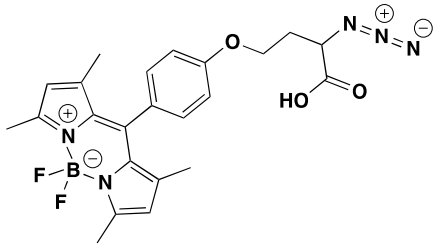

4,4-Difluoro-8-(methyl 2-azido-4-(4-formyl))phenyl-2,6-dimethyl-4-bora-3a,4adiaza-s-indacene **123** (20 mg, 0.42 mmol) was dissolved in MeOH/water (2:5 mL). LiOH (5 mg, 2.1 mmol) was added over ice and the reaction was stirred for three hours. The MeOH was evaporated and the aqueous phase was washed with DCM (2 x 10mL). The aqueous layer was acidified with 1M HCl and the product was extracted with DCM (3 x 10mL). The organics were washed with brine, dried and concentrated to yield a red solid (34 mg, quantitative yield).

^{1}H NMR: δ 1.43 (6H, s, CH_3), 2.20-2.22 (1H, m, CH$\underline{CH_2}$), 2.40-2.47 (1H, m, CH$\underline{CH_2}$), 2.55 (6H, s, CH_3), 4.16-4.20 (2H, m, OCH_2), 4.20-4.26 (1H, m, CH), 5.97 (2H, s, 6.96, CH),7.00 (2H, d, *J* 8.9, ArCH), 7.81 (2H, d, *J* 8.9, ArCH).

^{13}C NMR: δ 14.60 (CH_3), 22.62 ($\underline{CH_2}CHN_3$), 41.34 ($\underline{CH}N_3$), 63.36 (OCH_2), 115.05 (phenyl CH), 121.11 (pyrrole CH), 127.64 (Phenyl C), 129.34 ($N\underline{C}CCH_3$), 131.8 (Phenyl CH), 141.40 ($CH_3C\underline{C}$), 143.14 (PhenylC-$\underline{C}$), 155.37 ($N\underline{C}CH_3$), 158.87 (Phenyl CO), 174.80 (COOH).

Mpt: 136-138 °C

ES-MS MH+ calc. For $C_{23}H_{25}BF_2N_5O_3$ 468.2013 found 468.2175

Synthesis of 4,4-difluoro-8-(4-(2-(2-azido-4-(4-formyl)phenoxy)butanamido))phenyl-2,6-dimethyl-4-bora-3a,4adiaza-s-indacene 127

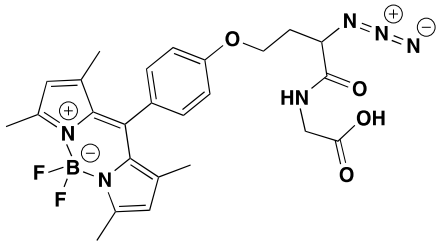

4,4-difluoro-8-(4-(2-azido-4-(4-formyl)phenoxy))phenyl-2,6-dimethyl-4-bora-3a,4adiaza-s-indacene **126** (15 mg, 0.32 mmol) and HBTU (12 mg, 0.35 mmol) were dissolved in DCM (5 mL). DIPEA (12.3 μL, 0.35 mmol) was added and the reaction mixture was stirred for 30 seconds before the addition of glycine methyl ester **125** (3.6 mg, 0.035 mmol). The reaction mixture was stirred overnight and the reaction mixture was concentrated. Deprotection of the methyl ester with LiOH (15mg, 6.3 mmol) dissolved in water/MeOH (2:5mL) and stirred for six hours. The MeOH was evaporated and the aqueous phase was washed with DCM (2 x 10mL). The aqueous layer was acidified with 1M HCl and the product was extracted with DCM (3 x 10mL). The organics were washed with brine, dried and concentrated to yield a red solid (16 mg, 16%).

^{1}H NMR: δ 1.42 (6H, s, CH_3), 2.54 (6H, s, CH_3), 2.82 (2H, s, $\underline{CH_2}COOH$), 4.16-4.20 (2H, m, OCH_2), 4.20-4.26 (1H, m, CH), 5.97 (2H, s, 6.96, CH), 7.00 (2H, d, *J* 8.9, ArCH), 7.81 (2H, d, *J* 8.9, ArCH).

^{13}C NMR: δ 14.60 (CH_3), 22.62 ($\underline{CH_2}CHN_3$), 41.34 ($\underline{CH}N_3$), 63.36 (OCH_2), 115.05 (phenyl CH), 121.11 (pyrrole CH), 127.64 (Phenyl C), 129.34 ($N\underline{C}CCH_3$), 131.8 (Phenyl CH), 141.40 ($CH_3C\underline{C}$), 143.14 (PhenylC-$\underline{C}$), 155.37 ($N\underline{C}CH_3$), 158.87 (Phenyl CO), 174.80 (COOH).

Mpt: 154-156 °C.

Synthesis of (*R*)-1-(3-(4,4-difluoro-8-(4-(2-azido-(4-formyl)phenoxy)phenyl-2,6-dimethyl-4-bora-3a,4adiaza-s-indacene -1*H*-1,2,3-triazol-4-yl)propyl)-3-(2-hydroxy-2,2-diphenylacetoxy) quinuclidinium chloride 128a

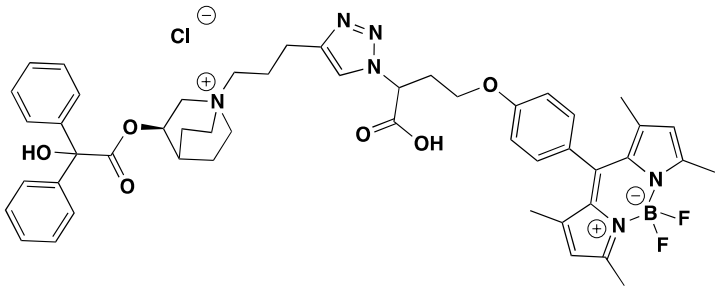

Using general procedure 1 starting with 4,4-difluoro-8-(4-(2-azido-4-(4-formyl)phenoxy))phenyl-2,6-dimethyl-4-bora-3a,4adiaza-s-indacene **124** (1eq) and (*R*)-3-(2-hydroxy-2,2-diphenylacetoxy)-1-(pent-4-yn-1-yl)quinuclidinium chloride **111c** (1.1eq) yielded a red solid after HPLC purification (3.9mg, 57%).

HPLC Rt: 12.48 (System 1), 15.28 (System 2).

ES-MS M-Cl+ calc. For $C_{49}H_{56}BF_2N_6O_6$ 872.4239 found 872.4245

Synthesis of (*R*)-1-(3-(4,4-difluoro-8-(4-(2-(2-azido-4-(4-formylphenoxy)butanamido)))phenyl-2,6-dimethyl-4-bora-3a,4adiaza-s-indacene -1*H*-1,2,3-triazol-4-yl)propyl)-3-(2-hydroxy-2,2-diphenylacetoxy) quinuclidinium chloride 128b

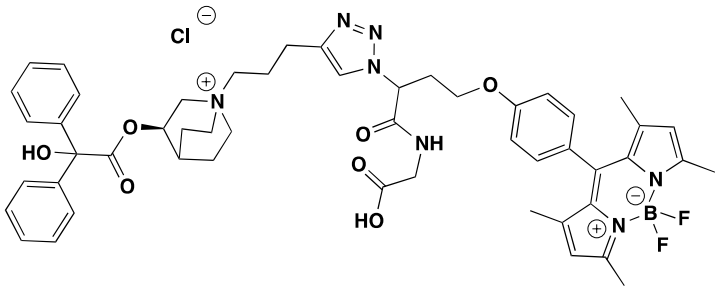

Using general procedure 1 starting with 4,4-difluoro-8-(4-(2-(2-azido-4-(4-formyl)phenoxy)butanamido))phenyl-2,6-dimethyl-4-bora-3a,4adiaza-s-indacene **127** (1eq) and (*R*)-3-(2-hydroxy-2,2-diphenylacetoxy)-1-(pent-4-yn-1-yl)quinuclidinium chloride **111c** (1.1eq) yielded a red solid after HPLC purification (2.9mg, 47%).

HPLC Rt: 12.48 (System 1), 15.28 (System 2).

ES-MS M-Cl+ calc. For $C_{51}H_{58}BF_2N_7O_7$ 929.4448 found 929.4427

Synthesis of (*R*)-1-(3-(2-sulfonate-1,3,5,7-tetramethyl-8-(4-(3-azidopropoxy))phenyl -4,4-difluoro-4-bora-3a, 4a-diaza-s-indacence -1*H*-1,2,3-triazol-4-yl)propyl)-3-(2-hydroxy-2,2-diphenylacetoxy) quinuclidinium 129

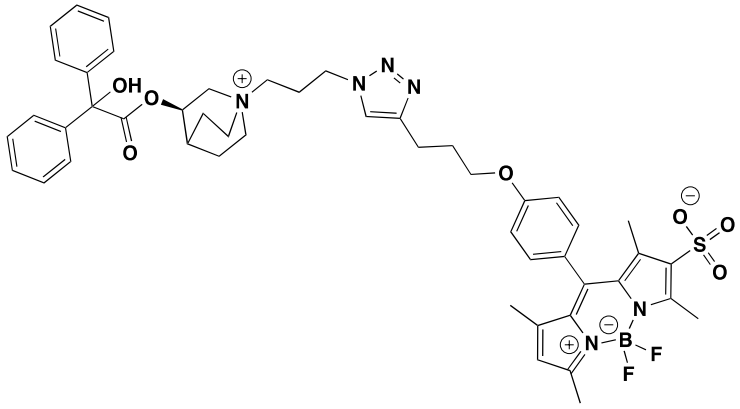

Using general procedure 1 sodium 2-sulfonate-1,3,5,7-tetramethyl-8-(4-(3-azidopropoxy))phenyl -4,4-difluoro-4-bora-3a, 4a-diaza-s-indacence **119** (1eq) and (*R*)-3-(2-hydroxy-2,2-diphenylacetoxy)-1-(pent-4-yn-1-yl)quinuclidinium chloride **111c** (1.1eq) yielded a red solid after HPLC purification (2.9mg, 47%).

HPLC Rt: 10.70 (System 1), 12.15 (System 2).

ES-MS M-Cl+ calc. For $C_{51}H_{58}BF_2N_7O_7$ 908.3909 found 908.3910

Pharmacology

Whole Cell Culture

All reagents used were obtained from Sigma chemicals (Poole, Dorset, UK), unless otherwise stated. All plates were obtained from Corning Costar (Corning Incorporated, Corning, NY, USA), unless otherwise stated.

CHO-K1-β_1, CHO-K1-β_2 and CHO M_3 cells were used throughout this study. CHO-K1 cells were obtained from Dr Jillian Baker who performed the transfection, dilution cloning and isolation of a stable clone. CHO M_3 cells were obtained from Dr Lauren May who performed the transfection, dilution cloning and isolation of a stable clone.

All cell lines were cultured in Dulbecco's modified Eagle's medium/nutrient mix F12 (DMEM/F12) supplemented with 2mM L-glutamine and 10% heat-inactivated foetal calf serum (FCS) (PAA Laboratories, Teddington, Middlesex, UK). CHO cells were incubated at 37 °C, 5% CO_2. All cell culture procedures were performed in a class II laminar flow hood using sterile techniques.

Passaging of cells

All CHO cell lines were passaged once they had grown to confluence in a T75 flask. Media was removed and the cells were washed with warm Dulbecco's phosphate buffered saline (PBS) (5-10 mL). PBS was removed and cells were then incubated with warm trypsin/EDTA (T/E) (1 mL) for 2-3minutes or until cells were loosened from the bottom of the flask. Once detached, the T/E was neutralised with media (10 mL) and the resulting suspension was spun at 1000 rpm for fiveminutes. The pellet was re-suspended in media (1 mL); this step involved rapid agigtation to ensure a uniform suspension was produced. The media was then added to make the volume 20mL and the resulting suspension was dispensed as appropriate into 75 mL flasks. All CHO cell lines were generally split 1:20.

Seeding into cell plates

All CHO cells from confluent T75 flasks were removed from the flask and centrifuged as described above. Cell required for radioligand binding assays were seeded 24 hours prior to

experiments. One T75 flask was used to set up a maximum of four 96-well. Cells required For intracellular calcium assays were seeded 24 hours prior to experiment One T75 flask was used to set up a maximium of six 96 well plates.

Cell freezing and thawing

Cells from confluent T150 flasks were removed from the flask and centrifuged as described previously. One pellet from a T150 flask was carefully re-suspended in the freezing medium (5 mL, 10% DMSO in FCS). 1 mL of cell suspension was transferred to each cryovail (Nalgene, Rochester, NY, USA) and cooled in an isopropanol filled freezing chamber to reduce the temperature at a rate of approximately 1 °C/min for 24 hours. The following day, cryovials were transferred to the liquid nitrogen dewars for freezing.

Cells were thawed by removing one cyrovial from the storage in liquid nitrogen and rapidly warmed to 37 °C. The contents of the vial were suspended into growth media (10 mL) and the resulting suspension was spun at 1000rpm for fiveminutes. The pellet was resuspended in media (1 mL) and transferred to a 75 mL flask containing 20 mL of media. After 8-12 hours, growth media was removed and replaced wth fresh growth media, removing the cell debris that did not survive the freezing/thawing process.

Assays

Radioligand binding assays

Cells were seeded into 96-well white sided plates 24 hours prior to the assay. On the day of experimentation, all media was aspirated and different concentrations of the ligand were added (100µl/well) in triplicate. Total and non-specific binding was defined by adding serum free media in triplicate (total binding) and 1 µl propranolol (non specific binding). [^{3}H]-CGP 12177 was made at a concentration of 0.5 nM in serum free media and as added to all wells (100 µl/well). The cells were incubated for 2 hours at 37 °C, 5% CO_2. After 2 hour incubation, the cells were washed twice with cold PBS (200 µl/well) in order to wash any unbound ligand from the cells. White backing was added to each plate and 100 µl of microscintillent was added to each well. Finally the plates were sealed and counted on a Topcount Microplate Illuminator.

Data Analysis

All data are represented as mean ± s.e. of triplicate determinations unless otherwise stated. The n in the text refers to the number of separate experiments (a separate experiment requires cells plated from a separate plate and separate drug dilution used throughout the experiment).

In order to determine the actual concentration of radioligand, 50 µl was added in triplicate to scintillation vials. Scintillation fluid (10 mL) was added to each vial and the vial was counted on a scintillation counter.

The dpm was then converted to concentration of [^{3}H]-CGP 12177 from the following:

1 Ci = 2.22 x 10^{12}. Specific activity of ^{3}H-CGP 12177 = 45 Ci/mmol

therefore 1dpm = 1/(45 x 2.22 x10^{12}) mmol.

K_d values were then determined from the IC_{50} values and concentration of radioligand according to the expression[141]

$$K_d = \frac{IC_{50}}{(1 + {}^{A}/_{K_{d(CGP)}})}$$

Where [A] is the concentration of [^{3}H]-CGP 12177 used in the displacement and K_d is the dissociation constant (K_d) of [^{3}H]-CGP 12177.

Intracellular calcium assay

Cells were seeded into 96-well black sided plates 24 hours prior to the assay. On the day of experimentation, all media was aspirated and different concentrations of the ligand were added (20 µl) with assay buffer (Hank's Buffered Salt Solution, brilliant black (0.5mM), fura-2 (2 mM) and probenacid (2 mM). The plates were incubated for 0.5 hours at 37 °C, 5% CO_2 then assay plates were then placed onto the flexstation 1 fluorescence plate reader for measuring the changes of intracellular calcium in response to the GPCR activation. The fluorescent signal was recorded for 200 seconds with carbachol (10 µl) added at 20 seconds.

Data analysis

All data are represented as mean ± s.e.m of triplicate determinations unless otherwise stated. The n in the text refers to the number of separate experiments (a separate experiment requires cells plated from a separate plate and separate drug dilution used throughout the experiment).

Kd values were determined from the IC_{50} values and concentration of carbachol according to the expression[171]

$$DR = 1 + \frac{[A]}{K_b}$$

Where DR (dose ± ratio) is the ratio of the concentrations of agonist required to produce an identical response in the presence and absence of antagonist, [A] is the concentration of antagonist and K_b is the antagonist inhibitory constant.

Binding kinetic assays

Cell Membranes were pre-prepared using established procedures[37] by Mr David Sykes (Novartis Institute for Biomedical Research).

On the day of experimentation, different concentrations using of antagonist were diluted in assay buffer (10 mM HEPES, 1 mM $MgCl_2$, pH 7.4) and were added (100 µl/well) in triplicate. Assay buffer (200 µl) was added to each well. Non specific was defined by adding assay buffer in triplicate and 100 µl atropine (5 µM). [^{3}H]-NMS was made at a concentration of 1 nM in buffer and was added (100µl/well). Membranes were prepared and at each time point cell membranes (100 µl (10 µg/well) were added. The plates were sealed and shaken at 37 °C. Termination of reaction by rapid vacuum filtration onto pretreated unfiltered GF/B plates and washed three times with ice cold buffer. Plates were dried at 48 °C for two hours in a controlled temperature incubator. White backs were placed onto the filter plates and 40 µl of microscintillent was added to each well. Finally the plates were sealed and counted on a Topcount Microplate Illuminator.

In order to determine the actual concentration of radioligand, 50 µl was added in triplicate to scintillation vials. Scintillation fluid (5 mL) was added to each vial and the vial was counted on a scintillation counter.

Data analysis

The dpm was then converted to concentration of [^{3}H]-NMS from the following:

1 Ci = 2.22 x 10^{12}. Specific activity of [^{3}H]-NMS = 82 Ci/mmol

therefore 1dpm = 1/(82 x 2.22 x10^{12}) mmol.

The association (k_3) and disassociation rate (k_4) for antagonists were calculated in line with

Sykes *et al*.[37]

Confocal microscopy

Confocal microscopy was performed using a Zeiss LSM510 laser-scanning microscope. All experiments used a Zeiss 40 x 1.3 NA oil immersion lens.

Imaging

Cells were seeded into 8-well plates 24 hours prior to experiment. (If wells needed preincuation with poly- L -lysine, (1mg/mL) was incubated for one hour, followed aspiration and washing with PBS.) On the day of the experiment, all media was aspirated and the cells were washed twice with warmed 500 μl HBS. HBS (300 μl) was added to each well which provided a media into which the antagonists could be added. The holder was transferred to a heated stage on the microscope, which allowed cells to be maintained at 37 °C throughout the experiments. Cells were allowed to settle for 15minutes before each antagonist (30 μl) was added. When competition antagonist were used, cells were incubated for 15minutes before addition of fluorescent antagonist. All images were taken at 1024 x 1024 pixels.

Stability Experiments

Antagonists were diluted from DMSO stock solution to 10^{-4} M concentration in serum free media and incubated for a maximum of six hours. This incubation time was chosen as it above and beyond the time length in which the antagonists would be in solution for. HPLC analytical traces were performed with 20 μL of antagonist/serum free media and were injected at 0 hr, 0.5 hr, 1 hr, 2 hr 3 hr and 6 hr in order to observe if the media had caused any decomposition of the ligands. Results showed that there was no decomposition of any antagonists.

6. References

(1) Rang, H. P.; Dale, M. M.; Ritter, J. M.; Moore, P. K. *Pharmacology*; 5th ed.; Churchill Livingstone, 2003.

(2) Fredriksson, R.; Lagerström, M. C.; Lundin, L.-G.; Schiöth, H. B. *Mol Pharmacol* **2003**, *63*, 1256.

(3) Vassilatis, D. K.; Hohmann, J. G.; Zeng, H.; Li, F. S.; Ranchalis, J. E.; Mortrud, M. T.; Brown, A.; Rodriguez, S. S.; Weller, J. R.; Wright, A. C.; Bergmann, J. E.; Gaitanaris, G. A. *Proc. Natl. Acad. Sci. U. S. A.* **2003**, *100*, 4903.

(4) Congreve, M.; Langmead, C. J.; Mason, J. S.; Marshall, F. H. *J.Med.Chem.* **2011**, *54*, 4283.

(5) Ji, T. H.; Grossmann, M.; Ji, I. H. *J. Biol. Chem.* **1998**, *273*, 17299.

(6) Hopkins, A. L.; Groom, C. R. *Nat. Rev. Drug Discov.* **2002**, *1*, 727.

(7) Thomas P, S. *Curr. Opin. Struct. Biol.* **2002**, *14*, 189.

(8) Ji, T. H.; Grossmann, M.; Ji, I. *J. Biol. Chem.* **1998**, *273*, 17299.

(9) Perez, D. M. *Mol Pharmacol* **2003**, *63*, 1202.

(10) Sam R.J, H. *Drug Discov. Today* **2005**, *10*, 417.

(11) Parmentier, M. L.; Prezeau, L.; Bockaert, J.; Pin, J. P. *Trends Pharmacol. Sci.* **2002**, *23*, 268.

(12) Hamm, H. E. *J. Biol. Chem.* **1998**, *273*, 669.

(13) Lappano, R.; Maggiolini, M. *Nat Rev Drug Discov* **2011**, *10*, 47.

(14) Overington, J. P.; Al-Lazikani, B.; Hopkins, A. L. *Nat. Rev. Drug Discov.* **2006**, *5*, 993.

(15) Druker, B. J.; Lydon, N. B. *J. Clin. Invest.* **2000**, *105*, 3.

(16) Wall, M. E.; Wani, M. C. *Cancer. Res.* **1995**, *55*, 753.

(17) Wainwright, M.; Swan, H. T. *Med. Hist.* **1986**, *30*, 42.

(18) Masuer, H.; Guba, W. *Curr. Opin.Drug. Discov. Devel.* **2008**, *11*, 365.

(19) Hecht, D.; Fogel, G. B. *J.Chem. Inf. Model.* **2009**, *49*, 1105.

(20) Jhoti, H. In *Sparking Signals: Kinases as Molecular Signal Transducers and Pharmacological Drug Targets in Inflammation*; Baier, G., Schraven, B., Zugel, U., VonBonin, A., Eds.; Springer-Verlag Berlin: Berlin, 2008; Vol. 3, p 169.

(21) Honma, T. *Med. Res. Rev*. **2003**, *23*, 606.

(22) Caflisch, A.; Miranker, A.; Karplus, M. *J.Med.Chem*.**1993**, *36*, 2142.

(23) Nishibata, Y.; Itai, A. *Tetrahedron.* **1991**, *47*, 8985.

(24) Firth-Clark, S.; Todorov, N. P.; Alberts, I. L.; Williams, A.; James, T.; Dean, P. M. *J. Chem. Inf. Model*. **2006**, *46*, 1168.

(25) de Graaf, C.; Rognan, D. *Curr.Pharm.Des*. **2009**, *15*, 4026.

(26) Rasmussen, S. G. F.; Choi, H.-J.; Rosenbaum, D. M.; Kobilka, T. S.; Thian, F. S.; Edwards, P. C.; Burghammer, M.; Ratnala, V. R. P.; Sanishvili, R.; Fischetti, R. F.; Schertler, G. F. X.; Weis, W. I.; Kobilka, B. K. *Nature.* **2007**, *450*, 383.

(27) Palczewski, K.; Kumasaka, T.; Hori, T.; Behnke, C. A.; Motoshima, H.; Fox, B. A.; Le Trong, I.; Teller, D. C.; Okada, T.; Stenkamp, R. E.; Yamamoto, M.; Miyano, M. *Science.* **2000**, *289*, 739.

(28) Dorè, A. S.; Robertson, N.; Errey, J. C.; Ng, I.; Hollenstein, K.; Tehan, B.; Hurrell, E.; Bennett, K.; Congreve, M.; Magnani, F.; Tate, C. G.; Weir, M.; Marshall, F. H. *Structure,* **2011**, *19*, 1283.

(29) Wu, B. L.; Chien, E. Y. T.; Mol, C. D.; Fenalti, G.; Liu, W.; Katritch, V.; Abagyan, .; Brooun, A.; Wells, P.; Bi, F. C.; Hamel, D. J.; Kuhn, P.; Handel, T. M.; Cherezov, V.; Stevens, R. C. *Science* **2010**, *330*, 1066.

(30) Chien, E. Y. T.; Liu, W.; Zhao, Q.; Katritch, V.; Won Han, G.; Hanson, M. A.; Shi, L.; Newman, A. H.; Javitch, J. A.; Cherezov, V.; Stevens, R. C. *Science.* **2010**, *330*, 1091.

(31) Bokoch, M. P.; Zou, Y. Z.; Rasmussen, S. G. F.; Liu, C. W.; Nygaard, R.; Rosenbaum, D. M.; Fung, J. J.; Choi, H. J.; Thian, F. S.; Kobilka, T. S.; Puglisi, J. D.; Weis, W. I.; Pardo, L.; Prosser, R. S.; Mueller, L.; Kobilka, B. K. *Nature.* **2010**, *463*, 108.

(32) Warne, T.; Moukhametzianov, R.; Baker, J. G.; Nehme, R.; Edwards, P. C.; Leslie, A. G. W.; Schertler, G. F. X.; Tate, C. G. *Nature.* **2011**, *469*, 241.

(33) Shimamura, T.; Shiroishi, M.; Weyand, S.; Tsujimoto, H.; Winter, G.; Katritch, V.; Abagyan, R.; Cherezov, V.; Liu, W.; Han, G. W.; Kobayashi, T.; Stevens, R. C.; Iwata, S. *Nature.* **2011**, *475*, 65.

(34) Zhukov, A.; Andrews, S. P.; Errey, J. C.; Robertson, N.; Tehan, B.; Mason, J. S.; Marshall, F. H.; Weir, M.; Congreve, M. *Journal of Medicinal Chemistry* **2011**, *54*, 4312.

(35) Cherezov, V.; Rosenbaum, D. M.; Hanson, M. A.; Rasmussen, S. G. F.; Thian, F. S.; Kobilka, T. S.; Choi, H.-J.; Kuhn, P.; Weis, W. I.; Kobilka, B. K.; Stevens, R. C. *Science*. **2007**, *318*, 1258..

(36) Qume, M. *Methods Mol. Biol.* **1998**, *106*, 3.

(37) Sykes, D. A.; Dowling, M. R.; Charlton, S. J. *Curr. Protoc. Pharmacol.* **2001.**50:9.14.1-9.14.30.

(38) Harrison, C.; Traynor, J. R. *Life Sci.* **2003**, *74*, 489.

(39) Weber, M.; Ferrer, M.; Zheng, W.; Inglese, J.; Strulovici, B.; Kunapuli, P. *Assay.drug. dev. technol.* **2004**, *2*, 39.

(40) Williams, C. *Nat Rev Drug Discov* **2004**, *3*, 125.

(41) Hill, S. J.; Baker, J. G.; Rees, S. *Curr. Opin. Pharmacol* **2001**, *1*, 526.

(42) Cheng, Z.; Garvin, D.; Paguio, A.; Stecha, P.; Wood, K.; Fan, F. *Curr. chem. genomics* **2010**, *4*, 84.

(43) Webb, B. L. J.; Hirst, S. J.; Giembycz, M. A. *Br. J. Pharmacol.* **2000**, *130*, 1433.

(44) Hansen, K. B.; Brauner-Osborne, H. *Method.Mol.Biol.* **2009**; Vol. 552, 269.

(45) Briddon, S. J.; Cordeaux, Y.; Middleton, R. J.; Kellam, B.; Hill, S. J. *Br. J. Pharmacol.* **2002**, *136*.

(46) Briddon, S. J.; Middleton, R. J.; Yates, A. S.; George, M. W.; Kellam, B.; Hill, S. J. *Faraday. Discuss*. **2004**, *126*, 197.

(47) Briddon, S. J.; Middleton, R. J.; Cordeaux, Y.; Flavin, F. M.; Weinstein, J. A.; George, M. W.; Kellam, B.; Hill, S. J. *Proc. Natl. Acad. Sci. U. S. A.* **2004**, *101*, 4673.

(48) Alonso, D.; Vázquez-Villa, H.; Gamo, A. M.; Martínez-Esperón, M. F.; Tortosa, M.; Viso, A.; Fernandez de la Pradilla, R.; Junquera, E.; Aicart, E.; Martian-Fontecha, M.; Benhamú, B.; López-Rodríguez, M. L.; Ortega-Gutiérrez, S. *Med. Chem. Lett.* **2010**, *1*, 249.

(49) Daly, C. J.; Ross, R. A.; Whyte, J.; Henstridge, C. M.; Irving, A. J.; McGrath, J. C. *Br. J. Pharmacol.* **2010**, *159*, 787.

(50) Bonnet, D.; Riche, S.; Loison, S.; Dagher, R.; Frantz, M. C.; Boudier, L.; Rahmeh, R.; Mouillac, B.; Haiech, J.; Hibert, M. *Chem.-Eur. J.* **2008**, *14*, 6247.

(51) Brand, F.; Klutz, A. M.; Jacobson, K. A.; Fredholm, B. B.; Schulte, G. *Eur. J. Pharmacol.* **2008**, *590*, 36.

(52) Lacivita, E.; Leopoldo, M. *J. Med. Chem.* **2008**, *51*, 1492.

(53) Xie, S.-X.; Petrache, G.; Schneider, E.; Ye, Q.-Z.; Bernhardt, G. n.; Seifert, R.; Buschauer, A. *Bioorg. Med. Chem. Lett* **2006**, *16*, 3886.

(54) Degorce, F.; Card, A.; Soh, S.; Trinquet, E.; Knapik, G. P.; Xie, B. *Current chemical genomics* **2009**, *3*, 22.

(55) Zhang, R.; Xie, X. *Acta Pharmac Sinic.* **2012**, *33*, 372.

(56) McGrath, J. C.; Arribas, S.; Daly, C. J. *Trends Pharmacol. Sci.* **1996**, *17*, 393.

(57) Aubin, J. E. *J.Histochem. Cytochem.* **1979**, *27*, 36.

(58) Waters, J. C. *J.Cell.Bio.* **2009**, *185*, 1135.

(59) Schwille, P. *Cell Biochem. Biophys.* **2001**, *34*, 383.

(60) Valeur, B. *Molecular Fluorescence: Principles and Applications*; Wiley-VCH, 2001.

(61) Mueller, M. *Introduction to Confocal Fluorescence Microscopy*; 2 ed.; The International society for optical engineering, 2005.

(62) Petrov, R. R.; Ferrini, M. E.; Jaffar, Z.; Thompson, C. M.; Roberts, K.; Diaz, P. *Bioorg. Med. Chem. Lett.* **2011**, *21*, 5859.

(63) Briddon, S. J.; Middleton, R. J.; Kellam, B.; Hill, S. J. *Br. J. Pharmacol.* **2002**, *137*.

(64) Baker, J. G.; Adams, L. A.; Salchow, K.; Mistry, S. N.; Middleton, R. J.; Hill, S. J.; Kellam, B. *J.Med.Chem.* **2011**, *54*, 6874.

(65) Vukojevic, V.; Ming, Y.; D'Addario, C.; Hansen, M.; Langel, U.; Schulz, R.; Johansson, B.; Rigler, R.; Terenius, L. *Faseb J.* **2008**, *22*, 3537.

(66) Leopoldo, M.; Lacivita, E.; Berardi, F.; Perrone, R. *Drug. Discov. Today.* **2009**, *14*, 706.

(67) Adamczyk, M.; Reddy, R. E.; Yu, Z. *Bioorg. Med. Chem. Lett.* **2002**, *12*, 1283.

(68) Briddon, S. J.; Hill, S. J. *Trends Pharmacol. Sci.* **2007**, *28*, 637.

(69) Pramanik, A.; Rigler, R. *Biol. Chem.* **2001**, *382*, 371.

(70) Ambrosio, M.; Zürn, A.; Lohse, M. J. *Neuropharmacology* **2011**, *60*, 45.

(71) Hovius, R.; Vallotton, P.; Wohland, T.; Vogel, H. *Trends Pharmacol. Sci.* **2000**, *21*, 266.

(72) You, X.; Nguyen, A. W.; Jabaiah, A.; Sheff, M. A.; Thorn, K. S.; Daugherty, P. S. *Proc. Natl. Acad. Sci.* **2006**, *103*, 18458.

(73) Joo, C.; Balci, H.; Ishitsuka, Y.; Buranachai, C.; Ha, T. In *Annu. Rev. Biochem.* **2008**; 77, 51.

(74) Middleton, R. J.; Kellam, B. *Curr. Opin. Chem. Bio.* **2005**, *9*, 517.

(75) Cottet, M.; Faklaris, O.; Zwier, J. M.; Trinquet, E.; Pin, J.-P.; Durroux, T. *Pharmaceuticals*, *4*, 202.

(76) Briddon, S. J.; Kellam, B.; Hill, S. J.; Willars, G. B.; Challiss, R. A. J.; Humana Press: 2011; Vol. 746, p 211.

(77) Bohme, I.; Beck-Sickinger, A. J.; *Cell. Commu. Signal* .**2009**, *7*, 16.

(78) Cowart, M.; Gfesser, G. A.; Bhatia, K.; Esser, R.; Sun, M.; Miller, T. R.; Krueger, K.; Witte, D.; Esbenshade, T. A.; Hancock, A. A. *Inflamm. Res.* **2006**, *55*, S47.

(79) Bonnet, D.; Ilien, B.; Galzi, J. L.; Riche, S.; Antheaune, C.; Hibert, M. *Bioconjugate Chem.* **2006**, *17*, 1618.

(80) Lacivita, E.; Masotti, A. C.; Jafurulla, M.; Saxena, R.; Rangaraj, N.; Chattopadhyay, A.; Colabufo, N. A.; Berardi, F.; Perrone, R.; Leopoldo, M. *Bioorg. Med. Chem. Lett*.**2010**, *20*, 6628.

(81) Leopoldo, M.; Lacivita, E.; Passafiume, E.; Contino, M.; Colabufo, N. A.; Berardi, F.; Perrone, R. *J. Med. Chem.* **2007**, *50*, 5043.

(82) Middleton, R. J.; Briddon, S. J.; Cordeaux, Y.; Yates, A. S.; Dale, C. L.; George, M. W.; Baker, J. G.; Hill, S. J.; Kellam, B. *J. Med. Chem.* **2007**, *50*, 782.

(83) Cordeaux, Y.; Briddon, S. J.; Alexander, S. P. H.; Kellam, B.; Hill, S. J. *Faseb J.* **2008**, *22*, 850.

(84) Baker, J. G.; Middleton, R.; Adams, L.; May, L. T.; Briddon, S. J.; Kellam, B.; Hill, S. J. *Br. J. Pharmacol.* **2010**, *159*, 772.

(85) Jones, L. H.; Randall, A.; Napier, C.; Trevethick, M.; Sreckovic, S.; Watson, J. *Bioorg. Med. Chem. Lett.* **2008**, *18*, 825.

(86) Baker, J. G.; Hall, I. P.; Hill, S. J. *Br. J. Pharmacol.* **2003**, *139*, 232.

(87) Hegener, O.; Prenner, L.; Runkel, F.; Baader, S. L.; Kappler, J.; H√ § berlein, H. *Biochemistry.* **2004**, *43*, 6190.

(88) Hartmuth C. K; Finn, M. G.; Sharpless, K. B. *Angew. Chem.* **2001**, *40*, 2004.

(89) Tornoe, C. W.; Christensen, C.; Meldal, M. *The Journal of Organic Chemistry* **2002**, *67*, 3057.

(90) Huisgen, R. *Proc. Chem.Soc.* **1961**, 357.

(91) Alder, K.; Stein, G.; Finzenhagen, H. *Liebigs Ann.* **1931**, *485*, 211.

(92) Bock, V. D.; Hiemstra, H.; van Maarseveen, J. H. *Eur. J. Org. Chem.* **2006**, *2006*, 51.

(93) Zhang, L.; Chen, X.; Xue, P.; Sun, H. H. Y.; Williams, I. D.; Sharpless, K. B.; Fokin, V. V.; Jia, G. *J. Am. Chem. Soc.* **2005**, *127*, 15998.

(94) Himo, F.; Lovell, T.; Hilgraf, R.; Rostovtsev, V. V.; Noodleman, L.; Sharpless, K. B.; Fokin, V. V. *J. Am. Chem. Soc.* **2004**, *127*, 210.

(95) Saxon, E.; Bertozzi, C. R. *Science* **2000**, *287*, 2007.

(96) Kiick, K. L.; Saxon, E.; Tirrell, D. A.; Bertozzi, C. R. *Proc. Natl. Acad. Sci.* **2002**, *99*, 19.

(97) Rostovtsev, V. V.; Green, L. G.; Fokin, V. V.; Sharpless, K. B. *Angew. Chem.***2002**, *41*, 2596.

(98) Yilmaz, M. D.; Bozdemir, O. A.; Akkaya, E. U. *Org. Lett.* **2006**, *8*, 2871.

(99) Evans, R. A. *Aust. J. Chem* **2007**, *60*, 384.

(100) Lynch, G. S.; Ryall, J. G. *Physiol. Rev.* **2008**, *88*, 729.

(101) Jacoby, E.; Bouhelal, R.; Gerspacher, M.; Seuwen, K. *Chem.Med.Chem* **2006**, *1*, 760.

(102) Strosberg, A. D. *Protein. Sci.* **1993**, *2*, 1198.

(103) Strosberg, A. D. *Annu. Rev.Pharmacol.Toxicol.***1997**, *37*, 421.

(104) Dzimiri, N. *Pharmaco.l Res.* **1999**, *51*, 465.

(105) Black .J.W.; Duncan W.A.M.; Shanks. R.G. *Br. J. Pharmacol.* **2010**, *160*, S28.

(106) Baker, J. G. *Br. J. Pharmacol.* **2005**, *144*, 317.

(107) Wu, G.; Tian, H.; Han, K.; Xi, Y.; Yao, Y.; Ma, A. *Clin. Exp. Hyperte* **2006**, *28*, 489.

(108) Haslam, D. W.; James, W. P. T. *The Lancet* **2005**, *366*, 1197.

(109) Dickson, M. E.; Sigmund, C. D. *Hypertension* **2006**, *48*, 14.

(110) Cruickshank, J. M. *The Lancet* **2010**, *376*, 415.

(111) Siebenhofer, A.; Jeitler, K.; Berghold, A.; Waltering, A.; Hemkens, L. G.; Semlitsch, T.; Pachler, C.; Strametz, R.; Horvath, K. *Cochrane Database Syst Rev.* **2011**.

112) Banach, M.; Rysz, J. *Expert Opin. Pharmacother.* **2010**, *11*, 2575.

(113) Chobanian, A. V.; Bakris, G. L.; Black, H. R.; Cushman, W. C.; Green, L. A.; Izzo, J. L.; Jones, D. W.; Materson, B. J.; Oparil, S.; Wright, J. T.; Roccella, E. J. *Hypertension.* **2003**, *x42*, 1206.

(114) Koester, R.; Kaehler, J.; Ebelt, H.; Soeffker, G.; Werdan, K.; Meinertz, T. *Clin. Res. Cardio.* **2010**, *99*, 665.

(115) Sacks, F. M.; Moy, L. A.; Davis, B. R.; Cole, T. G.; Rouleau, J. L.; Nash, D. T.; Pfeffer, M. A.; Braunwald, E. *Circulation* **1998**, *97*, 1446.

(116) Roe, M. T.; Chen, A. Y.; Thomas, L.; Wang, T. Y.; Alexander, K. P.; Hammill, B. G.; Gibler, W. B.; Ohman, E. M.; Peterson, E. D. *Am. Heart J.* **2011**, *162*.

(117) Yusuf, S.; Peto, R.; Lewis, J.; Collins, R.; Sleight, P. *Prog. Cardiovas. Dis.* **1985**, *27*, 335.

(118) The task force of the working group on arrhythmias of the European society of cardiology, *Eur. Heart J.* **1991**, *12*, 1112.

(119) Martinez, F. D. *Eur. Respir. J.* **2007**, *29*, 179.

(120) O,Byrne, P. M. *J. Allergy. clin. immunol.* **2011**, *128*, 257.

(121) Halbert, R. J.; Natoli, J. L.; Gano, A.; Badamgarav, E.; Buist, A. S.; Mannino, D. M. *Eur. Respir. J.* **2006**, *28*, 523.

(122) Silverman, E. Ä.; Chapman, H. Ä.; Drazen, J. Ä.; Weiss, S. Ä.; Rosner, B.; Campbell, E. Ä.; O'Donnell, W. Ä.; Reilly, J. Ä.; Ginns, L.; Mentzer, S.; Wain, J.; Speizer, F. Ä. *Am. J. Respir. Crit. Care. Med.* **1998**, *157*, 1770.

(123) Cazzola, M.; Molimard, M. *Pulm. Pharmacol. Ther.* **2010**, *23*, 257.

(124) Baker, J. G.; Hall, I. P.; Hill, S. J. *Mol. Pharmacol.* **2003**, *64*, 1357.

(125) Warne, T.; Serrano-Vega, M. J.; Baker, J. G.; Moukhametzianov, R.; Edwards, P. C.; Henderson, R.; Leslie, A. G. W.; Tate, C. G.; Schertler, G. F. X. *Nature* **2008**, *454*, 486.

(126) Rosen, O. M.; Erlichman, J.; Rosen, S. M. *Mol. Pharmacol.* **1970**, *6*, 524.

(127) Bilezikian, J. P.; Dornfeld, A. M.; Gammon, D. E. *Biochem. Pharmacol.* **1978**, *27*, 1445.

(128) Ariëns, E. J. *Ann. NY. Acad. Sci.* **1967**, *139*, 606.

(129) Loudet, A.; Burgess, K. *Chem. Rev.* **2007**, *107*, 4891.

(130) Briddon, S. J.; Middleton, R. J.; Kellam, B.; Hill, S. J. *Br. J. Pharmacol.* **2003**, *138*, U63.

(131) Hajos, G.; Messmer, A.; Neszmelyi, A.; Parkanyi, L. *J. Org. Chem.* **1984**, *49*, 3199.

(132) Parker, R. E.; Isaacs, N. S. *Chemical Reviews* **1959**, *59*, 737.

(133) Hughes, D. L.; Reamer, R. A.; Bergan, J. J.; Grabowski, E. J. J. *J. Am. Chem. Soc.* **1988**, *110*, 6487.

(134) Li, Z.; Bittman, R. *J. Org. Chem.* **2007**, *72*, 8376.

(135) Thomas J, N. *Anal. Biochem*, *419*, 40.

(136) Colombano, G.; Travelli, C.; Galli, U.; Caldarelli, A.; Chini, M. G.; Canonico, P. L.; Sorba, G.; Bifulco, G.; Tron, G. C.; Genazzani, A. A. *J. Med.Chem.* **2009**, *53*, 616.

(137) Cintas, P.; Barge, A.; Tagliapietra, S.; Boffa, L.; Cravotto, G. *Nat. Protocols*, *5*, 607.

(138) Miller, N.; Williams, G. M.; Brimble, M. A. *Org. Lett.* **2009**, *11*, 2409.

(139) Mohapatra, D. K.; Maity, P. K.; Shabab, M.; Khan, M. I. *Bioorg. Med. Chem. Lett.* **2009**, *19*, 5241.

(140) Wolff, H.; Zenger, K.; Kraus, B. *BioTechniques* **2009**, *47*, 976.

(141) Cheng, Y.-C.; Prusoff, W. H. *Biochem. Pharmacol.* **1973**, *22*, 3099.

(142) Yu, T.B.; Bai, J. Z.; Guan, Z. *Angew. Chem.* **2009**, *48*, 1097.

(143) L'abbé, G.; Leurs, S.; Sannen, I.; Dehaen, W. *Tetrahedron* **1993**, *49*, 4439.

(144) Valko, K.; Du, C. M.; Bevan, C. D.; Reynolds, D. P.; Abraham, M. H. *J. Pharm. Sci.* **2000**, *89*, 1085.

(145) Kerns, E. H.; Di, L.; Petusky, S.; Kleintop, T.; Huryn, D.; McConnell, O.; Carter, G. *J. chromatogr. B.* **2003**, *791*, 381.

(146) Buschmann, V.; Weston, K. D.; Sauer, M. *Bioconjugate. Chem.* **2002**, *14*, 195.

(147) Behrens, O. K.; Corse, J.; Huff, D. E.; Jones, R. G.; Soper, Q. F.; Whitehead, C. W. *J. Biol. Chem.* **1948**, *175*, 771.

(148) Meltola, N.; Soini, A.; Patent, W., Ed. 2003.

(149) Kang, H. C.; Haugland, R. P.; Patent, U. S., Ed. 1993; Vol. US 5, 187,288.

(150) Belmonte, K. E. *Proc. Am. Thoracic Soc.* **2005**, *2*, 297.

(151) Gross, N. J. *New. Engl. J. Med.* **1988**, *319*, 486.

(152) Gross, N. J.; Skorodin, M. S. *New. Engl. J. Med* **1984**, *311*, 421.

(153) Gross, N. J.; Skorodin, M. S. *Am. Rev. Respir.Dis.* **1984**, *129*, 856.

(154) Roffel, A. F.; Elzinga, C. R. S.; Zaagsma, J. *Pulm. Pharmacol.* **1990**, *3*, 47.

(155) Coulson, F. R.; Fryer, A. D. *Pharmacol. Therapeut.* **2003**, *98*, 59.

(156) Hulme, E. C.; Birdsall, N. J. M.; Buckley, N. J. *Annu. Rev. Pharmacol. Toxicol.* **1990**, *30*, 633.

(157) Wess, J. *Crit. Rev. Neurobiol.* **1996**, *10*, 69.

(158) Haga, K.; Kruse, A. C.; Asada, H.; Yurugi-Kobayashi, T.; Shiroishi, M.; Zhang, C.; Weis, W. I.; Okada, T.; Kobilka, B. K.; Haga, T.; Kobayashi, T. *Nature* **2012**, *advance online publication*.

(159) Kruse, A. C.; Hu, J.; Pan, A. C.; Arlow, D. H.; Rosenbaum, D. M.; Rosemond, E.; Green, H. F.; Liu, T.; Chae, P. S.; Dror, R. O.; Shaw, D. E.; Weis, W. I.; Wess, J.; Kobilka, B. K. *Nature* **2012**, *482*, 552.

(160) Sommer, A.; Tielsch, J. M.; Katz, J.; Quigley, H. A.; Gottsch, J. D.; Javitt, J.; Singh, K.; Baltimore Eye Survey Research Group *Arch Ophthalmol* **1991**, *109*, 1090.

(161) Leffler, C.; Amini, L. *BMC Ophthalmology* **2007**, *7*, 17.

(162) Milsom, I.; Abrams, P.; Cardozo, L.; Roberts, R. G.; Thüroff, J.; Wein, A. J. *BJU International* **2001**, *87*, 760.

(163) Ko, Y.; Malone, D. C.; Armstrong, E. P. *Pharmacotherapy* **2006**, *26*, 1694.

(164) Mete, A.; Bowers, K.; Chevalier, E.; Donald, D. K.; Edwards, H.; Escott, K. J.; Ford, R.; Grime, K.; Millichip, I.; Teobald, B.; Russell, V. *Bioorg. Med. Chem. Lett.* **2011**, *21*, 7440.

(165) Prat, M.; Fernandez, D.; Buil, M. A.; Crespo, M. I.; Casals, G.; Ferrer, M.; Tort, L.; Castro, J.; Monleon, J. M.; Gavalda, A.; Miralpeix, M.; Ramos, I.; Domenech, T.; Vilella, D.; Anton, F.; Huerta, J. M.; Espinosa, S.; Lopez, M.; Sentellas, S.; Gonzalez, M.; Alberti, J.; Segarra, V.; Cardenas, A.; Beleta, J.; Ryder, H. *J. Med. Chem.* **2009**, *52*, 5076.

(166) Dowling, M. R.; Charlton, S. J. *Br. J. Pharmacol.* **2006**, *148*, 927.

(167) Disse, B.; Speck, G. A.; Rominger, K. L.; Witek Jr, T. J.; Hammer, R. *Life Sci.* **1999**, *64*, 457.

(168) Lopez, A. D.; Shibuya, K.; Rao, C.; Mathers, C. D.; Hansell, A. L.; Held, L. S.; Schmid, V.; Buist, S. *Eur. Respir. J.* **2006**, *27*, 397.

(169) Mathers, C. D.; Loncar, D. *PLoS Med* **2006**, *3*, e442.

(170) Patrick, G. L. *An Introduction to Medicinal Chemisrty*; 3rd ed.; Oxford University Press: Oxford, 2005.

(171) Schild, H. O. *Br. J.Pharmacol. Chemother.* **1949**, *4*, 277.

(172) Barnes, P. J.; Belvisi, M. G.; Mak, J. C. W.; Haddad, E.-B.; O'Connor, B. *Life Sci.* **1995**, *56*, 853.

(173) Li, L.; Han, J.; Nguyen, B.; Burgess, K. *J. Org. Chem.* **2008**, *73*, 1963.

(174) Hill, A. V. *J. .Physiol.* **1909**, *39*, 361.

(175) Pujala, B.; Rana, S.; Chakraborti, A. K. *J. Org. Chem. 76*, 8768.

(176) Timo Mayer, M. E. M. *Eur. J. Org. Chem.* **2007**, *2007*, 4711.

(177) Reux, B.; Weber, V.; Galmier, M.-J.; Borel, M.; Madesclaire, M.; Madelmont, J.-C.; Debiton, E.; Coudert, P. *Bioorg. Med. Chem.* **2008**, *16*, 5004.

(178) Le Sann, C.; Baron, A.; Mann, J.; van den Berg, H.; Gunaratnam, M.; Neidle, S. *Org. Biomol. Chem.* **2006**, *4*, 1305.

(179) Gao, Y.; Zhang, X.; Ma, C.; Li, X.; Jiang, J. *J. Am. Chem. Soc.* **2008**, *130*, 17044.

(180) Angell, Y.; Burgess, K. *J. Org. Chem.* **2005**, *70*, 9595.

(181) Engel, N.; Steglich, W. *Angew. Chem.* **1978**, *17*, 676.

(182) Munno, G. D.; Lucchesini, F.; Neidlein, R. *Tetrahedron* **1993**, *49*, 6863.

(183) Ketcham, R.; Jambotkar, D.; Martinelli, L. *J. Org. Chem.* **1962**, *27*, 4666.

(184) Orsini, F.; Pelizzoni, F.; Bellini, B.; Miglierini, G. *Carbohydr. Res.* **1997**, *301*, 95.

(185) Jones, R. A.; Pojarlieva, T.; Head, R. J. *Tetrahedron* **1968**, *24*, 2013.

(186) Huang, L.; Shi, A.; He, F.; Li, X. *Bioorg. Med. Chem.* **2010**, *18*, 1244.

(187) Abedin, M. J.; Liepold, L.; Suci, P.; Young, M.; Douglas, T. *J. Am. Chem. Soc* **2009**, *131*, 4346.